# Feasibility Studies of the Exhaust-Gas Reforming of Hydrocarbon and Alcohol Fuels

By
Martin Richard Jones

Thesis submitted to the
University of Birmingham
for the degree of
Doctor of Philosophy

Automotive Engineering Centre
School of Manufacturing
and Mechanical Engineering
University of Birmingham

April 1992

## SYNOPSIS

The feasibility of a proposed exhaust-gas reforming process, as applied to hydrocarbon and alcohol spark-ignition engine fuels, has been studied.

In the first instance, a theoretical approach is reported. Complex chemical equilibria and energy balance software has been developed, and used to simulate exhaust-gas reforming reactions for n-heptane and methanol feedstocks. Engine combustion of reformed fuel compositions thus predicted has then been modelled by means of in-house developed cycle analysis software. An important preliminary part of the cycle simulation exercise was the calculation of reformed fuel laminar flame speed, and hence heat-release duration and commencement values. The results of the simulations have enabled comparisons of predicted engine thermal efficiency and pollutant emission levels for reformed and conventional fuelling strategies.

Conclusions of the theoretical studies were sufficiently encouraging to warrant a practical investigation, and hence the design, construction and commissioning of a prototype reforming reactor and test rig are described. A test programme was then conducted, in order that the effect of various relevant parameters on reformer performance could be established. The findings of this study were encouraging in terms of the fuel compositions which could be produced, and in the case of an n-heptane feedstock, results were found to correlate well with those of the earlier predictive work. Major limitations highlighted by the practical work, however, relate to high reformer temperature requirements, and low reformed fuel generation rates.

The findings of the studies are drawn together in a discussion of the practical feasibility of a vehicle installation, and project conclusions.

## ACKNOWLEDGEMENTS

Dr M L Wyszynski of the School of Manufacturing and Mechanical Engineering is gratefully acknowledged for his enthusiastic encouragement and supervision over the past four years or so. This was particularly valuable in the early stages of the work, when a project strategy leading towards achievable objectives had to be established in the light of very limited knowledge in the field.

Thanks are also extended to Dr J W Dunn, Director of the Automotive Engineering Centre, especially for his efforts in respect of the business aspects of the project; this has resulted in committed industrial sponsorship of the study throughout its duration. Mrs M Morby is gratefully acknowledged for her efficiency in dealing with administrative matters relating to the work, and Mr C Hingley is thanked for the many hours spent on the construction and commissioning of the laboratory test rig.

Sincere thanks to the sponsoring company, Jaguar Cars, for their financial and technical support. Mr R Lee is acknowledged for his valuable suggestions over the past 18 months or so, and Mr B N V Parsons for originating the project concept some eight years ago.

Finally, Dr's P Hawker, R Brisley and E Shutt of Johnson Matthey Catalytic Systems Division, and Mr M Shaw of Inco Alloys International, are gratefully acknowledged for their technical assistance, and for the provision of free-issue materials. Mr G Davies of W B Combustion is thanked for help in the design and commissioning of the test-rig combustion apparatus.

# NOTATION

| | |
|---|---|
| $A$ | Helmholtz Function, eqn 4.14 |
| AFR | mass air to fuel ratio |
| $a_{ij}$ | stoichiometric coefficients, kg-atoms of element i per kg-mole of species j |
| $a_i$ (i=1-7) | least squares coefficients, eqn's 4.40 to 4.42 |
| $b_i$ | kg-atoms of element i per kg of mixture |
| $b_i^0$ | kg-atoms of element i per kg of reactants |
| $C$ | dimensionless standard state constant pressure specific heat |
| $(C_p^0)_j$ | standard state constant pressure specific heat of species j |
| $C_A$ | mole fraction of air in eqn 6.9 |
| $C_F$ | mole fraction of fuel in eqn 6.9 |
| $C_H$ | mole fraction of hydrogen in eqn 6.9 |
| $CO_{RC}$ | rate-controlled carbon monoxide level in eqn 5.6 |
| $CO_{EQ}$ | equilibrium carbon monoxide level in eqn 5.6 |
| $CO_{PEQ}$ | peak equilibrium carbon monoxide level in eqn 5.6 |
| $F_S$ | stoichiometric mass fuel to air ratio |
| $f$ | total mass fraction of inert diluents in fuel/air mixture, eq 6.7 |
| $f_{CO}$ | carbon monoxide kinetics calibration factor, eqn 5.6 |
| G | total Gibbs free energy of mixture |
| $\mathcal{G}$ | dimensionless Gibbs free energy |
| GHSV | catalyst gas hourly space velocity |
| g | specific Gibbs free energy |
| H | total enthalpy |
| $\mathcal{H}$ | dimensionless enthalpy |
| $H_{P,298}$ | standard state standardized enthalpy of products |

| | |
|---|---|
| $H_{R,298}$ | standard state standardized enthalpy of reactants |
| $(H_T^0)_j$ | standardized enthalpy of species j |
| HCV/HHV | higher calorific or heating value of a fuel |
| h | specific enthalpy |
| $h_o$ | specific enthalpy of reactants |
| $h_{FE}$ | specific enthalpy of feedstock at reformer entry |
| $h_{RE}$ | specific enthalpy of reforming exhaust gases at reformer entry |
| $h_{RF}$ | specific enthalpy of reformed fuel at reformer outlet |
| $h_{SE1}$ | specific enthalpy of surplus exhaust gases at reformer entry |
| $h_{SE2}$ | specific enthalpy of surplus exhaust gases at reformer outlet |
| IMEP | indicated mean effective pressure |
| LCV/LHV | lower calorific or heating value of a fuel |
| M | molecular mass |
| $\dot{m}$ | mass flow rate |
| $\dot{m}_{FE}$ | mass flow rate of reformer feedstock |
| $\dot{m}_{RE}$ | mass flow rate of reforming exhaust gases |
| $\dot{m}_{RF}$ | mass flow rate of reformed fuel |
| $\dot{m}_{SE}$ | mass flow rate of surplus exhaust gases |
| $n_j$ | kg-moles of species j per kg of mixture |
| n | total kg-moles per kg of mixture |
| OXF | assigned reforming oxidant to fuel ratio |
| p | partial pressure |
| P | total pressure |
| $P_{evo}$ | pressure at exhaust valve opening |
| $P_{max}$ | peak cycle pressure |
| $P_o$ | assigned equilibrium pressure |
| Q | heat transfer |

| | |
|---|---|
| $Q_{RP,298}$ | heat of reaction for products and reactants at 298K |
| R | specific gas constant |
| $R_H$ | quantity of relative hydrogen addition, eqn 6.9 |
| $R_o$ | universal gas constant, 8314.3 J/kmolK |
| S | total entropy |
| $\mathcal{S}$ | dimensionless entropy |
| $S_j$ | standardized entropy of species j in a mixture |
| $(S^0_T)_j$ | standardized entropy of species j in isolation |
| s | specific entropy |
| $s_o$ | specific entropy of reactants |
| $S^o_{L(i)}$ | laminar flame speed of fuel i |
| $S^o_{L(f)}$ | laminar flame speed modified by addition of mass fraction *f* of inert diluents |
| $S^o_{L(f,H)}$ | laminar flame speed modified by addition of mass fraction *f* of inert diluents and addition of hydrogen |
| $S^o_{L(hept)}$ | laminar flame speed of n-heptane |
| $S^o_{L(Rel)}$ | laminar flame speed of fuel relative to $S^o_{L(hept)}$, eqn 6.5 |
| T | temperature |
| $T_{evo}$ | temperature at exhaust valve opening |
| $T_{FE}$ | temperature of feedstock at reformer inlet |
| $T_{max}$ | peak cycle temperature |
| $T_o$ | assigned equilibrium temperature |
| $T_{RE}$ | temperature of reforming exhaust gases at reformer inlet |
| $T_{req}$ | exhaust gas temperature required at inlet to reformer |
| $T_{RF}$ | temperature of reformed fuel at reformer outlet |
| $T_{SE1}$ | temperature of surplus exhaust gases at reformer inlet |
| $T_{SE2}$ | temperature of surplus exhaust gases at reformer outlet |

| | |
|---|---|
| $T_{130}$ | temperature at crank angle of 130° ATDC |
| $T_{180}$ | temperature at crank angle of 180° ATDC |
| U | internal energy |
| V | volume |
| x | ratio of surplus to reforming exhaust gases |
| | |
| $\alpha$ | flame speed calculation constant, eqn 6.8 |
| $\eta_{cycle}$ | engine cycle thermal efficiency |
| $\eta_{overall}$ | overall reformer/engine cycle thermal efficiency |
| $\eta_{rth}$ | reforming reactor thermal efficiency |
| $\lambda_c$ | iteration correction control factor, eqn 4.35 |
| $\lambda_e$ | engine excess air factor |
| $\lambda_i$ | Lagrangian multiplier, eqn 4.19 |
| $\lambda_r$ | reformer excess oxidant factor |
| $\lambda_1$ | iteration correction control factor, eqn 4.36 |
| $\lambda_2$ | iteration correction control factor, eqn 4.37 |
| $\mu_i$ | chemical potential of species i |
| $\pi_i$ | iteration correction variable |
| $\theta$ | engine crank angle |
| $\theta_b$ | heat release duration in crank angle degrees |
| $\theta_s$ | commencement of heat release, crank angle degrees |
| $\zeta$ | Gibbs free energy with constraints, eqn 4.19 |

Indices:

| | |
|---|---|
| i | counter |
| j | counter |

| | |
|---|---|
| k | counter |
| $l$ | number of discrete elements in system |
| m | number of possible gaseous species |
| n | number of possible gaseous and condensed species |

CONTENTS

## LIST OF FIGURES

## LIST OF PHOTOGRAPHS



## LIST OF TABLES

# 1 INTRODUCTION

The search for viable alternative fuels for the spark-ignition internal combustion engine is a field of research study which has grown steadily over the past 25 years or so. Initial impetus was provided by the American Environmental Protection Agency (EPA), who began to introduce vehicle emissions legislation in the late 1960's, whilst further stimulus arose in late 1973, when oil prices increased sharply as a result of the Middle East oil embargo. The realization that fossil fuels are a rapidly diminishing finite resource, and the recent increased awareness of the need to reduce carbon-derived emissions to the atmosphere, have also become predominant factors driving the search for alternatives.

Various definitions of the term 'alternative fuels' can be found in the literature; throughout this thesis the term will be defined in the widest possible sense, thereby including the use of a conventional fuel in a non-conventional or alternative manner. It is hoped that this definition is justified in later stages of the thesis, where it is proposed that significant improvements in engine thermal efficiency and pollutant emissions might result from the non-conventional use of an otherwise conventional motor fuel.

Much of the work in the field of alternative fuels for spark-ignition engines has suggested that the use of hydrogen would address three fundamental problems: pollutant emissions, long term availability, and economy of usage (1, 2, 3). The respective reasons are that hydrogen can be combusted to give products consisting almost entirely of water vapour, it can be produced in several ways from a wide variety of feedstocks, and it has an extremely lean flammability limit. The major limitations of hydrogen as an

automotive fuel, however, relate to the storage of the fuel onboard the vehicle.

Storage as a compressed gas or a cryogenic liquid are possibilities (4), but have generally been considered to be unsuitable on the grounds of cost, inconvenience, and inherent danger. The onboard storage of hydrogen dissolved in a metal hydride might also be feasible (5), but again there are limitations, not least of which is the relatively low mass of hydrogen which can be liberated as a free gas per unit mass of hydride. Studies carried out in the late 1970's suggested that the maximum hydrogen storage capacity of hydrides was around 5% by mass (6), but more recent work indicates that the true value is somewhat less than 2% (7, 8). The lower levels quoted most recently are due to correct allowances being made for the masses of the hydride packaging and the heating medium, the latter being required in order to desorb hydrogen gas from the hydride (9).

Consideration can also be given to the storage of hydrogen as a constituent element of a more convenient compound such as gasoline or methanol; with this form of storage, the technical problem becomes one of releasing the hydrogen from its parent molecule. This can be accomplished in a number of ways, but the methods generally used in the chemical industry are based either on partial oxidation or catalytic steam reforming (10, 11, 12).

As partial oxidation involves the reaction of a feedstock with a limited quantity of air, the process is exothermic, and the resulting hydrogen-containing fuel gas typically has a calorific value some 20% lower than that of the original feedstock. For this reason the process is not usually considered to be attractive in terms of efficiency, although it does represent an interesting

means of generating free hydrogen gas for use as a charge supplement in ultra-lean combustion exercises (13).

The second major process, steam reforming, can be highly endothermic, and generally involves a catalysed reaction between steam and a hydrocarbon feedstock at high temperatures. The gas thus produced has an improved calorific value as compared with the feedstock, and the efficiency of the process can therefore be quite favourable, particularly if the heat energy requirement is supplied from a source which would otherwise be wasted.

It follows that for onboard vehicle applications, such a heat energy requirement might be provided by the hot engine exhaust gases. In addition, because such gases contain a certain quantity of steam, it is proposed that a hydrocarbon or alcohol feedstock could be catalytically reformed by direct contact with a portion of the hot products of combustion leaving the engine. The fuel gas generated should thus contain quantities of hydrogen, carbon monoxide and nitrogen, and might have a potential for lean combustion, leading to low emissions of currently regulated pollutants, and improvements in engine thermal efficiency.

The initial objective of the work reported in this thesis is to establish the theoretical thermodynamic feasibility of a proposed exhaust-gas reforming process, and to predict benefits for engine operation on gaseous exhaust-reformed fuels. The results of this study lead into the second major phase of the work, the objective of which is to design and construct a prototype reforming reactor and test rig, and hence evaluate the process in a laboratory-based test programme.

# 2 LITERATURE SURVEY OF ONBOARD FUEL REFORMING TECHNIQUES

As the work reported here is concerned mainly with the onboard production of hydrogen-containing gaseous fuels from liquid hydrocarbon and alcohol feedstocks, published research relating to the onboard storage of hydrogen in pressurized, cryogenic, or metal hydride form has not been considered. Previous work of interest in the current project concerns the processes by which relatively large hydrogen-containing molecules can be broken down to mixtures containing free hydrogen gas, and the feasibility of adapting such processes for onboard vehicle operation.

On-line searches of the Society of Automotive Engineers (SAE) and Chemical Abstracts databases were carried out via the ORBIT and STN host computer systems, and a survey of the SAE MOVE CD-ROM disk was conducted. Searches of hard copy sources such as SAE Index/Transactions, I Mech E Proceedings, and the American Chemical Society Abstracts were also carried out. In addition, certain text books were found to be useful, particularly from the point of view of describing the various industry-proven reforming processes currently in use. Although such books invariably deal with large scale chemical plant rather than miniaturized onboard automotive plant, the information on such subjects as reforming equilibria and catalysis contained therein is of considerable interest.

Much of the early work in the field of onboard hydrogen generation was carried out in the USA, with initial research in the 1970's directed mainly at reducing pollutant emissions from the spark-ignition engine. The potential for fuel economy improvements was soon identified, however, and later work has also been aimed, therefore, at improving engine operating

efficiency. Research in the USA has been sponsored by organizations such as the National Aeronautics and Space Administration (NASA), and the Environmental Protection Agency (EPA), and has been carried out at such establishments as the Jet Propulsion Laboratory (California Institute of Technology), the Institute of Gas Technology (Chicago), and various universities; Ford and General Motors have also run in-house research programmes.

Outside the USA, the onboard reforming of hydrocarbon and alcohol fuels has been investigated at The Royal Institute of Technology (Sweden), Volkswagen (Germany), in Japan, by companies such as Nissan and Mitsubishi, and at various academic institutions.

Almost without exception, the onboard reforming techniques investigated fall into one or more of the following general categories:

i) Steam Reforming
ii) Partial Oxidation
iii) Thermal Dissociation
iv) Exhaust-Gas Reforming

Each of these processes is outlined below, with a discussion of selected research publications.

## 2.1 Onboard Steam Reforming Techniques

The steam reforming of hydrocarbons to produce hydrogen-containing gas mixtures has been an established industrial process since the mid-1930's, when ICI first commissioned plant to reform a feedstock of gases ranging

from methane to butane in the presence of steam and a catalyst (10). Lee and Wimmer suggested the use of steam-reformed gaseous mixtures as automotive fuels in 1968 (14), but the first attempt at adapting the reforming technique as an onboard process was by Newkirk and Abel in 'The Boston Reformed Fuel Car' project (15).

### 2.1.1 The Boston Reformed Fuel Car

Under contract to the EPA, Newkirk and Abel of the International Materials Corporation proposed a system where gasoline is steam reformed into a hydrogen-rich gaseous fuel. Idealizing gasoline as n-heptane, ($C_7H_{16}$), the chemical reactions thought to be of prime importance are defined as follows:

$$C_7H_{16} + 14H_2O + \text{Heat} \rightarrow 7CO_2 + 22H_2 \quad \text{(Summary Equation)} \qquad (2.1)$$

$$C_7H_{16} + 7H_2O + \text{Heat} \rightarrow 7CO + 15H_2 \qquad (2.2)$$

$$C_7H_{16} + \text{Heat} \rightarrow 7C + 8H_2 \qquad (2.3)$$

$$C + H_2O + \text{Heat} \rightarrow CO + H_2 \qquad (2.4)$$

$$CO + H_2O \rightarrow CO_2 + H_2 + \text{Heat} \quad \text{(Water-Gas Shift)} \qquad (2.5)$$

In the first four of these idealized equations, the addition of heat on the left-hand side indicates that the reaction is endothermic, and requires a heat input in order to proceed from left to right. Conversely, the water-gas shift reaction, eqn 2.5, is exothermic, liberating heat as the reaction moves from left to right.

Newkirk and Abel decided against the use of a catalyst to promote the reforming reactions on the grounds that this would introduce unnecessary cost and complexity. A block diagram of their system is shown in Fig 2.1a, whilst a detailed cross-section of the reformer itself is shown in Fig 2.1b.

To briefly describe the operation of the system, water is condensed from the engine exhaust gases and fed to the reactor where it is vaporized and superheated to a temperature of around 1000°C. Preheated gasoline is then injected into the steam flow, and it is proposed that reforming reactions proceed to give a gaseous fuel comprising hydrogen and carbon dioxide. A portion of this fuel is then recirculated into the reactor, where it is burned with air to provide the heat requirement of the endothermic reforming reactions. That portion of reformed fuel not combusted in the reformer is then available to fuel the engine.

In view of the fact that no attempt is made to reclaim heat energy from the engine system, and that about 40% of the heat of combustion available as reformed fuel is required to drive the reformer, the proposed process is rather inefficient. A theoretical reformer thermal efficiency of 59.7% is quoted, this figure giving a measure of reformed fuel lower heating value (LHV) available to the engine compared with the LHV of the feedstock, with both values expressed on a heat-release per kg of feedstock basis. This implies that the heat release available to the engine would be considerably less with reformed gasoline fuel than would be the case with normal gasoline, for a constant feedstock flow rate, which in turn implies a detrimental effect on fuel economy.

It is stated, however, that the objective of the work is to minimize emissions, and in this respect significant improvements are predicted. The

findings of Murray and Schoeppel (16) are cited as being representative of oxides of nitrogen ($NO_x$) levels which might be expected from the reformate-fuelled engine (see Fig 2.2). The levels quoted from Ref 16 certainly appear to show significant reductions in $NO_x$ levels, but the predictions are not substantiated by test results, and there is no evidence in the literature of any further work on the Boston Car project.

### 2.1.2 Catalytic Steam Reforming - M D Martin - University of Arizona

Martin looked at the steam reforming/engine system as a total energy concept, and attempted to utilize as much of the engine's waste heat as possible in order to promote the endothermic reforming reactions (17). His proposed system is shown in Fig 2.3.

Martin describes the catalytic steam reforming of gasoline at a reactor temperature of around 620°C, with the reformer energy requirements met by indirect heat-exchange with hot engine exhaust gases. Careful use is made of all convenient sources of otherwise wasted heat energy, such as coolant and exhaust systems and the hot reformed fuel stream, in order that the reactants are preheated and reformed as efficiently as possible.

On the whole the work is of considerable interest, and equilibrium computations carried out at the proposed reaction temperature of 620°C predict a product composition comprising combustible mole fractions of 48% hydrogen ($H_2$), 8% methane ($CH_4$) and 9% carbon monoxide (CO); it is predicted that such a fuel would raise the brake thermal efficiency value of a test engine from a gasoline-fuelled level of 18.6% to a value of 26% when operating at the same speed/load condition on the reformed fuel. This improvement would result, it is claimed, from the improvement in fuel

heating value which would be characterized by the reforming process, and from reduced pumping losses. The latter benefit arises from the potential to run the engine fuelled lean to give the required part-load power output, thus precluding the necessity for charge throttling. It is a widely-studied phenomenon with hydrogen-enriched fuels made possible by the extension of the lean flammability limit of the mixture (18, 19). Notably, the lean flammability limit of pure hydrogen in air occurs at an air to fuel mass ratio of approximately 346:1 (20), which compares with a much lower ratio of around 24:1 for gasoline and air (21).

Martin presents some fundamental and rather optimistic thermodynamic calculations, which claim that sufficient energy can be recovered from the engine system in order to drive the reforming process, but it should be pointed out that the analysis is open to criticism on the following grounds:

i) The probability of carbon solids (C(s)) formation in the reactor under the quoted operating conditions would be high, as demonstrated later in the current work.

ii) It is assumed that the reformer will be isothermal, but in fact temperatures would tend to reduce significantly through the vessel as a result of the endothermic reactions. This should be accounted for when assigning the equilibrium temperature in computational predictions of fuel composition.

iii) No recognition is given to the fact that only a small portion of the energy available in the exhaust gases exists at temperatures high enough to drive the reforming reactions.

The work undertaken at Arizona appears to represent one of the first investigations into onboard catalytic steam reforming as a means of improving both pollutant emissions and fuel economy, and as such it is unfortunate that no further work on the project can be traced in the literature.

### 2.1.3 Other Work on Onboard Steam Reforming of Hydrocarbons.

Houseman and Cerini of the Jet Propulsion Laboratory, California, have been involved in many aspects of research into onboard reforming techniques, and summarized much of their work in a paper entitled "Onboard Hydrogen Generation for Automobiles" (22). The paper gives the results of predictive studies of chemical equilibria for various reforming processes involving both hydrocarbon and alcohol feedstocks, and presents the findings of laboratory-based rig tests conducted in order to verify the theoretical work.

The hydrocarbon work was conducted using a JP-5 feedstock, $(CH_{1.92})_x$, which was considered to be a good approximation to the Federal Test gasoline Indolene, $(CH_{1.86})_x$, for which the requisite thermodynamic data was not available. The proposed idealized reforming reaction is as follows:

$$CH_{1.92} + H_2O + Heat \rightarrow CO + 1.96H_2 \qquad (2.6)$$

Which gives a stoichiometric steam to feedstock mass ratio of around 1.3.

Reactor thermal efficiency, $\eta_{RTH}$, is defined as follows:

$$\eta_{RTH} = \frac{\text{Lower Heating Value of Product Gases}}{\text{Lower Heating Value of Tanked Feedstock}} \qquad (2.7)$$

where lower heating value (LHV) is expressed as a heat release per unit mass of feedstock in each case. This gives a theoretical thermal efficiency value of 118% based on computations at an equilibrium temperature of 760°C, and a steam to feedstock mass ratio of 3.5. Steam to fuel mass ratios well in excess of the stoichiometric value of 1.3 are generally used in order to avoid soot formation problems, which according to equilibria predictions would exist at all ratios lower than 1.7 at the assigned temperature of 760°C (see Fig 2.4).

Experimental work was restricted to rig testing of the reactor vessel utilizing an electrically-heated unit loaded with a 2.4kg charge of commercial grade steam-reforming catalyst (Girdler G56B, 25% Ni on alumina beads). Reformed fuel gas compositions very close to those predicted theoretically were produced, and it is stated that significant improvements in fuel heating value could be achieved across the reactor. An approximately linear decrease in temperature was also observed as the reactants passed through the reformer, which is attributed to heat conversion in the endothermic reactions.

A limited amount of other work was also reported in the 1970's, ranging from steam reforming using reactors driven by engine exhaust gas energy, to "cracking" carburettors, where it was proposed that the feedstock could be reformed within the carburettor itself (23, 24, 25, 26).

### 2.1.4 Steam Reforming of Methanol

There has for some time been considerable interest in the potential of methanol as an automotive fuel, one of the main reasons for this being the wide variety of means by which it can be produced (27, 28, 29, 30). A characteristic of the fuel which is of particular interest in the current project,

however, is the ease with which the alcohol can be steam reformed; much lower temperature requirements than those needed for gasoline have been reported, whilst carbon solids formation problems can apparently be easily avoided.

The idealized chemical equation for the steam reforming of methanol is given as:

$$CH_3OH + H_2O + Heat \rightarrow 3H_2 + CO_2 \qquad (2.8)$$

Product gases of the reaction have a lower calorific value some 8% higher than that for gaseous methanol, giving a reactor thermal efficiency of 108% (31). When product gases are compared with a liquid tanked feedstock, the thermal efficiency of the reaction becomes 114%, with the 6% increase being attributed to the heat of vaporization of the methanol. Hence, a fuel gas having a calorific value improved by some 14% could be produced, and if the energy requirement of the reforming reaction is provided by otherwise wasted engine thermal energy, an improvement in overall engine efficiency should result.

Fig 2.5 shows the results of equilibria computations presented by Houseman and Cerini for the steam reforming of methanol over a range of temperature. Steam to fuel mass ratio is 0.5, which is slightly lower than the stoichiometric ratio of 0.56 derived from eqn. 2.8. The plot shows carbon-solids-free compositions above approximately 500K, with maximum $H_2$ yields of around 60% occurring at 1000K.

Test results are quoted for an engine running on a simulated steam-reformed methanol gas having a molar composition of $3H_2 + CO_2 + 1.36H_2O$.

This fuel could apparently be produced by a reformer driven by energy reclaimed from hot engine exhaust gases, and represents a 7% improvement in fuel heating value as compared with a gaseous feedstock. It is claimed that the use of the fuel under lean operating conditions could lead to increases in engine thermal efficiency of the order of 30% as compared with normal gasoline operation. As in earlier work, the low maximum power output potential of the engine is acknowledged, and it is suggested that turbo-charging or the use of larger displacement engines could overcome this limitation.

McCall et al (32) report a 22% improvement in fuel heating value arising from the steam reforming of methanol, but this calculation is based on the LHV of a tanked mixture of methanol and water, which is naturally much lower than the true LHV of the liquid methanol feedstock. The paper reports the results of engine trials using neat methanol and gas mixtures simulating dissociated and steam-reformed methanol; results of particular interest are those relating to pollutant emissions, where significant reductions in unburned fuel and carbon monoxide levels are claimed for engine operation on the steam-reformed fuel in place of liquid methanol. In addition, the emission levels of aldehydes, which have generally been found to be rather high from alcohol-fuelled engines (33, 34, 35) were measured, using the 3-Methyl-2-Benzothiazolone Hydrazone test technique (36, 37); the results indicate very considerable reductions in aldehyde levels when the engine is fuelled with the steam-reformed fuel mixture. This reduction is attributed to the virtual non-existence of certain intermediate compounds which normally form during the combustion process of unreformed alcohols, and subsequently become oxidized to form aldehydes.

## 2.2 Partial Oxidation Reforming Processes

Partial oxidation techniques involve the exothermic reaction of a feed fuel in a limited quantity of air, such that incomplete combustion only can result. The gaseous products of the reaction can thus have a relatively high heating value - typically around 80% of the original feedstock.

### 2.2.1 Partial Oxidation of Hydrocarbons

In terms of hydrogen yield, the ideal partial oxidation reaction for the Federal Test gasoline Indolene, $(CH_{1.86})_x$, is given by:

$$CH_{1.86} + 0.5(O_2 + 3.76N_2) \rightarrow CO + 0.93H_2 + 1.88N_2 + Heat \qquad (2.9)$$

In practice, operation at the air to fuel mass ratio (AFR) of 4.95 indicated in eqn 2.9 would lead to the formation of carbon solids (C(s)), and hence operation at slightly leaner AFR's is essential. Equilibria predictions given by Houseman and Cerini were again computed using JP-5 as an approximation to Indolene, and the results given in Fig 2.6 clearly show that the equilibrium C(s) formation limit lies at an AFR of around 5.2 (13).

Experimental work reported in Ref 13 indicates that partial oxidation over a nickel catalyst of the type usually used in the steam reforming process gives compositions close to those predicted by equilibria computations. The system developed gave a reformer thermal efficiency of 78.5%, which corresponds to 96% of the maximum theoretical value, with hydrogen and carbon monoxide yields of 21.6 and 23.6% by volume respectively. Although no actual engine trials are reported, it is proposed that the generated fuel gas would be injected into the engine along with a gasoline/air charge, in order to

extend the lean flammability limit of the mixture. It is claimed that this could lead to improvements in engine thermal efficiency and to better part-load economy, as a result of mixture leaning rather than throttling to give reduced output operation.

Further work on the hydrogen enrichment programme at the Jet Propulsion Lab was undertaken by Finegold (38) and Menard et al (39). A block diagram of the rig used by Finegold is shown in Fig 2.7, and it is stated that the gas produced by the reformer is much the same as that generated by Houseman and Cerini, as discussed in the previous paragraph. The reformed fuel produced is mixed with a gasoline/air charge, and improvements in $NO_x$ levels and fuel economy are reported as a result of the ultra-lean operation which was possible. Stebar and Parks also quote similar results for work which they conducted (40).

The partial oxidation of hydrocarbons to generate hydrogen in a small-scale reactor has been the subject of some work carried out in the UK by Johnson Matthey (41). Their "Hot Spot" technology has led to the development of a small, self-contained reformer which can produce a hydrogen-rich gas from a hydrocarbon feedstock in the presence of a noble metal catalyst. The technique is still under development, and would not currently be capable of producing a fuel gas in large enough quantities to run an automotive engine.

### 2.2.2 Partial Oxidation of Alcohols

Although in principle the partial oxidation of alcohols such as methanol is a feasible means of producing a hydrogen-containing gas, very little work has been traced on the subject. The process is similar to that

applied to gasoline, being exothermic and having a maximum theoretical thermal efficiency of around 82.5%. Air to fuel ratios used with the alcohol are generally much lower than for gasoline, and optimum equilibrium and hence efficiency conditions occur at an air to fuel ratio of around 1.4, which represents the soot limit (see Fig 2.8).

Again, Johnson Matthey have carried out a limited amount of work in the area (42), along the same lines as their efforts mentioned above. In addition, a study into the feasibility of methanol decomposition through rich oxidation, as a cold-start method for methanol engines, has recently been conducted in the USA (43)

## 2.3 Thermal Dissociation of Methanol

An interesting characteristic of methanol is that it can be thermally decomposed, in the absence of any other reactant, into a 2 to 1 molar mixture of hydrogen and carbon monoxide, in accordance with the following reaction:

$$CH_3OH + \text{Heat} \rightarrow 2H_2 + CO \qquad (2.10)$$

This is an endothermic reaction, requiring a heat input of around 4.0 MJ/kg of liquid methanol. The energy input manifests itself as a gain in chemical energy, as combustion of the product gases would yield 24.0 MJ/kg of methanol feed, as compared with a value of around 20.0 MJ/kg for the standard liquid fuel; this increase represents an improvement of the order of 20% (44, 45).

The temperature at which the dissociation reaction occurs appears to be strongly dependent upon the type of catalyst used. Equilibrium yields computed in Ref 22 suggest that reactor temperatures of over 1000K are required if complete conversion to the 2 to 1 molar mixture of $H_2$ and CO is to be approached; the effect of temperature on computed equilibria is shown in Fig 2.9. More recent work (46) suggests that the use of catalysts can reduce the temperature requirement levels to as low as 300°C, whilst still producing a gas containing 58% $H_2$ and 30% CO; the balance comprises $CO_2$, $H_2O$, $CH_4$ and small amounts of unreacted feedstock. Such temperatures naturally support the possibility of onboard dissociation using heat supplied from engine coolant and exhaust systems, and it is this concept which has been the subject of much recent research.

König et al (47) present a very interesting study of various methanol dissociation catalysts. Fig 2.10 shows the results obtained for catalytic dissociation of methanol over a copper-based catalyst at various temperatures; near equilibrium yields are observed at 300°C and above, with barely quantifiable levels of soot formation. In addition, a number of more expensive noble metal catalysts were examined. It was found that a certain precious metal formulation gave product compositions comparable with those observed over copper, and that the performance of this catalyst was largely unaffected by the introduction of air into the system, which under certain conditions was desirable, but could not be tolerated by the copper catalyst. The suitability of the noble metal was confirmed when it successfully completed a 220hr ageing test carried out under alternating reducing and oxidizing conditions.

Similar studies of noble metal and base metal catalysts conducted by Sato et al (48) indicated that a base metal material containing quantities of

copper, NiO and $Cr_2O_3$ gave good methanol conversion at temperatures as low as 200°C; a 100hr durability test failed to affect the performance of this base metal catalyst.

There have been two main approaches addressing the issue of how the dissociated methanol fuel gas should then be used in the engine. It has been used as a fuel in its own right, with the engine aspirating and combusting a charge consisting of dissociated gas and air, and it has been used as a supplementary fuel, where it is mixed with a charge of unreformed fuel and air, thus permitting operation at very lean air to fuel ratios. It has generally been concluded that the use of dissociated methanol alone is most suitable for low power operation at very lean equivalence ratios, where unthrottled running and hence reduced pumping losses should be possible. Higher power operation at richer air to fuel ratios has led to pre-ignition and flashback into the inlet manifold when running with hydrogen-enriched fuels, and it is therefore suggested that a liquid methanol/gasoline fuelling strategy should be used for high load conditions.

After applying a correction to account for the difference in fuel calorific value of gasoline and methanol fuels, fuel economy improvements of up to 20% have been reported for a dissociated methanol vehicle using reclaimed exhaust-gas energy to drive the reformer (49). Considerable reductions in pollutant emissions are also said to result from the combustion of the gaseous reformed fuel. In particular, as yet unregulated aldehyde levels, which tend to be high from alcohol-fuelled vehicles, are reported to be low for the dissociated methanol engine as compared not only with liquid methanol, but also gasoline-fuelled units. In this respect, the results of König et al are presented in Fig 2.11.

In view of the relative ease and the potential benefits of methanol dissociation, it is suggested that further development of systems such as those outlined above should be pursued. It must be said, however, that national fuel policy will ultimately dictate the extent to which such alternative fuel technologies are adopted.

## 2.4 Exhaust-Gas Reforming

Previous studies of exhaust-gas reforming are of particular interest in the current project, where it is hoped that the heat and steam requirements of reforming reactions can be met by direct contact between the feedstock and hot engine exhaust gases.

### 2.4.1 Exhaust-Gas Reforming of Hydrocarbon Fuels

The literature survey into exhaust-gas reforming techniques traced few publications. Lindström of the Swedish Royal Institute of Technology appears to have pioneered the work in the early 1970's, leading to a USA patent in 1975 (50). Lindström proposed that between 5 and 50% of the exhaust gases leaving the engine be directed to a reactor where they mix with a quantity of gasoline fuel. It is proposed that endothermic steam reforming reactions, driven by the heat energy and steam content of the exhaust gases, then proceed to produce a fuel containing hydrogen and carbon monoxide. Should additional heat energy be required to drive the reaction, this could be supplied by heat exchange with surplus exhaust gases, or by the combustion of small quantities of either gasoline or reformed fuel inside the reformer. A diagram showing Lindström's proposed system is given in Fig 2.12.

The reformed fuel gas generated is used to supplement the gasoline/air charge, thus permitting operation at ultra-lean air to fuel ratios. Unburned hydrocarbon and carbon monoxide emissions are thus claimed to be relatively low, as are $NO_x$ levels, which are said to be reduced by a factor of between 5 and 10 as compared with normal gasoline operation. Further work conducted in Sweden was reported by Sjöström, whose paper discusses the chemistry and catalysis of the exhaust-reforming process in some detail (51).

The chemistry of the exhaust-gas reforming process is also described by Parsons in an unpublished report and in a patent application relating to 'An Internal Combustion Engine and a Method of Operating the Engine' (52, 53); calorific value improvements of the order of 20% are predicted. The documents give chemical equations for the combustion and reforming of a generalized hydrocarbon. Transcribing these equations for the specific case of JP-5 gives:

i) Normal combustion:

$$CH_{1.92} + 1.48(O_2 + 3.76N_2) \rightarrow CO_2 + 0.96H_2O + 5.56N_2 + \text{Heat} \qquad (2.11)$$

ii) Reforming:

$$CH_{1.92} + 0.51(CO_2 + 0.96H_2O + 5.56N_2) + \text{Heat} \rightarrow 1.51CO + 1.45H_2 + 2.84N_2 \qquad (2.12)$$

iii) Combustion of reformed fuel:

$$1.51CO + 1.45H_2 + 2.84N_2 + 1.48(O_2 + 3.76N_2) \rightarrow 1.51CO_2 + 1.45H_2O + 8.40N_2 + \text{Heat} \qquad (2.13)$$

Similar equations describing the exhaust-gas reforming of octane are presented by Sepos (54).

Parsons's patent application makes no claims as to the potential emissions performance of an engine operated solely on the proposed fuels, but other sources suggest that significant hydrocarbons reductions should result from the combustion of such a gaseous reformed-fuel charge (14). Carbon monoxide emissions would still be largely a function of engine air to fuel ratio, whilst $NO_x$ levels should be significantly decreased, as a result of the reduced cycle temperatures which would characterize the combustion of an exhaust-reformed fuel having a relatively high nitrogen content (55, 56).

The initial findings of the current study being conducted here at Birmingham were published by the author in 1990, and a copy of the paper can be found in Appendix I (57).

### 2.4.2 Exhaust-Gas Reforming of Methanol

The only work relating to the exhaust-gas reforming of methanol which has been traced is a paper published in 1981 by Sjöström et al (58). An experimental programme of work is reported, where methanol is catalytically steam reformed to produce hydrogen and carbon monoxide; the steam necessary for the reactions is supplied directly by recirculated exhaust gases.

Experimental results using a reactor filled with a 1 litre charge of nickel catalyst (Girdler 56) indicated that near equilibrium compositions can be produced at reactor outlet temperatures of around 650°C, with a quoted conversion efficiency of 98% giving $H_2$ and CO yields of around 36 and 17% respectively. Engine operation at lean equivalence ratios meant that oxygen

contained in the recirculated reforming exhaust gases initiated exothermic partial oxidation reactions in the reformer, which was a useful source of heat input for the endothermic reforming reactions. Surplus exhaust gases not actually used in the reforming reactions were used to preheat and vaporize the reactants, and also to heat the reactor.

The published results of engine trials are limited, but plots showing brake thermal efficiency improvements of the order of 8% are given. It is confirmed that hydrogen enrichment of the normal fuel-air charge enables ultra-lean operation, which in turn leads to very low emissions of CO and $NO_x$; HC emissions are also said to be relatively low, as a result of the lean running conditions, and a high degree of after-burning in the well-insulated exhaust system.

## 2.5 Concluding Remarks on the Literature Survey

### 2.5.1 General Observations

This chapter has indicated the considerable level of interest in the general field of onboard fuel reforming shown over the past two decades or so. Steam reforming is obviously of interest from the point of view of improving fuel heating value, which results from the endothermic nature of process. It is usually proposed that this energy requirement might be met by the reclamation of otherwise wasted energy. Conversely, partial oxidation is attractive as a means of producing hydrogen-rich gaseous fuels without the need for any external supply of energy, as the reaction is itself exothermic. Unfortunately, the process consequently has a thermal efficiency of around 80%, implying a reduction in fuel heating value of around 20% across the reformer.

The endothermic dissociation of methanol has been a subject of great interest recently, but its commercial uptake will largely be governed by the fuel policies of the potential user-nations, which currently favour the use of gasolines.

### 2.5.2 Focus of Current Project

The exhaust-gas reforming of hydrocarbon/alcohol fuels represents a means of steam reforming where the required quantities of steam and thermal energy are supplied directly by hot engine exhaust gases. Potential benefits include improvements in overall engine thermal efficiency, and reductions in pollutant emissions, and as there is only a limited amount of knowledge in the field, it is this technique which will be investigated in the current project.

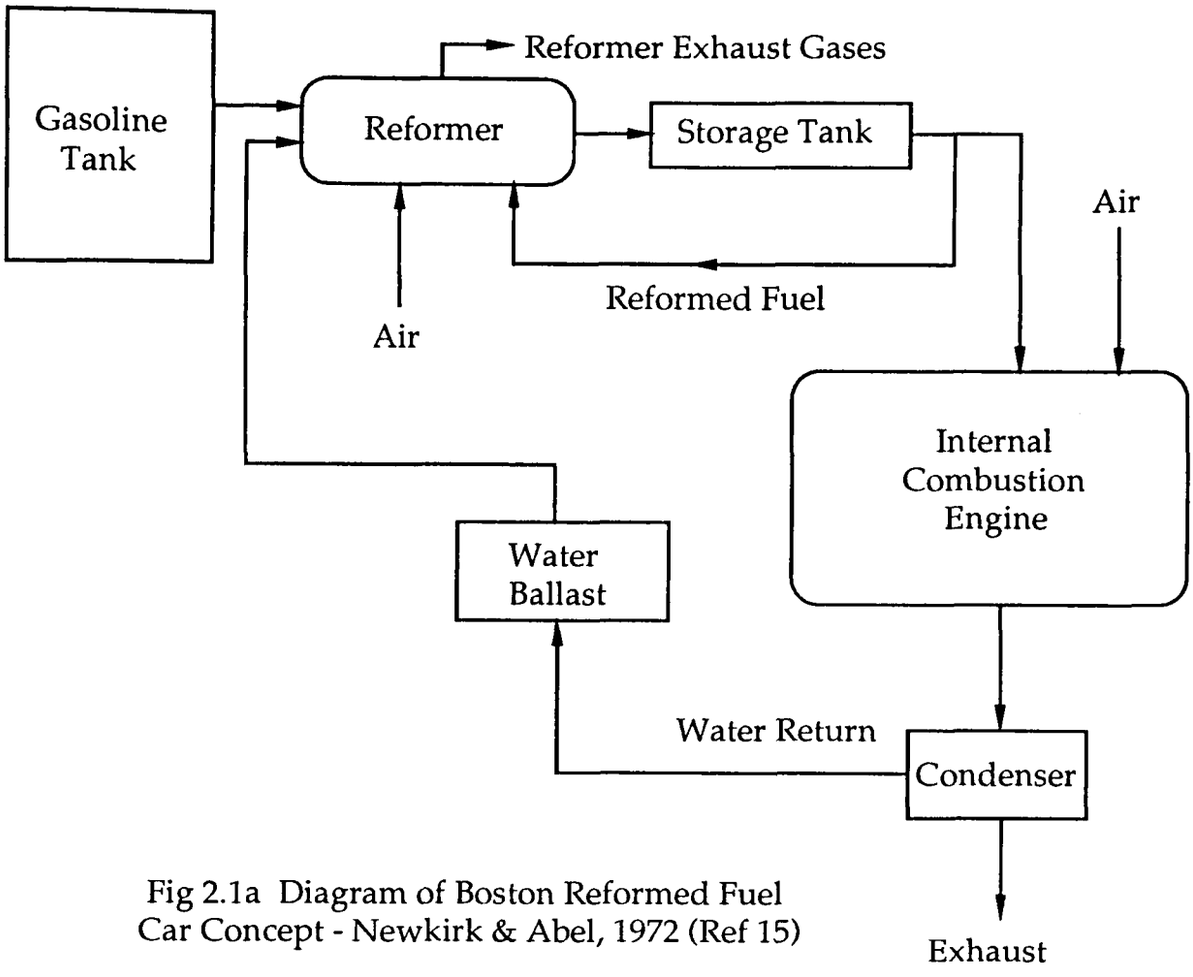


Fig 2.1a Diagram of Boston Reformed Fuel Car Concept - Newkirk & Abel, 1972 (Ref 15)

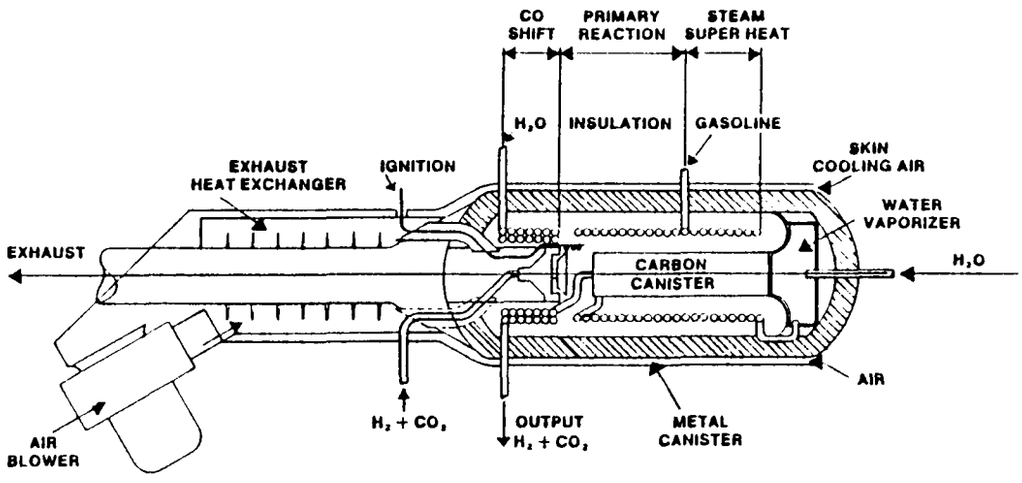


Fig 2.1b Diagram of Thermal Reactor

Boston Reformed Fuel Car - Newkirk & Abel 1972 (Ref 15)

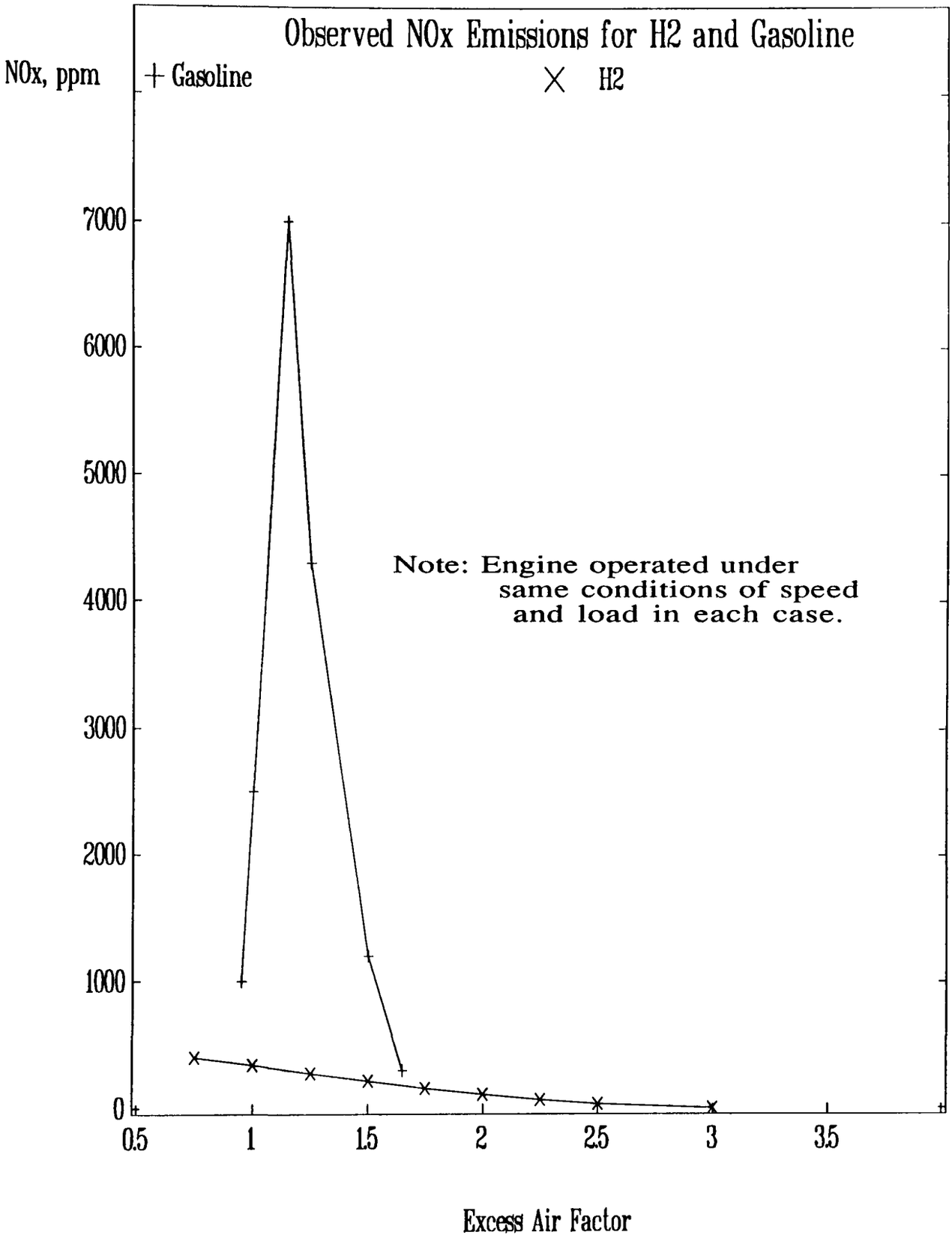


Fig 2.2 Plot of $NO_x$ Against Excess Air Factor

for Hydrogen and Gasoline-Fuelled Engines

(Results from Ref 16, cited by Ref 15)

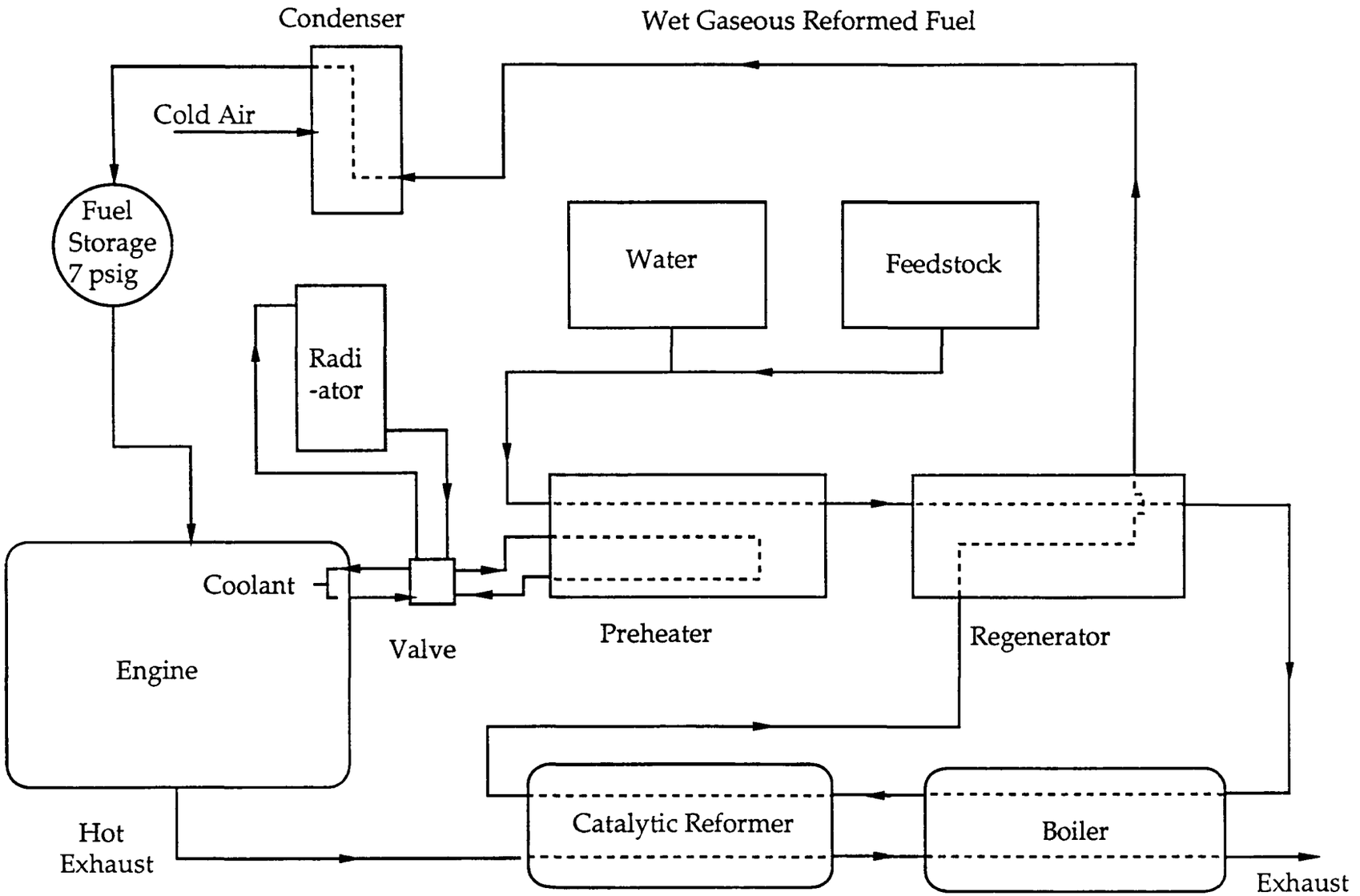


Fig 2.3 System Diagram for Onboard Fuel Reforming - M D Martin, 1978 (Ref 17)

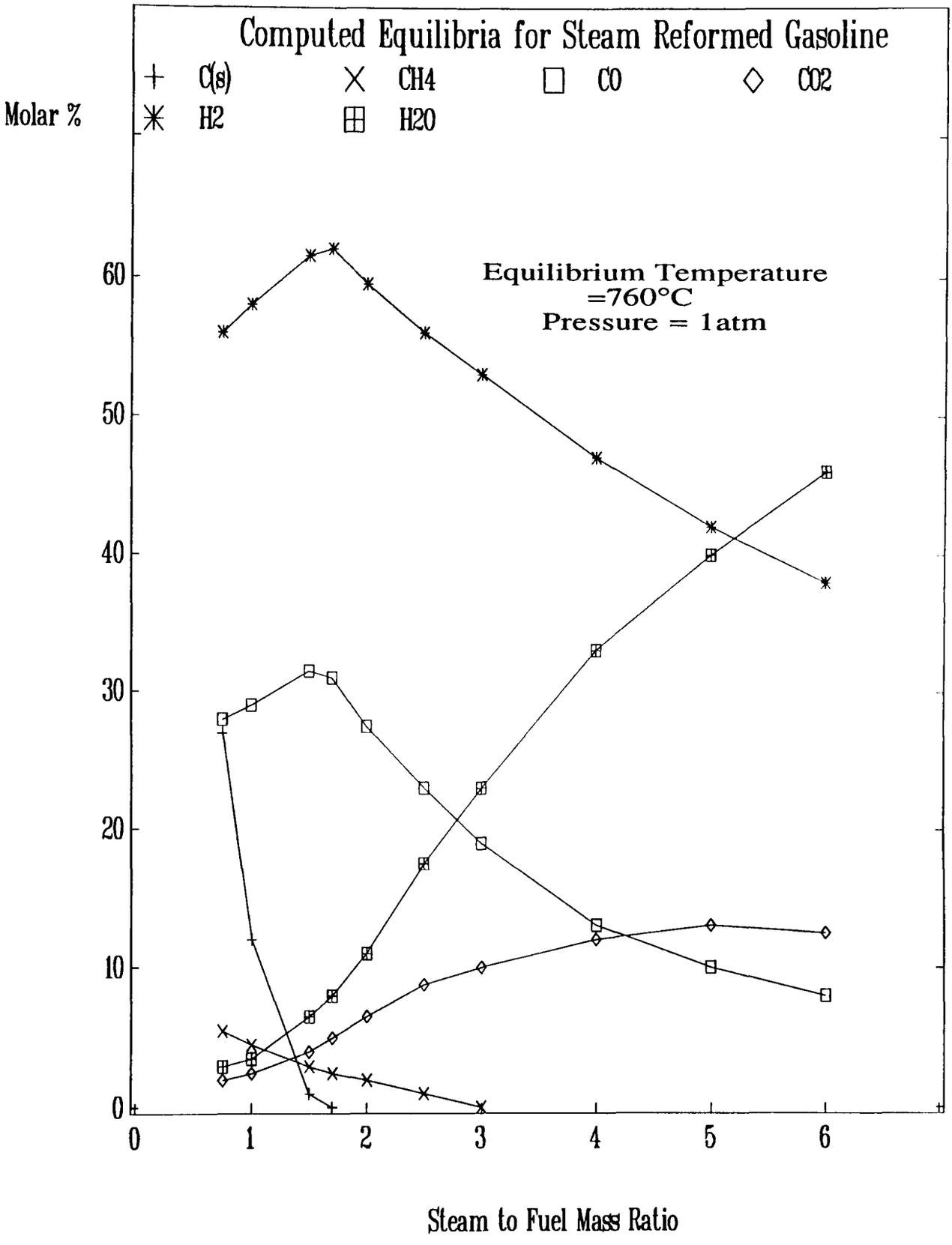


Fig 2.4 Plot of Computed Equilibria for Steam Reforming of JP-5 ($CH_{1.92}$) at 760°C (Results from Ref 22)

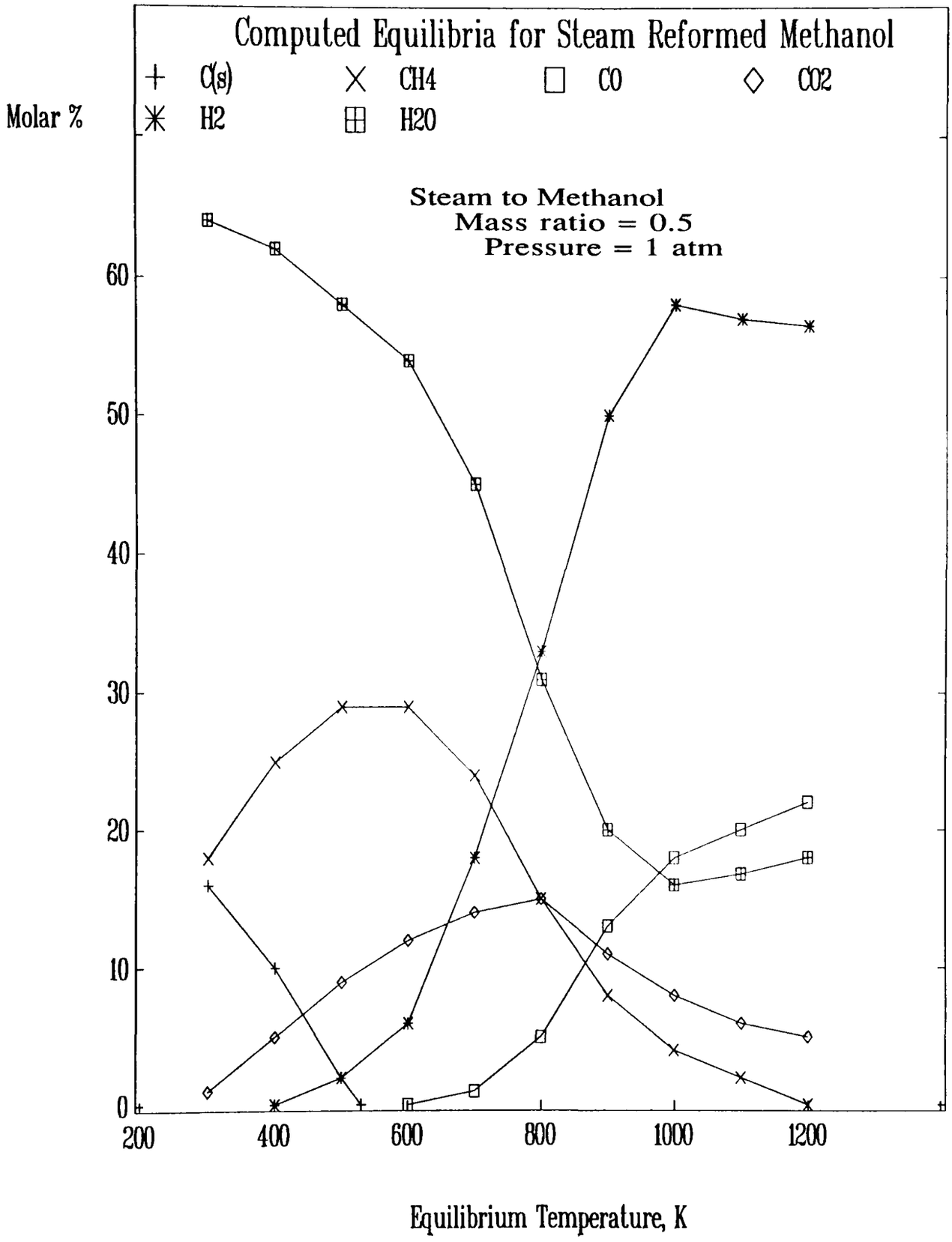


Fig 2.5 Plot of Computed Equilibria vs Equilibrium Temperature for Steam Reforming of Methanol (Results from Ref 22)

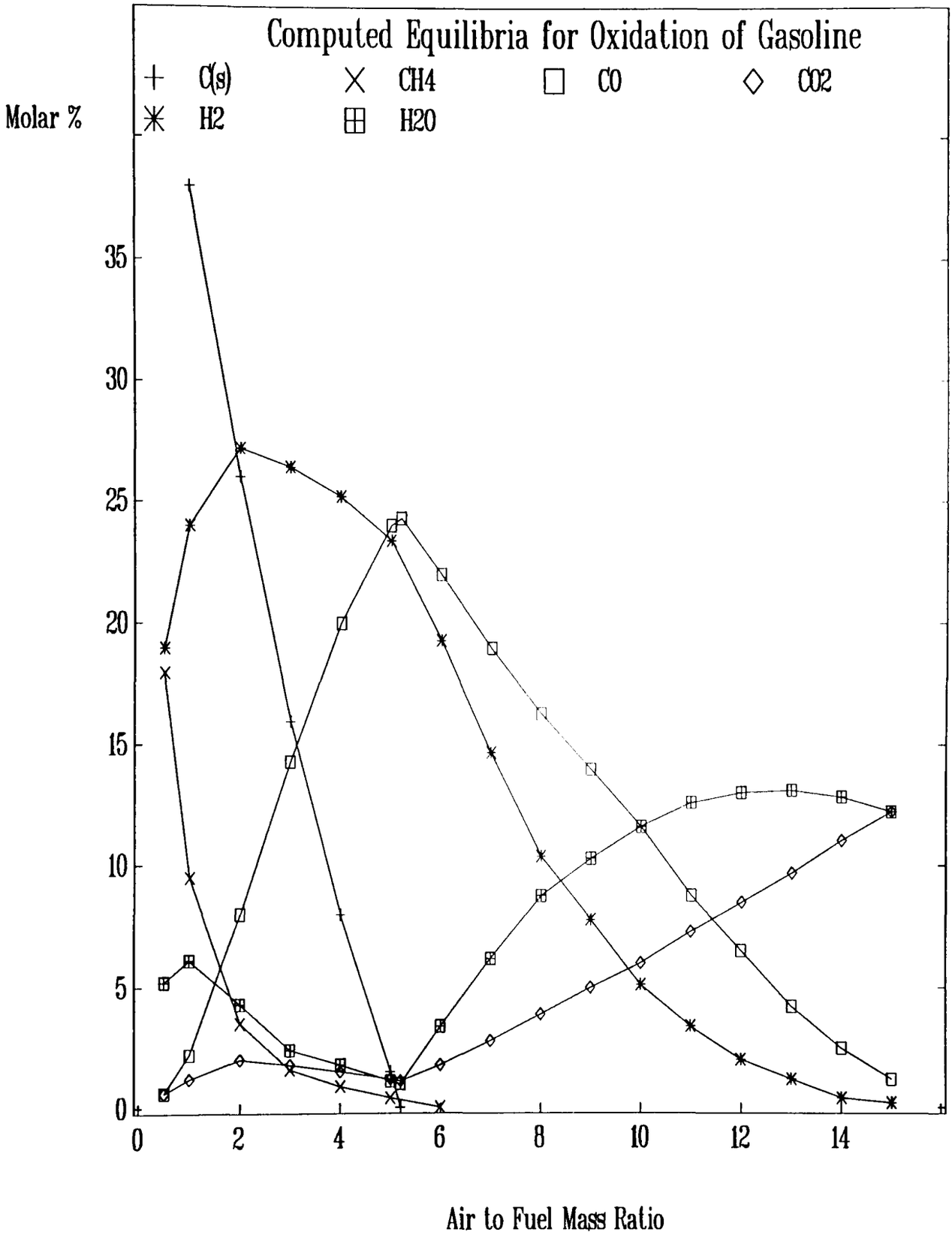


Fig 2.6 Plot of Computed Equilibria vs Air to Fuel Ratio for Oxidation of JP-5 (Results from Ref 13)

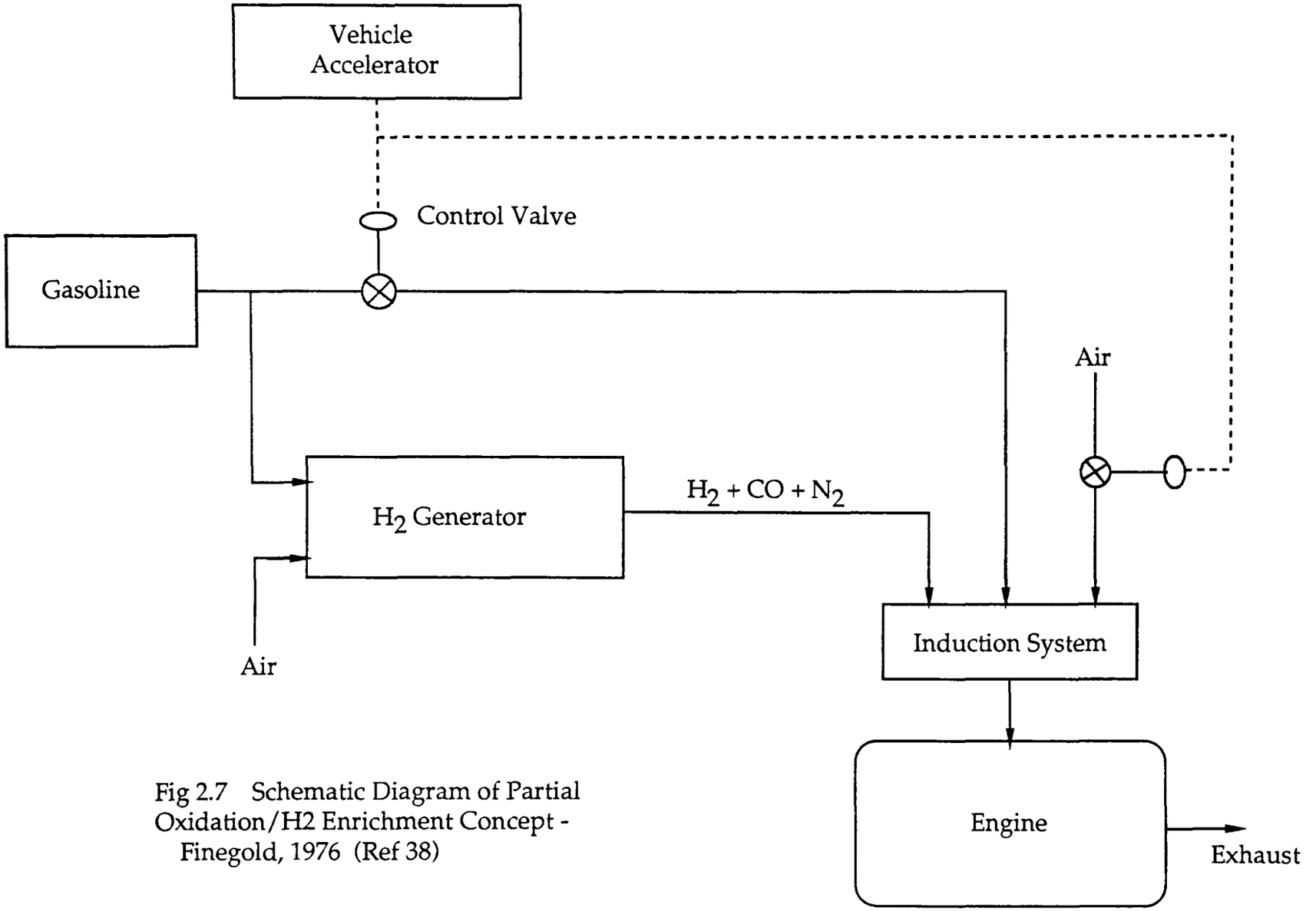


Fig 2.7 Schematic Diagram of Partial Oxidation/H2 Enrichment Concept - Finegold, 1976 (Ref 38)

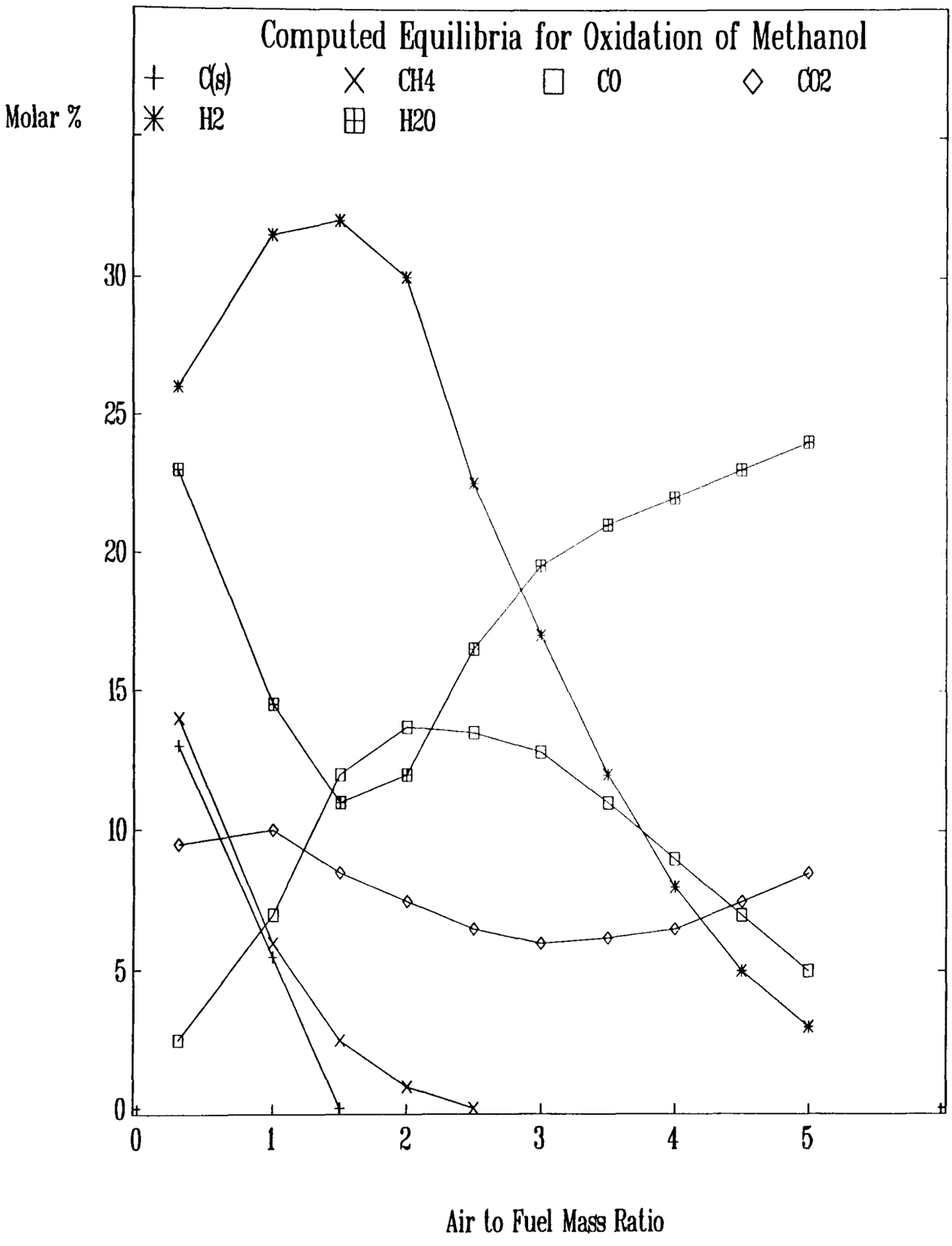


Fig 2.8 Plot of Computed Equilibria vs Air to Fuel Ratio for Oxidation of Methanol (Results from Ref 22)

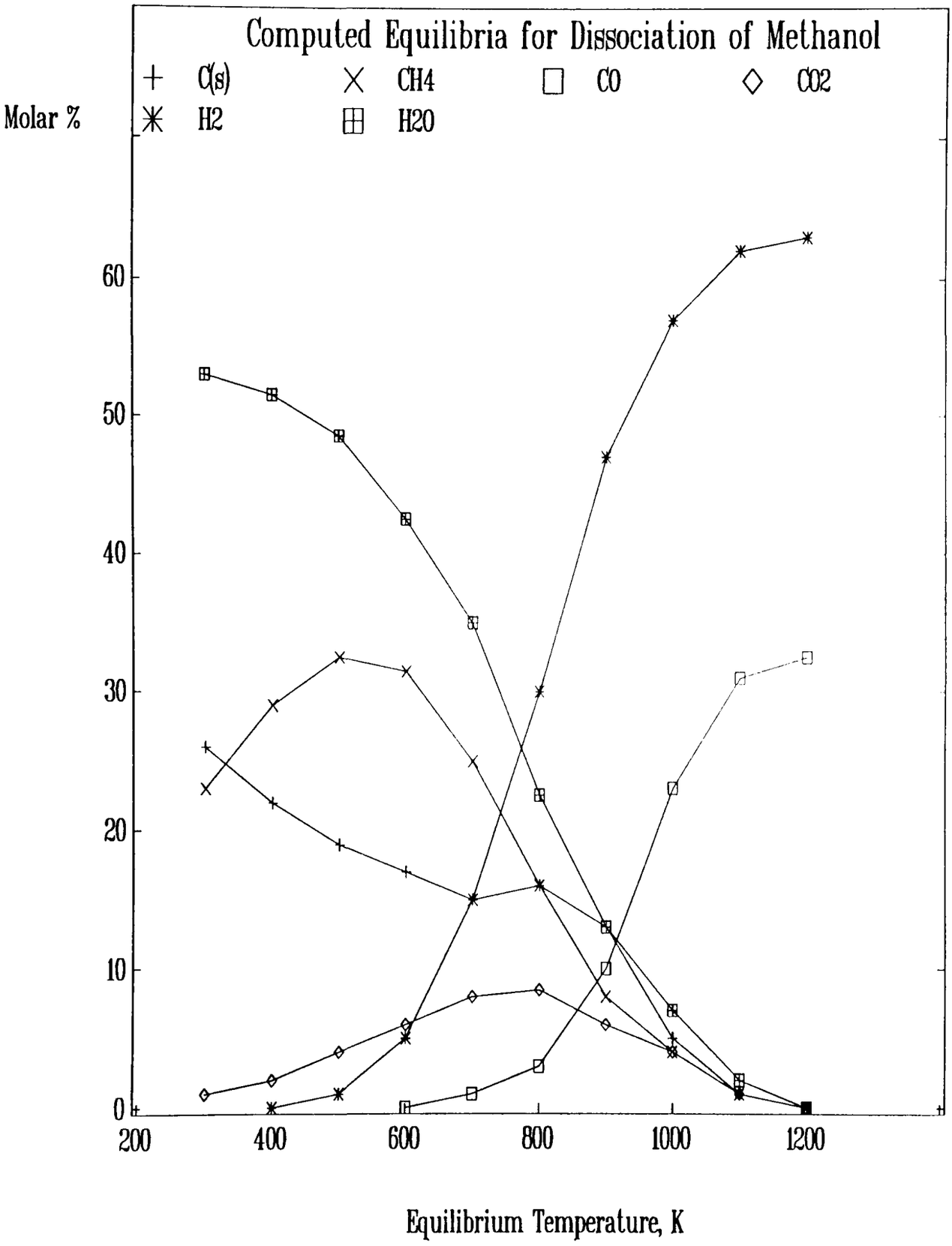


Fig 2.9 Plot of Computed Equilibria vs Equilibrium Temperature for Thermal Dissociation of Methanol (Results from Ref 22)

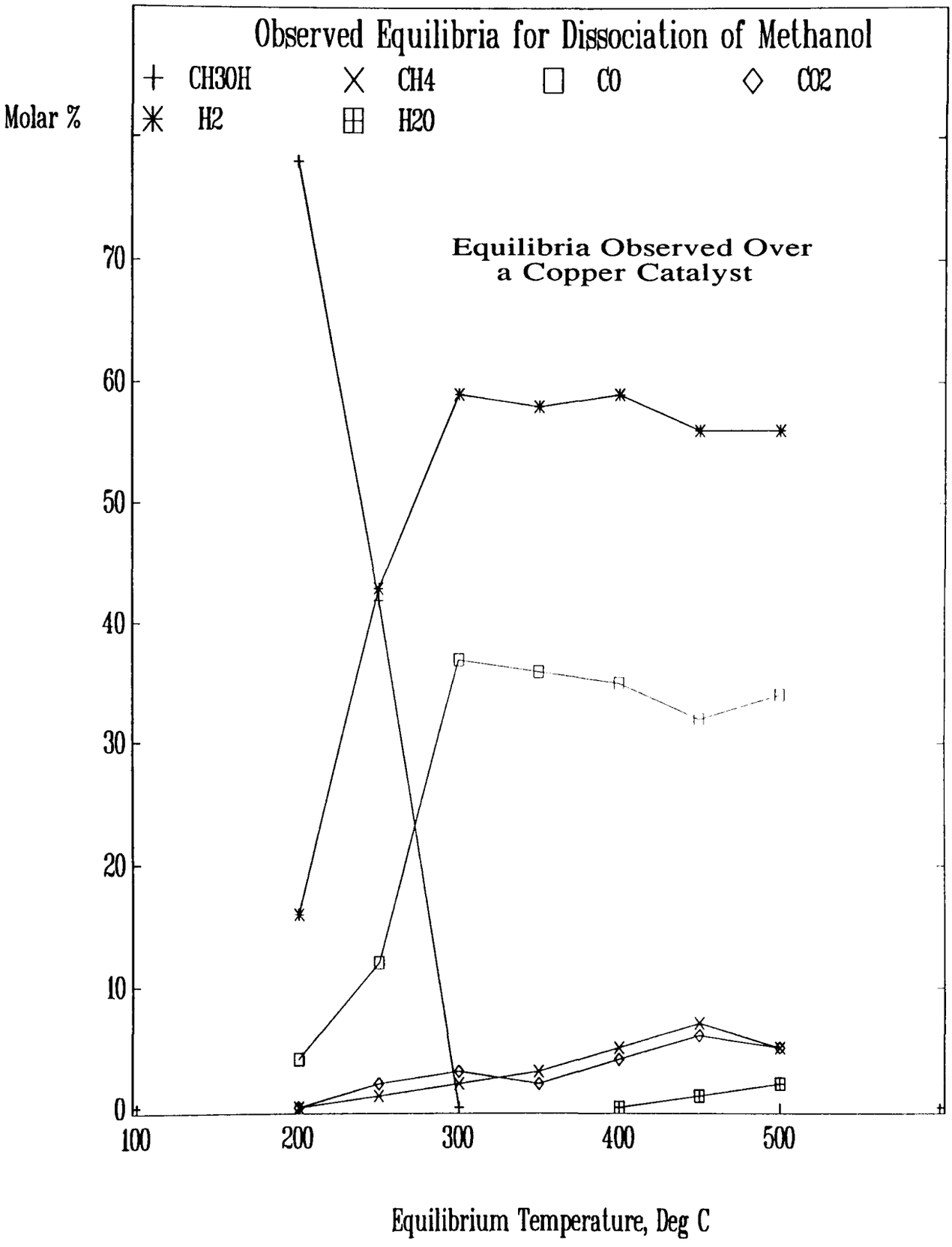


Fig 2.10 Plot of Observed Composition vs Equilibrium Temperature for Dissociated Methanol (Results form Ref 47)

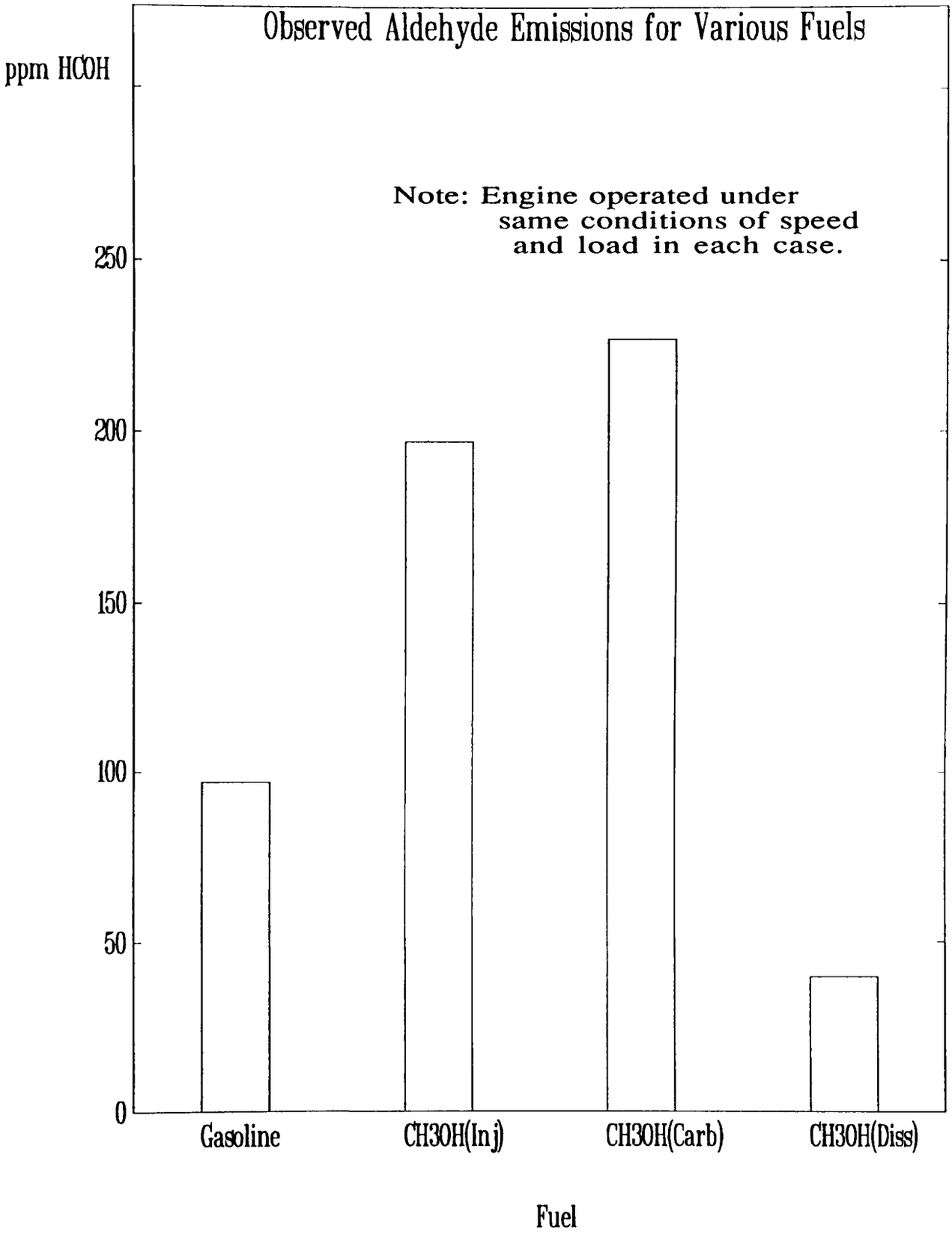


Fig 2.11 Plot of Aldehyde Emissions from an Engine Operated on Gasoline and Fuel-Injected, Carburetted, and Dissociated Methanol (Results from Ref 47)

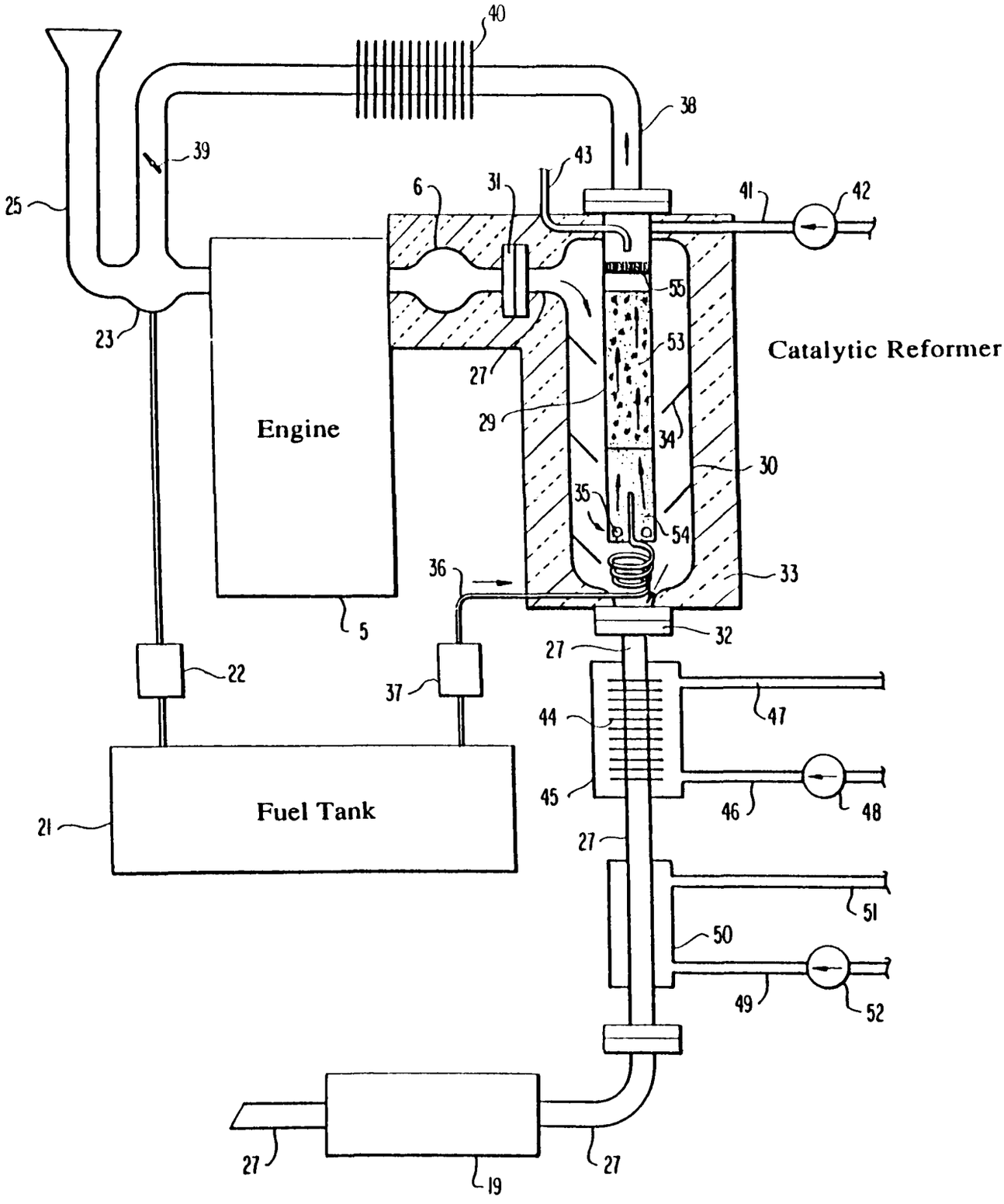


Fig 2.12 Diagram of Exhaust-Gas Reforming System - Lindström 1975

(Ref 50)

# 3 THE CHEMISTRY AND THERMODYNAMICS OF EXHAUST-GAS REFORMING

As mentioned in earlier sections of the thesis, the project work reported here is concerned mainly with the feasibility of reforming liquid hydrocarbon and alcohol feedstocks by means of direct contact with a portion of the hot exhaust gases leaving the engine. It is proposed that the mixture of feedstock and exhaust gases would undergo endothermic reactions similar to those proven in the industrial steam reforming process, leading to the production of a gaseous fuel containing hydrogen and carbon monoxide combustibles, along with quantities of nitrogen, carbon dioxide, and unreacted water. Fig 3.1 illustrates the proposed concept as an integrated part of the automotive power unit system.

Theoretical prediction of reformed fuel compositions is a complex task, as the effects of such variables as temperature, pressure and reforming oxidant (exhaust gas) to feedstock mass ratio are all of interest. In view of this, it was decided at the outset that a good chemical equilibria software routine, enhanced with application-specific energy balance sub-routines, would be required. Foundations for such a program had been laid by Machmouchi (59) and more significantly West (60), and a full discussion of the software package developed is given in the next chapter. At this stage, however, it is appropriate to discuss in some detail the ideal reforming processes under investigation.

## 3.1 Exhaust-Gas Reforming of Hydrocarbons

The study of hydrocarbon reforming was concerned mainly with the use of gasoline as a feedstock, as this fuel is freely available at present, and

will continue to be a major automotive fuel in the foreseeable future. Bearing in mind the large number of hydrocarbon compounds actually found in the blend of gasoline, a single 'average' hydrogen to carbon ratio is generally used to describe the fuel. Some researchers have assumed gasoline to be best approximated by $C_7H_{17}$ or $C_7H_{16}$, which have hydrogen to carbon ratios of 2.42 and 2.29 respectively, whilst others have used reference test fuels such as Indolene ($(CH_{1.86})_x$) and JP-5 ($(CH_{1.92})_x$) which clearly have respective ratios of 1.86 and 1.92. In view of the availability of the requisite thermodynamic data, it was decided that n-heptane, $C_7H_{16}$, should be chosen to represent gasoline in the current work. It has physical properties similar to those generally described for pump-grade petroleum motor fuels (61, 62), and as a discrete hydrocarbon is fully represented in tables of data.

### 3.1.1 Idealized Reforming Equations for n-Heptane

The ideal reforming equations representing the combustion, reforming and reformed-fuel combustion for an n-heptane feedstock are given below. Heats of reaction, $Q_{RP,298}$, are given for each equation, and are based on differences in standardized enthalpies of total reactants and total products. Note that the standardized enthalpy of a substance is equal to its enthalpy of formation as evaluated at standard conditions of 1atm and 298K, plus the 'sensible heat' which exists when the substance is at non-standard temperature conditions. By convention, the enthalpy of formation of elements such as C(s), $H_2$, $O_2$ etc. is set to zero. In the equations shown below, properties are all evaluated at standard conditions in order to enable direct comparison of the various reactions, and hence the standardized enthalpy of each species is equal to its enthalpy of formation (63, 64).

Note also that in each of the idealized equations given below for n-heptane, $H_2O$ is assumed to exist in the vapour phase; thermodynamic properties are taken from JANAF tables (65), and data given by Stull et al (66).

Sample calculation for n-heptane:

i) Normal stoichiometric combustion of 1 mole of $C_7H_{16}$

$$C_7H_{16} + 11(O_2 + 3.76N_2) \rightarrow 7CO_2 + 8H_2O + 41.36N_2 \qquad (3.1)$$

$H_{R,298} = -53630 + 1\cdot1(0 + 0) = -53630$ kcal

$H_{P,298} = 7(-94054) + 8(-57795) + 0 = -1120738$ kcal

Hence $Q_{RP,298} = H_{R,298} - H_{P,298} = 1067108$ kcal $= 4467.98$ MJ

$\rightarrow Q_{RP,298(i)} = 44.59$ MJ/kg $C_7H_{16}$

ii) Reforming of 1 mole of n-heptane using exhaust gases from (i)

$$C_7H_{16} + 0.47(7CO_2 + 8H_2O + 41.36N_2) \rightarrow 10.29CO + 11.76H_2 + 19.44N_2 \qquad (3.2)$$

$H_{R,298} = -53630 + 0.47(7(-94054) + 8(-57795) + 0) = -580377$ kcal

$H_{P,298} = 10.29(-26416) + 0 + 0 = -271821$ kcal

Hence $Q_{RP,298} = H_{R,298} - H_{P,298} = -308556$ kcal $= -1219.25$ MJ

$\rightarrow Q_{RP,298(ii)} = -12.89$ MJ/kg $C_7H_{16}$

iii) Stoichiometric combustion of reformed fuel produced in (ii)

$$10.29CO + 11.76H_2 + 19.44N_2 + 11.03(O_2 + 3.76N_2) \rightarrow 10.29CO_2 + 11.76H_2O + 60.91N_2 \qquad (3.3)$$

$H_{R,298}$ = -271821 kcal

$H_{P,298}$ = 10.29(-94054) + 11.76(-57795) + 0 = -1647485 kcal

Hence $Q_{RP,298} = H_{R,298} - H_{P,298}$ = 1375664 kcal = 5759.90 MJ

$\rightarrow Q_{RP,298(iii)}$ = 57.48 MJ/kg $C_7H_{16}$

And, as expected, it is apparent that:

$$Q_{RP,298(i)} - Q_{RP,298(ii)} = Q_{RP,298(iii)}$$

As

44.59 - (-12.89) = 57.48 MJ/kg $C_7H_{16}$

These idealized equations indicate the potentially significant improvements in fuel heating value which can result from the reforming process if the energy requirement of 12.89 MJ/kg of feedstock is made available. In theory, product gases give a heat release of around 57.48 MJ/kg of feed fuel, as compared with the original fuel value of 44.59 MJ/kg. In addition, it will be noted that the exhaust-gas composition shown in eqn 3.3 is essentially the same as that in eqn 3.1, and it is therefore proposed that a looped cycle involving only those reactions shown in 3.2 and 3.3 could be established.

Using the definition for reformer thermal efficiency given in eqn 2.7 gives :

$$\eta_{RTH} = 57.48/44.59 * 100\% = 128.9\%$$

which represents an improvement in fuel heating value of 28.9%. The initial objective of the current project is to ascertain how closely this goal can be approached, bearing in mind that the endothermic reaction is to be sustained by the recovery of heat energy which would otherwise be wastefully rejected by the engine.

### 3.2 Exhaust-Gas Reforming of Alcohols.

As mentioned in the literature review, considerable interest has been shown in the use of alcohols as automotive fuels, both in a conventional and non-conventional sense. In the case of methanol, much effort has been directed at reforming the fuel by means of thermal dissociation prior to aspiration into the engine, whilst there has also been a limited amount of interest in the exhaust-gas reforming of the alcohol feedstock (58).

The higher alcohol, ethanol, has tended to be used in a more conventional manner as an alternative automotive fuel, particularly in regions where sugar and starch crops which can be fermented to produce the fuel are plentiful. Usable feedstocks leading to the production of the fuel are, however, rather limited, and this probably explains why no interest appears to have been shown in the onboard reforming of ethanol.

As methanol can be produced from a wide variety of sources such as wood, natural gas, coal, bio-mass etc, it was decided that an investigation into the exhaust-gas reforming of methanol should be undertaken.

### 3.2.1 Idealized Reforming Equations for Methanol.

As pure methanol is a relatively straightforward chemical, $CH_3OH$, there is no ambiguity regarding the fuel composition, as is the case with gasoline.

The overall equations describing methanol combustion, reforming and the combustion of reformed fuel are given below, and, as in the case of n-heptane, heats of reaction based on standardized properties are shown. It has been assumed that all carbon in the feedstock will appear as carbon dioxide in the reformed fuel, as opposed to appearing as carbon monoxide which was assumed in the case of n-heptane. The reason for this is that the presence of oxygen in the methanol fuel makes it impossible to write a simple reforming equation with only hydrogen, carbon monoxide and nitrogen in the products - in the case of steam or exhaust-gas reforming, there is too much oxygen in the system to permit such simple idealized chemistry.

Note again that in each reaction shown below, $H_2O$ is assumed to exist in the vapour phase, with thermodynamic properties taken from JANAF tables (65) and data given by Stull et al (66).

Sample calculation for methanol: (see over)

i) Normal stoichiometric combustion of 1 mole of methanol

$$CH_3OH + 1.5(O_2 + 3.76N_2) \rightarrow CO_2 + 2H_2O + 5.64N_2 \qquad (3.4)$$

$H_{R,298} = -57020 + 0 = -57020$ kcal

$H_{P,298} = -94054 + 2(-57795) = -209644$ kcal

Hence $Q_{RP,298} = H_{R,298} - H_{P,298} = 152624$ kcal $= 639.04$ MJ

$\rightarrow Q_{RP,298(i)} = 19.97$ MJ/kg $CH_3OH$

ii) Reforming of 1 mole of methanol using part of exhaust from (i)

$$CH_3OH + 0.5(CO_2 + 2H_2O + 5.64N_2) \rightarrow 1.5CO_2 + 3H_2 + 2.82N_2 \qquad (3.5)$$

$H_{R,298} = -57020 + 0.5(-94054 + 2(-57795) + 0) = -161842$ kcal

$H_{P,298} = 1.5(-94054) + 0 + 0 = -141081$ kcal

Hence $Q_{RP,298} = -20761$ kcal $= -86.93$ MJ

$\rightarrow Q_{RP,298(ii)} = -2.72$ MJ/kg $CH_3OH$

iii) Stoich. combustion of reformed fuel produced in (ii) above

$$1.5CO_2 + 3H_2 + 2.82N_2 + 1.5(O_2 + 3.76N_2) \rightarrow 1.5CO_2 + 3H_2O + 8.46N_2 \qquad (3.6)$$

$H_{R,298} = 1.5(-94054) = -141081$ kcal

$H_{P,298} = 1.5(-94054) + 3(-57795) = -314466$ kcal

Hence $Q_{RP,298}$ = 173385 kcal = 725.96 MJ

$\rightarrow Q_{RP,298(iii)}$ = 22.69 MJ/kg $CH_3OH$

And again:

$$Q_{RP,298(i)} - Q_{RP,298(ii)} = Q_{RP,298(iii)}$$

As

19.97 - (-2.72) = 22.69 MJ/kg $CH_3OH$

Also thermal efficiency is given by:

$$\eta_{RTH} = (22.69/19.97) * 100\% = 113.6\%$$

which indicates a 13.6% improvement in LCV resulting from exhaust reforming the fuel.

### 3.3 Discussion of Idealized Reactions vs True Equilibria

The reaction equations given above for n-heptane and methanol fuels represent the simplest approach to the chemistry of reforming and combustion. In practice it is known, for example, that dissociation plays an important role in the high temperature oxidation of hydrocarbon and alcohol fuels, where conditions drive endothermic reactions which tend to form combustible product species such as hydrogen and carbon monoxide (67, 68).

In addition to these high temperature mechanisms, a large number of 'side-reactions' can occur within the reacting systems, leading to the formation of many compounds not considered in the simple equations given above.

Neglecting kinetic considerations, the product compositions of the proposed reformed fuels will be those resulting when equilibrium conditions for reactions such as those shown below are established:

$$3H_2 + CO \leftrightarrow CH_4 + H_2O \quad (3.7)$$

$$4H_2 + CO_2 \leftrightarrow CH_4 + 2H_2O \quad (3.8)$$

$$2CO \leftrightarrow CO_2 + C \quad (3.9)$$

$$CH_4 \leftrightarrow 2H_2 + C \quad (3.10)$$

$$CO + H_2O \leftrightarrow CO_2 + H_2 \quad (3.11)$$

In addition, of course, are the general steam reforming and oxidation reactions mentioned earlier.

Sjöström states in relatively simple terms that the overall steam reforming of hydrocarbons can be regarded as a primary reduction of the fuel to hydrogen and carbon monoxide, followed by establishment of equilibrium for eqn's 3.7 and 3.11 above (51). This is a pleasantly straightforward approach, but it neglects, for example, the possibility of C(s) formation which has generally been found to be a problem by other workers. It will be appreciated that many fractional reactions including those outlined above can occur simultaneously, and prediction of the outcome, which is dependent amongst other things on temperature, pressure and initial conditions, is thus a complex problem.

## 3.4 Approach to the Equilibria Prediction Problem

Simple chemical systems can often be dealt with adequately using tabulated or curve-fitted equilibrium constant data, which describe the extent to which reactions are proceeding in either a forward or reverse direction as a function of temperature. The use of such data usually leads to a set of simultaneous equations which can be solved using matrix methods to predict the chemical equilibria under the specified conditions (69, 70).

More complex systems, however, render this technique very laborious, and even the use of sophisticated computer techniques does not overcome all of the associated problems. Large amounts of equilibrium constant data need to be accessed, and some degree of guess-work must be used in order to predict which of the reactions mentioned earlier will be important.

In view of this, an alternative technique involving the minimization of Gibbs free energy of the system is adopted. Although the derivation of the requisite mathematical expressions is involved, the result is a set of general equations which enable a very accurate determination of equilibria for the most complex of systems. The means by which equilibrium compositions can be computed on the basis of minimization methods is a field of study which has generated a great deal of interest over the past two decades or so; this interest has notably developed in the light of increasingly powerful computing facilities. The following chapter gives an insight into the subject, and focuses specifically on the technique used for the purpose of computing equilibrium reformed fuel compositions in the current project.

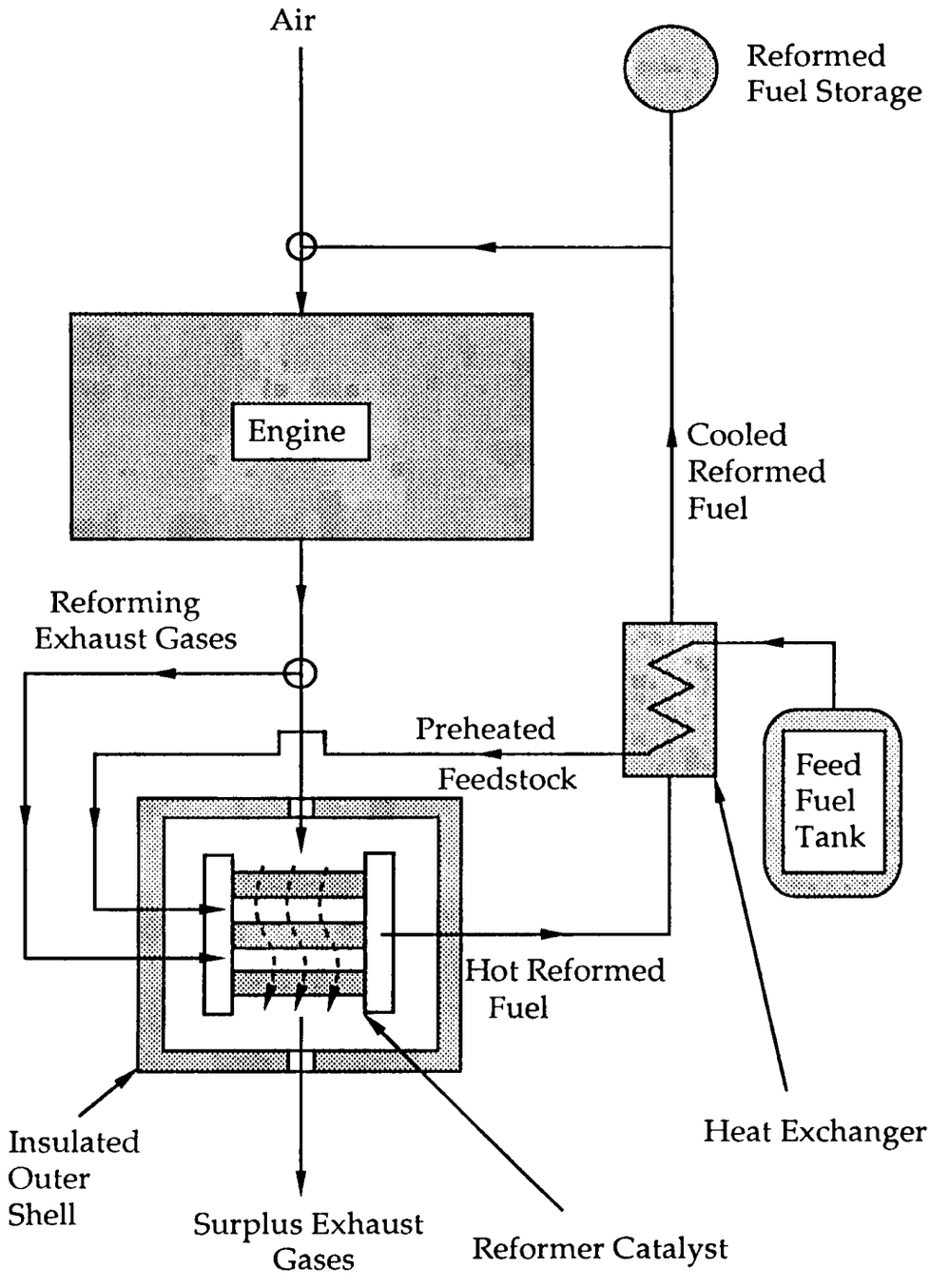


Fig 3.1 Diagram of Proposed Exhaust-Gas Reforming System

# 4 THE COMPUTATION OF COMPLEX CHEMICAL EQUILIBRIA

The condition for chemical equilibrium in a reacting system is generally described by one of the following techniques: the solution of a set of equations incorporating equilibrium constant data, or the optimization of a function or property such as Gibbs free energy or entropy (71).

Van Zeggeren and Storey discuss a wide variety of methods for solving the chemical equilibrium problem, but acknowledge the fact that much of the published work simply represents modified versions of earlier research (72). It is stated that the two major methods of solution involve either a search for the extremum of a thermodynamic function, or the numerical solution of a set of non-linear simultaneous equations (73). Some solution methods combine certain aspects of the two general techniques, and it is one such approach, the minimization of Gibbs free energy via the solution of a set of non-linear equations, that was used to determine theoretical equilibrium compositions in this project. The reason for this choice was that the approach was researched extensively by NASA in the 1950's and 60's (74), and led to the development of a computer program for calculating complex chemical equilibrium compositions; a copy of the code had been obtained by the university, and was available for use in the current project (75, 76).

Unfortunately, it was found that the NASA routine, which was written in FORTRAN, would not run satisfactorily on the university mainframe computer; despite several attempts at debugging the routine, no reliable results could be generated. On examination, it was found that the software was far more complex than was needed for the purposes of the current work, and it was therefore decided that a simpler, PC-based routine should be written. This led to the EQCOMP.PAS program, which omitted many of the

complexities found in the NASA code, and provided a much more streamlined approach to the current problem (60). The minimization technique adopted in the EQCOMP routine is the Gibbs free energy method developed at NASA, and is described below.

## 4.1 The Optimization of a Thermodynamic Function

### 4.1.1 The Minimization of Gibbs Free Energy

Gibbs free energy, G, can in general terms be considered a function of all independent variables of a system. Considering variables pressure, P, temperature, T, and number of moles of gaseous species j, $n_j$, it can be seen that an infinitesimal change in either or all of the variables will tend to effect a small change in G, in accordance with the basic principles of partial differentiation as applied to the problem of small increments (77).

To take a general example, if z is a function of two independent variables x and y, ie. z = f(x, y), increases in x and y by small amounts $\delta x$, $\delta y$, result in a small increase $\delta z$. It can easily be shown that $\delta z$ is given by:

$$\delta z = \left(\frac{\partial z}{\partial x}\right)_y \delta x + \left(\frac{\partial z}{\partial y}\right)_x \delta y \tag{4.1}$$

Where $\frac{\partial z}{\partial x}$ and $\frac{\partial z}{\partial y}$ are the partial derivatives of the original function.

Applying this to the case in question, where G = f(P, T, $n_j$), it follows that :

$$\delta G = \left(\frac{\partial G}{\partial T}\right)_{P,n_j} \delta T + \left(\frac{\partial G}{\partial P}\right)_{T,n_j} \delta P + \sum_{j=1}^{n} \left(\frac{\partial G}{\partial n_j}\right)_{T,P} \delta n_j \tag{4.2}$$

where index n is the total number of species in the system.

Convenient substitutions given by Zemansky (78) can then be used to replace two of the three partial derivatives, as follows:

$$\left(\frac{\partial G}{\partial T}\right)_{P,n_j} = -S \quad \text{and} \quad \left(\frac{\partial G}{\partial P}\right)_{T,n_j} = V$$

So that

$$\delta G = -S\,\delta T + V\,\delta P + \sum_{j=1}^{n} \left(\frac{\partial G}{\partial n_j}\right)_{T,P} \delta n_j \tag{4.3}$$

where S is system entropy, and V is volume.

Partial derivatives $\frac{\partial G}{\partial n_j}$ are properties of the system which indicate the change in Gibbs free energy which would result from the addition of small amounts of species j. As the derivative occurs frequently, it is usually denoted $\mu_j$, and is called the chemical potential, in this case of species j. Eqn 4.3 is thus generally written in the form:

$$\delta G = -S\,\delta T + V\,\delta P + \sum_{j=1}^{n} \mu_j \delta n_j \tag{4.4}$$

Now, in a system where pressure and temperature are constant, it follows that $\delta T$ and $\delta P$ will equal zero, and hence:

$$\delta G = \sum_{j=1}^{n} \mu_j \delta n_j \tag{4.5}$$

It can then be shown that: (see over)

$$G = \sum_{j=1}^{n} \mu_j n_j \qquad (4.6) \quad \text{(Ref 72)}$$

The importance of these results will be shown below, but first, having derived a concise expression for G, (eqn 4.6), the intrinsic relevance of Gibbs free energy to the equilibrium problem will be discussed.

Consider a hydrostatic system, in mechanical and thermal but not in chemical equilibrium, in contact with a reservoir at a temperature T and undergoing an infinitesimal irreversible heat exchange process with the reservoir. By definition, such a heat exchange process, $\delta Q$, will be accompanied by changes in entropy of the system and the reservoir, denoted $\delta S$ and $\delta S_o$ respectively, such that the entropy of the system/reservoir increases as follows (78):

$$\delta S_o + \delta S > 0 \qquad (4.7)$$

And, since $\delta S_o = -\frac{\delta Q}{T}$, it follows that:

$$\delta Q - T\delta S < 0 \qquad (4.8)$$

The first law of thermodynamics can be written in differential form as follows:

$$\delta Q = \delta U + P\delta V$$

and eqn 4.8 can therefore be written as

$$\delta U + P\delta V - T\delta S < 0 \qquad (4.9)$$

In the case where pressure and temperature are constant, $P\delta V = \delta(PV)$ and $T\delta S = \delta(TS)$ and hence:

$$\delta(U + PV - TS) < 0$$

$$\rightarrow \delta(H - TS) < 0 \qquad (4.10)$$

Now, Gibbs free energy, G, is specifically defined as follows:

$$G = (H - TS) \qquad (4.11)$$

And hence 4.10 becomes:

$$\delta G < 0 \qquad (4.12)$$

It is thus shown that the Gibbs free energy or Gibbs function of a system at constant temperature and pressure decreases during an irreversible process (78).

Moreover, consideration of Eqn 4.5 above indicates that G reaches an optimized value at chemical equilibrium for the system under investigation, by virtue of the fact that the condition of chemical equilibrium is defined by each value of $\delta n_j$ being equal to zero. This gives $\delta G_{T,P,n_j} = 0$, which in this case obviously represents a minimum point.

Having demonstrated the nature of the relationship between Gibbs free energy and chemical equilibria, a number of simple side conditions are introduced which are used with the equations given above in order to compute equilibrium compositions. Before outlining these side conditions,

however, it is worth mentioning briefly the corresponding methods employed for systems which are not at constant temperature and pressure.

### 4.1.2 The Maximization of System Entropy

Consider a system undergoing an irreversible process under conditions of constant internal energy and constant volume. In such a system, $\delta U$ and $\delta V$ are both equal to zero, and hence from Eqn 4.9, it can be shown that:

$$(\delta S)_{U,\,V} > 0 \qquad (4.13)$$

Thus the irreversible process is always attended by an increase in entropy. Using similar arguments to those given above, it can be shown that system entropy will reach its maximum value at equilibrium in a system under conditions of constant energy and volume (78).

### 4.1.3 The Minimization of Helmholtz Free Energy

Similarly, minimization techniques can be used to define chemical equilibrium under conditions of constant volume and temperature. In such cases, the Helmholtz function given below is relevant:

$$\text{Helmholtz function, } A = U - TS \qquad (4.14)$$

Again, using the same reasoning as above, it can be shown that:

$$\delta A + S\,\delta T + P\,\delta V < 0 \qquad (4.15)$$

And, for $\delta T = 0$ and $\delta V = 0$, it follows that: (see over)

$$\delta A < 0 \qquad (4.16)$$

Hence, as the irreversible process progresses under conditions of constant temperature and volume, the Helmholtz function decreases, and will reach a minimum at chemical equilibrium (78).

The system conditions under consideration therefore determine which of the above three minimization techniques are adopted. In the current project it was decided that the most suitable conditions to constrain would be pressure and temperature, and thus the minimization of Gibbs free energy was chosen as the optimization technique.

### 4.2 Note on Side Conditions

In order to compute those values of $n_j$ which give the minimum value of Gibbs free energy, G, for the system, it is apparent that certain additional constraints must be applied.

Firstly, the mole numbers, $n_j$, which represent the number of moles of each chemical species existing in the system, must obviously meet the following requirement:

$$n_j \geq 0 \qquad (4.17)$$

since negative mole numbers would clearly be physically inadmissible.

Secondly, there is a mass balance requirement across the process. Although the given species mole numbers will be variable, particularly in the case of a highly reactive mixture, the actual numbers of atoms of each discrete

element, and hence the total mass of the system, must remain constant. The mass conservation equation is written as:

$$\sum_{j=1}^{n} a_{ij} n_j = b_i \qquad (i = 1....l) \tag{4.18}$$

where stoichiometric coefficients $a_{ij}$ are the number of atoms of element i per kg-mole of species j, n is the total number of species present in the system, $n_j$ is the number of kg-moles of species j per kg of mixture, and $b_i^0$ and $b_i$ are the assigned number of kg-atoms of element i per kg of total reactants and per kg of mixture respectively. The equation given above must be applied for values of i from 1 to *l*, where *l* is the number of discrete elements in the system.

### 4.3 Concluding Remarks on Minimization Fundamentals

Having considered the relationship of Gibbs function to chemical equilibrium in conjunction with the above-mentioned mole number and mass balance constraints, it can be stated that the equilibrium problem for a system undergoing an irreversible process under conditions of constant temperature and pressure reduces to that of finding the set of $n_j$ values which minimize the function

$$G = \sum_{j=1}^{n} \mu_j n_j \quad (=(H - TS)) \tag{4.6}$$

subject to the side conditions

$$\sum_{j=1}^{n} a_{ij} n_j = b_i \qquad (i = 1....l) \tag{4.18}$$

and $n_j \geq 0$ (4.17)

Fig 4.1 gives a graphical illustration of how the principle of free energy minimization can be applied as a criterion for chemical equilibrium, and is based on data given in Ref 79. The simple system considered consists of a mixture of H and $H_2$ at constant temperature and pressure conditions of 3000K and 1 atm respectively. The value of Gibbs free energy is calculated for various compositions ranging from a system containing almost 100% diatomic hydrogen to one containing a high proportion of monatomic hydrogen. The graph demonstrates that the minimum free energy value of -62.06 kcal/g occurs at a partial pressure, $p_{H2}$, of 0.855 atm, with $p_H$ at 0.145 atm. This composition therefore represents that observed at equilibrium, and can easily be verified using the equilibrium constant method.

This graphical approach can actually be used in practice to define equilibria in very simple systems, but it can be appreciated that more complex systems soon render the technique inapplicable. In these situations, computational techniques provide a far-superior means of solving the minimization problem.

## 4.4 Development of Equations for the Minimization of Gibbs Free Energy in a Complex System - The NASA Method.

The approach used here to minimize free energy is based on the NASA method, and is discussed below (74, 75, 76). The technique involves the derivation of equations describing the condition of chemical equilibrium in terms of Gibbs free energy and constraining side conditions (eqn's 4.6, 4.17, 4.18). The method of Lagrangian multipliers is then applied, leading to a set of non-linear simultaneous equations which must be solved using iterative techniques. In this particular case, the non-linear equations are solved by means of a Newton-Raphson method, which itself involves a Taylor series

expansion of the equations, with all resulting terms truncated at levels higher than the first derivative. These intermediate equations, which contain various thermodynamic functions, are made dimensionless, and the number of expressions reduced by algebraic substitution and manipulation. This leads to a set of reduced Gibbs iteration equations which can be solved in matrix format using a Gaussian elimination technique. The resulting solution vector contains correction variables which are then multiplied by a control factor, $\lambda_c$, before being applied to the initial estimates of composition. An updated matrix is then formed and solved, to give a vector of new correction variables, and hence an improved estimate of the equilibrium composition. This iterative loop continues until the change in the value of the correction variables from one loop to the next satisfies certain criteria, indicating that convergence to a specified level of accuracy has been achieved.

A summary of the mathematical steps which lead to the all-important Gibbs iteration equations is given below.

### 4.4.1 Derivation of Gibbs Iteration Equations

In order to find the extremum of a function such as Gibbs free energy (Eqn 4.6) subject to a mass balance constraint (Eqn 4.18) it is convenient to define a Lagrangian function, $\zeta$, as follows (74):

$$\zeta = G + \sum_{i=1}^{l} \lambda_i ( b_i - b_i^0 ) \qquad (4.19)$$

where G, $b_i$ and $b_i^o$ are as defined in Eqn's 4.6 and 4.18, and $\lambda_i$ are Lagrangian multipliers (72, 78).

The condition for equilibrium becomes (74):

$$\delta\zeta = \sum_{j=1}^{n} (\mu_j + \sum_{i=1}^{l} \lambda_i a_{ij})\, \delta n_j + \sum_{i=1}^{l} (b_i - b_i^0)\delta\lambda_i = 0 \qquad (4.20)$$

and, since for mass conservation, $b_i = b_i^0$ for i=1 to $l$ it follows that if $\delta n_j$ is treated as independent of $\delta\lambda_i$, then:

$$\mu_j + \sum_{i=1}^{l} \lambda_i a_{ij} = 0 \qquad (j = 1, \ldots, n) \qquad (4.21)$$

At this stage in the derivation it is appropriate to introduce standard expressions for chemical potential, $\mu$, and the enthalpy and entropy of the mixture, h and s respectively. The expressions given below are standard text-book statements.

Firstly, chemical potential may be written as:

$$\mu_j = \begin{cases} \mu_j^0 + RT\ln(n_j/n) + RT\ln P_{atm} & (j = 1, \ldots, m) \\ \mu_j^0 & (j = m+1, \ldots, n) \end{cases} \qquad (4.22)$$

where $\mu_j^o$ is the chemical potential at the standard state, R is the specific gas constant, and the "n" appearing in the denominator of the log term is defined as follows:

$$n = \sum_{j=1}^{m} n_j \qquad (4.23)$$

The expression for j = 1 , ... , m (eqn 4.22) deals with gaseous species, whilst that for j > m relates to condensed species.

The general term for enthalpy is:

$$h = \sum_{j=1}^{n} n_j \left(H_T^0\right)_j \tag{4.24}$$

where $\left(H_T^0\right)_j$ is the standardized molar enthalpy of species j at temperature T.

Finally, entropy, s is given by:

$$s = \sum_{j=1}^{n} n_j S_j \tag{4.25}$$

where $S_j$ is defined as follows:

$$S_j = \begin{cases} \left(S_T^0\right)_j - R \ \ln(n_j/n) - R \ \ln P_{atm} & (j + 1, \ldots, m) \\ \left(S_T^0\right)_j & (j = m+1, \ldots, n) \end{cases} \tag{4.26}$$

and $\left(S_T^0\right)_j$ is the standardized molar entropy of species j at temperature T.

The manner in which thermodynamic functions such as entropy and enthalpy are actually computed is discussed further in sub-section 4.4.4

Having thus derived the general equations required to describe and constrain the equilibrium problem, (Eqn's 4.18, 4.21, 4.23), all that remains to be done to complete the set of expressions is to specify the thermodynamic state. If, for example, it is decided that the state be defined by temperature and pressure, variables T and P have to be set to the assigned values $T_o$ and $P_o$, which gives the following trivial equations:

$$T = T_o \tag{4.27}$$

$$P = P_o \tag{4.28}$$

Similar equations are written for enthalpy and entropy if these functions are chosen to define the thermodynamic state of the system. As mentioned above, a Taylor series expansion is then carried out on the appropriate equations, with truncation of terms higher than the first derivative. The resulting equations are then manipulated to give a reduced set of Gibbs iteration equations which are shown below:

$$\sum_{i=1}^{l}\sum_{j=1}^{m} a_{kj}a_{ij}n_j\pi_i + \sum_{j=m+1}^{n} a_{kj}\Delta n_j + \sum_{j=1}^{m} a_{kj}n_j\Delta\ln n + \left[\sum_{j=1}^{m}\frac{a_{kj}n_j(H_T^o)_j}{RT}\right]\Delta\ln T$$

$$= (b_k^o - b_k) + \sum_{j=1}^{m}\frac{a_{kj}n_j\mu_j}{RT} \qquad (k=1,\ldots,l\,) \tag{4.29}$$

$$\sum_{i=1}^{l} a_{ij}\pi_i + \left[\frac{(H_T^o)_j}{RT}\right]\Delta\ln T = \frac{\mu_j}{RT} \qquad (j=m+1,\ldots.,n) \tag{4.30}$$

$$\sum_{i=1}^{l}\sum_{j=1}^{m} a_{ij}n_j\pi_i + \left(\sum_{j=1}^{m} n_j - n\right)\Delta\ln n + \left[\sum_{j=1}^{m}\frac{n_j(H_T^o)_j}{RT}\right]\Delta\ln T$$

$$= n - \sum_{j=1}^{m} n_j + \sum_{j=1}^{m}\frac{n_j\mu_j}{RT} \tag{4.31}$$

$$\sum_{i=1}^{l}\left[\sum_{j=1}^{m}\frac{a_{ij}n_j(H_T^o)_j}{RT}\right]\pi_i + \sum_{j=m+1}^{n}\left[\frac{(H_T^o)_j}{RT}\right]\Delta n_j + \left[\sum_{j=1}^{m}\frac{n_j(H_T^o)_j}{RT}\right]\Delta\ln n$$

$$+\left[\sum_{j=1}^{n}\frac{n_j(C_p^o)_j}{R} + \sum_{j=1}^{m}\frac{n_j(H_T^o)_j^2}{R^2T^2}\right]\Delta\ln T = \frac{h_o - h}{RT} + \sum_{j=1}^{m}\frac{n_j(H_T^o)_j\mu_j}{R^2T^2} \tag{4.32}$$

$$\sum_{i=1}^{l}\left[\sum_{j=1}^{m}\frac{a_{ij}n_jS_j}{R}\right]\pi_i+\sum_{j=m+1}^{n}\left(\frac{S_j}{R}\right)\Delta n_j+\left[\sum_{j=1}^{m}\frac{n_jS_j}{R}\right]\Delta\ln\ n$$

$$+\left[\sum_{j=1}^{n}\frac{n_j(C_p^o)_j}{R}+\sum_{j=1}^{m}\frac{n_j(H_T^o)_jS_j}{R^2T}\right]\Delta\ln T=\frac{S_o-S}{R}+n-\sum_{j=1}^{m}n_j+\sum_{j=1}^{m}\frac{n_jS_j\mu_j}{R^2T} \qquad (4.33)$$

Indices m and n represent the number of gaseous species and the total number of gaseous plus condensed species respectively, and $l$ is the number of discrete elements in the system. i, j and k are counters, and $\pi_i$ (i = 1,...,$l$) are Lagrangian correction variables.

Certain terms which occur frequently in the above equations are given symbols as follows:

$$\left\{\begin{array}{ll} \mathcal{H}_j=\dfrac{(H_T^o)_j}{RT} & \mathcal{H}=\dfrac{h}{RT} \\ \mathcal{G}_j=\dfrac{\mu_j}{RT} & \mathcal{H}_o=\dfrac{h_o}{RT} \\ \mathcal{S}_j=\dfrac{S_j}{R} & \mathcal{S}=\dfrac{s}{R} \\ C_j=\dfrac{(C_p^o)_j}{R} & \mathcal{S}_o=\dfrac{S_o}{R} \end{array}\right\} \qquad (4.34)$$

It can be seen that equations 4.29 to 4.33 given above fit logically into a matrix format, as shown in Table 4.1. The matrix is solved using a modified Gaussian elimination technique, to give a solution vector of correction variables $\pi_i$ (i = 1,...,$l$), $\Delta n_j$ (j = m+1,...n), $\Delta\ln$ n, $\Delta\ln$ T, which enables the calculation of gaseous species correction variables $\Delta \ln n_j$ (j = 1,...m).

### 4.4.2 Iteration, Correction and Convergence

As is usually the case with iterative techniques, estimates of species mole numbers, $n_j$, are used to form the initial matrix. On this basis, an initial solution vector can be computed, which enables improvements to be made to the original compositional estimates and in turn permits the formation of a new matrix. It is pointed out in Ref 76 that applying the correction variables directly to the previous estimates can lead to divergence in the iterative process, as corrections can, on occasion, be rather large. In order to prevent such problems, a control factor, $\lambda_c$, is introduced to limit the size of the applied correction as follows:

$$\lambda_c = \min( 1, \lambda_1, \lambda_2 ) \tag{4.35}$$

where:

$$\lambda_1 = \frac{2}{\max \left( |\Delta \ln T|, |\Delta \ln n|, |\Delta \ln n_j| \right)} \qquad (j=1,\ldots,m) \tag{4.36}$$

and:

$$\lambda_2 = \min \left| \frac{-\ln (n_j/n) - 9.2103404}{\Delta \ln n_j - \Delta \ln n} \right| \qquad (j=1,\ldots,m) \tag{4.37}$$

$\lambda_1$ is calculated for gaseous species having mole fractions greater than $10^{-8}$, whilst $\lambda_2$ is used for those having mole fractions less than or equal to $10^{-8}$. As shown, the overall factor, $\lambda_c$, is defined as the minimum of 1, $\lambda_1$, and $\lambda_2$, and it can be seen that the value will be somewhat less than unity when estimates for composition are far from equilibrium values, and will be equal to 1 as convergence is approached.

The correction variables obtained in the matrix solution vector are multiplied by the value of $\lambda_c$ calculated for that particular iteration, and added to the previous estimates as follows:-

$$\left\{\begin{array}{ll} \ln n_j^{(i+1)} = \ln n_j^{(i)} + \lambda_c^{(i)} (\Delta \ln n_j)^{(i)} & (j=1,\ldots,m) \\ n_j^{(i+1)} = n_j^{(i)} + \lambda_c^{(i)} (\Delta n_j)^{(i)} & (j=m+1,\ldots,n) \\ \ln n^{(i+1)} = \ln n^{(i)} + \lambda_c^{(i)} (\Delta \ln n)^{(i)} & \\ \ln T^{(i+1)} = \ln T^{(i)} + \lambda_c^{(i)} (\Delta \ln T)^{(i)} & \end{array}\right\} \qquad (4.38)$$

where (i) is a counter which represents the number of times the iteration loop has been completed.

As mentioned, the revised values obtained from eqn set 4.38 are used to form an updated matrix, and the loop repeated until compositional corrections satisfy each of the following criteria:

$$\left\{\begin{array}{ll} \dfrac{n_j \left|\Delta \ln n_j\right|}{\sum_{j=1}^{m} n_j} \le 0.5*10^{-5} & (j=1, \ldots, m) \\ \dfrac{\left|\Delta n_j\right|}{\sum_{j=1}^{m} n_j} \le 0.5*10^{-5} & (j=m+1, \ldots, n) \\ \left|\Delta \ln n\right| \le 0.5*10^{-5} & \end{array}\right\} \qquad (4.39)$$

Having satisfied the convergence criteria, the program gives an output of compositional mole fractions, and thermodynamic properties such as enthalpy and entropy under the specified conditions.

### 4.4.3 Note on Constant Temperature/Pressure Problems

As mentioned earlier, it was decided that for the purpose of this project, temperature and pressure would be those conditions constrained as constants to define the thermodynamic state. This being the case, it can be seen that a number of the Gibbs iteration equations given above become simplified, by virtue of the fact that $\Delta \ln T = 0$. For example, terms multiplied by $\Delta \ln T$ in eqn's 4.29 to 4.33 disappear, which leads to the elimination of a complete column of the matrix shown in Table 4.1. In addition, eqn 4.30 can be eliminated if gaseous species only are of interest, since it is applied only to condensed phases. Similarly, eqn's 4.32 and 4.33 are required only for problems involving conditions of constant H,P or constant S,P respectively (76).

In addition, the determination of $\lambda_1$ (eqn 4.36) is simplified, and the final equation in set 4.38 is not required.

### 4.4.4 Computation of Thermodynamic Properties

Generally, when a thermodynamic property such as specific heat, enthalpy or entropy is required, it can be ascertained by reference to tabulated data. For computational purposes, however, it is often useful to be able to derive these thermodynamic properties from equations which have been curve-fitted to the data. Zeleznik and Gordon (80) developed a set of equations which describe the above-mentioned properties in terms of temperature and constant coefficient data, as follows:

$$\frac{C_p^o}{R} = a_1 + a_2T + a_3T^2 + a_4T^3 + a_5T^4 \qquad (4.40)$$

$$\frac{H_T^o}{RT} = a_1 + \frac{a_2}{2}T + \frac{a_3}{3}T^2 + \frac{a_4}{4}T^3 + \frac{a_5}{5}T^4 + \frac{a_6}{T} \qquad (4.41)$$

$$\frac{S_T^o}{R} = a_1 \ln T + a_2 T + \frac{a_3}{2}T^2 + \frac{a_4}{3}T^3 + \frac{a_5}{4}T^4 + a_7 \qquad (4.42)$$

Values of constants $a_1$ to $a_7$ representing a wide range of species are stored in a data file, enabling the accurate determination of the properties over a range of temperature extending from 300 to 5000K. Problems associated with tabular interpolation and the storage of vast amounts of data are thus avoided.

## 4.5 Concluding Remarks on Discussion of Chemical Equilibria Computation

This chapter has presented a discussion of the equilibria problem and the means by which it can be solved. Particular reference is made to the Gibbs free energy minimization technique developed at NASA, as it is this method which has been used in the in-house written equilibria routine for the purpose of predicting exhaust-gas reformed fuel compositions. The EQCOMP.PAS program written, but not fully debugged by West (60), provided an invaluable lead-in to the project work reported here, and has been developed and used extensively. The following chapter outlines the findings of the predictive studies undertaken using this software, and also discusses certain modifications/improvements which were incorporated into EQCOMP.PAS in order to produce a more comprehensive program, better suited to the requirements of the current investigation.

TABLE I. - ITERATION EQUATIONS TO DETERMINE EQUILIBRIUM COMPOSITIONS FOR EITHER ASSIGNED TEMPERATURE AND PRESSURE, ENTHALPY AND PRESSURE, OR ENTROPY AND PRESSURE

| Variables / Equation | $\pi_1$ | $\pi_2$ | --- | $\pi_\ell$ | $\Delta n_{m+1}$ | --- | $\Delta n_n$ | $\Delta \ln n$ | $\Delta \ln T$ (a) | Right side |
|---|---|---|---|---|---|---|---|---|---|---|
| (24) | $\sum_{j=1}^{m} a_{1j}a_{1j}n_j$ | $\sum_{j=1}^{m} a_{1j}a_{2j}n_j$ | --- | $\sum_{j=1}^{m} a_{1j}a_{\ell j}n_j$ | $a_{1,m+1}$ | --- | $a_{1n}$ | $\sum_{j=1}^{m} a_{1j}n_j$ | $\sum_{j=1}^{m} a_{1j}n_j \mathcal{H}_j$ | $\left(b_1^o - b_1\right) + \sum_{j=1}^{m} a_{1j}n_j \mathcal{G}_j$ |
| | $\sum_{j=1}^{m} a_{2j}a_{1j}n_j$ | $\sum_{j=1}^{m} a_{2j}a_{2j}n_j$ | --- | $\sum_{j=1}^{m} a_{2j}a_{\ell j}n_j$ | $a_{2,m+1}$ | --- | $a_{2n}$ | $\sum_{j=1}^{m} a_{2j}n_j$ | $\sum_{j=1}^{m} a_{2j}n_j \mathcal{H}$ | $\left(b_2^o - b_2\right) + \sum_{j=1}^{m} a_{2j}n_j \mathcal{G}_j$ |
| | --- | --- | --- | --- | --- | --- | --- | --- | --- | --- |
| | $\sum_{j=1}^{m} a_{\ell j}a_{1j}n_j$ | $\sum_{j=1}^{m} a_{\ell j}a_{2j}n_j$ | --- | $\sum_{j=1}^{m} a_{\ell j}a_{\ell j}n_j$ | $a_{\ell,m+1}$ | --- | $a_{\ell n}$ | $\sum_{j=1}^{m} a_{\ell j}n_j$ | $\sum_{j=1}^{m} a_{\ell j}n_j \mathcal{H}_j$ | $\left(b_\ell^o - b_\ell\right) + \sum_{j=1}^{m} a_{\ell j}n_j \mathcal{G}_j$ |
| (25) | $a_{1,m+1}$ | $a_{2,m+1}$ | --- | $a_{\ell,m+1}$ | 0 | --- | 0 | 0 | $\mathcal{H}_{m+1}$ | $\mathcal{G}_{m+1}$ |
| | --- | --- | --- | --- | --- | --- | --- | --- | --- | --- |
| | $a_{1n}$ | $a_{2n}$ | --- | $a_{\ell n}$ | 0 | --- | 0 | 0 | $\mathcal{H}_n$ | $\mathcal{G}_n$ |
| (26) | $\sum_{j=1}^{m} a_{1j}n_j$ | $\sum_{j=1}^{m} a_{2j}n_j$ | --- | $\sum_{j=1}^{m} a_{\ell j}n_j$ | 0 | --- | 0 | $\sum_{j=1}^{m} n_j - n$ | $\sum_{j=1}^{m} n_j \mathcal{H}_j$ | $n - \sum_{j=1}^{m} n_j + \sum_{j=1}^{m} n_j$ j |
| (27) (b) | $\sum_{j=1}^{m} a_{1j}n_j \mathcal{H}_j$ | $\sum_{j=1}^{m} a_{2j}n_j \mathcal{H}_j$ | --- | $\sum_{j=1}^{m} a_{\ell j}n_j \mathcal{H}_j$ | $\mathcal{H}_{m+1}$ | --- | $\mathcal{H}_n$ | $\sum_{j=1}^{m} n_j \mathcal{H}_j$ | $\sum_{j=1}^{n} n_j \mathcal{G}_j + \sum_{j=1}^{m} n_j \mathcal{H}_j \mathcal{H}_j$ | $\mathcal{H}_o - \mathcal{H} + \sum_{j=1}^{m} n_j$ |
| (28) (c) | $\sum_{j=1}^{m} a_{1j}n_j \mathcal{S}_j$ | $\sum_{j=1}^{m} a_{2j}n_j \mathcal{S}_j$ | --- | $\sum_{j=1}^{m} a_{\ell j}n_j \mathcal{S}_j$ | $\mathcal{S}_{m+1}$ | --- | $\mathcal{S}_n$ | $\sum_{j=1}^{m} n_j \mathcal{S}_j$ | $\sum_{j=1}^{n} n_j \mathcal{G}_j + \sum_{j=1}^{m} n_j$ j | $\mathcal{S}_o - \mathcal{S} + n - \sum_{j=1}^{m} n_j + \sum_{j=1}^{m} n_j$ j |

[a] Column not used for assigned temperature and pressure.

[b] Row used only for assigned enthalpy and pressure.

[c] Row used only for assigned entropy and pressure.

Table 4.1 Matrix of Reduced Gibbs Iteration Equations (From Ref 76)

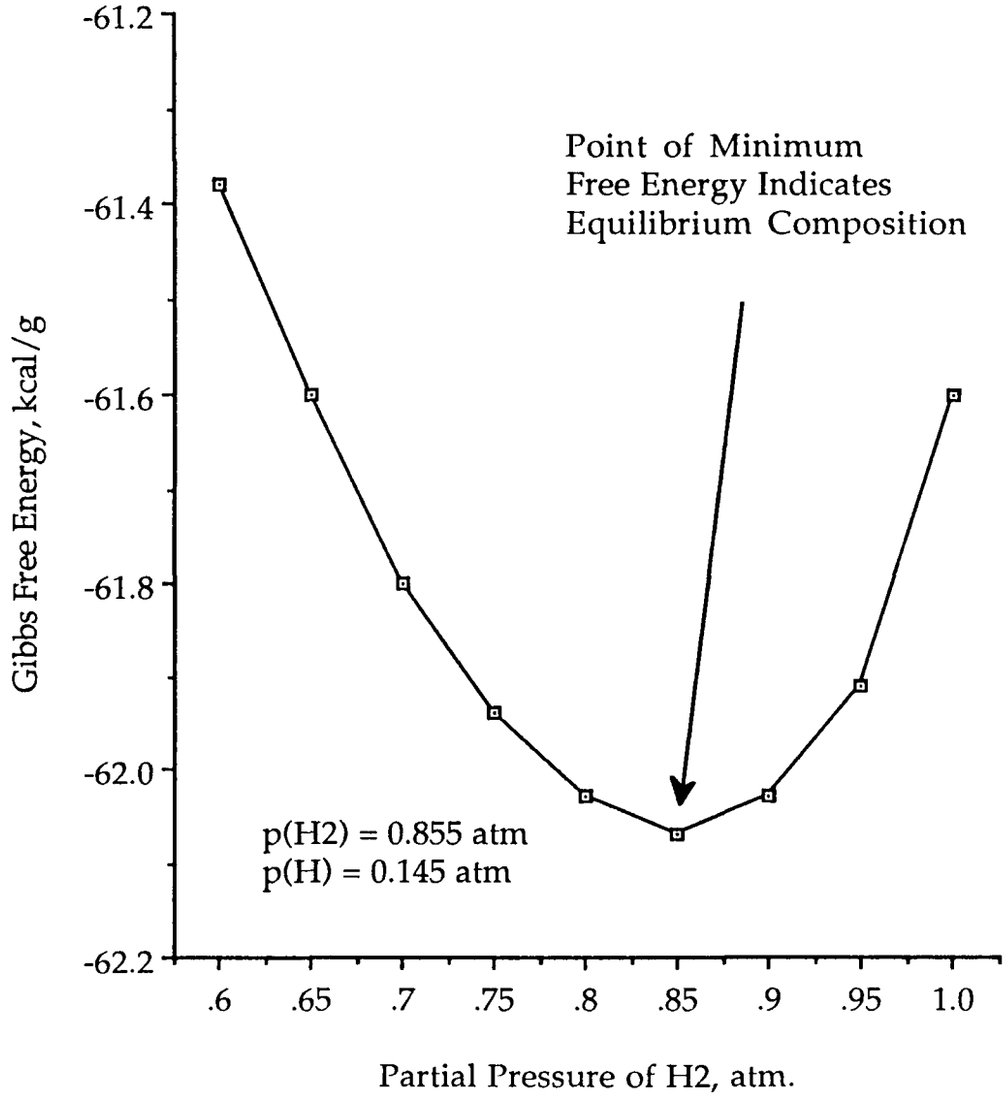


Fig 4.1 Plot of Equilibria vs Free Energy, G, for a Simple System Containing only H and $H_2$ at T=3000K and P=1atm.

(Results from Ref 79)

# 5 EQUILIBRIA AND ENERGY-REQUIREMENT PREDICTIONS FOR EXHAUST-GAS REFORMING REACTIONS

Having developed the software required for the prediction of chemical equilibrium compositions, the next stage of the study is to apply the code to the process of immediate interest - the exhaust-gas reforming of hydrocarbon and alcohol fuels.

In the first instance, however, it was necessary to validate the EQCOMP routine. This is done by comparing program output with previously published equilibria results relating to the type of reaction under consideration in the current project. An input file was written in order to simulate the adiabatic oxidation of JP-5, $(CH_{1.92})_x$, with air over a range of air to fuel ratio, and the output of the program compared with equilibria computations presented for the same reaction by Houseman and Cerini (13). Plots of the two sets of results are overlaid on the same axes in Fig 5.1, and a good level of agreement is confirmed - the small discrepancies which can be seen are most probably attributable to errors introduced when transferring values from the graph plot of Ref 13. Comparisons of output with data presented by ICI were also carried out, leading to a high degree of confidence in the operation of the in-house developed equilibria software.

The examination of the exhaust-gas reforming process begins with a consideration of the exhaust-gas compositions which would be available for the reforming process. In order to do this a set of generalized statements describing the proposed process as a whole are written, as follows:

Feed fuel + Air $\rightarrow$ 1st Generation Combustion Products (5.1)

1st Generation Combustion Products + Feed Fuel

→ 1st Generation Reformed Fuel (5.2)

1st Generation Reformed Fuel + Air

→ 2nd Generation Combustion Products (5.3)

2nd Generation Combustion Products + Feed Fuel

→ 2nd Generation Reformed Fuel (5.4)

2nd Generation Reformed Fuel + Air

→ 3rd Generation Combustion Products (5.5)

## 5.1 Predicted Composition of Combustion Products for n-Heptane

The initial stage of this part of the theoretical study involved the prediction of equilibrium exhaust-gas compositions for the combustion of a selected hydrocarbon and air. As outlined earlier, it was decided that n-heptane, $C_7H_{16}$, should be used to represent gasoline at this stage, as its molecular structure is a good overall approximation of the complex motor fuel, and thermodynamic data for the single hydrocarbon is readily available.

Simulation of engine combustion of the fuel in order to predict exhaust-gas compositions would usually require the application of a good cycle analysis package, incorporating chemical equilibria routines and kinetics models for $NO_x$ and CO formation. A cycle analysis package having limited chemical equilibria capabilities was available, and it was decided that the model should in the first instance be used to compute cycle temperature and pressure conditions for the combustion of n-heptane. The 'static' Gibbs free energy routine is subsequently used to more accurately compute equilibrium

gas compositions based on the predicted cycle conditions. The general reaction under examination is as follows:

Feed Fuel (n-Heptane) + Air $\rightarrow$ 1st Generation Combustion Products

The cycle analysis package used is described in the following chapter. Trials were conducted over a range of air to fuel ratio, and the resulting cycle pressure and temperature data used as a basis for more accurate computations of equilibrium composition using the superior Gibbs free energy software. Cycle conditions chosen for the more accurate calculations of gas composition were those giving the peak cycle temperature, which occurred around top dead centre (TDC), and those predicted at 130 crank angle degrees after TDC, which represents a typical exhaust-valve opening angle.

Predictably, the general effect of air to fuel ratio (AFR) was to give increasing quantities of excess air as AFR moved lean of stoichiometric, and progressively larger fractions of $H_2$ and CO as richer mixtures were examined. As this is a well known trend, it was decided that the study should be limited to one of stoichiometric combustion at this stage, thus eliminating one of the many variables. The effect of cycle temperatures and pressures on computed equilibria was also as expected, with levels of dissociation of $H_2O$ and $CO_2$ tending to increase with temperature and reduce with rising pressure.

The tendency to form small quantities of monatomic H, O and N etc was not significant. Equilibrium $NO_x$ levels were also generally low, and were not considered to be important in the context of exhaust-gas reforming, although they would naturally be of interest in later stages when considering actual engine emissions. CO levels were sufficiently high to warrant consideration, however, and in view of the fact that such levels are highly

dependent on reaction kinetics under engine combustion conditions, it was felt that a means of predicting non-equilibrium CO levels should be examined.

The rate-controlled CO formation mechanism in the engine leads to a pollutant emission level which falls somewhere between the equilibrium level predicted at peak cycle temperature, and that computed at exhaust-valve opening (EVO) conditions. Benson et al (81) propose a relatively simple mathematical means of dealing with this problem in predictive studies, as follows:

$$CO_{RC} = CO_{EQ} + f_{CO}(CO_{PEQ} - CO_{EQ}) \qquad (5.6)$$

where $CO_{RC}$ is the calculated rate-controlled CO emission level, $CO_{EQ}$ is the equilibrium CO concentration under the conditions of interest (in this case EVO), $CO_{PEQ}$ is cycle peak equilibrium CO level, and $f_{CO}$ is a calibration factor, which experiment has shown can be set to 0.5 for most engines (82).

The computed composition for the stoichiometric combustion of n-heptane and air, as based on cycle simulation results and subsequent equilibria computations using the Gibbs free energy software, therefore comprises the composition predicted at exhaust valve opening conditions, with CO levels modified in accordance with eqn 5.6. Arbitrarily neglecting mole fractions of less than 0.002, the composition predicted is:

$$0.012CO + 0.110CO_2 + 0.140H_2O + 0.733N_2 + 0.005O_2 \qquad (5.7)$$

$\lambda_e = 1.0$

$T_{evo} = 1426.7K$

$P_{evo} = 4.85$ bar abs

## 5.2 Predicted Equilibria of 1st Generation Reformed n-Heptane Fuels

A predictive study of the reformed fuel compositions produced by the interaction of 1st generation exhaust gas with n-heptane was then undertaken over a range of temperature, pressure and reforming oxidant to fuel ratio. The general stoichiometric equation describing the process as applied using the exhaust gas composition shown in eqn 5.7 above is as follows:

$$C_7H_{16} + 26.923(0.012CO + 0.110CO_2 + 0.140H_2O + 0.733N_2 + 0.005O_2) \rightarrow 10.285CO + 11.769H_2 + 19.734N_2 \quad (5.8)$$

Taking masses of reactants and products gives:

$$(100.2\ kg + 764.1\ kg)_R = (864.3\ kg)_P \quad (5.9)$$

which indicates a stoichiometric reforming oxidant (1st generation exhaust-gas) to feedstock mass ratio of 7.64:1.

At this stage it is convenient to define a term $\lambda_r$, reforming excess oxidant factor, as follows:

$$\lambda_r = \frac{\text{Actual Reforming Oxidant to Feedstock Mass Ratio}}{\text{Stoich. Reforming Oxidant to Feedstock Mass Ratio}} \quad (5.10)$$

$\lambda_r$ will be greater than 1 for mixtures containing an excess of oxidant relative to stoichiometric, and less than 1 for fuel-rich mixtures.

Several reformed fuels were predicted using the EQCOMP software in a study based on eqn 5.8 over a range of temperature and pressure, and a

$$C_7H_{16} + 26.415(0.003CO + 0.122CO_2 + 0.139H_2O + 0.734N_2 + 0.002O_2)$$
$$\rightarrow 10.302CO + 11.672H_2 + 19.389N_2 \quad (5.12)$$
(Ideal 2nd Generation Reformed Fuel)

By mass:

$$(100.2\ kg + 754.7\ kg)_R = (854.9\ kg)_P \quad (5.13)$$

which in this case gives a stoichiometric reforming oxidant to feedstock mass ratio of 7.55:1.

In the first instance, a general exploratory study of 2nd generation exhaust-gas reforming was conducted, and this highlighted a number of inadequacies in the EQCOMP.PAS software; it was decided that the equilibria software should be further developed before proceeding with a more rigorous investigation.

Specific modifications were implemented, leading to the computation of carbon solids (C(s)) mole fractions, endothermic reaction energy input demand (and hence exhaust-gas temperature requirements), and the effect of preheating the reactor feedstock. These enhancements are discussed below.

## 5.3 Further Development of the EQCOMP Routine

### 5.3.1 Inclusion of Condensed Species

The original EQCOMP.PAS routine was not able to deal with condensed species such as carbon solids in the equilibrium composition. The

first step taken to overcome this limitation was to include a simple test for the effect of a condensed species in the composition, in the form given below:

$$\frac{\partial G}{\partial n_j} = \left(\frac{\mu_j^0}{RT}\right)_c - \sum_{i=1}^{I} \pi_i a_{ij} < 0 \qquad (5.14)$$

This test is conducted for each condensed species of interest after the gaseous equilibrium composition has been computed. If the test proves positive, and indicates that the inclusion of the condensed species would further reduce the Gibbs free energy of the mixture, it is concluded that the species should form part of the equilibrium composition.

The implementation of this relatively simple procedure immediately indicated that C(s) would exist in the predicted equilibrium composition under a number of simulated reforming conditions, and it was therefore decided that further work should be directed towards quantifying such levels. In order to do this, an additional line and column have to be incorporated into the matrix of Gibbs iteration equations in the software, as outlined in Table 4.1.

Having included these amendments the operation of the EQCOMP routine was again verified against previously published results which included C(s) in the equilibria. The steam reforming of JP-5 was simulated at a temperature of 1033K, and results checked against those given by Houseman and Cerini (22); a good level of agreement was found to exist across a wide range of steam to fuel mass ratio in line with the earlier comparison shown in Fig 5.1

### 5.3.2 Theoretical Energy Balance Across Reactor

#### 5.3.2.1 Prediction of Exhaust-Gas Temperature Requirement

An energy balance procedure was written into the program, in order to predict those engine exhaust-gas temperatures which would be required at entry to the reactor/heat exchange unit in order to drive the endothermic reforming reactions. The energy balance is based on the following assumptions:

i) The reactor reformed fuel outlet temperature defines equilibrium conditions for computational purposes, which in most cases would be considerably lower than the exhaust-gas temperature existing at entry to the reactor.

ii) The reactor/heat exchange unit is adiabatic with respect to heat transfer to the surroundings.

iii) Any exhaust gases not actually required for the reforming reactions (ie surplus exhaust) are used to heat the reactor.

iv) Good heat transfer conditions exist between the catalyst and surplus exhaust-gas sides of the heat exchange unit, such that surplus exhaust gases leave the unit at the same temperature as the reformed fuel product gas.

v) The feedstock fuel is vaporized and preheated to the reformer outlet temperature prior to injection into the reformer.

The notation used in the energy balance procedure is illustrated below:

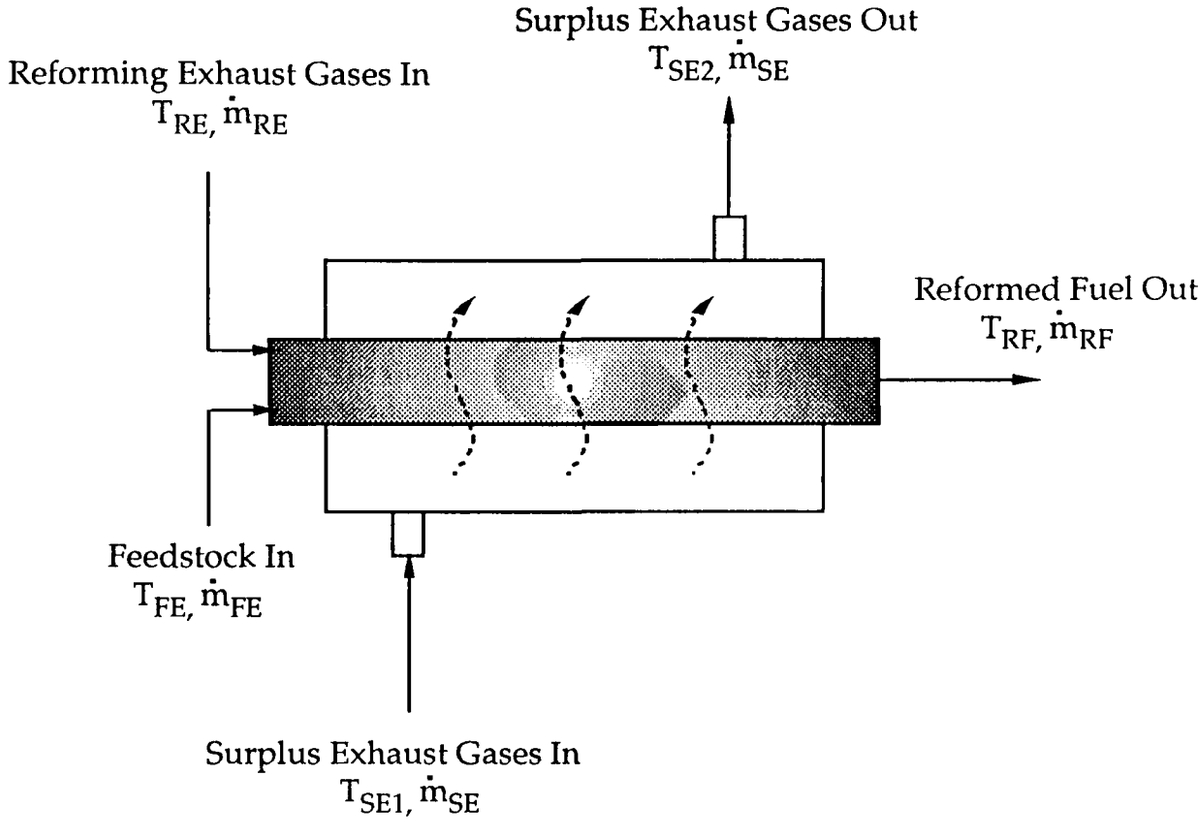


Fig 5.2 Diagram Showing Energy Balance Notation

Referring to Fig 5.2 and the assumptions given above, the following statements can be made:

$$T_{RF} = T_{SE2} = T_{FE} = \text{Assigned Equilibrium Temperature} \quad (5.15)$$

$$T_{SE1} = T_{RE} = \text{Exhaust-Gas Inlet Temperature} \quad (5.16)$$

$$\dot{m}_{RF} = \dot{m}_{FE} + \dot{m}_{RE} \quad (5.17)$$

$$\dot{m}_{SE} = x\dot{m}_{RE} \quad (5.18)$$

$$\dot{m}_{FE} = \frac{\dot{m}_{RE}}{OXF} \tag{5.19}$$

where x is the mass flow ratio of surplus exhaust gases to reforming exhaust, and is determined from space velocity and total exhaust-gas flow rates through the system, and OXF is the specified reforming oxidant to feedstock ratio.

For an adiabatic reactor, where no work is done, and where changes in fluid kinetic and potential energy are negligible, the energy equation reduces to:

$$h_{RE}\dot{m}_{RE} + h_{FE}\dot{m}_{FE} + h_{SE1}\dot{m}_{SE} = h_{SE2}\dot{m}_{SE} + h_{RF}\dot{m}_{RF} \tag{5.20}$$

As the temperature and composition of reforming and surplus exhaust gases are assumed to be identical at inlet to the reactor, it follows that specific enthalpies $h_{RE}$ and $h_{SE1}$ will be the same. Taking substitutions from eqn's 5.17 to 5.19 and manipulating, gives the following expression for the unknown specific enthalpy of reforming exhaust gases at entry to the reformer:

$$h_{RE} = \frac{xh_{SE2} + h_{RF}\left(1 + \frac{1}{OXF}\right) - h_{FE}\left(\frac{1}{OXF}\right)}{(1 + x)} \tag{5.21}$$

As all terms on the right hand side are either derived from the specified stoichiometric initial conditions, or from the equilibrium computation of the reaction under investigation, the required enthalpy of exhaust gases at inlet to the reactor, $h_{RE}$, can be determined. As this gas composition is known, a trial and error solution is then applied to find the exhaust-gas temperature which gives the computed enthalpy. The

temperature is determined to an accuracy of $\pm$5K, which would normally be equivalent to an accuracy of within around 0.5% of the true value.

#### 5.3.2.2 Conditioning of Feedstock

It has been assumed that the tanked liquid feedstock will be supplied to the reactor in a vaporized and highly preheated state. The fractions of gasoline typically boil at temperatures of between 25 and 215°C, whilst n-heptane has a boiling point of 98°C (83), and it is therefore proposed that low temperature heating and partial vaporization could be achieved by heat exchange with hot engine coolant. Higher temperature heating requirements would be provided by heat exchange with surplus exhaust gases and the hot reformed fuel leaving the reformer, the latter means being particularly beneficial as the gaseous reformate would in any case have to be cooled prior to aspiration into the engine.

#### 5.3.2.3 Computation of Thermodynamic Properties of Feedstock Fuels

In order to calculate the standardized enthalpy of the various feedstock fuels at the specified preheat temperature, it has been necessary to curve-fit tabulated data presented by Stull et al (66), as coefficients compatible with eqn's 4.40 to 4.42 could not be found for the fuels of interest. Fuel enthalpy data derived from Ref 66 is therefore represented by second order polynomial functions of temperature, and associated sets of coefficients which relate to the chosen fuels. Within the temperature range of interest, the curve-fitted functions give computed enthalpy values to an accuracy of within $\pm$0.3% as compared with the original tabulated data.

#### 5.3.2.4 Heat of Reforming Reaction and Reactor Thermal Efficiency

In order to give an indication of the extent to which the simulated reforming reactions affect fuel calorific value, the standardized enthalpies of reactants and products are computed, at the standard reference state of 298K and 1 atm. This enables the heat of reforming reaction to be calculated on a MJ/kg of feedstock basis, which is a direct measure of any change in fuel chemical energy, and also leads to reaction thermal efficiency via eqn 2.7.

Having fully developed and validated the EQCOMP routine to give all the desired information regarding the simulation of exhaust-gas reforming reactions, the software can be applied directly to the task of predicting 2nd generation reformed fuel compositions and corresponding energy requirements. Sample input and output files which give an insight into the use of the EQCOMP.PAS package are given in Fig's A5.1 and A5.2 in Appendix II.

### 5.4 Equilibria and Energy Predictions for 2nd Generation Reformed n-Heptane Fuels

The reaction given in eqn 5.12 describes the idealized process of reforming n-heptane with the unmodified products of combustion of a first generation reformed fuel. It was decided at this stage that the predicted equilibria for second generation reformed fuels should be examined over a range of simulated reformer operating conditions. Earlier work had indicated that high temperature and low pressure conditions would be most favourable in terms of maximizing hydrogen yield, and that changes in temperature had a much greater effect on predicted composition than pressure, within the ranges examined. Three discrete equilibrium temperatures of 650, 750 and

850°C (923, 1023, 1123K) were therefore chosen for investigation at a simulated reactor pressure of 1atm; at each temperature, the reforming of the n-heptane feedstock was simulated over a range of excess oxidant factor, $\lambda_r$, extending from 0.5 to 3. Equilibrium compositions were also computed at $\lambda_r$=1.5 over a range of temperature, in order that the effect of temperature on such parameters as hydrogen and carbon solids yields could be examined in isolation. The temperature sweep was also conducted using the standard exhaust gas composition given in eqn 5.12 as the reforming oxidant.

In addition, it was thought that the effects of secondary steam and/or air injection into the reactor should be examined, and hence three additional simulated oxidants were created. To recap, the composition of the standard, unmodified exhaust-gas oxidant, designated OX1, is as follows:

$$OX1 = .003CO + .122CO_2 + .139H_2O + .734N_2 + .002O_2$$

In order to examine the effect of excess steam in the oxidant, the water fraction of OX1 is doubled and the resulting composition normalized to give:

$$OX2 = .003CO + .107CO_2 + .244H_2O + .644N_2 + .002O_2$$

The addition of steam was thought to be of interest as the literature suggests that in straightforward steam reforming, an excess of steam helps to suppress the formation of carbon solids.

Preliminary studies indicated that the exhaust temperatures required at inlet to the reformer might be rather high, and it was proposed that this high energy requirement might be met in part by the introduction of small quantities of secondary air into the reactor, thus initiating an exothermic

partial oxidation. Naturally, if an improvement in fuel calorific value is to be achieved, the endothermic reforming reaction would have to dominate the exotherm, but nevertheless the effect of simulated air injection on temperature requirement is of considerable interest. It was therefore decided to simulate the introduction of an air-borne 3% excess of oxygen into the exhaust gases, to give a third reforming oxidant as follows:

$$OX3 = .003CO + .108CO_2 + .123H_2O + .740N_2 + .026O_2$$

Finally, since the introduction of excess steam and air would both, hopefully, have some beneficial effect, a fourth simulated oxidant incorporating both strategies was created by adding 3% oxygen-in-air to the steam-enriched exhaust-gas composition OX2. The composition of the resulting oxidant is thus:

$$OX4 = .002CO + .096CO_2 + .220H_2O + .659N_2 + .023O_2$$

Thus, four simulated exhaust compositions were created in order to give an insight into reforming equilibria and energy requirements under varying conditions of secondary air and steam injection.

Reforming using each of these oxidants was simulated using the EQCOMP.PAS routine over a range of reactor excess oxidant factor extending from 0.5 to 3 at the above-mentioned equilibrium temperatures of 923, 1023, and 1123K, with pressure maintained at 1atm abs throughout. As also mentioned above, a temperature sweep was conducted from 800 to 1200K at a fixed $\lambda_r$ value of 1.5 with the standard exhaust composition, OX1. The results of predicted equilibrium composition, exhaust-temperature requirement and reactor thermal efficiency are plotted against an abscissa of reactor excess

oxidant factor, $\lambda_r$, in the case of the $\lambda_r$ sweeps, and against equilibrium temperature for the single temperature sweep. Results are arranged as outlined below.

## 5.5 Results and Discussion of n-Heptane Reforming Equilibria and Energy Predictions

### 5.5.1 Presentation of Results

The compositions of each of the four reforming oxidants, and their corresponding stoichiometric reforming oxidant to fuel ratios, are given in Table A5.1, which can be found in the Appendix II.

The list given below summarizes the presentation of the results of the second generation reforming predictions, as applied to the n-heptane feedstock. Note that on plots of gas composition the balance to 100% in all cases comprises atmospheric nitrogen which existed in the reforming oxidant.

| | Fig No |
|---|---|
| Equilibria/Energy Predictions at $\lambda_r$ =1.5, T=800 to 1200K, OX1 | 5.3a, b |
| Equilibria/Energy Predictions at 923K, $\lambda_r$ =0.5 to 3, OX1 | 5.4a, b |
| Equilibria/Energy Predictions at 1023K, $\lambda_r$ =0.5 to 3, OX1 | 5.5a, b |
| Equilibria/Energy Predictions at 1123K, $\lambda_r$ =0.5 to 3, OX1 | 5.6a, b |
| Equilibria/Energy Predictions at 923K, $\lambda_r$ =0.5 to 3, OX2 | 5.7a, b |
| Equilibria/Energy Predictions at 1023K, $\lambda_r$ =0.5 to 3, OX2 | 5.8a, b |
| Equilibria/Energy Predictions at 1123K, $\lambda_r$ =0.5 to 3, OX2 | 5.9a, b |
| Equilibria/Energy Predictions at 923K, $\lambda_r$ =0.5 to 3, OX3 | 5.10a, b |
| Equilibria/Energy Predictions at 1023K, $\lambda_r$ =0.5 to 3, OX3 | 5.11a, b |

Eight reformed fuel compositions were selected from the equilibria results for use in an engine cycle simulation exercise. The selected fuels are indicated on the relevant equilibria plots, and it will be noted that each fuel falls in a region around the carbon solids formation limit, and gives a significant predicted improvement in calorific value as compared with the n-heptane feedstock (see thermal efficiency values). The selection of the fuels was based on a careful examination of the results, in order that the combustion characteristics of a widely differing range of reformed fuels might be investigated.

### 5.5.2 Discussion of Results and Selection of Reformed n-Heptane Fuels for Engine Cycle Simulation Investigation

Fig 5.3 illustrates results for 2nd generation reforming of n-heptane, and clearly shows that high temperature operation is imperative in exhaust-gas reforming if carbon solids (C(s) formation is to be avoided; the equilibria plot shows a C(s) limit at an equilibrium temperature of around 1000K when reforming n-heptane with unmodified exhaust gases at the chosen value of $\lambda_r$=1.5. This temperature coincides with that which gives the maximum hydrogen yield of around 21.5%. Observation of subsequent plots indicates that as equilibrium temperature increases, the carbon solids limiting value of $\lambda_r$ approaches 1, ie stoichiometric reforming.

Figs 5.4, 5.5, and 5.6 indicate that equilibrium formation of C(s) is predicted at all values of $\lambda_r$ richer than (less than) 1.5 when reforming with standard exhaust gases, and, in the case of Fig 5.4, at $\lambda_r$=2.0 and below. As reforming with standard exhaust gases would obviously be desirable, it was thought that a reformed fuel should be chosen from each of the plots shown in Figs 5.4, 5.5, and 5.6 for the cycle analysis work. Hence the selection of reformed fuels RF1, RF2 and RF3, which occur at or around the carbon solids limit in each Fig, as indicated on the plots.

Fuel RF1, which occurs at $\lambda_r$=2.0, T=923K, comprises 17.4% $H_2$, 13.0% CO, and 0.6% $CH_4$ combustibles by volume, and has a predicted lower calorific value (LCV) some 24.5% higher than the n-heptane feedstock, as indicated on the plot of thermal efficiency (Fig 5.4b). The predicted exhaust gas temperature requirement for the production of RF1 is 1300K, and a major objective of the cycle analysis work will be to ascertain whether or not such a temperature can be achieved by the engine combustion products of the reformed fuel.

RF2 (Fig 5.5) results from the reforming of n-heptane with standard flue gases at $\lambda_r$=1.5 at an equilibrium temperature of 1023K. The reaction would require a high inlet flue gas temperature of around 1435K to proceed to completion, and has a predicted reactor thermal efficiency of around 127.2 %, indicating a 27.2% improvement in LCV. This fuel comprises combustible fractions of $H_2$, CO and $CH_4$ of 21.5, 18.4 and 0.1% respectively.

The third fuel chosen from the standard exhaust gas runs for cycle analysis investigation, RF3 (Fig 5.6), occurs at $\lambda_r$=1.5, T=1123K, with a very high inlet temperature requirement of 1535K. The main combustibles in this fuel are $H_2$ and CO at 21.2% and 19.0% respectively. Again, the fuel has a

predicted LCV some 27.8% greater than that of the n-heptane feedstock, but it remains to be seen whether the high temperature requirement at inlet can be achieved.

It had been hoped that reforming with exhaust gases enriched with 100% steam addition would show a reduced tendency to form carbon solids as compared with unmodified flue gases. In the first instance, observation of Fig's 5.7, 5.8 and 5.9 does not appear to support this, as the solids limit still falls around $\lambda_r$=1.5 to 2 as per Fig's 5.4 to 5.6. However, the stoichiometric reforming oxidant to fuel ratio with the steam-enriched exhaust gases is considerably lower than with standard gases at 5.38:1 compared with 7.55:1 respectively, and hence in terms of oxidant to fuel ratio there are potential benefits. For example, in the case of the excess-steam exhaust gas, mixtures containing much greater proportions of feedstock relative to exhaust-gas oxidant can be reformed without C(s) formation than is the case with standard oxidant under the same conditions of temperature and pressure. A major benefit of this is that proportionately lower quantities of nitrogen diluent then exist in the equilibrium composition, whilst the combustible mole fraction increases; this would prove to be advantageous when attempting to aspirate a given mass of combustible mixture into the engine cylinder. Hence the selection of fuel RF4 at the C(s) limit of $\lambda_r$=1.5 in Fig 5.8a, a plot of equilibria for reforming with 100% steam-enriched exhaust gases at T=1023K. The fuel comprises 29.5% $H_2$, 19.1% CO, and 0.2% $CH_4$, giving a total combustible fraction of around 49% as compared with a value of around 40% for reforming with unmodified flue gases under similar conditions (see RF2). $\eta_{RTH}$ is 126.0%, with a reactor inlet temperature requirement of 1395K.

Figs 5.10, 5.11 and 5.12 show the results of reforming with exhaust gases modified by the introduction of 3% oxygen in air. As expected, the influence

of excess air is to reduce exhaust gas temperature requirements, typically by around 150 to 250K, as compared with levels observed under similar conditions with unmodified oxidant. The fall in temperature requirement is accompanied by a commensurate reduction in reactor thermal efficiency, as part of the chemical energy of the feedstock is liberated as heat in the reaction. RF5 is indicated in Fig 5.10, and occurs at $\lambda_r$=2.0, T=923K. The fuel has relatively low $H_2$ and CO yields of 16.8 and 12.4% respectively, giving a total combustible fraction of just over 29.2%. The fuel has a computed LCV some 11.5% greater than the feedstock, and requires a predicted exhaust-gas temperature level of around 1105K at inlet to the reformer. A fuel was also identified at $\lambda_r$=1.5, T=1023K in Fig 5.11a, and was designated RF6. In the absence of excess steam, it can be seen that the combustible mole fraction is again below 40% at this value of $\lambda_r$, with the fuel containing 21.1% $H_2$ and 17.9% CO. The compromised reforming efficiency of 117.0% is achieved at an exhaust gas temperature requirement of 1290K.

The final set of plots, Fig's 5.13, 5.14, and 5.15 show the effects of both steam and air injection on equilibria and energy results. Fuel RF7 is indicated in Fig 5.13 at $\lambda_r$=1.5, which is just inside the C(s) zone at this temperature. Notwithstanding this, the fuel is of interest as it should require a relatively low exhaust gas temperature of around 1125K to drive the reaction, which has an efficiency of 113.3%. $H_2$, CO and $CH_4$ volume fractions are 25.4, 13.8 and 1.6% respectively.

Finally, fuel RF8 is selected at $\lambda_r$=1.5 in Fig 5.14. The fuel has a predicted combustible fraction approaching 48%, an LCV some 19.1% higher than that of the feedstock, and would require an oxidant inlet temperature of around 1305K.

In order to summarize the most relevant findings of the n-heptane equilibria study, Table A5.2 has been included in Appendix II. It contains information relating to the reactor conditions which would be required to generate mixtures RF1 to RF8, and various details pertaining to the fuels.

## 5.6 Study of Methanol Reforming - Prediction of Methanol and Reformed Methanol Combustion Products

As pointed out earlier, methanol is a strong candidate alternative fuel, primarily because of the variety of means by which it can be produced. In addition, its behaviour in the engine is not dissimilar to that of gasoline, and it can be distributed and stored using well-established techniques.

The idealized equations for methanol combustion, reforming and reformed-fuel combustion were given in section 3.2.1 (see eqn's 3.4 to 3.6), and they will not, therefore, be repeated here. In accordance with the generalized equations given at the beginning of this chapter, the first step in the examination of methanol reforming is to determine the equilibrium combustion products for standard methanol and air.

This was done in much the same way as discussed for n-heptane, with use being made of cycle analysis software as well as the EQCOMP routine. Again, restricting the study to stoichiometric combustion, it was found that product compositions changed little over the range of temperature and pressure predicted on the expansion stroke of the cycle simulation. The composition occurring at $130^{\circ}$ after TDC (exhaust valve opening angle) was chosen, taking account of the rate-controlled nature of CO formation, in order to enable the simulation of $1^{st}$ generation reforming of methanol. A range of exhaust reformed fuels were then predicted, and each subjected to a

combustion simulation in order to predict the composition of 1st generation reformed fuel + air exhaust gases. Again, as in the case of n-heptane, it was found that in the absence of secondary air or steam injection, the products of the stoichiometric combustion of 1st generation reformed fuels were essentially the same as those resulting from the combustion of the original feed fuel. Neglecting mole fractions of less than 0.002, which in this case precludes the small amount of rate-controlled CO predicted by applying eqn 5.6, gives 1st generation reformed methanol combustion products as follows:

$$\text{Reforming Oxidant } OX_m1 = .115CO_2 + .230H_2O + .655N_2$$

where subscript 'm' denotes that this is a methanol-derived exhaust-gas oxidant composition. This oxidant, which notably has a much higher water fraction than that for n-heptane, was thus used in the investigation of the production of second generation reformed fuels, ie those produced by reforming methanol in the presence of 1st generation reformed fuel combustion products.

## 5.7 Equilibria and Energy Predictions for 2nd Generation Reformed Methanol Fuels

As findings in the literature survey had indicated that carbon solids formation should be less of a problem with methanol fuel than with the hydrocarbons, it was decided that the equilibria for the exhaust-gas reforming of methanol should initially be examined at the stoichiometric reforming oxidant to fuel ratio. The idealized stoichiometric equation, based on the methanol feedstock and $OX_m1$, is as follows:

$$CH_3OH + 4.35(.115CO_2 + .230H_2O + .655N_2) \rightarrow 1.50CO_2 + 3.00H_2 + 2.85N_2 \qquad (5.21)$$

The stoichiometric reforming oxidant to fuel ratio derived from eqn 5.21 is 3.74:1 by mass, and reforming was initially simulated at this ratio over a range of temperature extending from 400 to 1200K. Pressure was maintained at 1 atm abs throughout, and results are presented in Fig 5.16a, b.

The results of the temperature sweep predict that for $\lambda_r$=1, the soot formation limit exists at an equilibrium temperature of around 900K, with compositions below this temperature invariably containing carbon solids. The next step in the investigation was to run the EQCOMP equilibria routine over a range of reactor excess oxidant factor, in order to examine the effect of operation at lean and rich reforming oxidant to fuel ratios; this exercise was carried out at equilibrium temperatures of 700, 800, 900, and 1000K, again at a fixed pressure of 1 atm abs.

## 5.8 Results and Discussion of Methanol Reforming Equilibria and Energy Predictions

### 5.8.1 Presentation of Results

It will be noted that all simulated second generation reformed methanol fuels are produced by reforming methanol with $OX_m1$, and that no attempt has been made to examine the effects of secondary steam or air injection. The reason for this apparent omission is that the exhaust-reforming of methanol is not such an endothermic reaction as is the case with n-heptane, and hence the introduction of secondary air in order to provide a heat energy input should not be necessary; the addition of steam should also be omissible on the grounds that the standard oxidant, $OX_m1$, has a relatively high water content, leading to a reduced tendency for C(s) problems.

The list below outlines the presentation of results for the methanol reforming investigation:

| | Fig No |
|---|---|
| Equilibria/Energy Predictions at $\lambda_r$ = 1.0, T= 400 to 1200K, $OX_m1$ | 5.16a, b |
| Equilibria/Energy Predictions at 700K, $\lambda_r$ = 0.5 to 2, $OX_m1$ | 5.17a, b |
| Equilibria/Energy Predictions at 800K, $\lambda_r$ = 0.5 to 2, $OX_m1$ | 5.18a, b |
| Equilibria/Energy Predictions at 900K, $\lambda_r$ = 0.5 to 2, $OX_m1$ | 5.19a, b |
| Equilibria/Energy Predictions at 1000K, $\lambda_r$ = 0.5 to 2, $OX_m1$ | 5.20a, b |

As in the case of n-heptane, compositions which appeared to give good reformed fuels have been indicated on the plots. The selection was based on the requirements of a soot-free fuel having an improved calorific value as compared to standard methanol, whilst being producible at realistic engine exhaust gas temperatures. The four fuels indicated on the plots are thus those used in the cycle simulation work discussed in the next chapter; fuel compositions are outlined in the following section.

### 5.8.2 Discussion of Results and Selection of Reformed Methanol Fuels for Engine Cycle Simulation Investigation

The methanol reforming results shown in Fig 5.16 indicate that, in the case of stoichiometric reforming, optimum hydrogen yields of around 28.2% are predicted at an equilibrium temperature of 1000K. At this point, carbon monoxide concentration is around 12.4%, with a predicted reactor thermal efficiency of 119.6%. Conditions are such that carbon solids formation is comfortably avoided, with a predicted exhaust temperature requirement of 1205K at inlet to the reactor.

It is encouraging to note, on observation of Fig's 5.17 and 5.18, that soot-free exhaust reforming of methanol should be possible at equilibrium temperatures as low as 700 and 800K, albeit at rather large reactor excess oxidant factors. Under such conditions, hydrogen and carbon monoxide yields tend to be relatively low, with high fractions of unreacted steam in the product composition.

Fig 5.19 shows results at an equilibrium temperature of 900K, and indicates C(s)-free fuel compositions at excess oxidant factors as rich as $\lambda_r$=0.75, and only a trace of soot at $\lambda_r$=0.5. As indicated on the equilibria plot, two fuels produced at 900K were selected for cycle analysis examination, and are denoted $RF_m1$, at $\lambda_r$=1, and $RF_m2$, at $\lambda_r$=1.5; both fuels have hydrogen yields well in excess of 20%. $RF_m1$ has an LCV some 15.8% higher than that of the methanol feedstock, whilst $RF_m2$ shows an improvement of around 17.1%. Respective temperature requirement predictions are 1060 and 1080K.

Fig 5.20 also shows encouraging results, as it is predicted that soot-free reforming at excess oxidant factors as low as 0.5 should be possible at the equilibrium temperature of 1000K. In the case of such rich oxidant to fuel ratios, relatively small quantities of exhaust gas are actually used to reform the fuel, leading to the production of a high-quality reformate exhibiting a good heating value per unit mass. The highest $H_2$ level predicted throughout the whole methanol reforming exercise was 38.8% at $\lambda_r$=0.5 and T=1000K, and as the corresponding thermal efficiency is 119.0%, the composition was denoted $RF_m3$ and selected for the cycle simulation exercise.

Finally, $RF_m4$ was selected at $\lambda_r$=1 and T=1000K, where a thermal efficiency value of 119.4% is predicted. This value was the highest observed for the exhaust reforming of methanol, and appears to represent optimum

conditions in terms of energy recovery. It will be noted that this level is somewhat higher than that quoted for the idealized reforming reaction (eqn's 3.4 to 3.6) - the reason for this is the presence in the true equilibria of carbon-based compounds other than just $CO_2$ as was assumed for the purpose of writing the simple stoichiometric equation. The predicted exhaust-gas temperature requirement for $RF_m4$ is 1205K.

The compositions and properties of the four selected reformed methanol fuels are drawn together in Table A5.3, which can be found in Appendix II.

## 5.9 Concluding Remarks on Equilibria/Energy Prediction Study

This chapter has outlined the approach adopted in tackling the equilibria problem with respect to the exhaust-gas reforming of n-heptane and methanol feedstocks, and has presented the results of the exercise. Enhancements which were implemented in order to derive as much useful information as possible from the EQCOMP routine have been discussed, and it is felt that these improvements have led to sound and accurate predictions of equilibria and energy requirements.

The ultimate result of the work reported thus far is the selection of eight reformed n-heptane fuels and four reformed methanol fuels for examination using engine cycle simulation techniques. This next phase of the study thus compares simulated engine performance using reformed fuels and conventional feedstocks, in terms of work output, engine thermal efficiency and pollutant emission levels.

Comparison of EQCOMP Software Output
With Data Published in Ref 13 for the
Adiabatic Combustion of JP-5

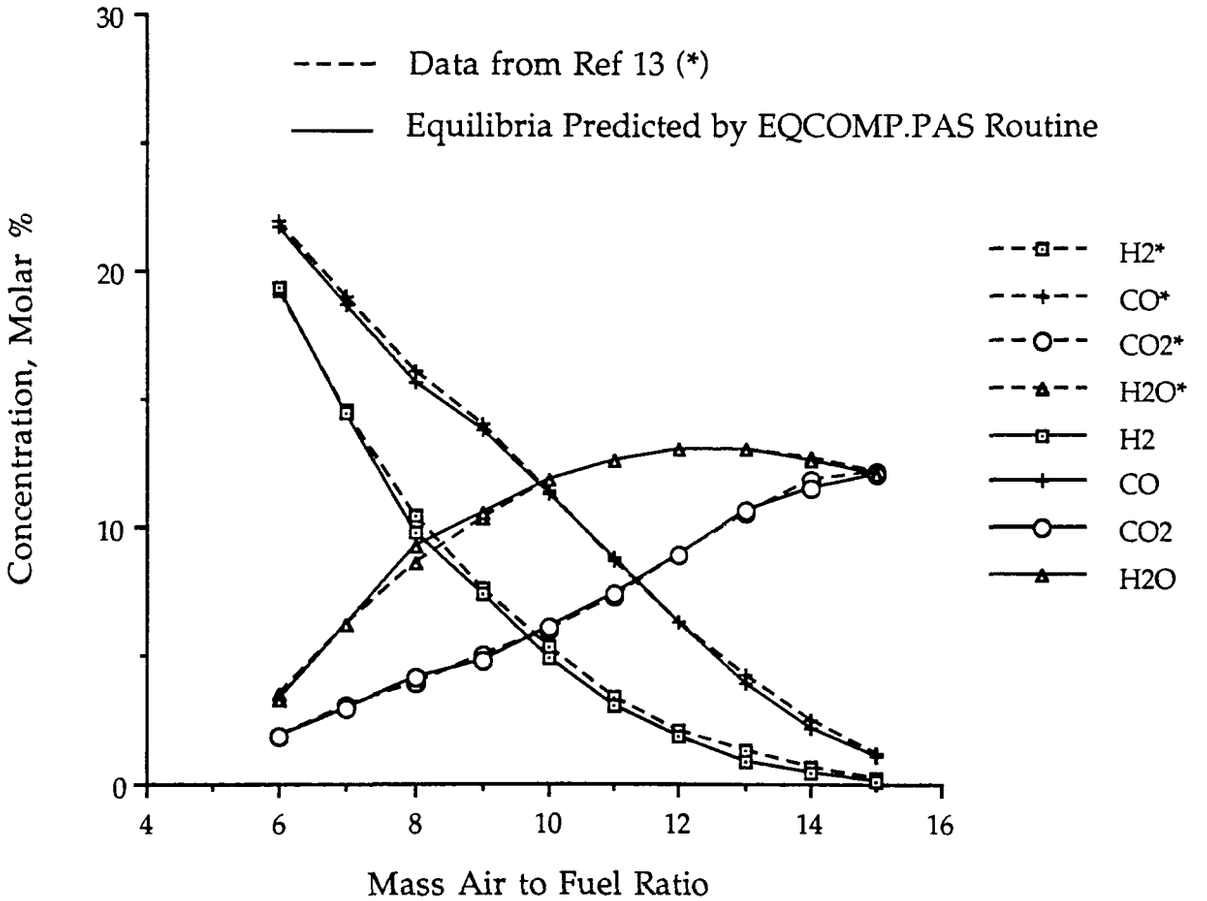


Fig 5.1

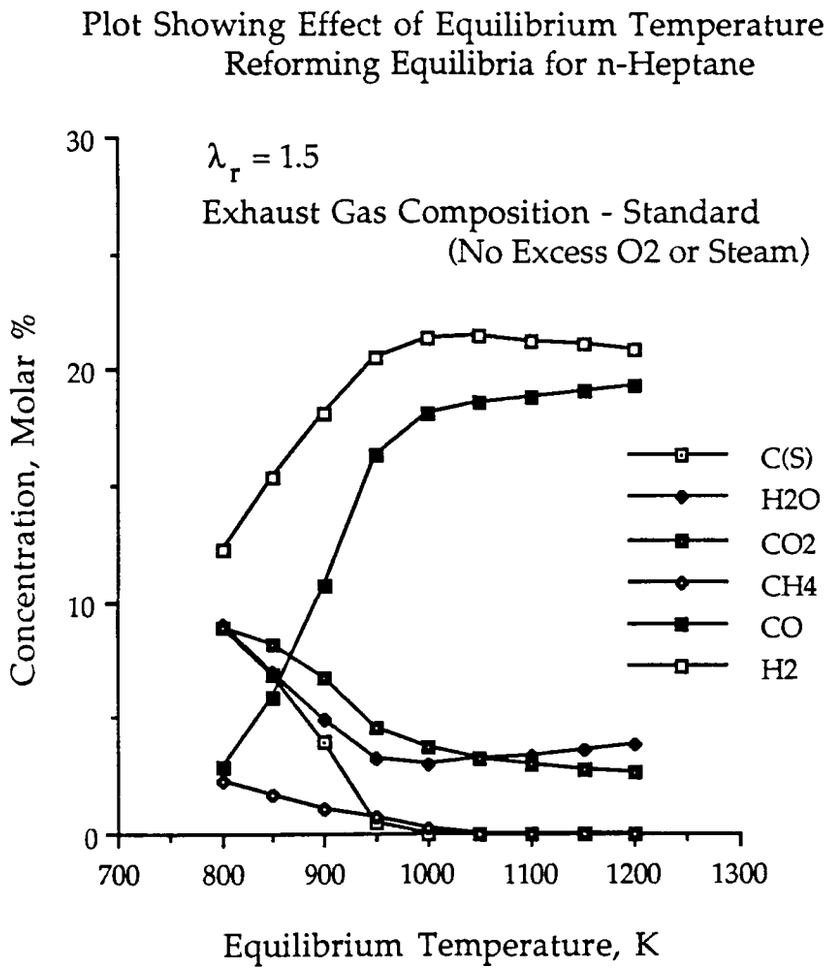


Fig 5.3a

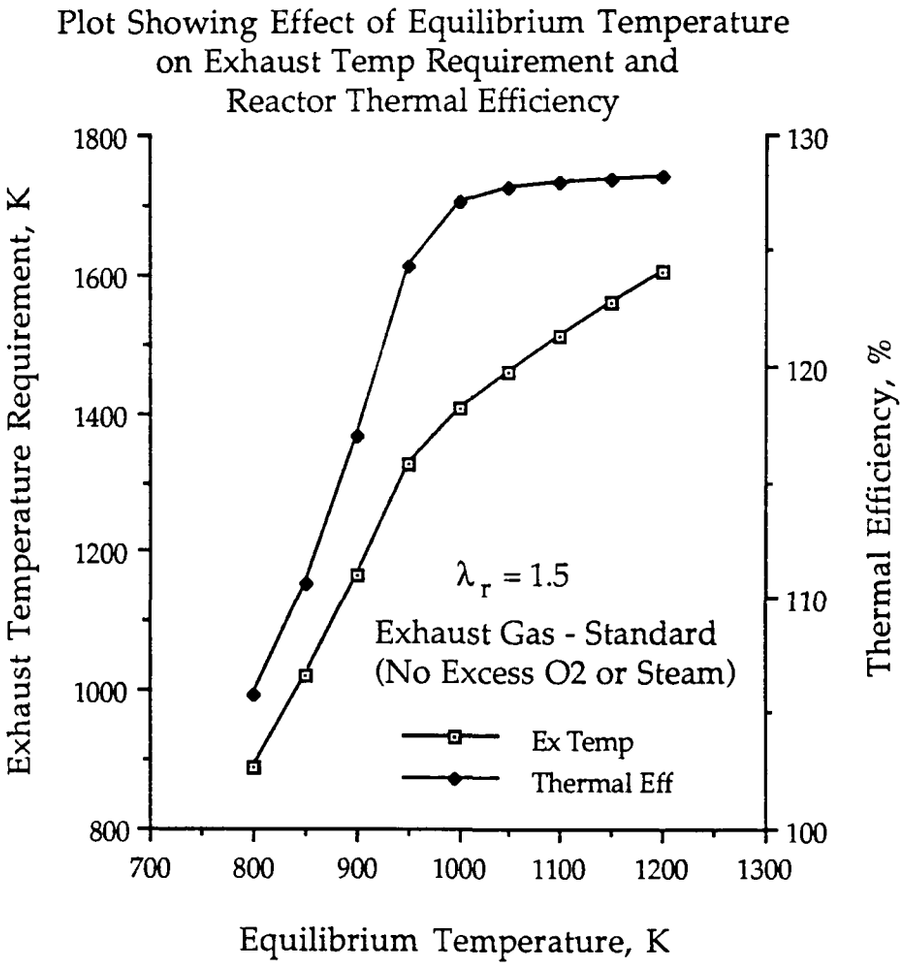


Fig 5.3b

Plot of Equilibrium Composition for Exhaust Reforming of n-Heptane

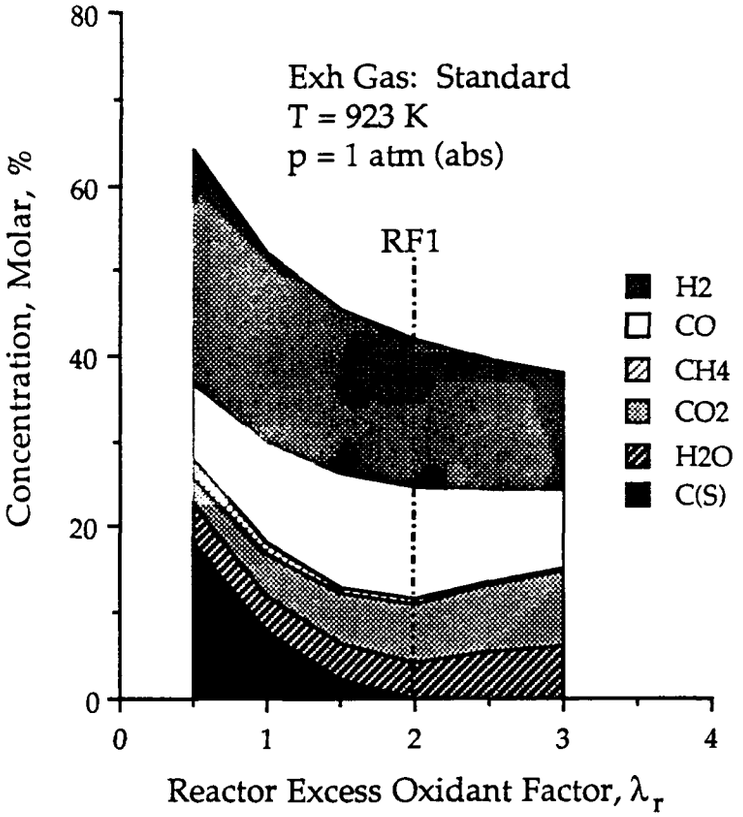


Fig 5.4a

Plot of Reactor Thermal Efficiency and Exhaust Temperature Requirement for Reforming of n-Heptane

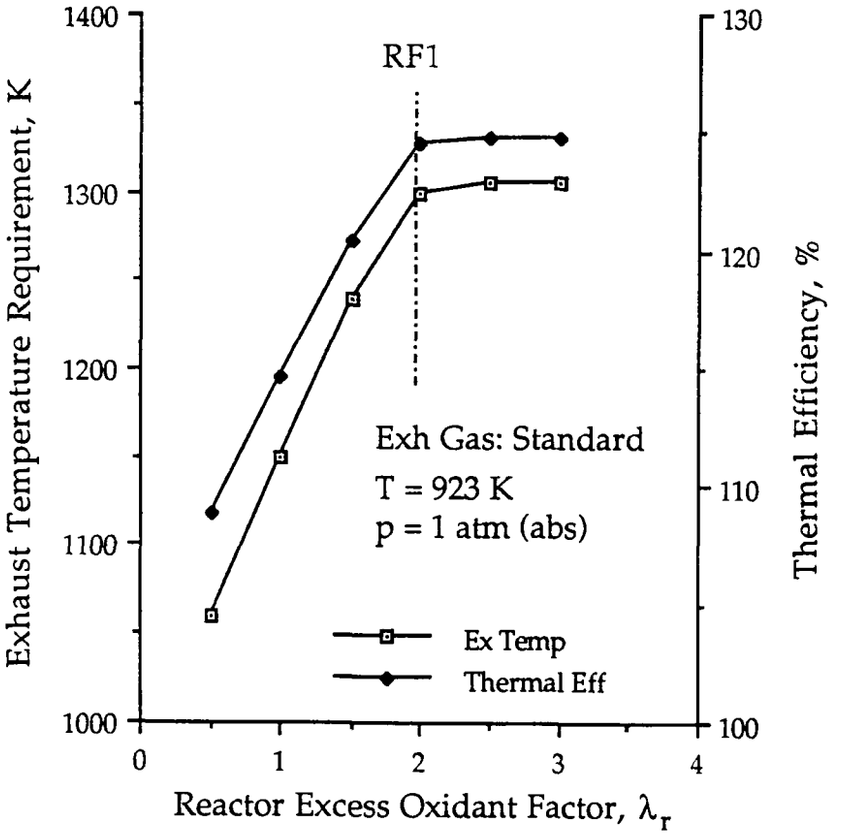


Fig 5.4b

Plot of Equilibrium Composition for Exhaust Reforming of n-Heptane

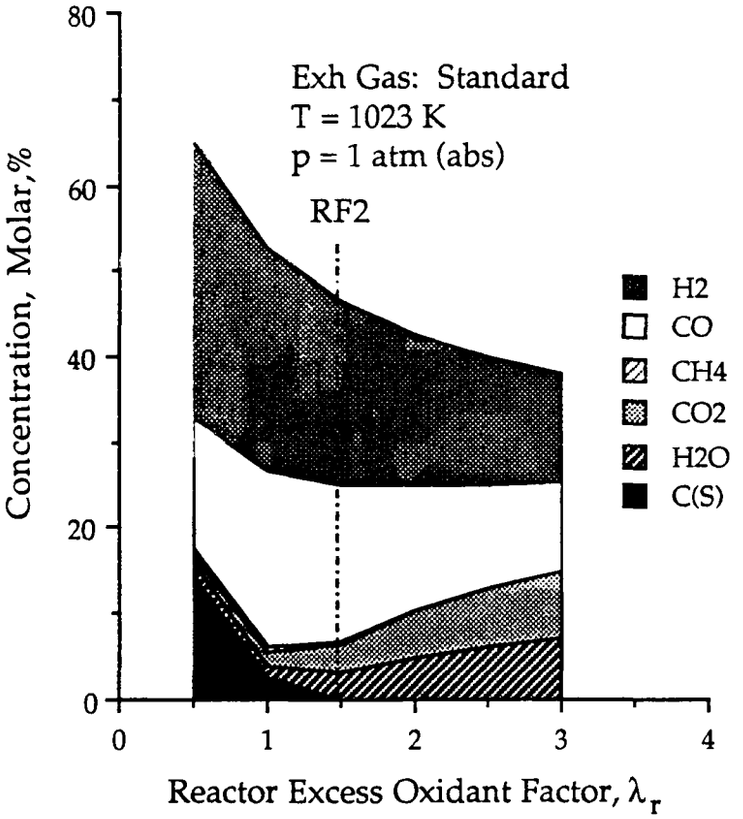


Fig 5.5a

Plot of Reactor Thermal Efficiency and Exhaust Temperature Requirement for Reforming of n-Heptane

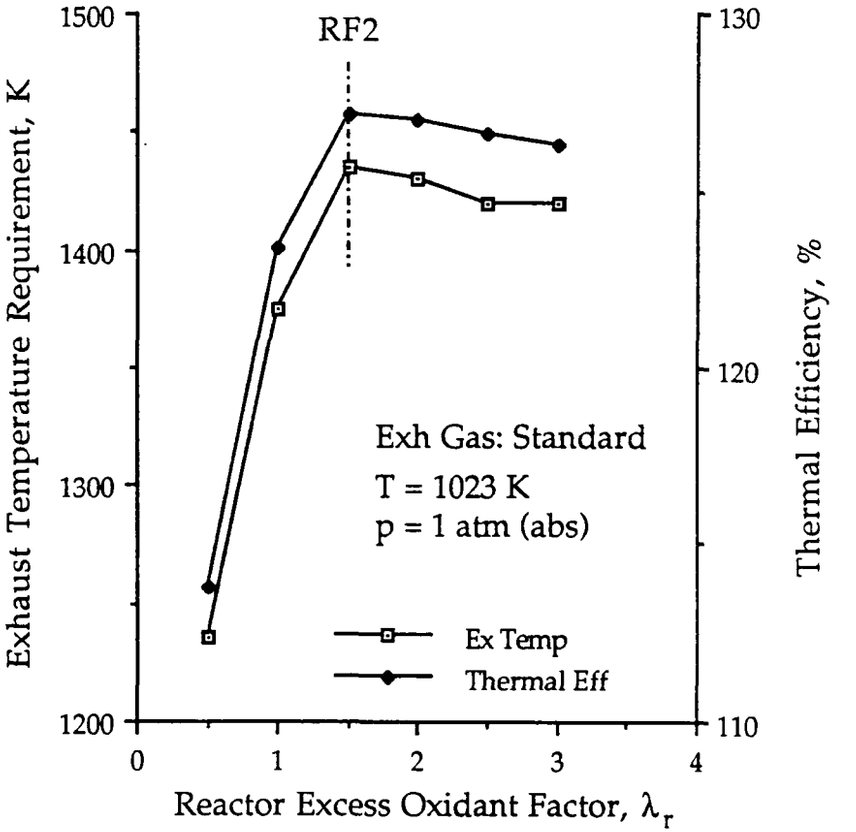


Fig 5.5b

Plot of Equilibrium Composition for Exhaust Reforming of n-Heptane

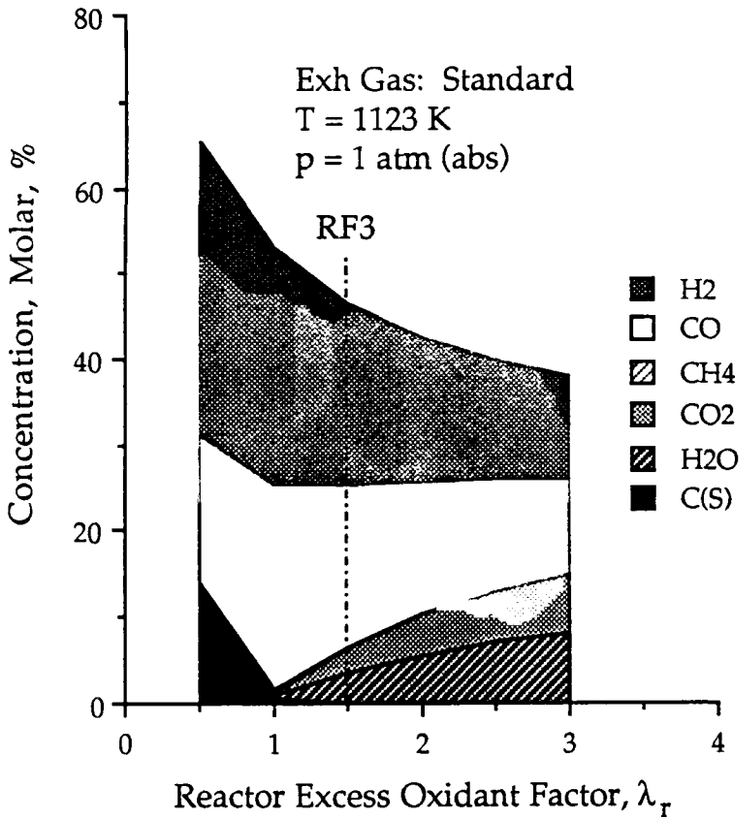


Fig 5.6a

Plot of Reactor Thermal Efficiency and Exhaust Temperature Requirement for Reforming of n-Heptane

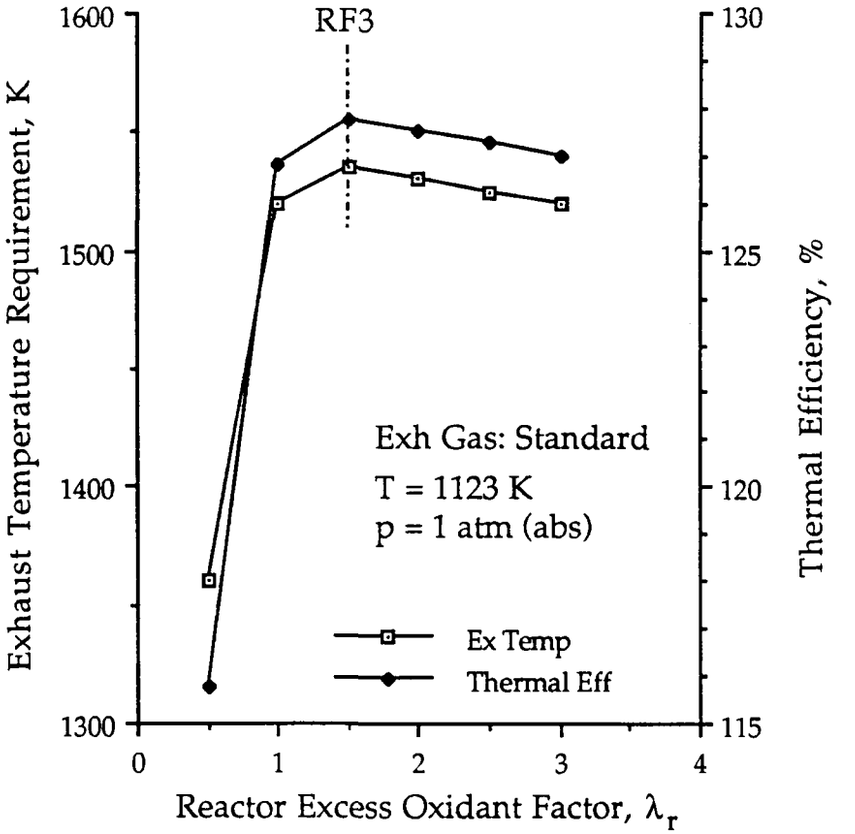


Fig 5.6b

Plot of Equilibrium Composition for Exhaust Reforming of n-Heptane

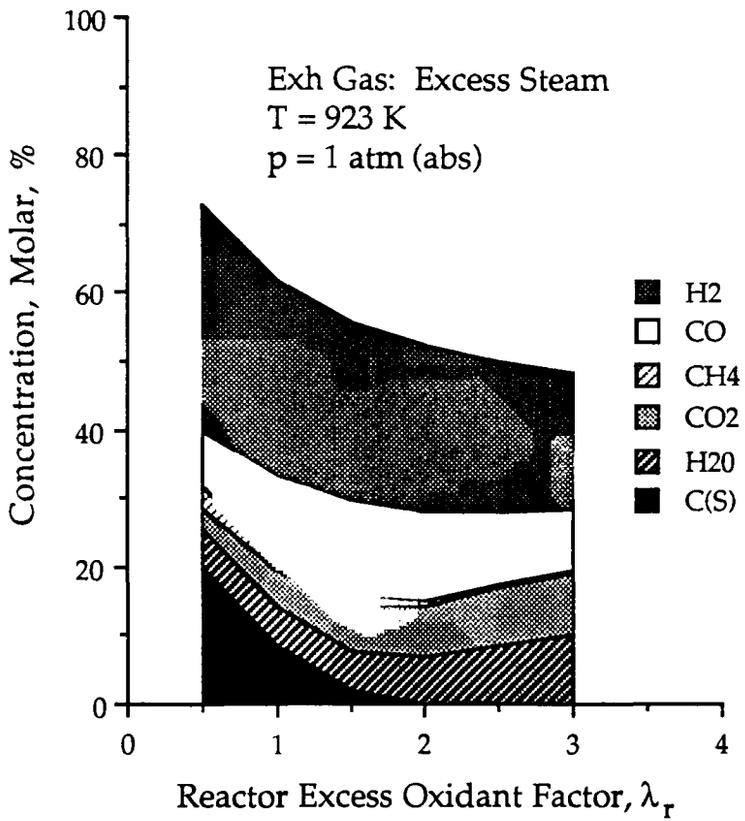


Fig 5.7a

Plot of Reactor Thermal Efficiency and Exhaust Temperature Requirement for Reforming of n-Heptane

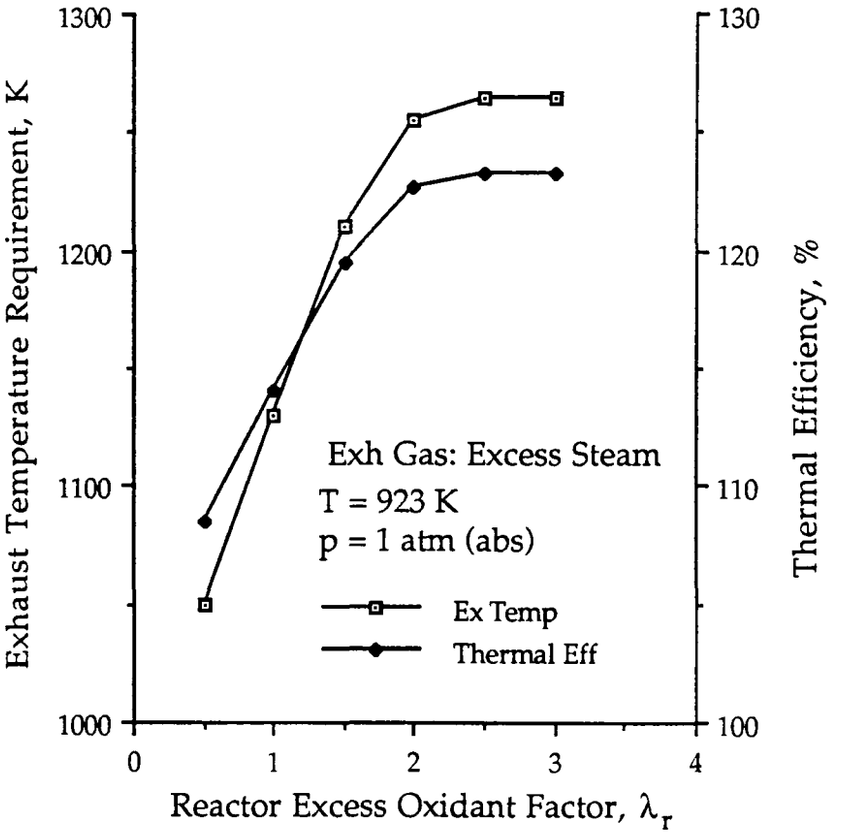


Fig 5.7b

Plot of Equilibrium Composition for Exhaust Reforming of n-Heptane

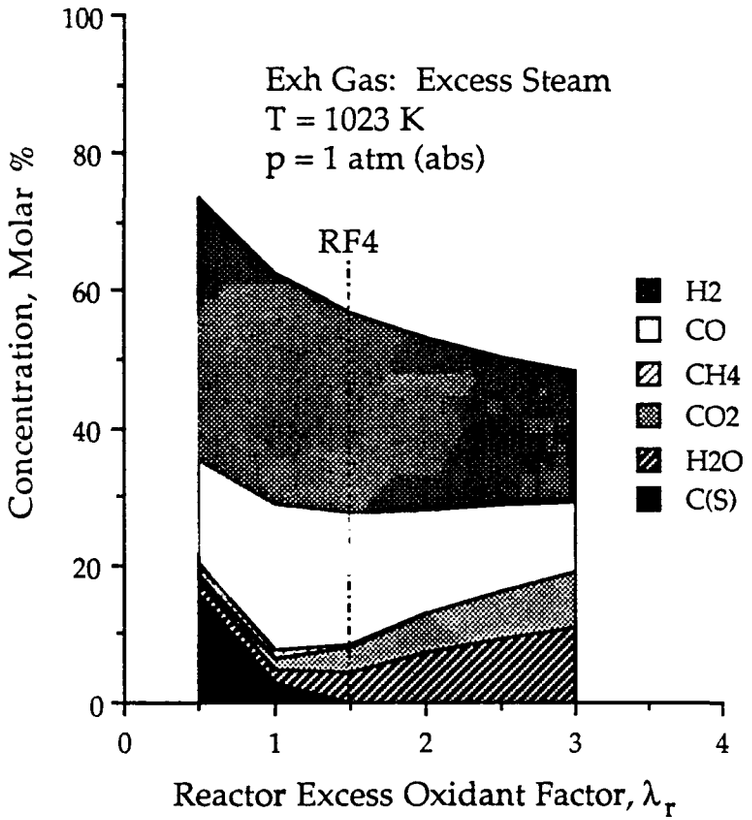


Fig 5.8a

Plot of Reactor Thermal Efficiency and Exhaust Temperature Requirement for Reforming of n-Heptane

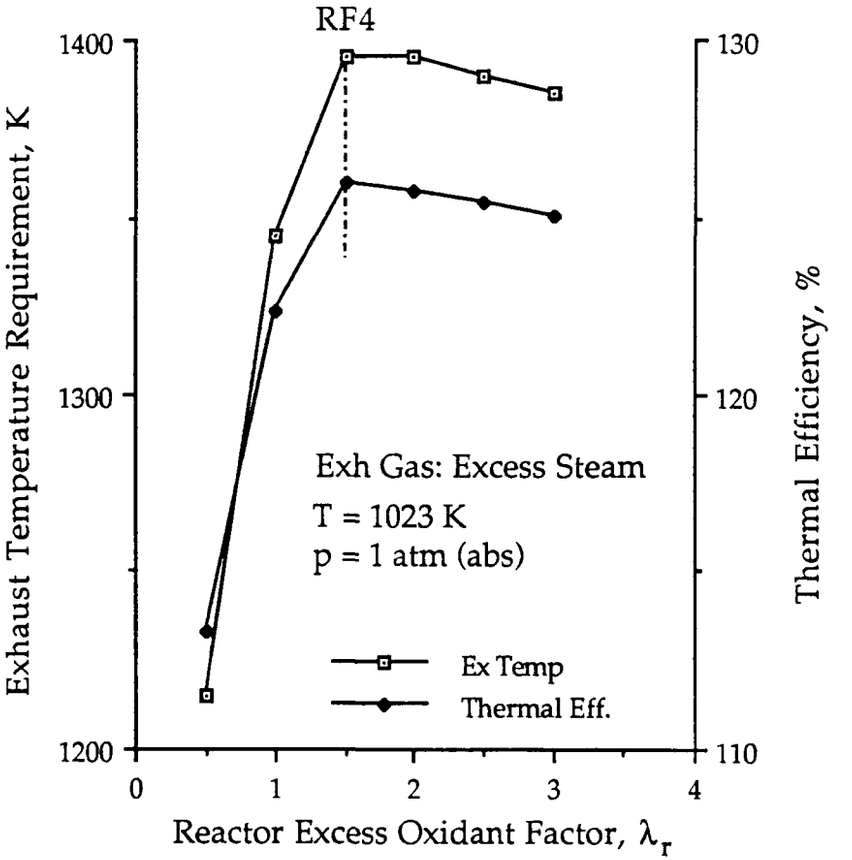


Fig 5.8b

Plot of Equilibrium Composition for Exhaust Reforming of n-Heptane

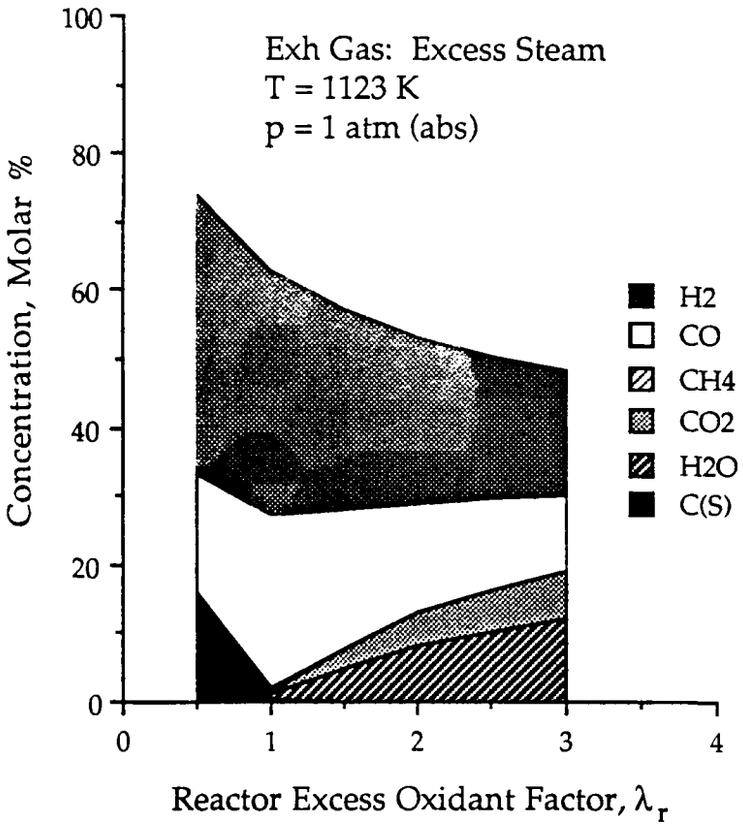


Fig 5.9a

Plot of Reactor Thermal Efficiency and Exhaust Temperature Requirement for Reforming of n-Heptane

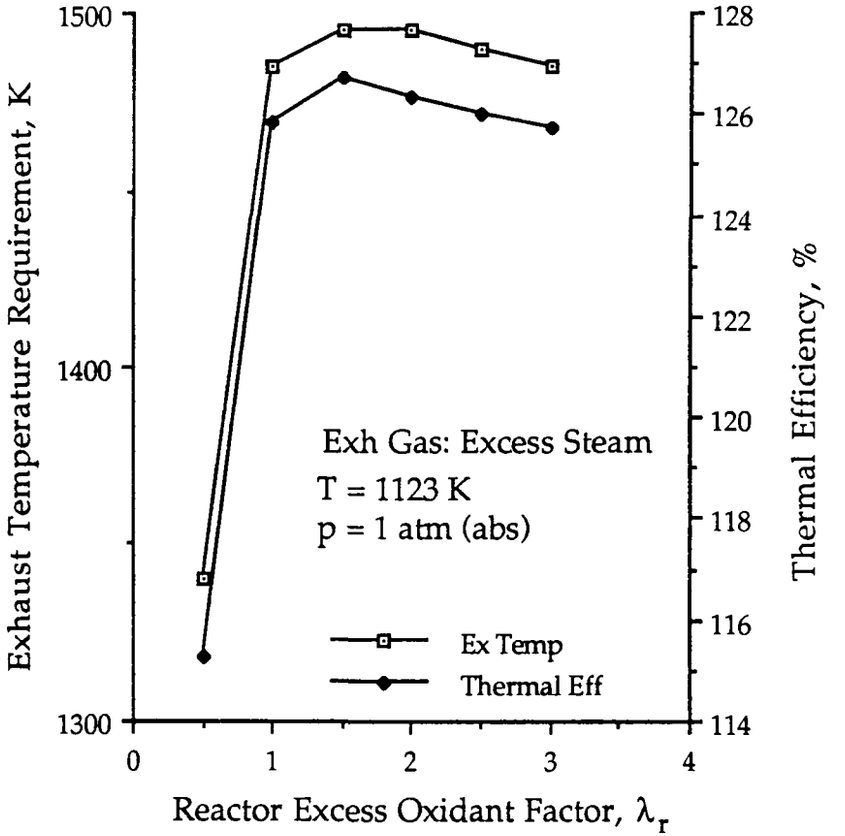


Fig 5.9b

Plot of Equilibrium Composition for Exhaust Reforming of n-Heptane

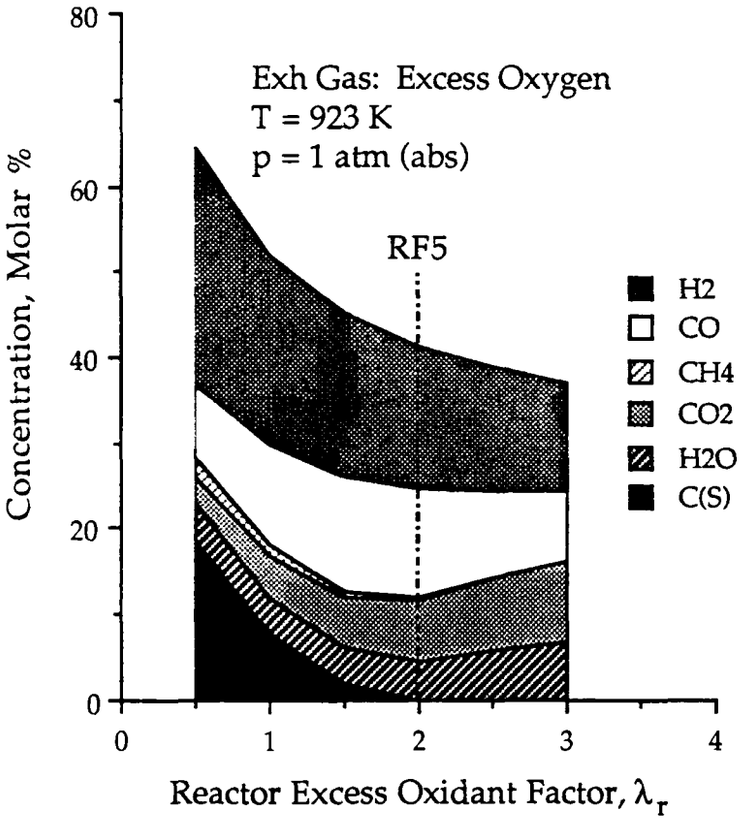


Fig 5.10a

Plot of Reactor Thermal Efficiency and Exhaust Temperature Requirement for Reforming of n-Heptane

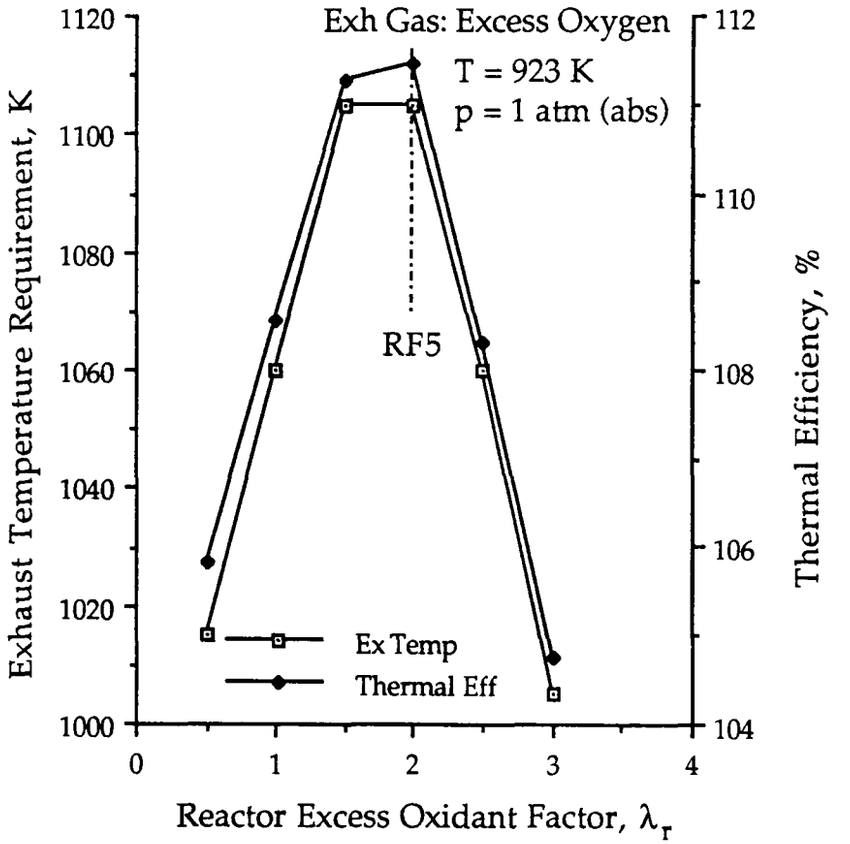


Fig 5.10b

Plot of Equilibrium Composition for Exhaust Reforming of n-Heptane

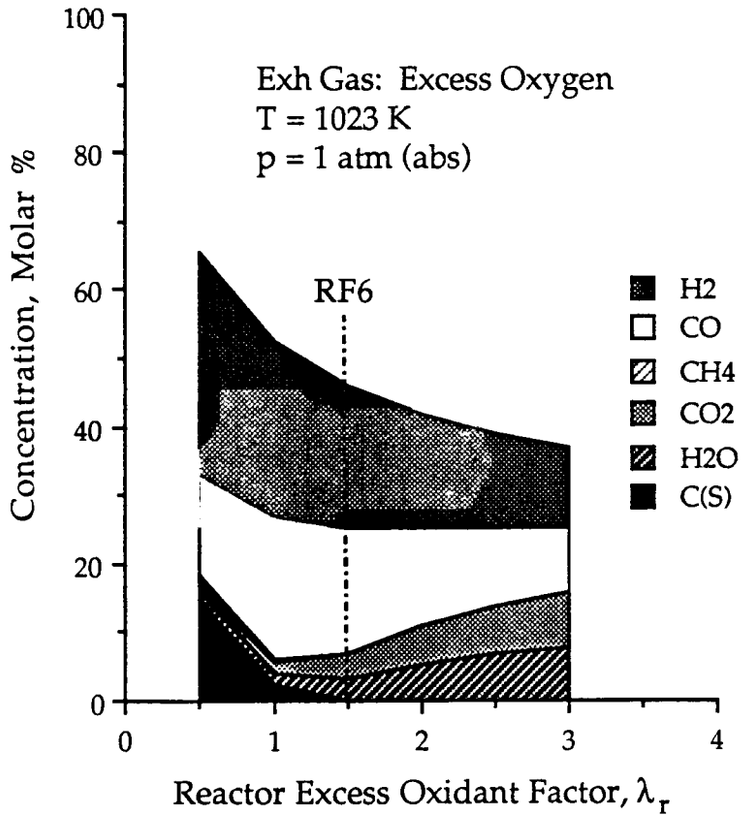


Fig 5.11a

Plot of Reactor Thermal Efficiency and Exhaust Temperature Requirement for Reforming of n-Heptane

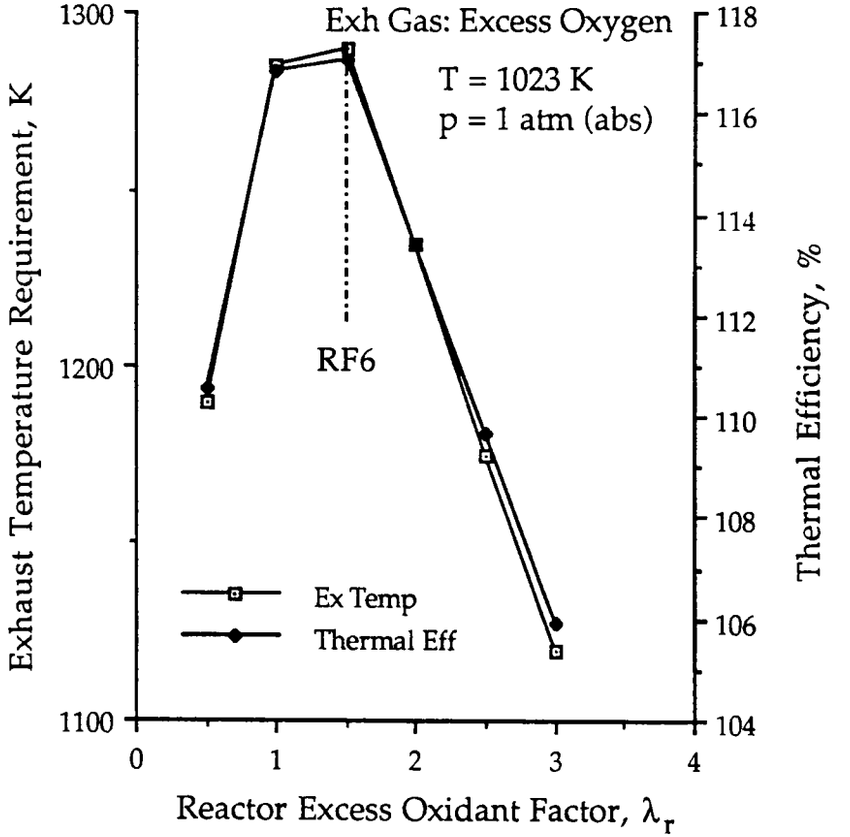


Fig 5.11b

Plot of Equilibrium Composition for Exhaust Reforming of n-Heptane

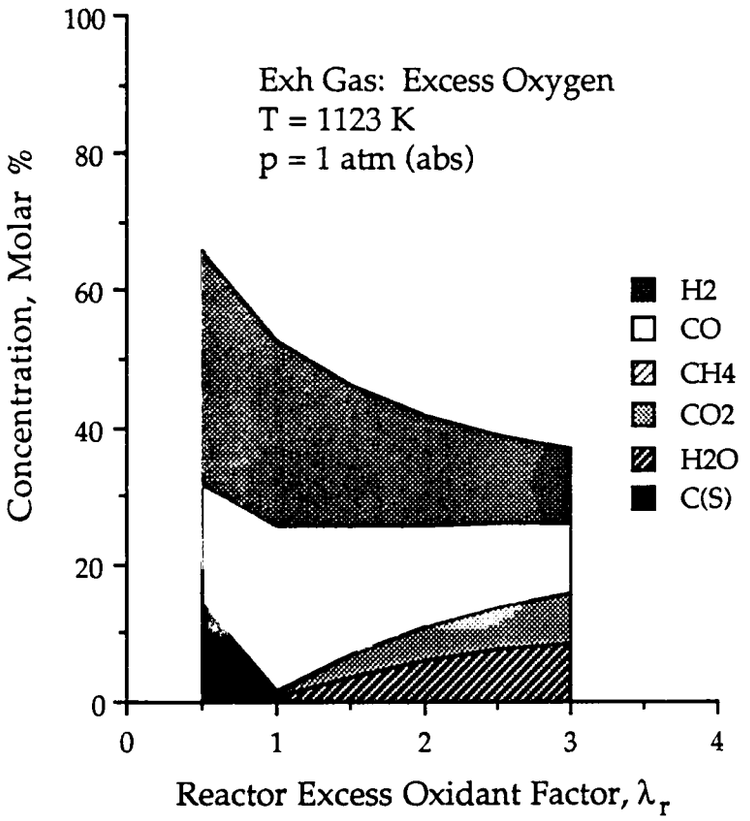


Fig 5.12a

Plot of Reactor Thermal Efficiency and Exhaust Temperature Requirement for Reforming of n-Heptane

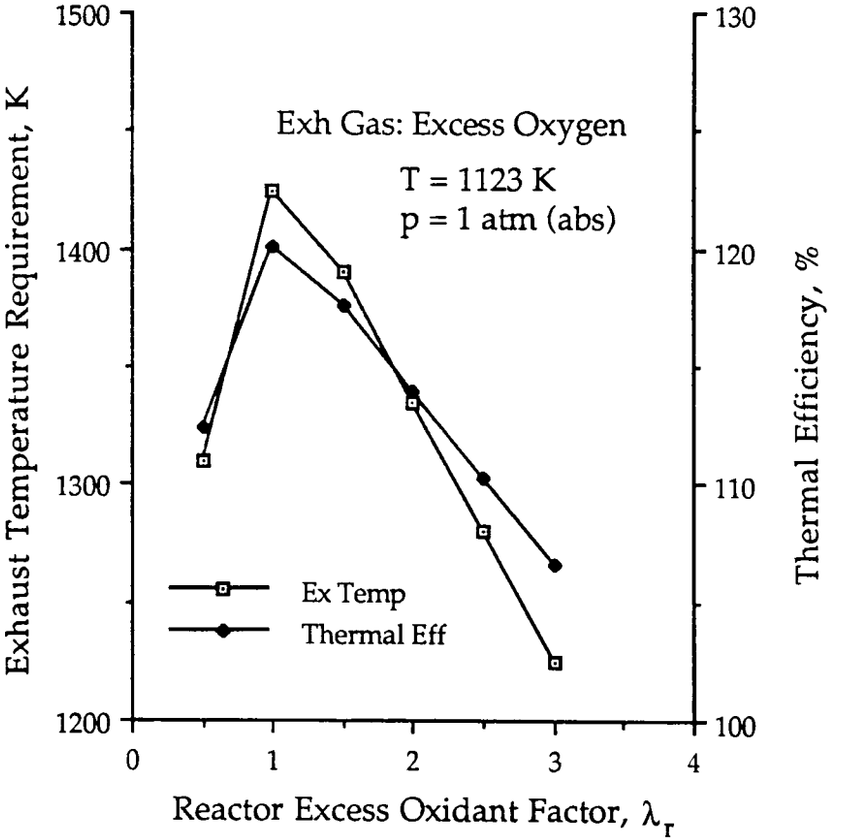


Fig 5.12b

Plot of Equilibrium Composition for Exhaust Reforming of n-Heptane

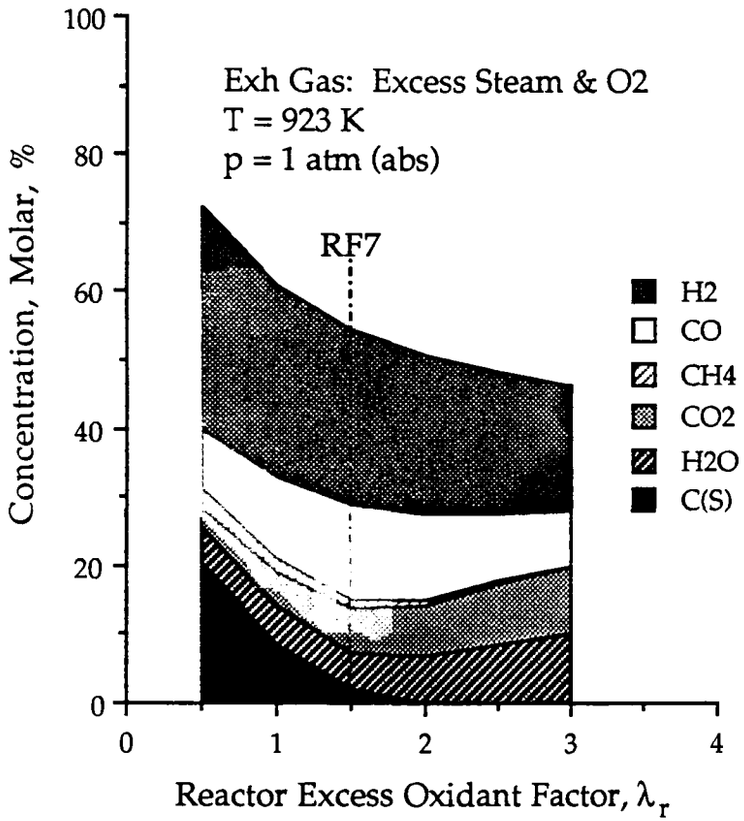


Fig 5.13a

Plot of Reactor Thermal Efficiency and Exhaust Temperature Requirement for Reforming of n-Heptane

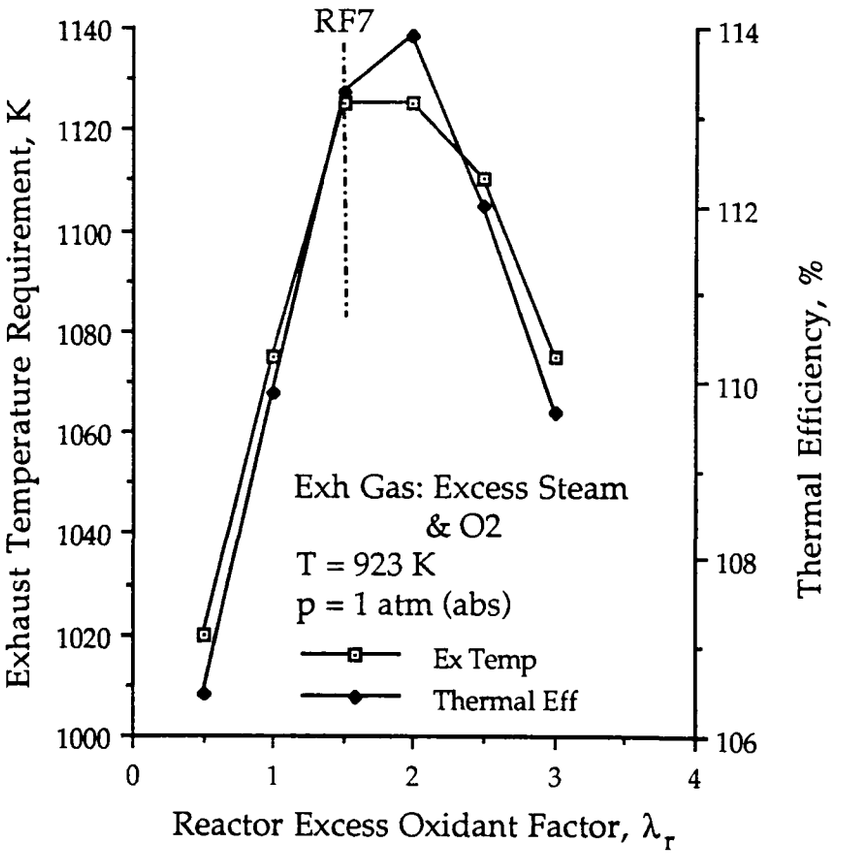


Fig 5.13b

Plot of Equilibrium Composition for Exhaust Reforming of n-Heptane

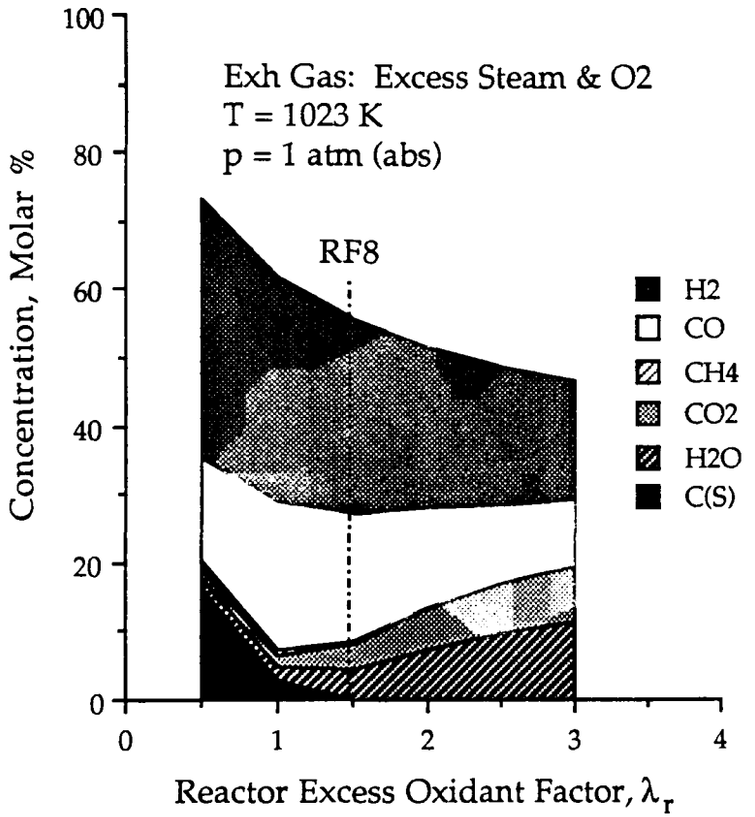


Fig 5.14a

Plot of Reactor Thermal Efficiency and Exhaust Temperature Requirement for Reforming of n-Heptane

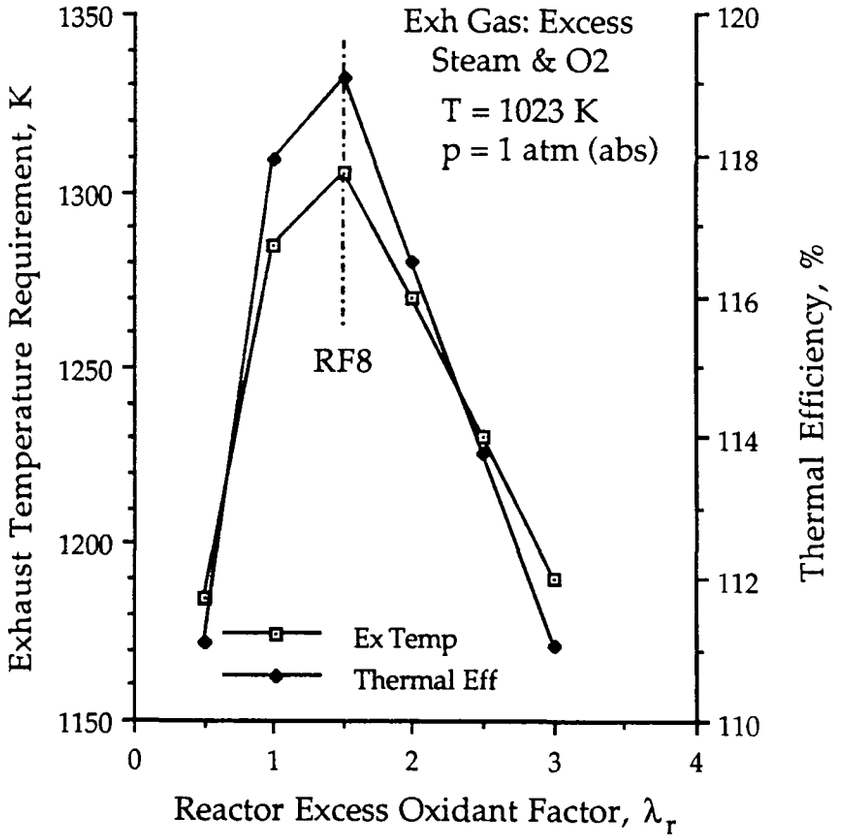


Fig 5.14b

Plot of Equilibrium Composition for Exhaust Reforming of n-Heptane

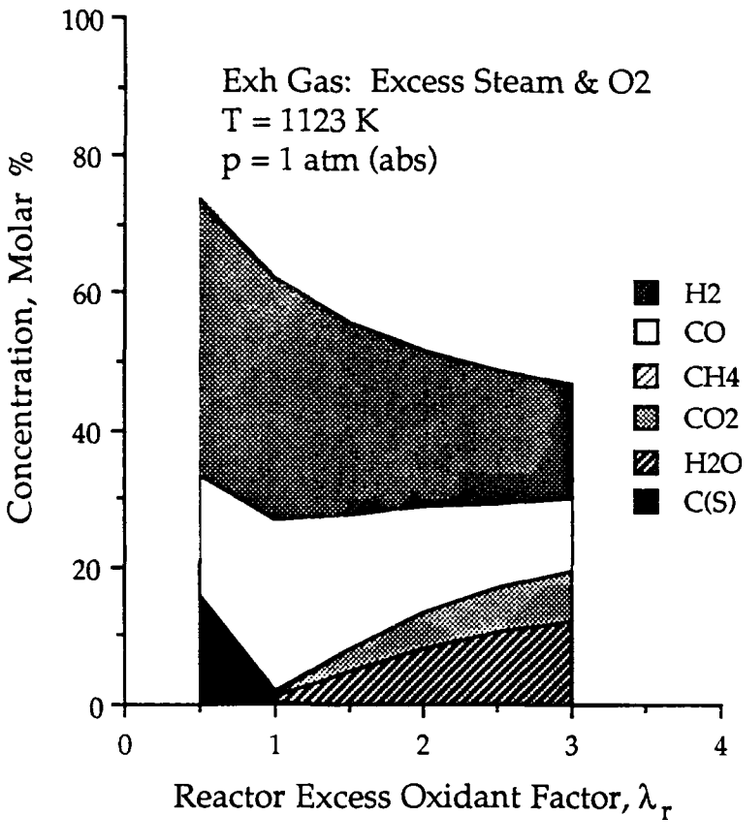


Fig 5.15a

Plot of Reactor Thermal Efficiency and Exhaust Temperature Requirement for Reforming of n-Heptane

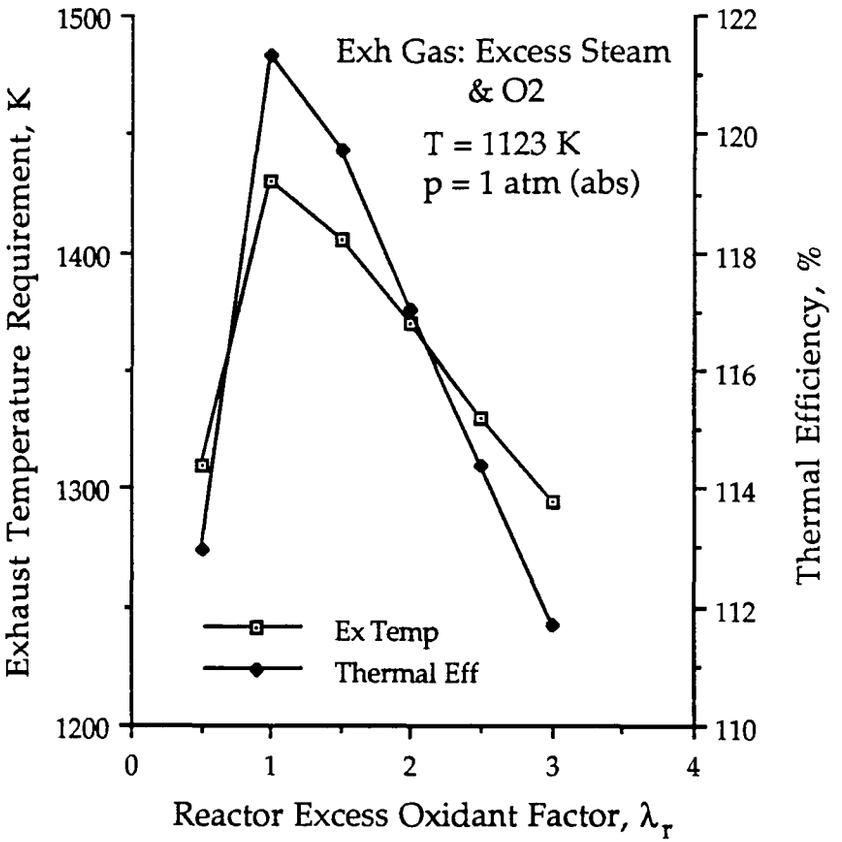


Fig 5.15b

Plot Showing Effect of Equilibrium Temperature on Reforming Equilibria for Methanol

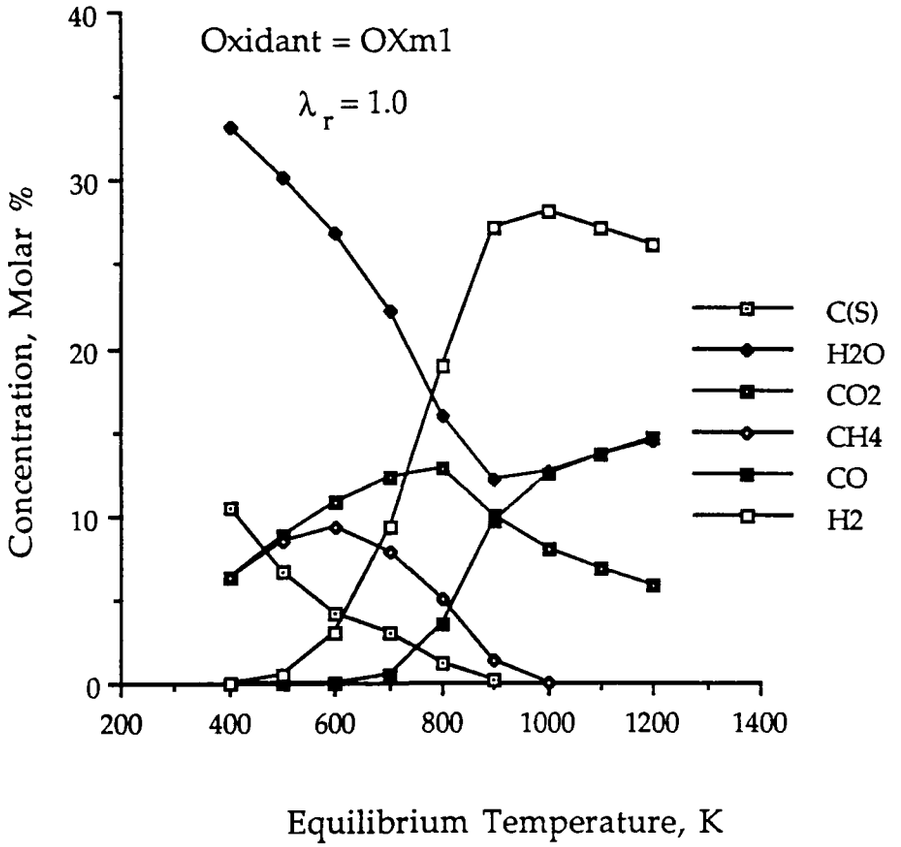


Fig 5.16a

Plot of Reactor Thermal Efficiency and Exhaust Temperature Requirement for Reforming of Methanol

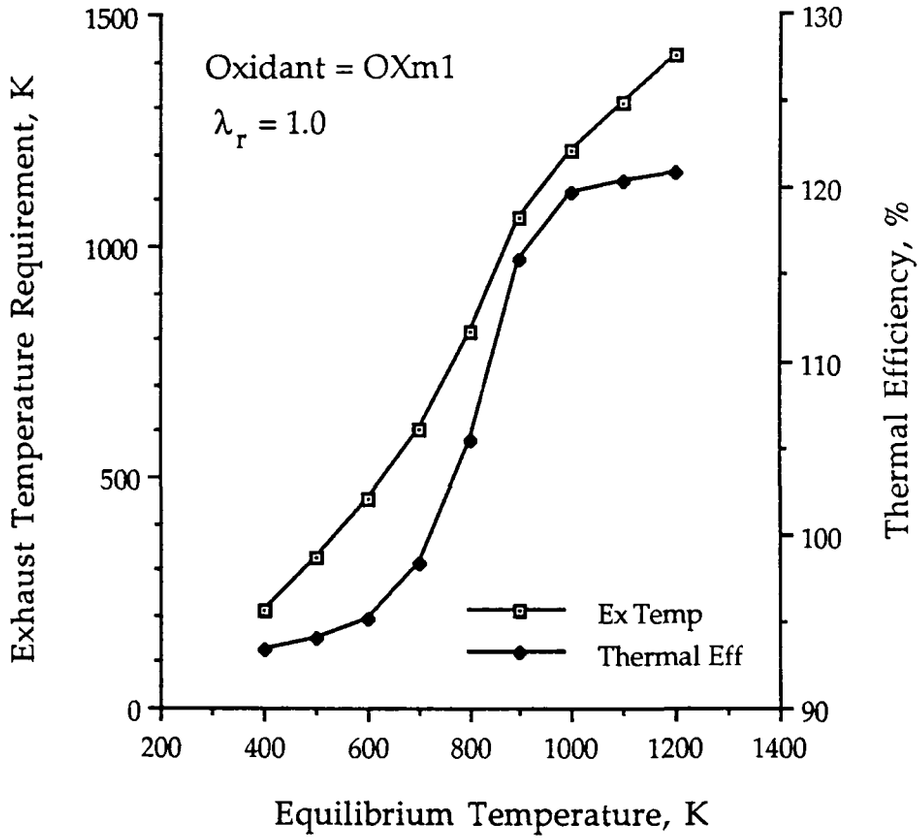


Fig 5.16b

Plot of Equilibria for the Reforming of Methanol at 700K

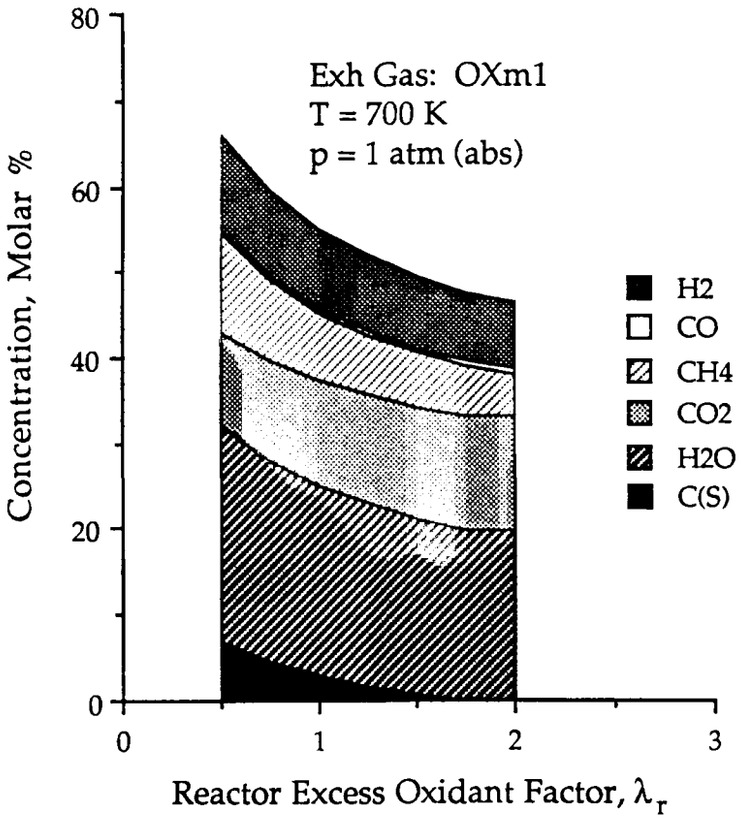


Fig 5.17a

Plot of Efficiency and Temperature Requirement for the Reforming of Methanol at 700K

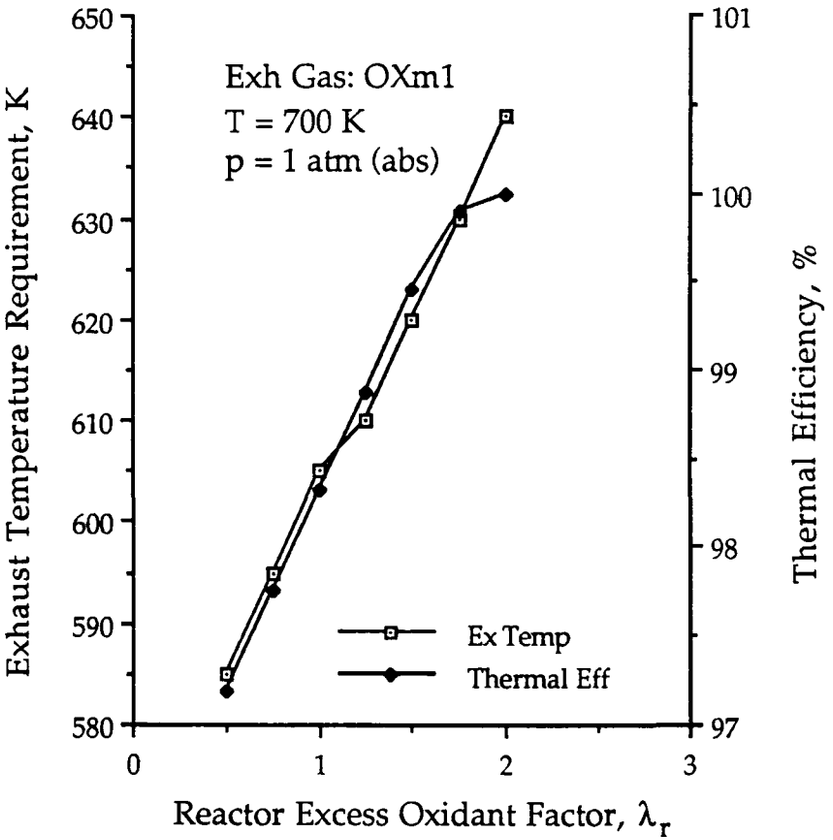


Fig 5.17b

Plot of Equilibria for the
Reforming of Methanol at 800K

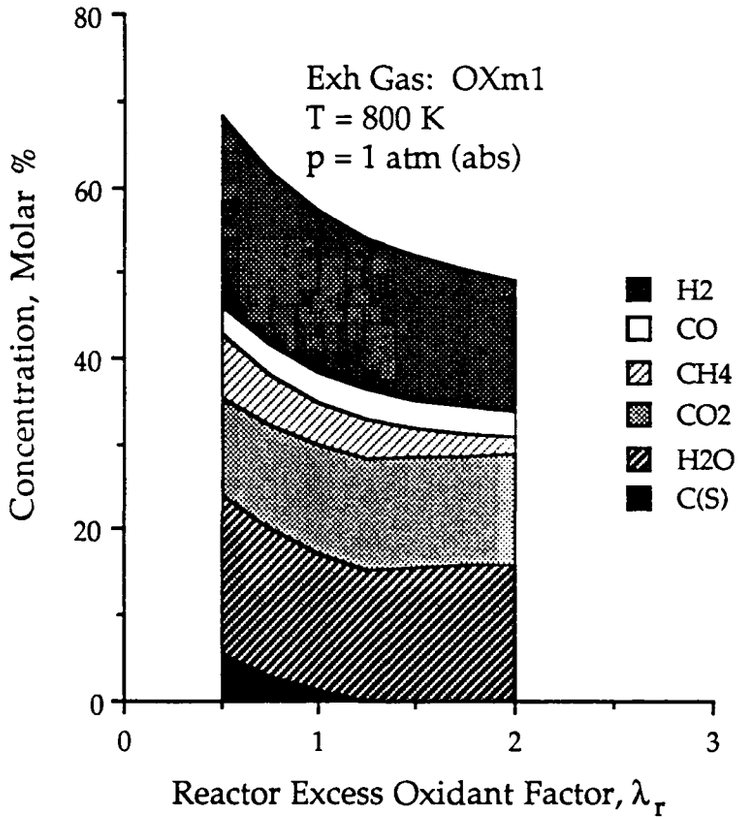


Fig 5.18a

Plot of Efficiency and Temperature Requirement
for the Reforming of Methanol at 800K

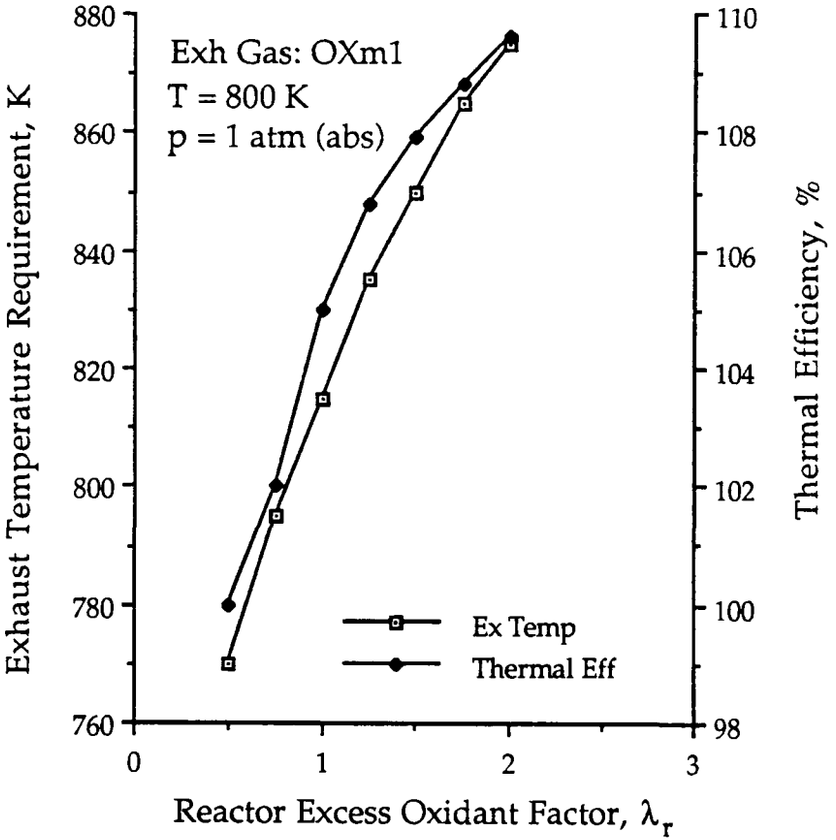


Fig 5.18b

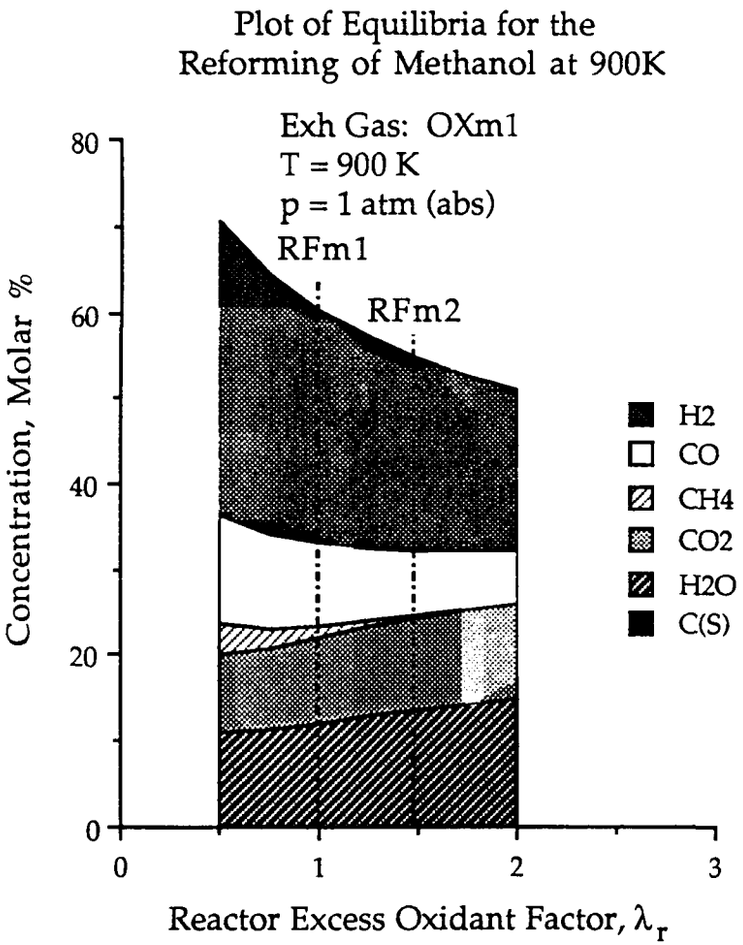


Fig 5.19a

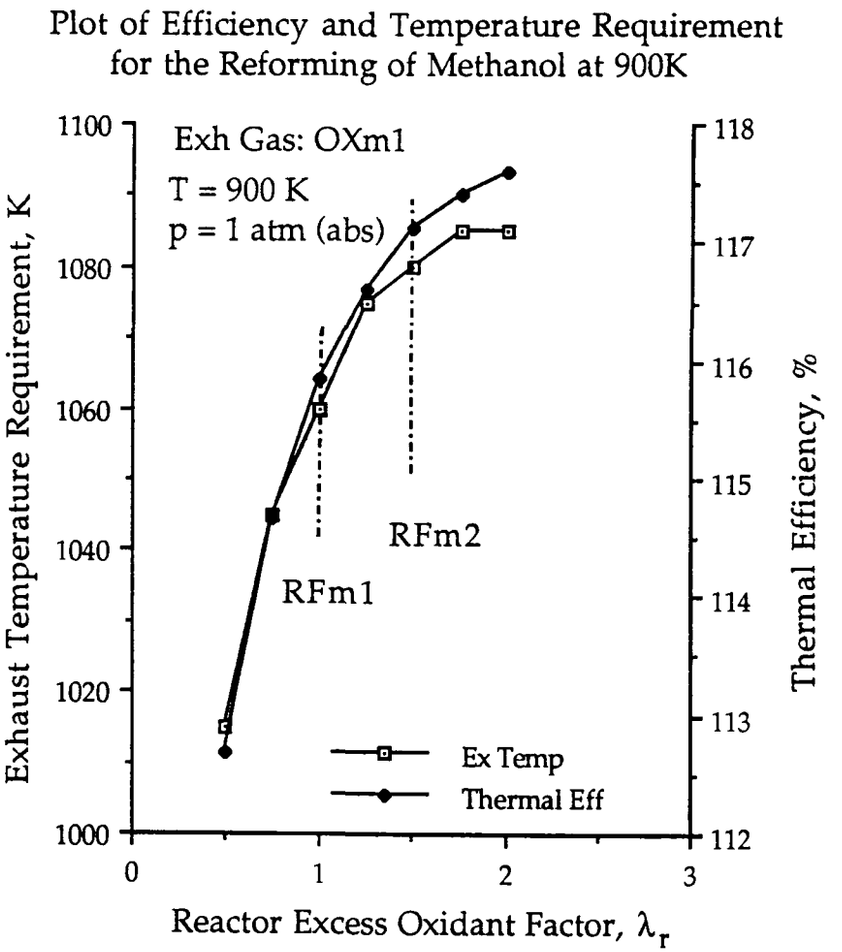


Fig 5.19b

Plot of Equilibria for the
Reforming of Methanol at 1000K

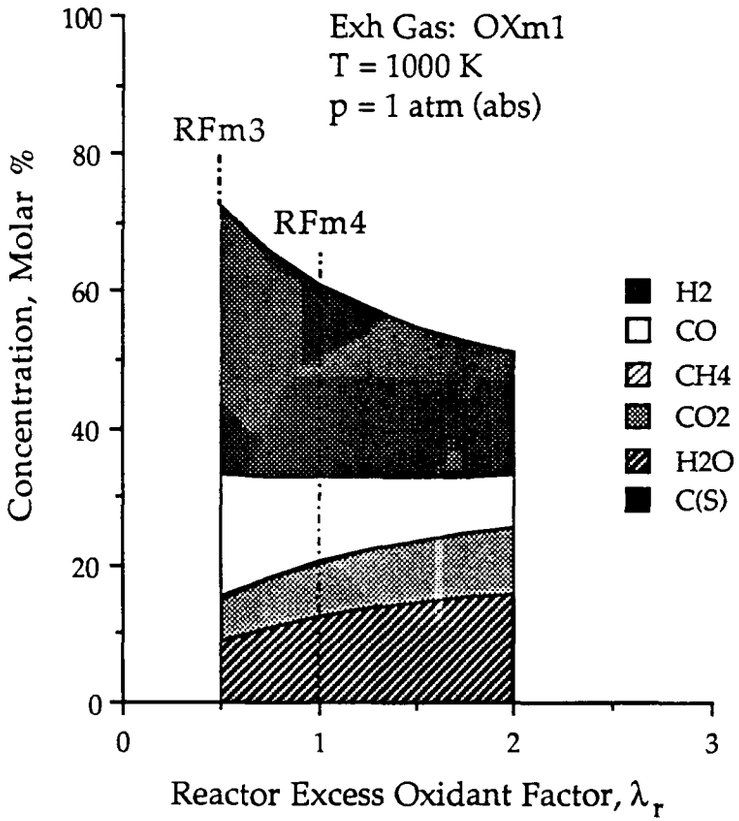


Fig 5.20a

Plot of Efficiency and Temperature Requirement
for the Reforming of Methanol at 1000K

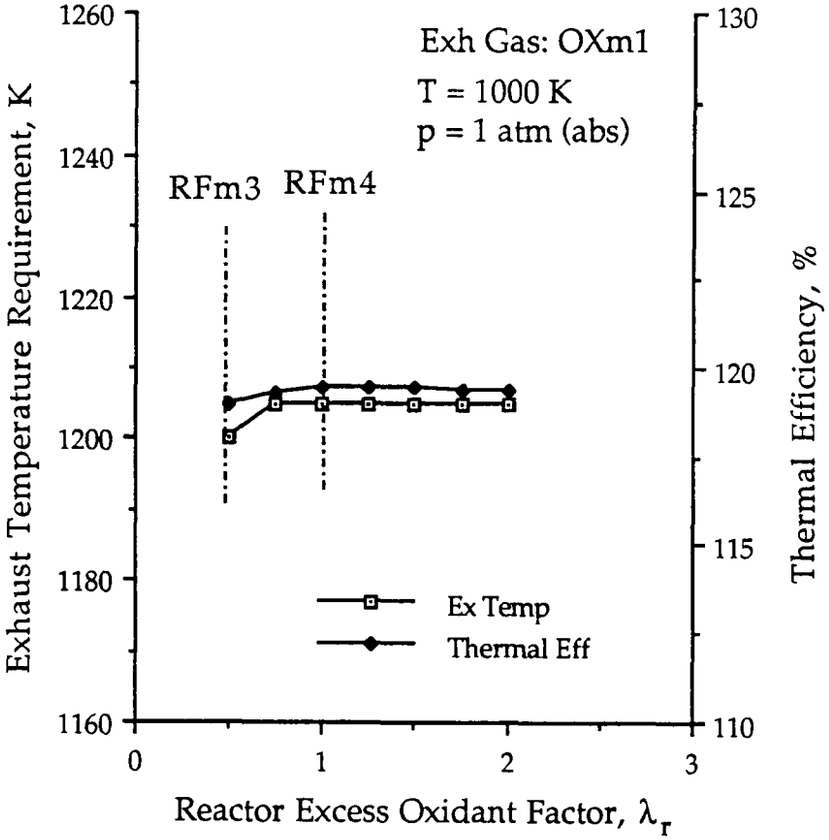


Fig 5.20b

# 6 THEORETICAL ENGINE CYCLE ANALYSIS INVESTIGATION USING CONVENTIONAL AND EXHAUST-GAS REFORMED FUELS

Towards the end of the previous chapter a number of predicted reformed n-heptane and methanol fuels were selected for examination using engine cycle analysis software. The prime objective of this exercise is to predict and compare engine performance in terms of power output and thermal efficiency for both standard and gaseous reformed fuels.

An important preliminary part of the exercise is to establish the levels of pressure charge which are required in order to aspirate representative quantities of the reformed fuel/air charge. It will be appreciated that if engine operation is to be compared on both standard and reformed fuels at a constant level of feed fuel consumption, a certain amount of pressure-charging will inevitably be required by the relatively low-density reformed fuel/air charge.

Another important aspect of the study relates to the laminar flame speed or burning velocity of the various fuel/air charges. The simulation software requires that burn duration, $\theta_b$, is specified in terms of crank angle degrees elapsing between start and end of combustion. This variable has a fundamental effect on the cycle simulation with, for example, low values of $\theta_b$ corresponding with fast flame speeds, leading to a potential for relatively high cycle efficiencies as the process tends towards the theoretically ideal case of constant volume combustion.

A further objective of the cycle analysis work is the prediction of reformed fuel/air combustion product temperatures, thus establishing the feasibility of sustaining reforming reactions by means of heat recovery from the hot engine exhaust gases.

## 6.1 Description of Engine Cycle Analysis Software.

The engine cycle analysis software used was written earlier by post-graduate students working within the Department of Mechanical Engineering at Birmingham (84); the code is written in Turbo Pascal and is based on a number of FORTRAN routines given by Ferguson (85). The general technique used to simulate the compression/heat release/expansion cycle of the four-stroke engine involves the solution of differential equations describing rate of change of cylinder pressure with respect to crank angle. These equations are used in conjunction with functions which describe the assumed heat release and heat and mass loss from the cylinder.

Chemical equilibria sub-routines based on equilibrium constant data compute the composition of the cylinder contents for each increment of crank angle, ensuring that thermodynamic properties are correctly assigned for the gas mixture, and cylinder volume is related to crank angle by the full form of the volume equation. The cosine burn law is assumed by Ferguson to describe the fractional heat release in terms of crank angle, and has also been adopted in the current work.

Prior to proceeding with the definition of engine modelling parameters, it was apparent that certain software modifications should be carried out. Firstly, a minor change in the structure of a nested iteration loop was implemented, reducing the run-time of a cycle simulation from around 4 hours on the Olivetti M24 PC to just 5 minutes on an Amstrad PC2286/40, with no significant effect on accuracy. Other enhancements included the addition of code to down-load cycle results to a data file compatible with a graphics package which had been written earlier by an undergraduate student (86). This modification has since been superseded by software which creates a

data file compatible with an Apple Macintosh text-translation application, enabling cycle data to be post-processed in the Macintosh Cricket Graph spreadsheet environment.

Finally, equilibria and gas property routines were enhanced in order that the combustion of reformed fuel gas mixtures could be simulated. In its original form the software was only able to handle standard fuels such as gasoline, methanol and diesel.

### 6.2 Assignment of Geometric, Heat and Mass Loss Parameters

Consideration has to be given to the form the combustion model should take, with respect to engine geometry and heat and mass transfer characteristics. After some deliberation, it was decided that a 'square' cylinder bore to stroke ratio and a compression ratio of 10:1 would be representative of a modern four-stroke engine. The cylinder wall temperature and piston blow-by variables were unchanged from those used by Ferguson, as listed below, whilst the cylinder gas-to-wall heat transfer coefficient was determined by means of a trial and error technique. It was found, after a number of program runs, that a heat transfer coefficient value of 1500W/$m^2$K appeared to give representative peak and expansion stroke pressures and temperatures for the combustion of gasoline, idealized for the purpose of this exercise as $C_7H_{17}$, at a simulated engine speed of 4000 rev/min. Predicted indicated mean effective pressure (IMEP) was also representative of levels observed from modern automotive engines.

. Modelling parameters chosen to describe the engine are thus as follows: (see over)

| | |
|---|---|
| Compression ratio ... ... ... ... ... | 10:1 |
| Engine Speed ... ... ... ... ... | 4000 rev/min |
| Piston Stroke ... ... ... ... ... | 90.00 mm |
| Cylinder Bore ... ... ... ... ... | 90.00 mm |
| Con-rod Length ... ... ... ... ... | 180.00 mm |
| Cylinder Wall Temp ... ... ... ... | 420K |
| Gas-to-Wall Heat Transfer Coefficient ... ... | $1500 W/m^2K$ |
| Cylinder Blow-by Coefficient ... ... ... | $0.8\ s^{-1}$ |
| Inert Residual Mass Fraction ... ... ... | 0.1 |

### 6.3 Assignment of Initial Pressure Conditions

In the case of the standard n-heptane and methanol fuels, initial pressure and temperature conditions were set to 1 bar and 350K respectively, thus simulating full-throttle operation with good cylinder filling.

In the case of the reformed fuel/air charge, however, it is apparent that the stoichiometry and molecular properties differ considerably from those of the standard fuels, meaning that the initial conditions must be modified if the two fuelling strategies are to be compared at a constant level of feedstock consumption. The stoichiometry of the reforming process dictates that a greater mass of fuel and air, and a far greater volume when considered under standard conditions, needs to be charged into the cylinder if a constant level of feedstock consumption is to be maintained for reformed fuel combustion as compared with the standard fuel case.

To illustrate, considering stoichiometric masses given in the idealized equation, eqn 3.1, we see that 1kg of n-heptane can be burned directly with 15.1kg of air to give a total charge mass of 16.1kg. Alternatively, if 1kg of n-

heptane is reformed stoichiometrically with 7.57kg of exhaust-gas oxidant as shown in eqn 3.2, and the fuel thus produced burned with its stoichiometric mass of air, (again 15.1kg) the total charge mass is 23.67kg. This gives a detrimental mass ratio of 1.47:1, and the problem is further exacerbated by the relatively low density of the reformed fuel charge, which results in a molar charge ratio of 1.76:1 when the two fuelling strategies are compared on a constant feed flow-rate basis.

Consequently, the initial charge pressure required in order to maintain the baseline-case feedstock consumption has to be calculated for each reformed fuel charge, in order that direct comparisons of the two fuelling modes can be made. The calculation is based on perfect gas law approximations, and it is assumed that the initial volume and temperature of the cylinder contents are constant, regardless of fuel type. Using subscripts 's' to denote a standard n-heptane/air charge and 'r' to denote the reformed fuel/air charge, the following relationships can be written:

$$PV = nR_oT \tag{6.1}$$

$$\frac{V}{T} = \frac{nR_o}{P} \tag{6.2}$$

and, as $V_r = V_s$ and $T_r = T_s$, it follows that:

$$\frac{n_rR_o}{P_r} = \frac{n_sR_o}{P_s} \tag{6.3}$$

and hence: $$\frac{P_r}{P_s} = \frac{n_r}{n_s} \tag{6.4}$$

Note that in the above equations, $n_s$ is the number of moles of n-heptane/air mixture for the stoichiometric combustion of a particular mass of

n-heptane. $n_r$ is then the number of moles of reformed fuel/air mixture required for the stoichiometric combustion of that quantity of reformed fuel produced by reforming the same particular mass of n-heptane feedstock.

The pressure ratio required to maintain constant feedstock consumption thus reduces to a ratio of the number of moles of the two stoichiometric mixtures, and as $P_s$, the initial pressure of the naturally aspirated n-heptane charge, was set to 1 bar throughout the baseline cycle analysis work, the level of pressure charge required to aspirate all of the reformed fuel/air charge is simply equal to $n_r/n_s$ bar. The calculated values of $P_r$ for each reformed fuel charge are shown in Table 6.1.

## 6.4 Assignment of Burn Duration Parameter, $\theta_b$

### 6.4.1 The Relevance of Laminar Flame Speed

In order that the respective burn duration and commencement parameters, $\theta_b$ and $\theta_s$, can be correctly assigned, it is apparent that some knowledge of the fuel/air flame propagation process is required. Although combustion within the engine is an inherently turbulent process, it is suggested that knowledge of a mixture's laminar flame speed gives a useful indiciation of burn duration in the engine cylinder (87).

Laminar flame speed data for the standard fuels of interest can be found in a variety of sources, some of which quote maximum flame speeds, which generally occur at air to fuel ratios considerably richer than stoichiometric, with other sources giving flame velocities under stoichiometric conditions, which are of more interest in the current work (88, 89). Stoichiometric laminar flame speed values of 39.7 cm/s for n-heptane

and 41.8 cm/s for methanol were chosen as being most representative of the somewhat scattered values found in the literature. The value for n-heptane is derived from a quoted maximum flame speed of 40.4 cm/s (90) corrected to a stoichiometric velocity using a simple equation presented by Metghalchi and Keck (91).

The combustion of n-heptane was designated the overall baseline case, and respective values of $\theta_b$ and $\theta_s$ of $60^\circ$ and $-30^\circ$ were assigned for the stoichiometric combustion of this fuel. Hence, the burn duration of $60^\circ$ commences $30^\circ$ before top dead centre (BTDC) and is thus centred around TDC of the simulated firing stroke. All other fuels will have $\theta_b$ and $\theta_s$ values related to those of n-heptane by the following expressions:

$$\theta_{b_i} = \theta_{b_{hep}} * \left[\frac{1}{\left(\frac{S^o_{l_i}}{S^o_{l_{hep}}}\right)}\right] \tag{6.5}$$

$$\text{and } \theta_{s_i} = -\left[\frac{\theta_{b_i}}{2}\right] \tag{6.6}$$

where $S^o_{l_{hep}}$ and $S^o_{l_i}$ are respective laminar flame speeds of heptane and fuel 'i', and the ratio $\frac{S^o_{l_i}}{S^o_{l_{hep}}}$ is defined as the relative flame speed, $S^o_{l_{i(Rel)}}$ of fuel 'i' as compared with n-heptane.

In the case of methanol, this gives:

$$S^o_{l_{i(Rel)}} = 41.8/39.7 = 1.053$$

$$\theta_{b_i} = 60^\circ * \frac{1}{1.053} = 56.98^\circ$$

$$\text{and } \theta_{s_i} = 28.49^\circ$$

Flame speeds of reformed fuels will also be related back to n-heptane in the same way, enabling $\theta_b$ and $\theta_s$ to be properly assigned for each fuel. The problem with the reformed fuels, however, lies in establishing the laminar flame speeds of the mixtures of different combustible gases and inert diluents. In the case of the standard fuels, the $S_{l_i}^o$ values can be read directly from tables, but for the reformed fuels, a more involved approach has to be adopted.

### 6.4.2 Prediction of Laminar Flame Speeds for Gas Mixtures

In a study of laminar flame speed for mixtures of hydrocarbon and hydrogen combustibles in air, Milton and Keck state that there is no simple relationship between burning velocity and any physical parameter such as H-atom fraction or overall hydrogen to carbon ratio (92). Furthermore, it is concluded that the laminar burning velocity of combustible gaseous fuel mixtures is a complex phenomenon requiring fundamental investigation. Significantly, however, it was found that in a mixture of two gases having widely differing flame speeds, the slower burning constituent appears to dominate the reaction, as measured velocities are considerably less than those calculated on a simple averaging basis.

In the case of the reformed fuels predicted in the current work, combustible components are hydrogen, carbon monoxide and methane, with the latter present in concentrations of around 1.0% vol. or less. There is also a significant inert fraction comprising nitrogen, carbon dioxide and water, which would have a considerable effect on flame velocity.

Hydrogen has a maximum flame speed of around 291 cm/s, and has been widely used in fuel enrichment studies as a means of increasing mixture flame velocity and/or lean flammability limit (5, 13, 18, 19). Contrary to the

findings of Milton and Keck, Yu et al established a linear correlation between hydrogen fraction and flame speed in studies of hydrocarbon/air mixtures with hydrogen addition. This work is of particular interest in the current project, where it is proposed that such a correlation might enable the prediction of reformed fuel laminar flame speeds (93).

Yu et al present equations for calculating flame speeds of mixtures of methane or propane with hydrogen in terms of the standard fuel's burning velocity and the level of hydrogen addition. These equations are used by Sher and Hacohen (19) in their work on hydrogen enrichment modelling, in conjunction with equations describing the effect of inert diluents presented by Metghalchi and Keck (91); the same approach is adopted in the current work.

### 6.4.3 Laminar Flame Speeds of Reformed Fuels

For the purpose of reformed fuel laminar flame speed predictions, the gas mixtures will be considered as consisting of a carbon monoxide combustible enriched with hydrogen, and diluted by a certain mass fraction of inert components. Any methane can justifiably be lumped together with the carbon monoxide in this exercise, as the methane fractions are relatively small, and any effect on flame speed would tend to be swamped by the slower-burning carbon monoxide.

#### 6.4.3.1 The Effect of Inert Diluents

The effect of inert diluents has been studied widely (94, 95), and as outlined above, the approach presented by Metghalchi and Keck will be adopted here. In this study, the effect on flame speed of *residual* inerts existing within the engine cylinder will be ignored, as the effect of such

diluents will be kept constant throughout the combustion simulations by fixing the engine residual mass fraction variable of the cycle analysis software at 0.1. It is the effect of the *intrinsic diluents* contained within the fresh fuel/air charge which is of primary interest here.

Firstly, consider the simple stoichiometric equation for the combustion of carbon monoxide in air:

$$CO + 0.5(O_2 + 3.76N_2) \rightarrow \text{Products}$$

Taking masses on the left-hand side we find that the inert mass fraction, which in this case consists solely of air-borne nitrogen, is 0.545 relative to the total charge. Considering now the stoichiometric combustion of the idealized reformed n-heptane fuel given in eqn 3.3 we have:

$$10.29CO + 11.76H_2 + 19.44N_2 + 11.03(O_2 + 3.76N_2) \rightarrow \text{Products}$$

which has a total inert nitrogen fraction of 0.719. It is thus apparent that the reformed fuel charge has a much higher diluent fraction than the pure CO charge, and it is this difference which must be accounted for.

It is proposed that the difference should be accounted for by subtracting the standard-case inert fraction of 0.545 from that calculated for the reformed fuel charge. Thus an inert mass fraction parameter $f$ is defined as zero for pure CO combustion in air, and is 0.174 for the idealized reformed fuel above. This methodology is applied to all of the predicted reformed n-heptane fuels, and gives values of $f$ ranging from 0.199 to 0.262.

The flame speed of a carbon monoxide and air mixture containing a mass fraction $f$ of diluents is then calculated using the following equation presented by Metghalchi and Keck:

$$S^{o}_{L(f)} = S^{o}_{L} * (1 - 2.1f) \tag{6.7}$$

where $S^{o}_{L}$ is the standard, undiluted flame speed, and $S^{o}_{L(f)}$ is the calculated value with diluents. The equation is derived from work which used a diluent comprising 85% nitrogen and 15% carbon dioxide, which has similar molecular mass and heat capacity properties to the inert fraction of the reformed fuel/air charge.

### 6.4.3.2 The Effect of Hydrogen Addition

Yu et al found a linear correlation between hydrogen fraction and laminar flame speed in studies of hydrocarbon/air mixtures with hydrogen addition. Although no reference is made to the combustion of carbon monoxide in the presence of hydrogen, it will be assumed that the process would be similar to that for the light hydrocarbons studied. The equation presented, which enables the calculation of laminar flame speed for a mixture of a single fuel, hydrogen and air, is as follows (93):

$$S^{o}_{L(H)} = S^{o}_{L} + \alpha R_H \tag{6.8}$$

where $\alpha$ is an empirically-derived constant which quantifies the effect that hydrogen addition has on the laminar flame speed of the mixture, and $R_H$ is defined as the relative amount of hydrogen addition. In the current work, $\alpha$ will be set to 80 cm/s which was found by Yu et al to represent light hydrocarbons such as methane, and $R_H$ is defined as follows: (see over)

$$R_H = \frac{C_H + C_H/(C_H/C_A)_{st}}{C_F + [C_A - C_H/(C_H/C_A)_{st}]} \qquad (6.9)$$

where, using the notation of Ref 93, $C_F$, $C_H$ and $C_A$ are the mole fractions of fuel, hydrogen and air respectively, and $(C_H/C_A)_{st}$ is the stoichiometric molar air to fuel ratio for hydrogen.

All that remains to be done in order to calculate reformed fuel laminar flame speeds is to write out the stoichiometric equations for each fuel in order to determine values of $f$, $C_H$, $C_F$ and $C_A$, and to determine the laminar flame speed of pure carbon monoxide.

#### 6.4.3.3 Calculation of Reformed Fuel Laminar Flame Speeds

Bradley states that it is difficult to establish a carbon monoxide oxidation flame, even in the presence of pure oxygen, if the reactants are completely dry, but that a small trace of water in the mixture can increase the flame speed by a factor of around 8 (96). Several other workers have studied this 'catalytic' effect which water has on the oxidation of CO and, in the case of reformed fuels which will invariably contain quantities of water, it is apparent that the effect is important (97, 98, 99). Data given by Lewis and von Elbe has been selected for the standard flame speed of CO here, which gives a value of 21.0 cm/s (100). This is the flame speed for the oxidation of CO gas containing 1.35% water in air, and it is felt that this level of water 'catalyst' effect should be representative of reformed fuels.

The calculation of reformed fuel laminar flame speeds is thus performed using equations given above in the following sequence: (see over)

$S^{o}_{L(CO)} = 21.0$ cm/s (Std Flame Speed of CO with small amount of $H_2O$) (6.10)

$S^{o}_{L(f)} = 21.0 * (1 - 2.1 f)$ (CO Flame Speed in cm/s with Diluents) (6.11)

$S^{o}_{L(f, H)} = S^{o}_{L(f)} + 80R_H$ (CO Flame Speed with Diluents & $H_2$) (6.12)

The burn duration crank angle, $\theta_b$, can then be calculated for each fuel using eqn 6.5, where $S^{o}_{Li} = S^{o}_{L(f, H)}$. Laminar flame speed and burn duration values thus derived for the two standard fuels and the total of twelve selected reformed fuels are presented in Table 6.2.

## 6.5 Cycle Simulation for n-Heptane Fuels

### 6.5.1 Standard n-Heptane

Having defined the physical parameters of the model, and established a strategy for describing the likely effect of fuel composition on flame speed and hence burn duration, the initial baseline simulation run on n-heptane can be conducted. It is appreciated that pure n-heptane would not usually be regarded as a suitable motor fuel, as by definition it has an octane number of zero and is used as a primary reference fuel in octane requirement studies. However, the cycle analysis software takes no account of a fuel's octane number, and is unable to model or recognize charge detonation. As n-heptane has heat release, flame speed and general thermodynamic properties in line with 'typical' gasolines, it can be used in the baseline combustion simulation exercise. This is desirable, as the objective of the study is to directly compare performance of the reformed n-heptane fuels with the unmodified liquid hydrocarbon feedstock.

As mentioned earlier, initial temperature and pressure conditions were set to 350K and 1 bar respectively, with a $\theta_b$ burn duration value of 60° for the standard n-heptane simulation. $\theta_s$, crank angle at commencement of heat release, is set at -30°, which is in effect the ignition timing of the simulated cycle. Pressure and burned-gas temperatures of the baseline run are plotted against crank angle $\theta$ in Figs 6.1 to 6.8 together with the results for the eight reformed fuels. In addition, discrete results of particular interest are given in Figs 6.10 to 6.13.

### 6.5.2 Procedure for Reformed n-Heptane Fuels

As outlined earlier in this chapter, various levels of initial pressure condition and burn duration parameter had to be calculated for each reformed fuel prior to commencement of this part of the study - the results of these calculations are summarized in Tables 6.1 and 6.2.

Cycle simulation runs were then conducted using the eight selected reformed n-heptane fuels (for compositions of these fuels see Fig A5.2). Initial temperature was set at 350K throughout, whilst initial pressures were set first at 1 bar and then at those levels of charge pressure required to maintain the same n-heptane consumption rate as in the baseline case. It was found that the naturally-aspirated trials gave a reduction in IMEP as compared with the baseline case, whilst the pressure-charged runs gave an improvement over baseline. On the basis of these results, a simple linear interpolation technique was applied, in order to calculate intermediate levels of initial pressure which should give similar reformed fuel cycle IMEP values to the standard-fuel baseline case. Simulation runs were then conducted for each of the eight reformed fuels at these intermediate levels of initial pressure.

The results of the work are presented as graphs of P-θ and T-θ, with reformed fuel plots overlaid on the n-heptane baseline cycle in each case for purposes of comparison. In addition, the most significant cycle results from the higher initial pressure conditions are again summarized in Fig's 6.10 to 6.13. Note that the bar chart of Fig 6.13 gives values for both overall and engine thermal efficiencies. The relevance of the two separate values is described in the discussion of the results.

At this stage it became apparent that a brief study of the effect of ignition timing should be undertaken; the reasons for this are also discussed below. Thus runs at $4^{\circ}$, $8^{\circ}$ and $12^{\circ}$ retarded from the calculated 'ideal' value were conducted using fuel RF7, from the higher level of initial pressure which gives constant feedstock consumption. The results of the exercise are given as plots of P-θ and T-θ in Fig 6.9.

### 6.5.3 Presentation of Results

The results of the cycle simulation study using n-heptane and the eight reformed n-heptane fuels are presented as follows:

| | Fig No |
|---|---|
| Simulation Cycle for RF1, $P_1$=1, 1.67, 2.23 bar | 6.1a, b |
| Simulation Cycle for RF2, $P_1$=1, 1.50, 2.01 bar | 6.2a, b |
| Simulation Cycle for RF3, $P_1$=1, 1.50, 2.00 bar | 6.3a, b |
| Simulation Cycle for RF4, $P_1$=1, 1.40, 1.81 bar | 6.4a, b |
| Simulation Cycle for RF5, $P_1$=1, 1.71, 2.05 bar | 6.5a, b |
| Simulation Cycle for RF6, $P_1$=1, 1.52, 1.86 bar | 6.6a, b |
| Simulation Cycle for RF7, $P_1$=1, 1.46, 1.65 bar | 6.7a, b |

| | |
|---|---|
| Simulation Cycle for RF8, $P_1$=1, 1.41, 1.74 bar | 6.8a, b |
| Simulation Cycle for RF7, $P_1$=1.65 bar, $\theta_s$= -6°, -2°, +2° | 6.9a, b |
| Bar Chart of Pressure Results and IMEP | 6.10 |
| Bar Chart of Peak and Exhaust-Gas Temperatures | 6.11 |
| Bar Chart of Cycle Heat Losses and Work Output | 6.12 |
| Bar Chart of Overall and Engine Thermal Efficiencies | 6.13 |

Note that Fig's 6.10 to 6.13 present results of reformed fuel cycle simulations from the higher level of initial pressure, ie at constant feedstock consumption. In addition, the most interesting results are tabulated in Appendix III, see Tables A6.1 and A6.2

### 6.5.4 Discussion of Results

The baseline cycle simulation using a pure n-heptane fuel gives an IMEP of 11.52 bar with maximum cycle pressure and temperature levels of 64.12 bar and 2863K respectively. This gives an indicated engine thermal efficiency value of 37.3% when work output is compared with cycle input, based on the fuel's higher heating value of 48.20 MJ/kg.

Again, comparing cycle work output with n-heptane input, reformed fuels 1 to 8 give significant improvements in overall thermal efficiency (see Fig 6.13). For a constant baseline level of fuel consumption, the overall thermal efficiency for RF2 is 51.2%, which represents the maximum predicted value, whilst RF7 gives the lowest reformed fuel level of 42.6%. It should be emphasized that these calculations are based on the cycle work output and n-heptane flow-rate and higher heating value at inlet to the reformer, and hence a large proportion of the improvement is a direct result of the increase in calorific value which occurs within the reformer itself. It is of interest to

eliminate this heating value effect and thus isolate specifically the *engine* thermal efficiency for operation on reformed fuels, and this is achieved by comparing work output with reformed fuel energy input. It is clear from Fig 6.13 that the resulting values of engine thermal efficiency are very similar for all reformed fuels, being in general slightly higher than the baseline n-heptane case. This indicates that improvements in overall thermal efficiency result not only from the improvement in fuel heating value in the reforming process, but also from a slightly more efficient combustion cycle.

The main reasons for this intrinsic improvement in cycle efficiency, which is over and above the effect of heating value improvements, are the reductions in burn duration and energy lost through cylinder-wall heat transfer. Cycle temperatures are invariably much lower for reformed fuel combustion than for standard n-heptane, and hence the temperature gradient which drives the heat transfer at the gas/cylinder wall interface is reduced throughout the cycle.

Heat loss and work output for the baseline and reformed fuel cycles are shown in Fig 6.12, for a constant level of feed fuel consumption, and it is clear that the ratio of work to heat loss is far superior in the case of the gaseous reformed fuels.

All reformed fuels give rather high peak cycle pressures when combusted from the higher pressure-charged initial conditions (see Figs 6.1 to 6.8). Levels range from 99.3 bar for RF7 (Fig 6.7a) to 120.5 bar for RF1 (Fig 6.1a), and it has to be said that these levels could not usually be tolerated in a real engine; in practice they would lead to very harsh engine operation, and, in all probability, uncontrolled combustion. The levels arise as a result of high

initial pressure conditions, and a relatively fast predicted flame speed in conjunction with near-optimum ignition timing.

Cycle runs at the intermediate levels of pressure boost, which enable a comparison of the two fuelling strategies at a constant work output level, give more acceptable peak pressures of around 85 to 90 bar, with overall system thermal efficiencies ranging from 42.2% for RF7 to 50.0% for RF2 and RF3. Again, these improvements result primarily from increases in fuel calorific value, as the respective engine thermal efficiencies are just 38.0 and 38.7%. These levels are still higher than the baseline, however, as a result of the lower relative levels of heat loss.

All naturally aspirated reformed fuel cycle simulations give substantial reductions in work output when compared to baseline, as a direct result of the inevitable reduction in feedstock consumption rate. IMEP values range from 6.32 bar for RF5 to 7.91 bar for RF4, representing reductions in indicated power of 45.1 and 31.3% respectively. Corresponding overall thermal efficiencies are 40.4 and 47.5% with respective engine efficiencies of 36.4 and 36.8%. It will be noted that these engine efficiencies are lower than the baseline level of 37.3%; this is a result of heat transfer losses becoming more significant as the initial pressure and hence reformed fuel charge mass reduce.

One of the most important aspects of the cycle simulation work is the prediction of exhaust-gas temperatures, and comparison with required levels predicted for the reforming reactions. Cycle temperature profiles for each fuel are shown in Fig's 6.1b to 6.8b, and are summarized for cycles having a constant level of feedstock consumption in Fig 6.11.

Combustion product temperatures existing at crank angles of 130 and 180 degrees after top dead centre (designated $T_{130}$ and $T_{180}$) are selected as being of interest, the former value representing a normal exhaust valve opening angle, and the latter signifying the end of the cycle. In the case of fuels RF1, 2, 3 and 4 it appears that temperature levels are not high enough to drive the reforming reactions. Taking the specific case of the combustion of RF4 from initial pressure conditions which give the baseline level of feedstock consumption, temperatures $T_{130}$ and $T_{180}$ are 1347 and 1199K respectively, which fall some way short of the predicted reformer requirement of 1395K. It must therefore be concluded that reforming with unmodified or steam-enriched exhaust gases, which were used to produce fuels 1 to 4, would not be feasible.

In the case of fuel RF5, which is produced from flue gases containing excess oxygen, there is some overlap, with the predicted reactor temperature requirement of 1105K being exceeded by $T_{130}$ values when burned from the two pressure-charged initial conditions.

Fuel RF7, produced from flue gases containing excess steam and oxygen, gave the most promising cycle analysis results. The fuel has a predicted reformer inlet temperature requirement of 1125K which is comfortably exceeded by $T_{130}$ values of 1264K and 1239K in the case of the cycle simulations from the two elevated levels of initial pressure, whilst $T_{180}$ values are only very slightly lower than the estimated requirements at 1119K and 1086K. The results of the simulated ignition timing swing are also encouraging, as increasing levels of ignition retard from the standard setting to 4, 8, and 12$^{\circ}$ retarded give progressively higher $T_{130}$ and $T_{180}$ values which exceed the predicted reformer temperature requirement for combustion from the higher pressure-charged initial conditions. This is at the expense of a

small drop-off in work output, with an IMEP at 12° retarded of 12.8 bar, which compares with a value of 13.2 bar for the fuel at optimum timing; overall system efficiency falls from 42.6 to 41.4%. This lower value still represents a useful efficiency improvement over the pure n-heptane level of 37.3%, being equivalent to an increase of around 10.9% over the baseline value. The effect of ignition retard on maximum cycle pressure is also beneficial, with the most retarded setting giving a peak of 75.9 bar compared with a standard level for this fuel of 99.3 bar.

Finally, the feasibility of producing fuel RF8 is at best marginal, as the reformer temperature requirement of 1305K is only just exceeded by a $T_{130}$ level of 1326K for the simulation under conditions of constant fuel consumption, whilst the $T_{180}$ level is considerably lower.

### 6.6 Cycle Simulation for Methanol Fuels

Four reformed methanol fuels were selected from the equilibria results for investigation in the cycle analysis investigation - the compositions of these fuels is given in Table A5.3. The procedure adopted for the methanol/reformed methanol study is essentially the same as that for n-heptane, and will therefore only be discussed briefly.

#### 6.6.1 Procedure for Methanol/Reformed Methanol Fuels

The geometry of the engine model defined in the earlier n-heptane work was unchanged, in order that a comparison of the whole range of fuelling strategies might be made if required.

The combustion of a naturally aspirated stoichiometric charge of methanol was simulated in order to provide a baseline against which to compare reformed methanol fuels. The standard fuel cycle initial conditions were again set at 1 bar and 350K, whilst burn duration and timing parameters were adjusted to account for the slightly faster flame speed of methanol fuel compared with n-heptane. $\theta_b$ and $\theta_s$ values had been set at $60^\circ$ and $-30^\circ$ respectively for n-heptane, and hence in the case of methanol, which has a flame speed relative to n-heptane of 1.053, $\theta_b$ becomes $56.98^\circ$. For the purpose of the cycle analysis work, this value is rounded to the nearest even number, $56^\circ$, giving a burn commencement value $\theta_s$ of $-28^\circ$.

The stoichiometric combustion of each of the reformed methanol fuels was then simulated from three initial pressure conditions: 1 bar (naturally aspirated), and the two higher levels giving the same levels of IMEP and fuel consumption as compared with the baseline methanol case. In all cases, $\theta_b$ and $\theta_s$ values were set to those calculated from the laminar flame speed predictions.

### 6.6.2 Presentation of Results

The results of this part of the study are presented as follows:

| | Fig No |
|---|---|
| Simulation Cycle for $RF_m1$, $P_1$=1, 1.50, 1.77 bar | 6.14a, b |
| Simulation Cycle for $RF_m2$, $P_1$=1, 1.72, 2.04 bar | 6.15a, b |
| Simulation Cycle for $RF_m3$, $P_1$=1, 1.31, 1.51 bar | 6.16a, b |
| Simulation Cycle for $RF_m4$, $P_1$=1, 1.51, 1.77 bar | 6.17a, b |

Again, Figs 6.18 to 6.21 give results from the higher level of initial pressure, and the most relevant results of the exercise are tabulated in Appendix III, see Tables A6.3 and A6.4.

### 6.6.3 Discussion of Results

The baseline methanol cycle gives an IMEP of 11.26 bar with maximum pressure and temperature conditions of 64.36 bar and 2770K. This gives an indicated thermal efficiency of 36.9% when work output is compared with energy input, based on methanol's higher heating value of 22.73 MJ/kg.

Again, all reformed methanol fuels give good predicted improvements in overall thermal efficiency when cycle work output is compared with the original methanol input into the reformer. At a constant level of baseline fuel consumption, ie. the higher level of initial pressure, the four reformed methanol fuels give overall thermal efficiencies in the range 43.3 to 44.3%. Corresponding engine thermal efficiencies based on reformed fuel energy input are 36.9 to 38.3%, ie generally higher than the baseline methanol case. This improvement, which is over and above the effect of increased calorific value, is again attributed to reductions in combustion duration and lower conductive heat loss relative to work output (Fig 6.20). Overall system and engine thermal efficiencies are shown in Fig 6.21.

Cycle peak pressures from the higher levels of initial charge-pressure tend again to be rather high, ranging from 96.4 to 107.6 bar, as shown in Fig's

6.14 to 6.17, and also in the summary plot of Fig 6.18. These levels are generally lower than those predicted for n-heptane reformed fuels, but would still be rather high for a running engine.

Cycle simulations from the constant-work intermediate level of pressure charge again give more acceptable maximum cycle pressures, ranging from 83.2 bar for $RF_m3$ to 90.6 bar for $RF_m2$. Overall efficiencies are 42.6% and 43.8% respectively, whilst the actual engine efficiencies are of a very similar level to the baseline methanol case, indicating that as charge mass reduces, thermal losses become more significant.

As expected, naturally aspirated simulations give low IMEP's. Predicted values range from 6.2 bar for $RF_m2$ to 8.3 bar for $RF_m3$ which represent respective reductions of 45.3 and 26.1% as compared with the pure methanol value of 11.26 bar. Overall system efficiency is still around 41% for each reformed fuel cycle, whilst engine thermal efficiencies have dropped below the baseline case level to around 35%.

Predicted cycle temperatures for the reformed methanol fuels are encouraging in terms of the feasibility of meeting predicted reformer temperature requirements. All pressure-charged runs give temperatures at 130° crank angle well in excess of predicted requirements, as shown in Fig 6.19. Fuels $RF_m1$ and $RF_m3$ also have temperatures at 180°crank angle in excess of the predicted requirements, and there are thus grounds to suggest that the reformer could be sustained by these exhaust gases.

The results for methanol reformed fuels are encouraging, with major advantages over reformed n-heptane fuels being largely attributable to the chemical composition of the alcohol fuel. This permits lower temperature

reforming at fuel-rich reforming oxidant to fuel ratios without C(s) problems. The relatively high hydrogen to carbon ratio of the fuel generates flue gases having a high steam content, leading to the production of fuels having lower levels of diluents, and a good heat release per unit volume as compared with the reformed n-heptane fuels.

High peak pressures, which tend to arise from pressure-charged initial conditions, could again be reduced by retarding ignition timing, as predicted in the timing swings carried out with the reformed n-heptane fuel RF7 (Fig 6.9). This would tend to give small reductions in IMEP and hence cycle thermal efficiency, with a useful increase in exhaust-gas temperatures.

### 6.7 Conclusions of Cycle Analysis Investigation

If standard baseline power output levels are to be maintained, a certain amount of pressure boosting will certainly be required by the reformed fuel/air charge. Levels of boost ranging from 0.4 to 1.0 bar above atmospheric would typically be necessary in the case of the reformed n-heptane and methanol fuels studied.

The approximately three-fold increase in predicted flame speeds of the hydrogen-containing reformed fuels compared with standard fuels leads to predicted improvements in cycle efficiency over and above those resulting from the enhanced heating value of the gaseous fuels. This is to be expected, as the heat release more closely approximates the thermodynamically ideal constant volume process. A disbenefit of the increased flame speeds, however, is the high peak cylinder pressure which tends to be generated by the rapid heat release, and it is proposed that this might best be dealt with by means of an ignition-retard strategy, which would also give beneficial increases in exhaust-gas temperatures.

It would certainly be difficult to sustain the reformer using flue gases alone in the case of n-heptane, even when flue gases are enriched with 3% oxygen which has the effect of reducing predicted reformer temperature requirements. However, as the predicted cycle temperature levels are close to the required values, it is suggested that the process is worthy of practical examination. It may be found that larger amounts of oxygen are required in order to sustain the reforming reaction, whilst accepting the inevitable reduction in calorific value improvement. The current study has predicted achievable improvements in overall thermal efficiency of around 10% over the baseline standard fuel level for fuel RF7, which is produced by reforming with an oxidant enriched with 3% oxygen and 100% excess steam. A small reduction in this improvement could be tolerated if the introduction of greater quantities of oxygen enhanced the feasibility of the process.

The exhaust-gas reforming of methanol appears to be rather more feasible than that of the hydrocarbon, as the reactions occur at lower temperatures and are less prone to carbon solids problems. On the basis of the cycle analysis results, it should be possible to drive these reactions with the exhaust-gases of the reformed fuel engine.

In conclusion, the theoretical study of the exhaust-reforming process, carried out in terms of equilibria, energy and engine cycle simulation predictions, indicates considerable potential. It is felt that the process should be examined practically in a laboratory-based study. Prior to this, however, it was thought that the theoretical work should be concluded with a study of the potential for pollutant emissions reductions from the reformed fuel engine. The findings of this brief investigation are reported in the following chapter.

| Fuel | $P_{(Const\ Fuel\ Cons)}$, bar | $P_{(Const\ Work\ Output)}$, bar |
|---|---|---|
| RF1 | 2.23 | 1.67 |
| RF2 | 2.01 | 1.50 |
| RF3 | 2.01 | 1.50 |
| RF4 | 1.80 | 1.40 |
| RF5 | 2.05 | 1.71 |
| RF6 | 1.86 | 1.52 |
| RF7 | 1.65 | 1.46 |
| RF8 | 1.74 | 1.41 |

Table 6.1a Calculated Levels of Pressure Charge Required for Reformed n-Heptane Fuels.

| Fuel | $P_{(Const\ Fuel\ Cons)}$, bar | $P_{(Const\ Work\ Output)}$, bar |
|---|---|---|
| $RF_m1$ | 1.77 | 1.50 |
| $RF_m2$ | 2.04 | 1.72 |
| $RF_m3$ | 1.51 | 1.31 |
| $RF_m4$ | 1.77 | 1.51 |

Table 6.1b Calculated Levels of Pressure Charge Required for Reformed Methanol Fuels

| Fuel | Flame Speed cm/s | Flame Speed Rel to n-Hept | $\theta_b$, Degrees | $\theta_s$, Degrees |
|---|---|---|---|---|
| n-Heptane | 39.7 | 1.00 | 60 | -30.0 |
| RF1 | 103.3 | 2.60 | 23.1 | -11.6 |
| RF2 | 103.2 | 2.60 | 23.1 | -11.6 |
| RF3 | 106.0 | 2.67 | 22.5 | -11.3 |
| RF4 | 131.2 | 3.30 | 18.2 | -9.1 |
| RF5 | 105.9 | 2.67 | 22.5 | -11.3 |
| RF6 | 103.2 | 2.60 | 23.1 | -11.6 |
| RF7 | 119.9 | 3.02 | 19.9 | -10.0 |
| RF8 | 129.2 | 3.25 | 18.4 | -9.2 |

Table 6.2a Predicted Flame Speed and Burn Duration/Commencement Values for Reformed n-Heptane Fuels

| Fuel | Flame Speed cm/s | Flame Speed Rel to n-Hept | $\theta_b$, Degrees | $\theta_s$, Degrees |
|---|---|---|---|---|
| Methanol | 41.8 | 1.05 | 57.0 | -28.5 |
| $RF_m1$ | 129.8 | 3.27 | 18.0 | -9.1 |
| $RF_m2$ | 128.6 | 3.23 | 18.2 | -9.1 |
| $RF_m3$ | 132.5 | 3.34 | 17.7 | -8.9 |
| $RF_m4$ | 130.5 | 3.29 | 17.9 | -9.0 |

Table 6.2b Predicted Flame Speed and Burn Duration/Commencement Values for Reformed Methanol Fuels

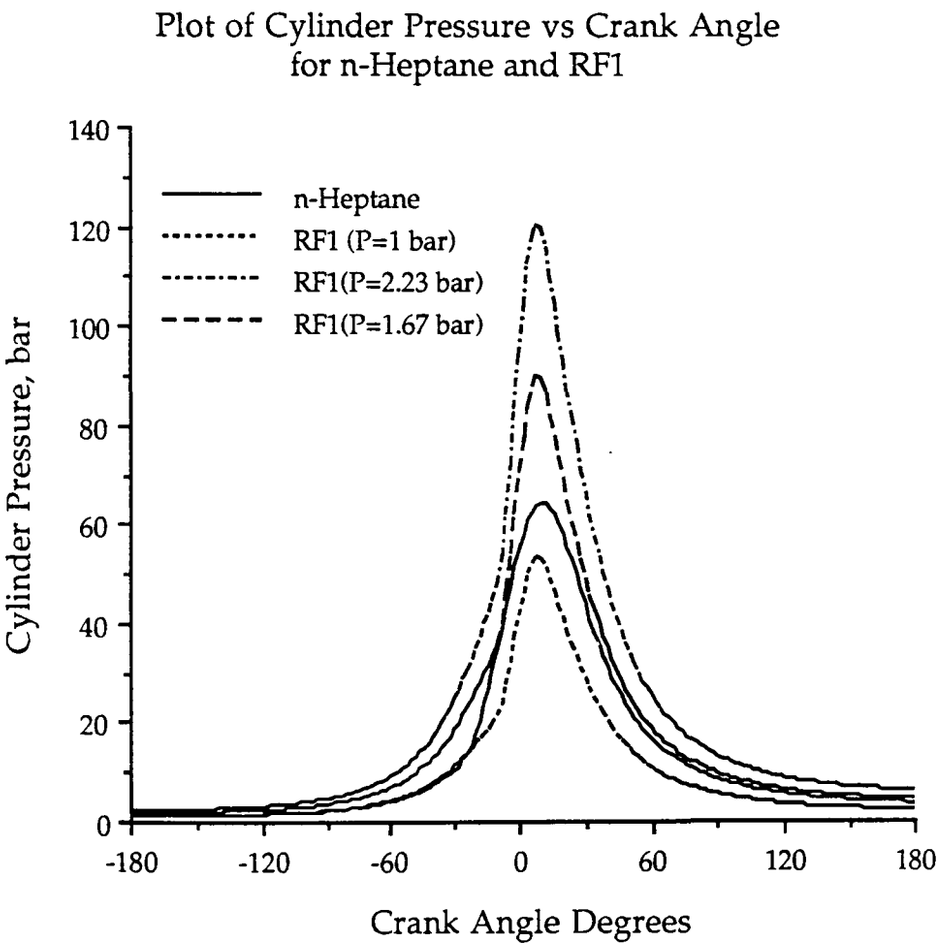


Fig 6.1a

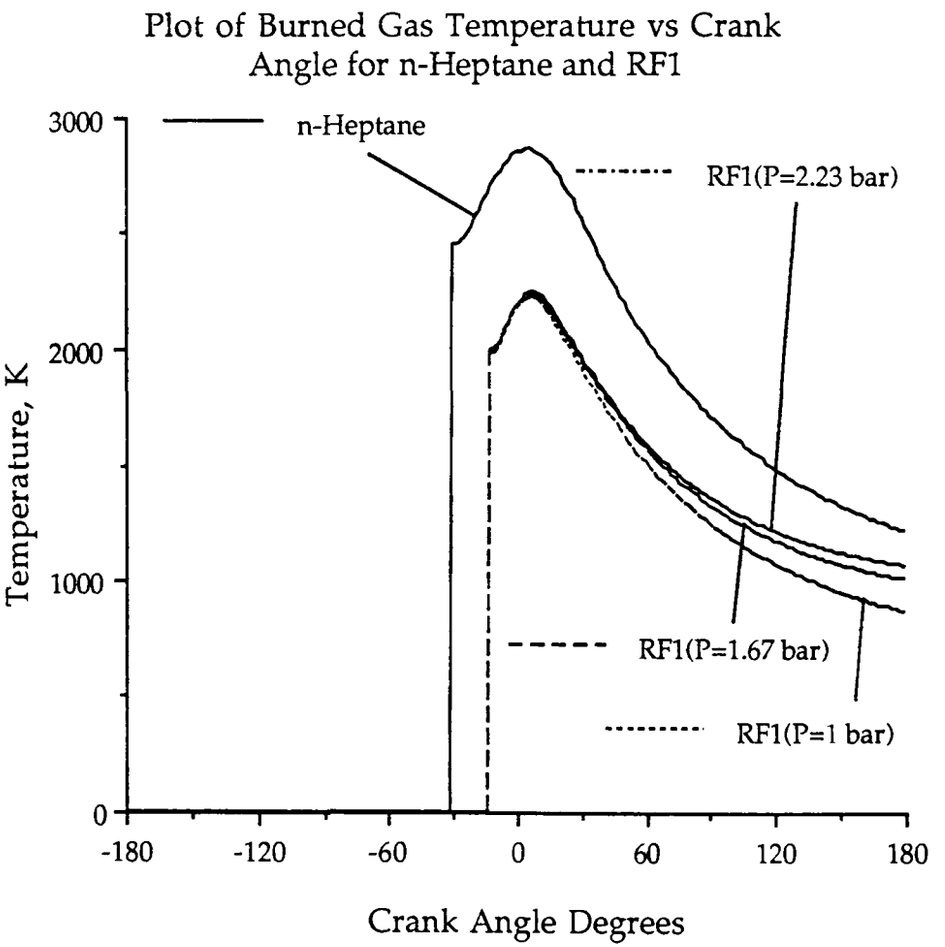


Fig 6.1b

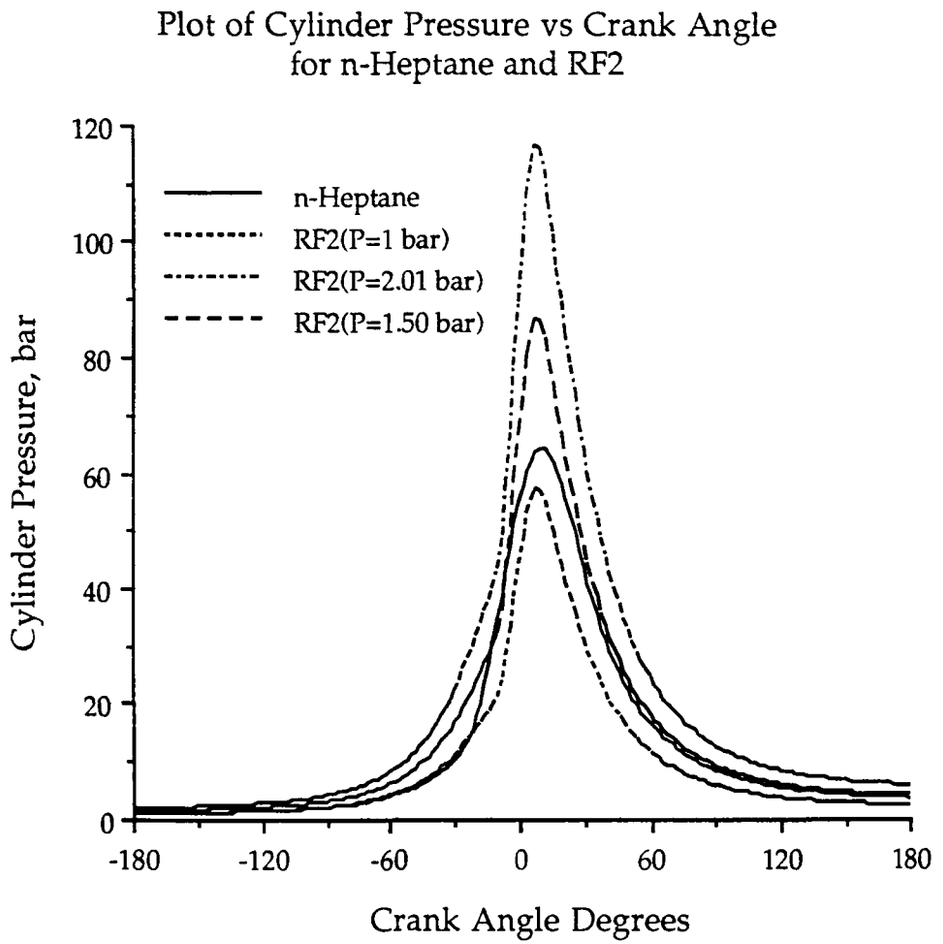


Fig 6.2a

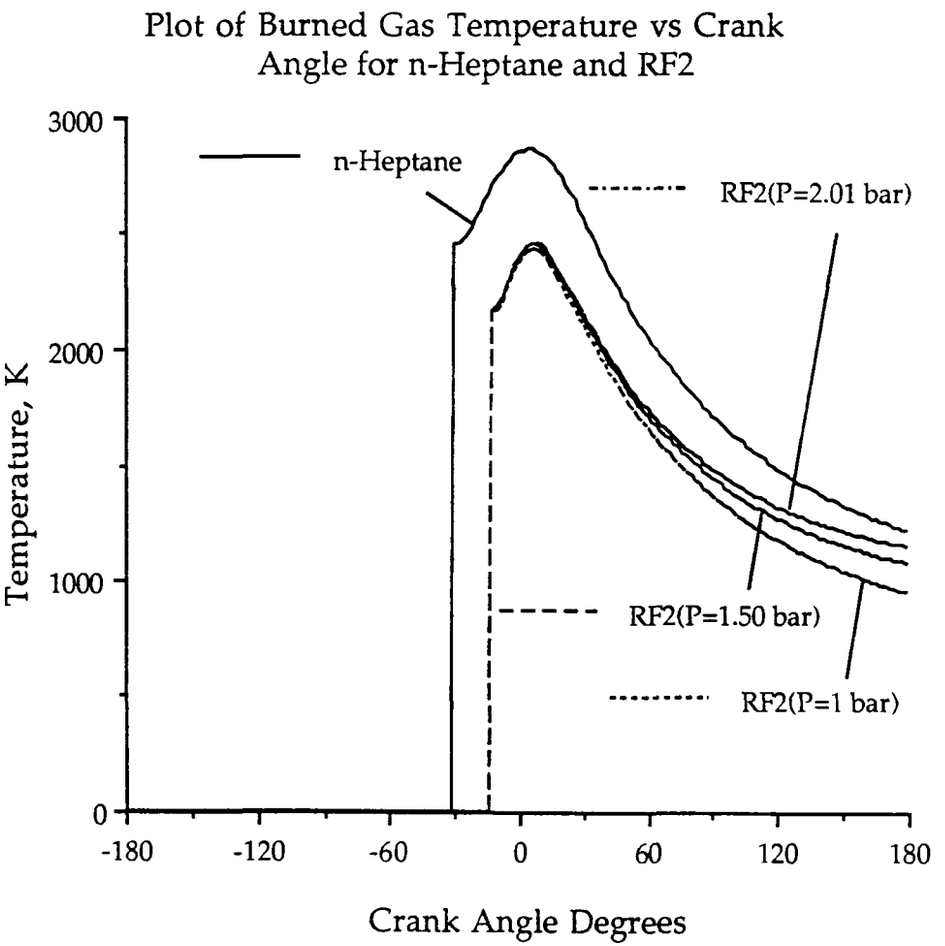


Fig 6.2b

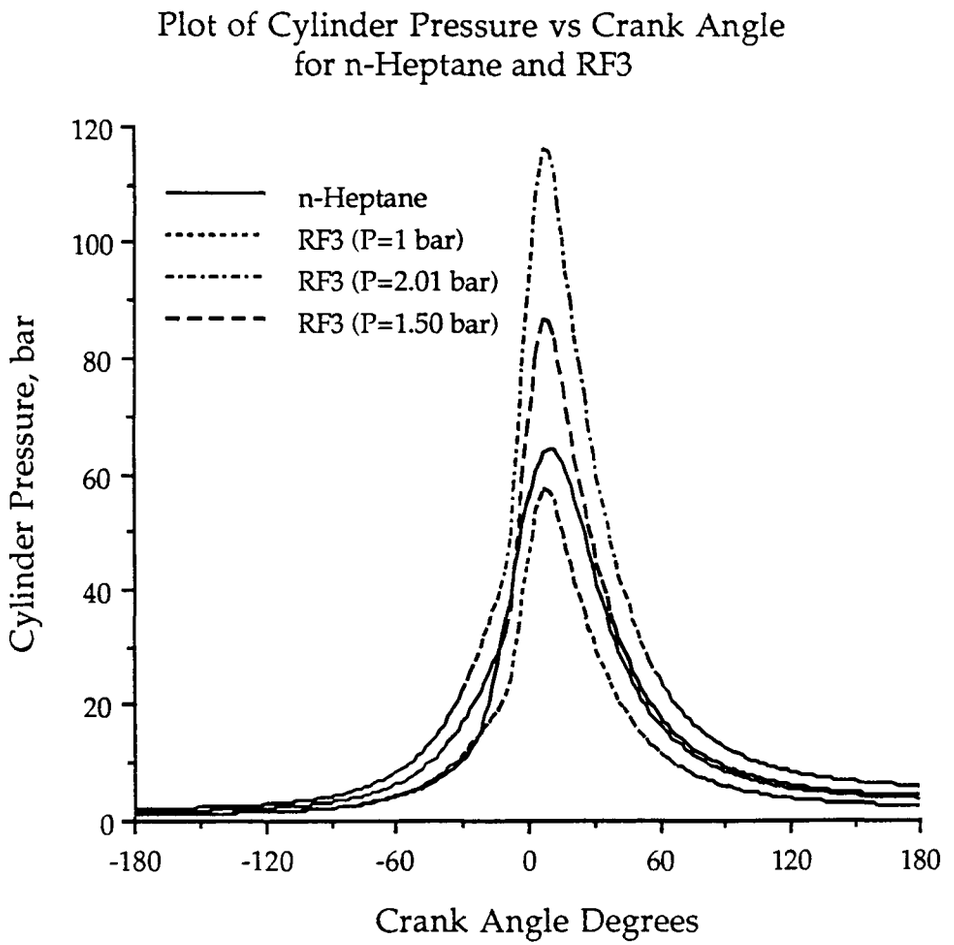


Fig 6.3a

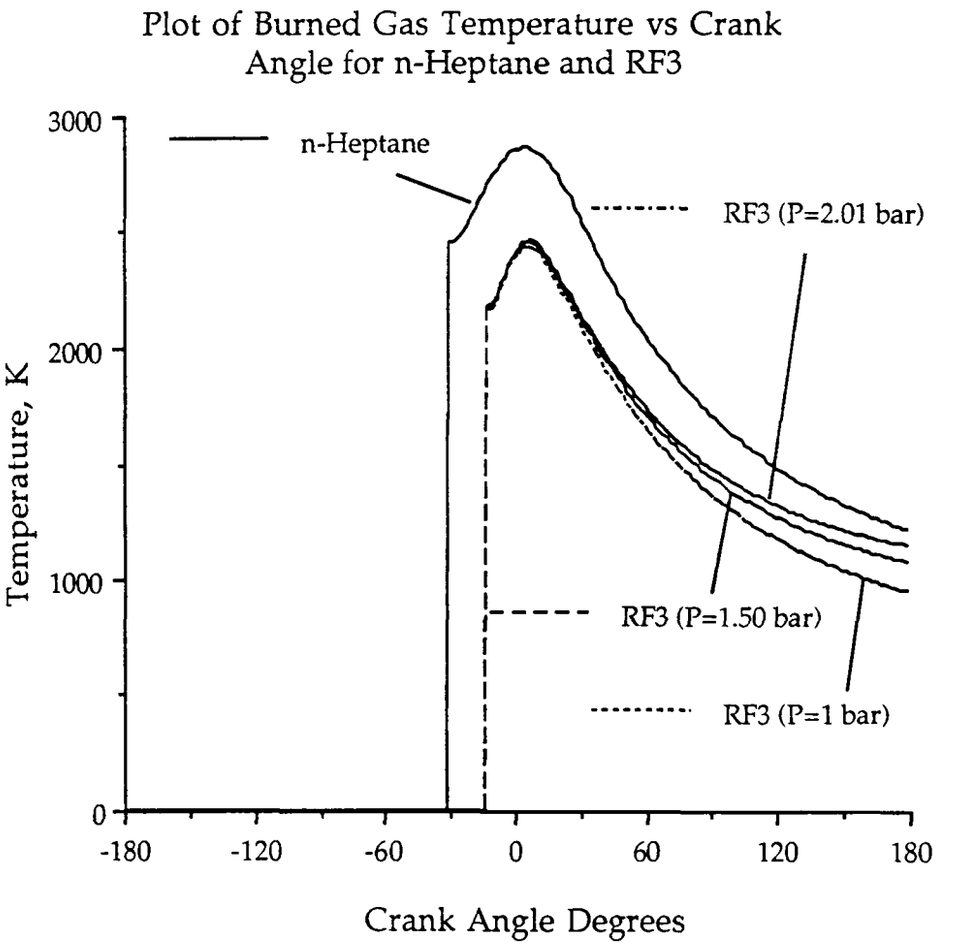


Fig 6.3b

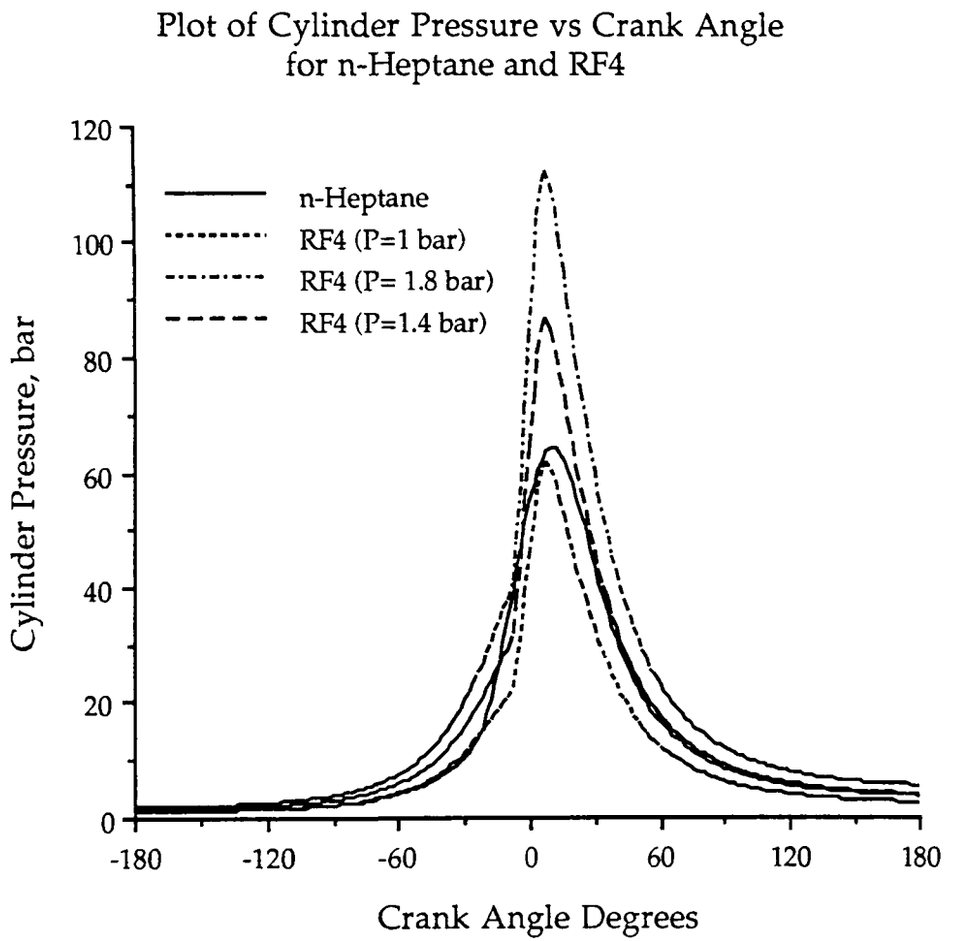


Fig 6.4a

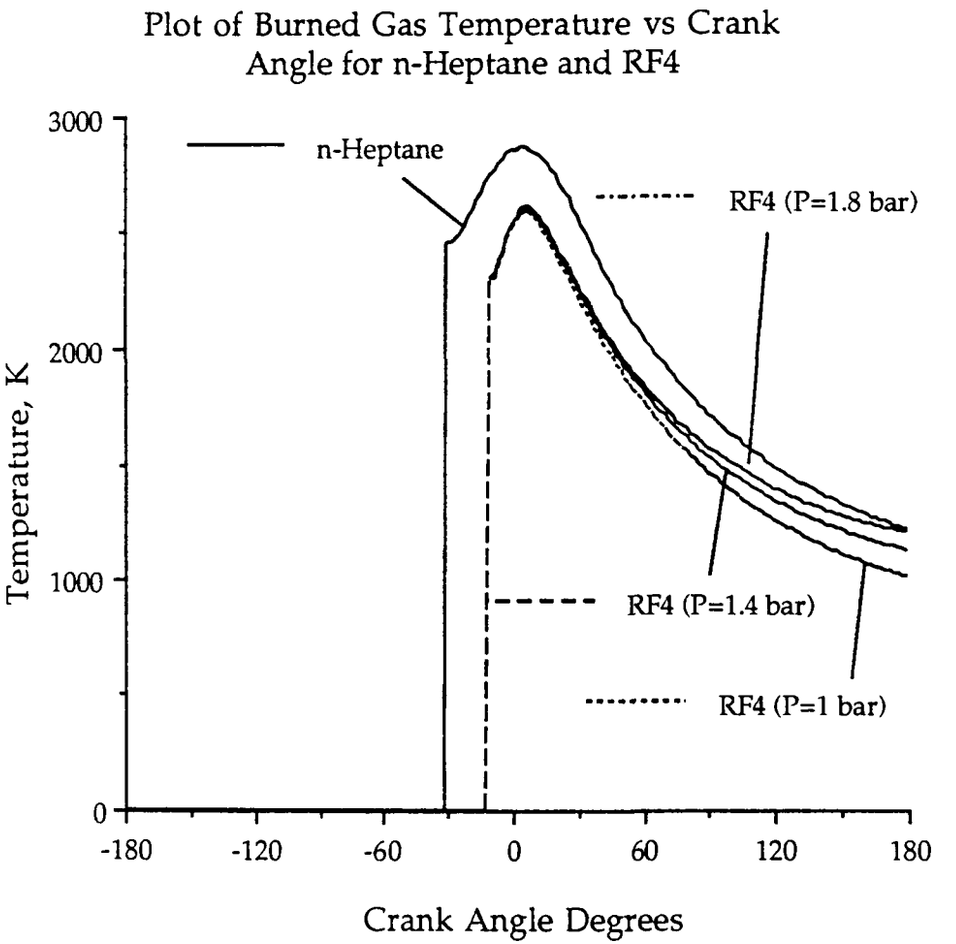


Fig 6.4b

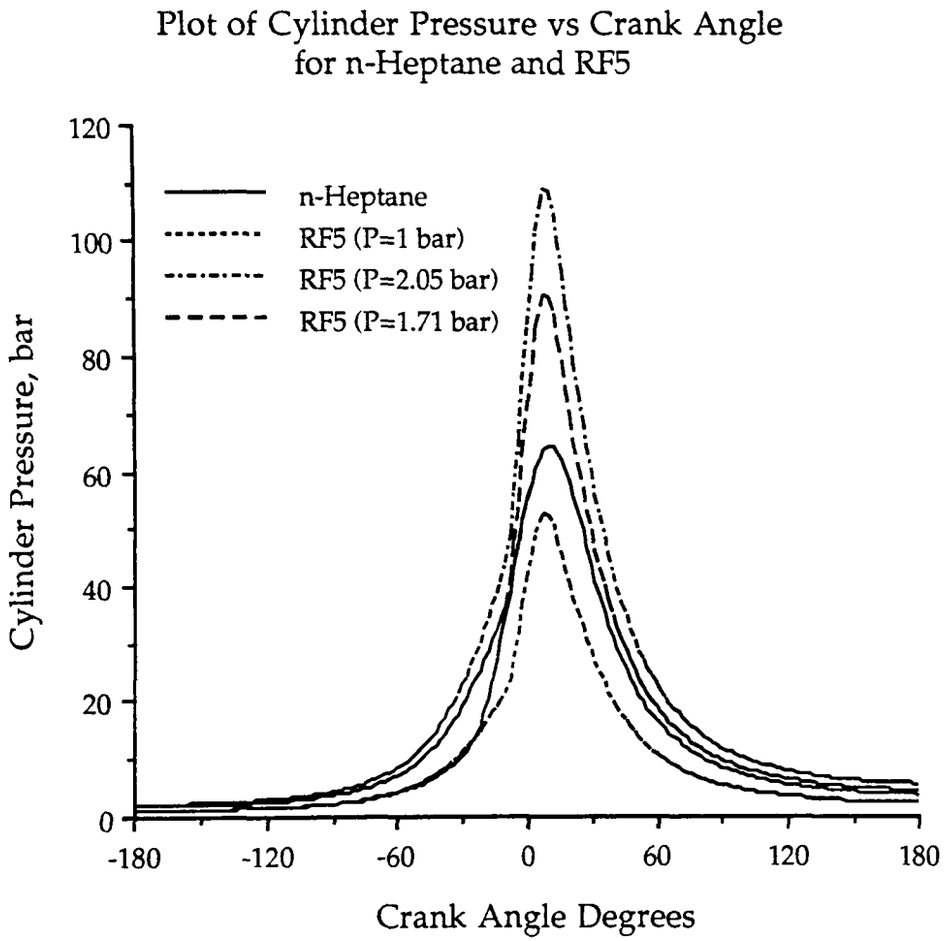


Fig 6.5a

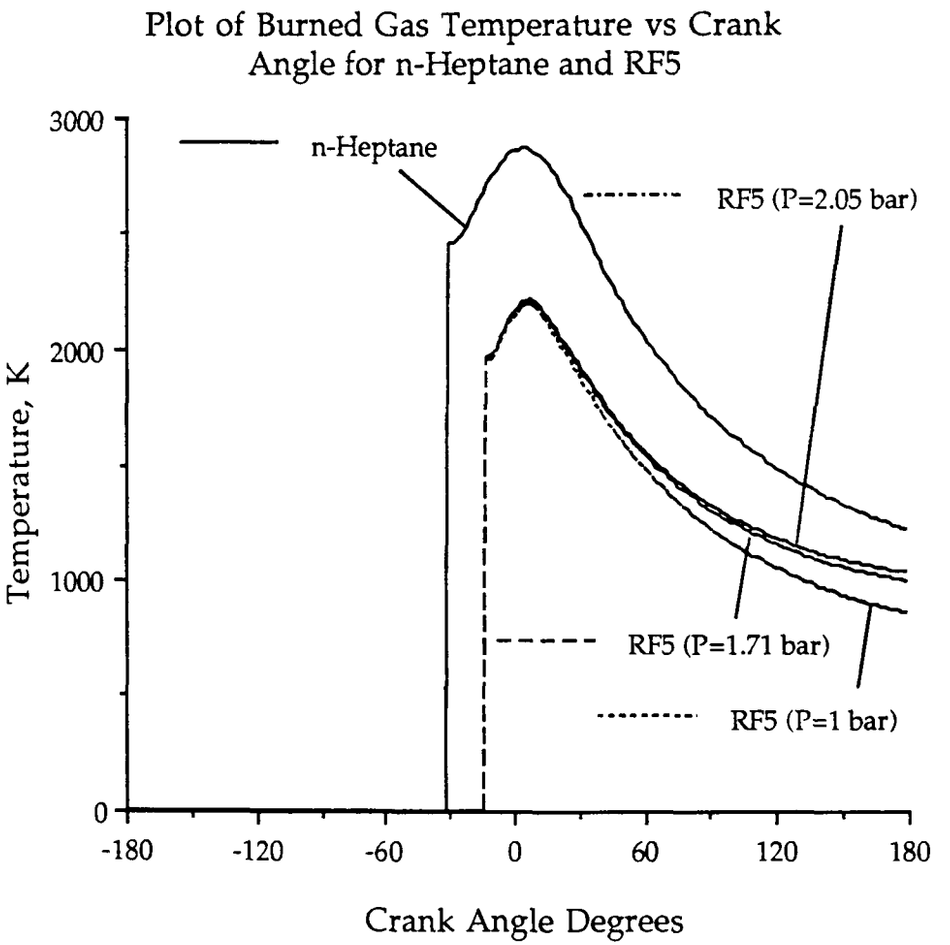


Fig 6.5b

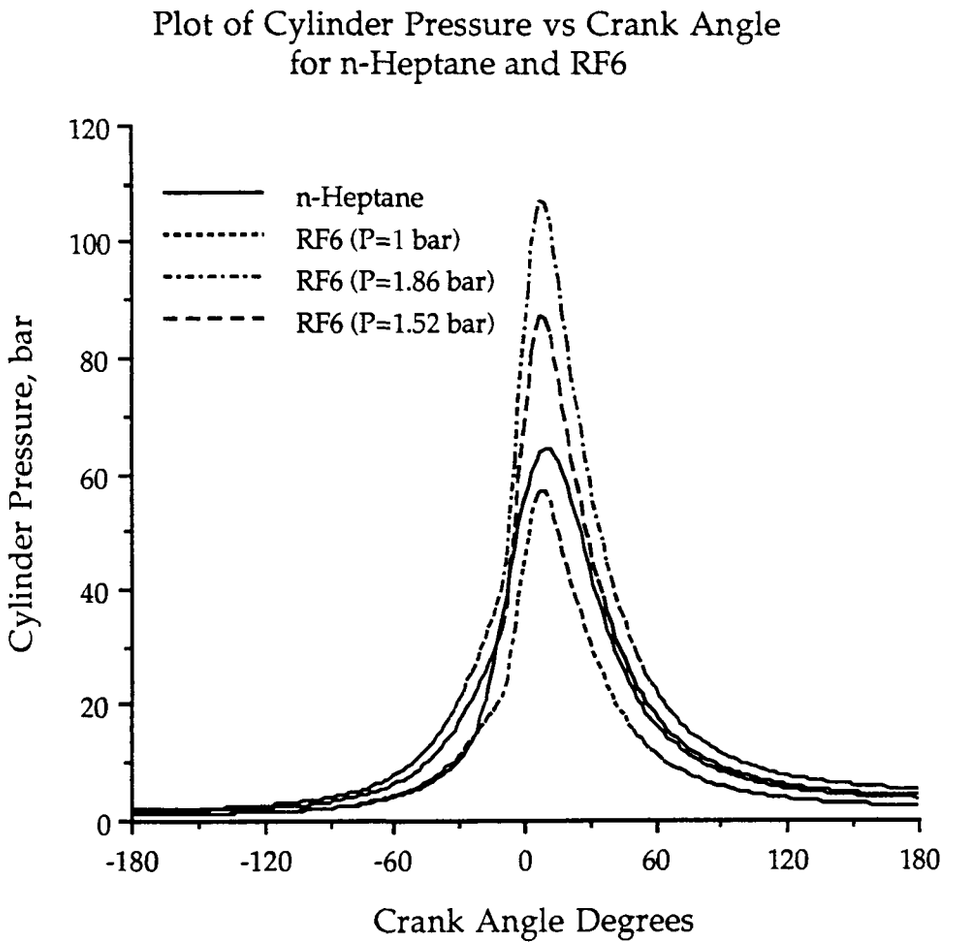


Fig 6.6a

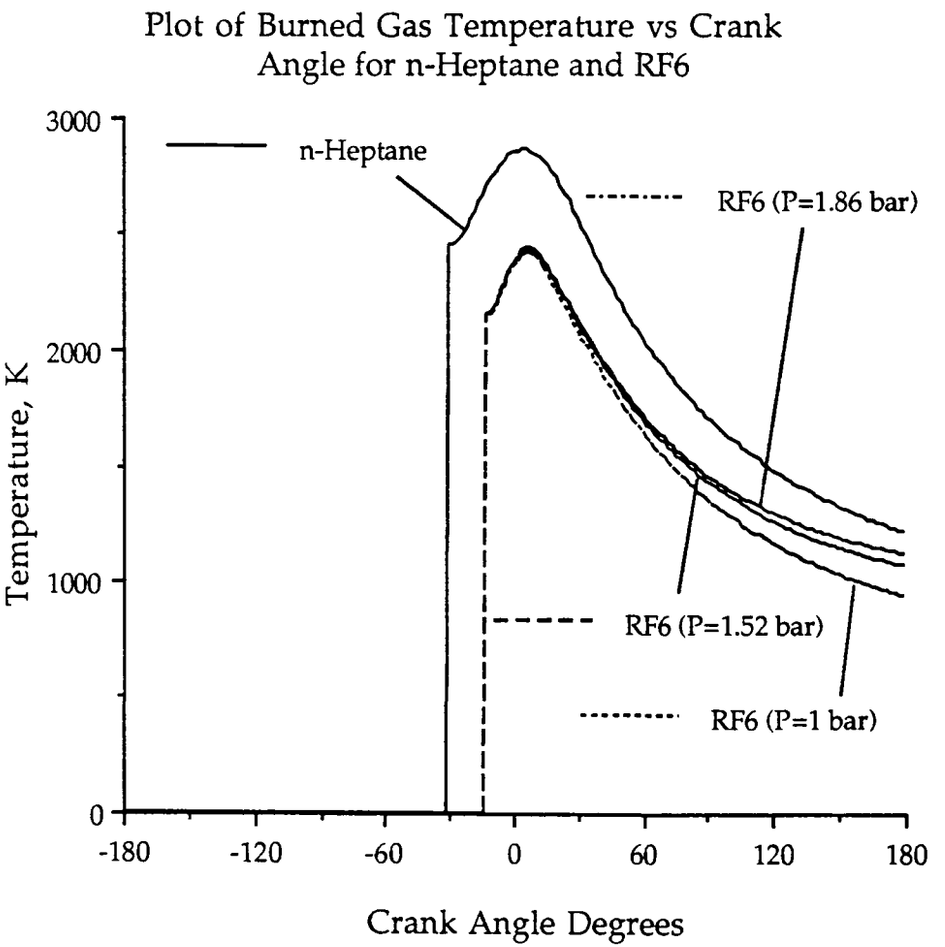


Fig 6.6b

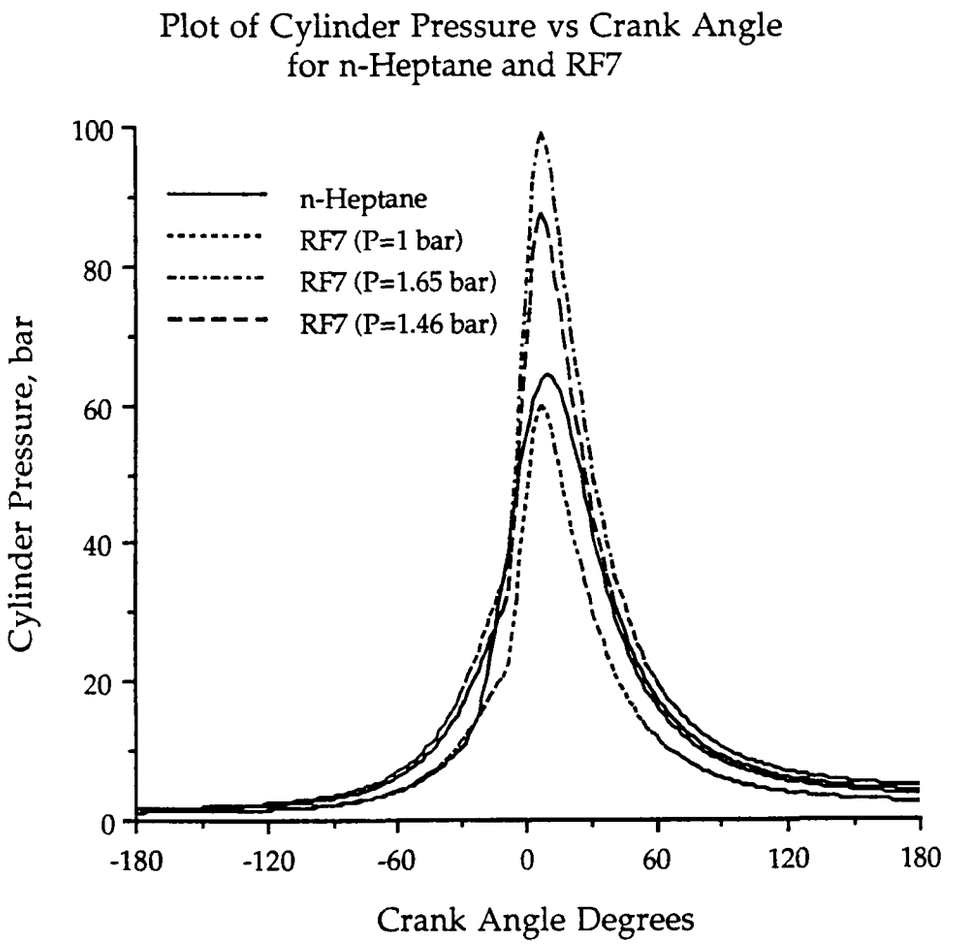


Fig 6.7a

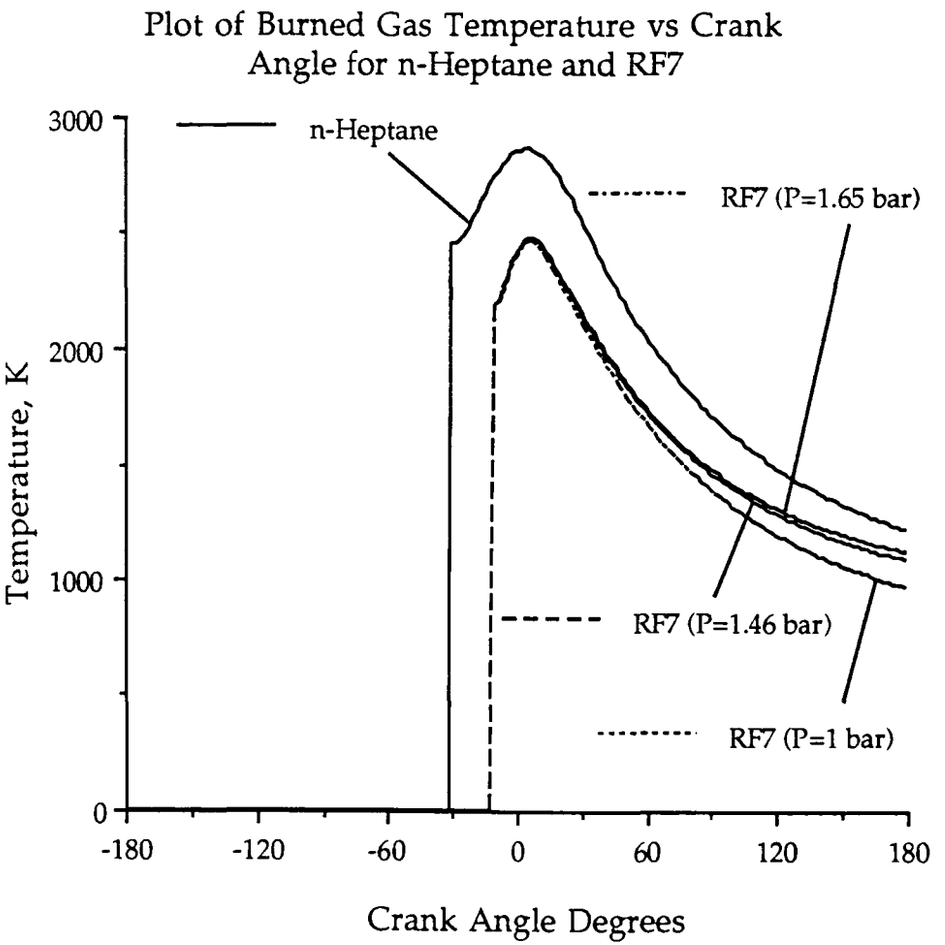


Fig 6.7b

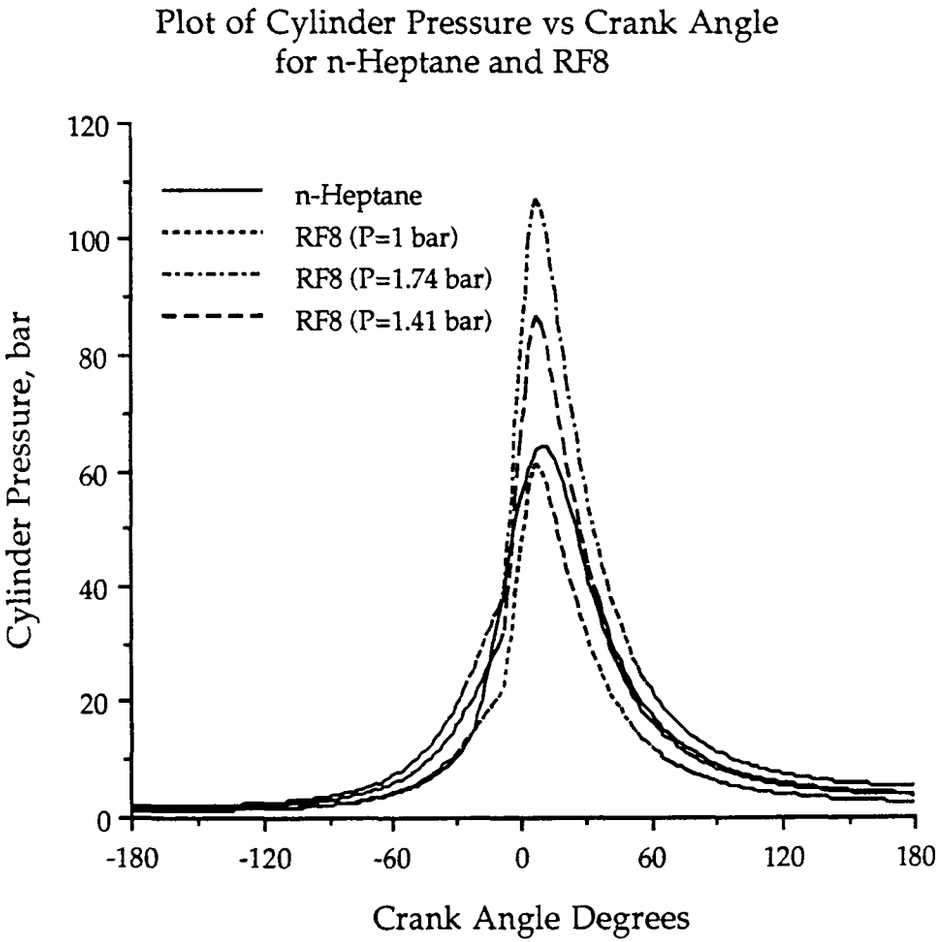


Fig 6.8a

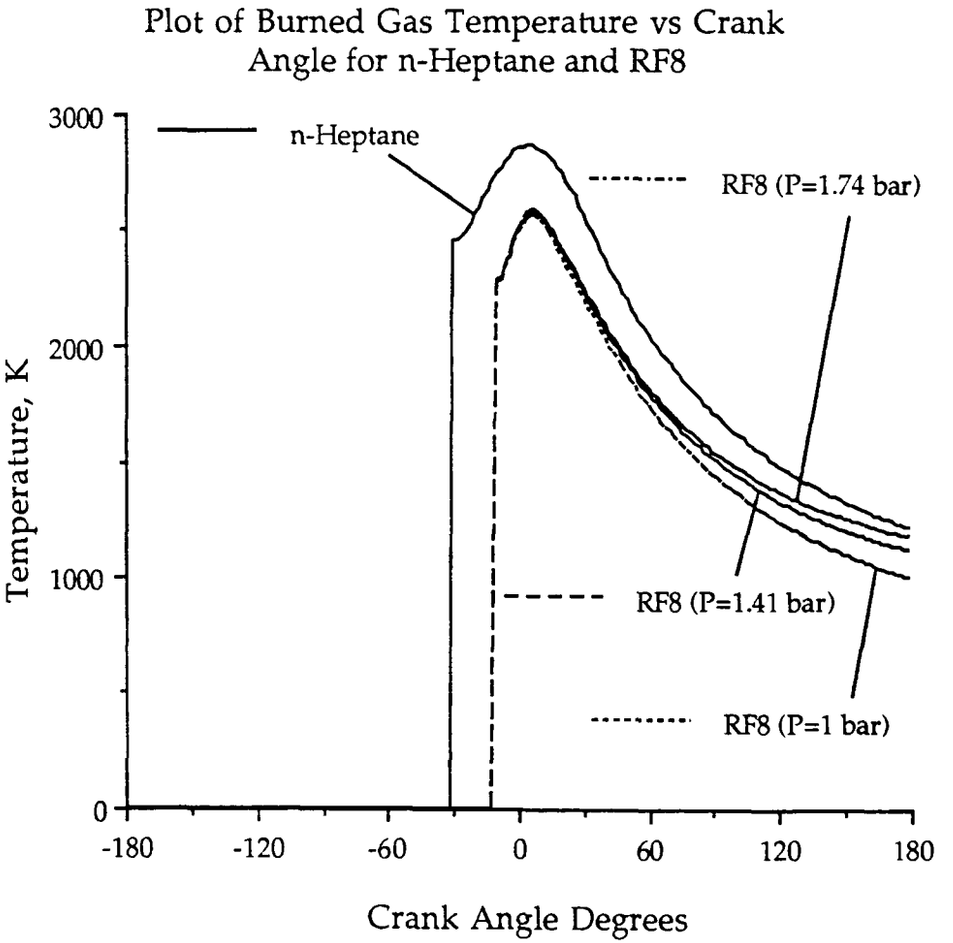


Fig 6.8b

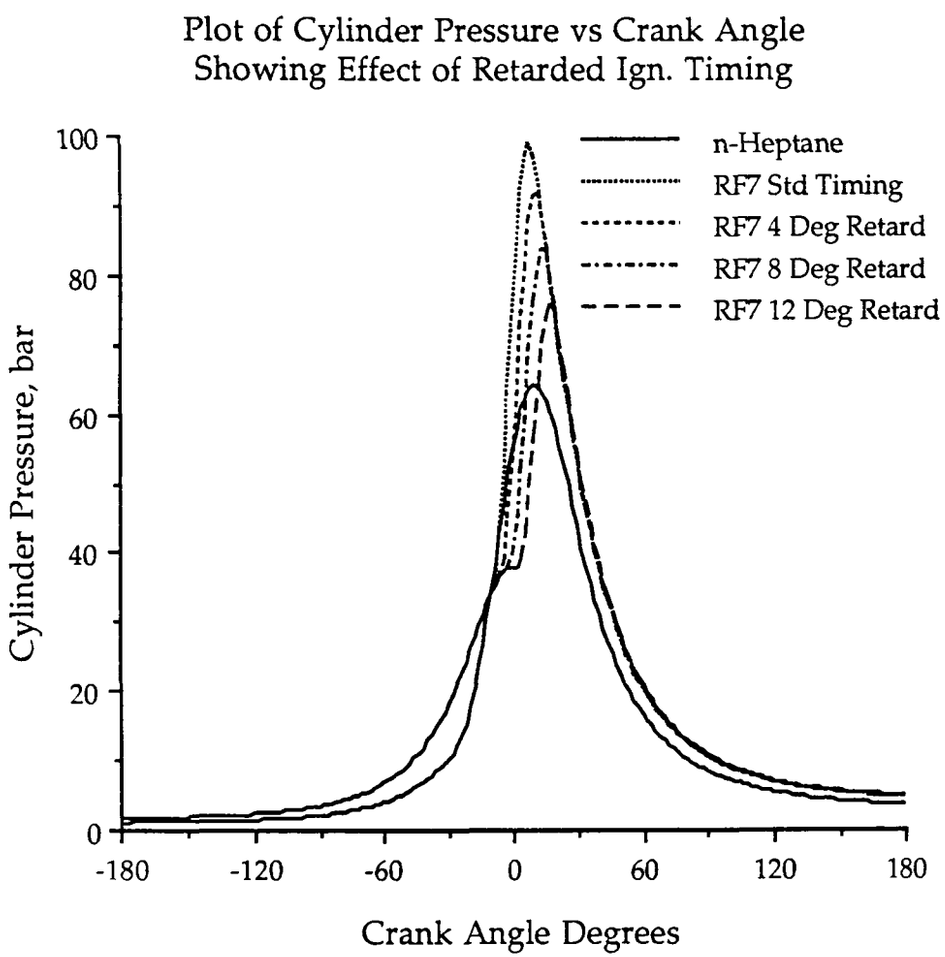


Fig 6.9a

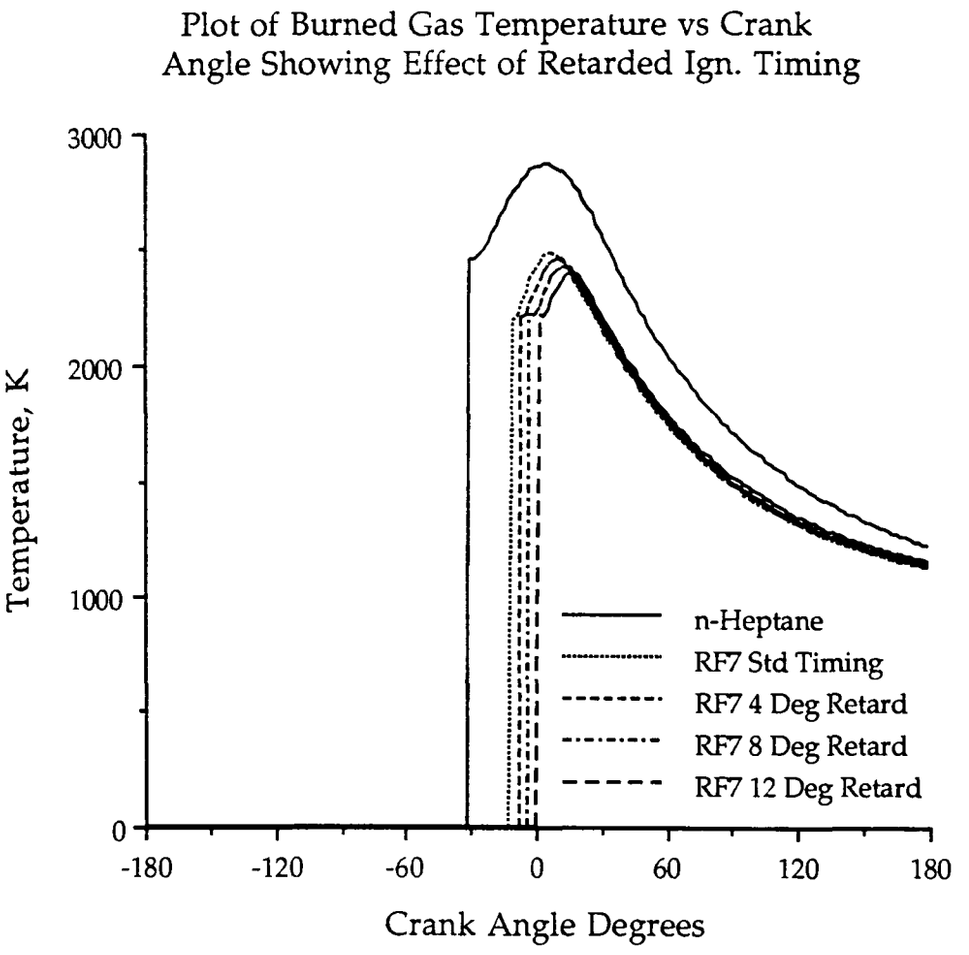


Fig 6.9b

Plot of Max Cycle Pressure and IMEP for n-Heptane and Reformed n-Heptane Fuels

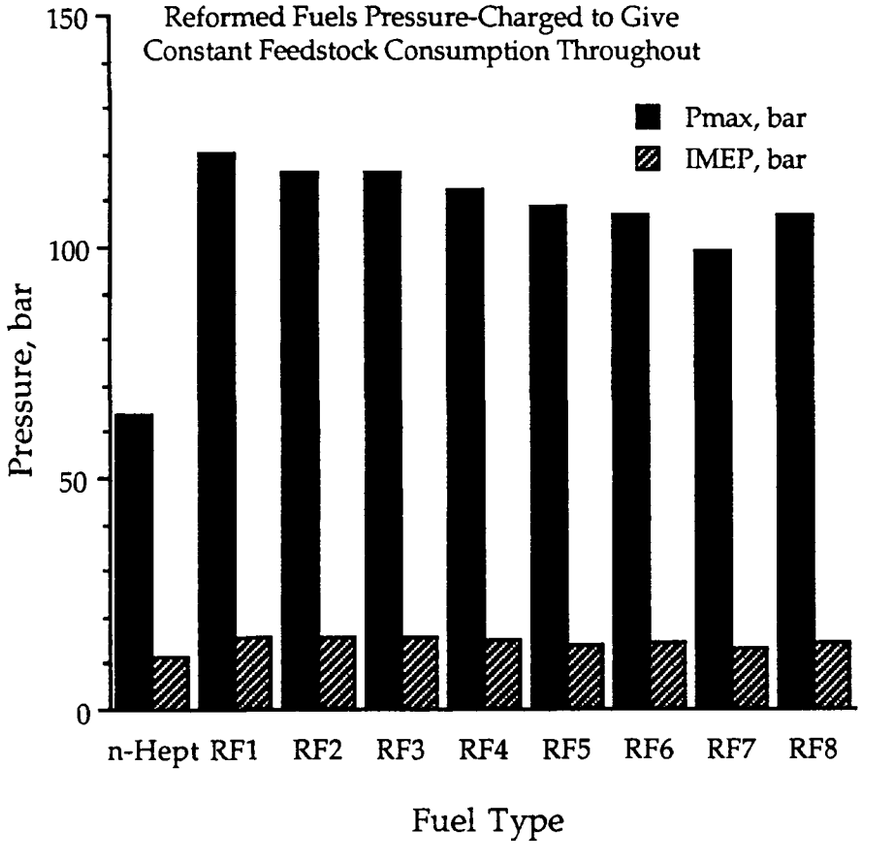


Fig 6.10

Plot of Cycle Burned Gas Temp and Reactor Temp Requirement for n-Heptane and Reformed n-Heptane Fuels

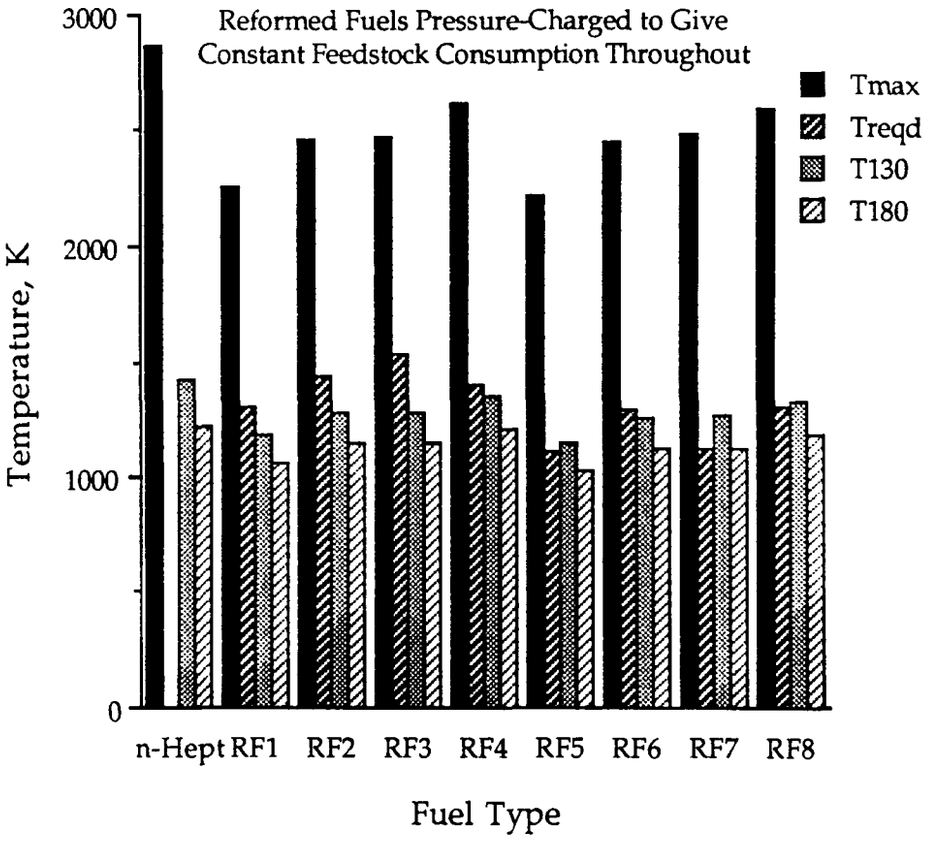


Fig 6.11

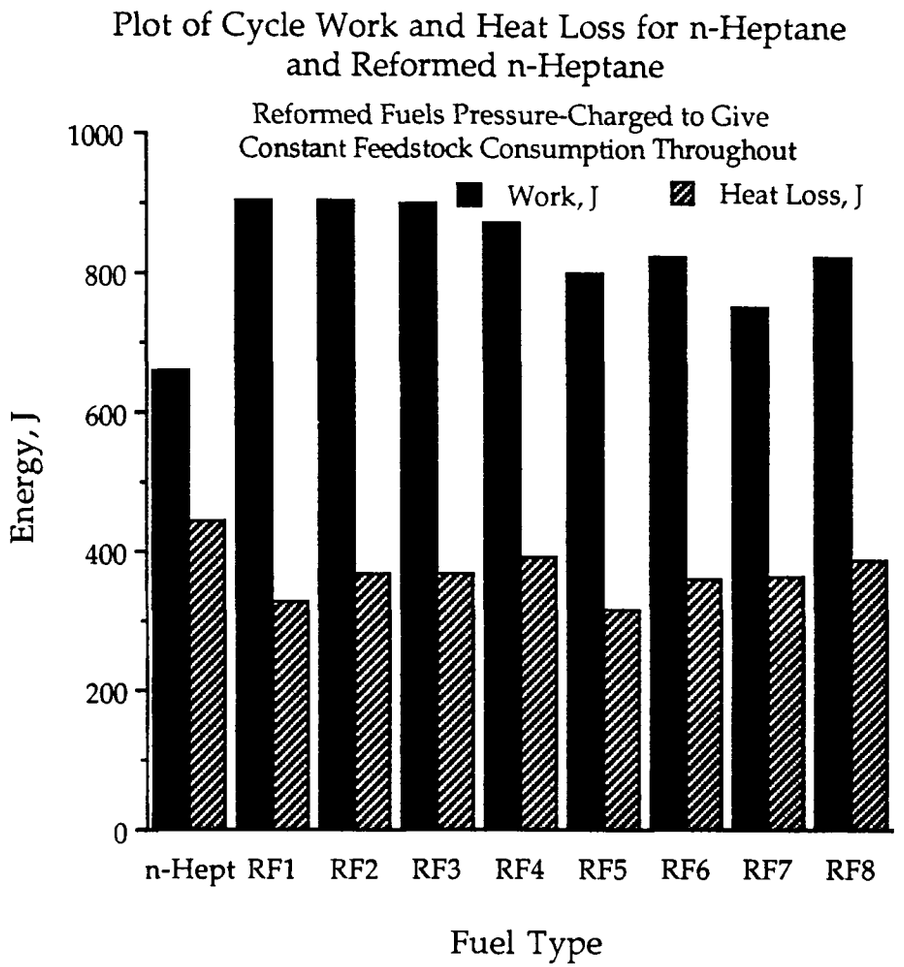


Fig 6.12

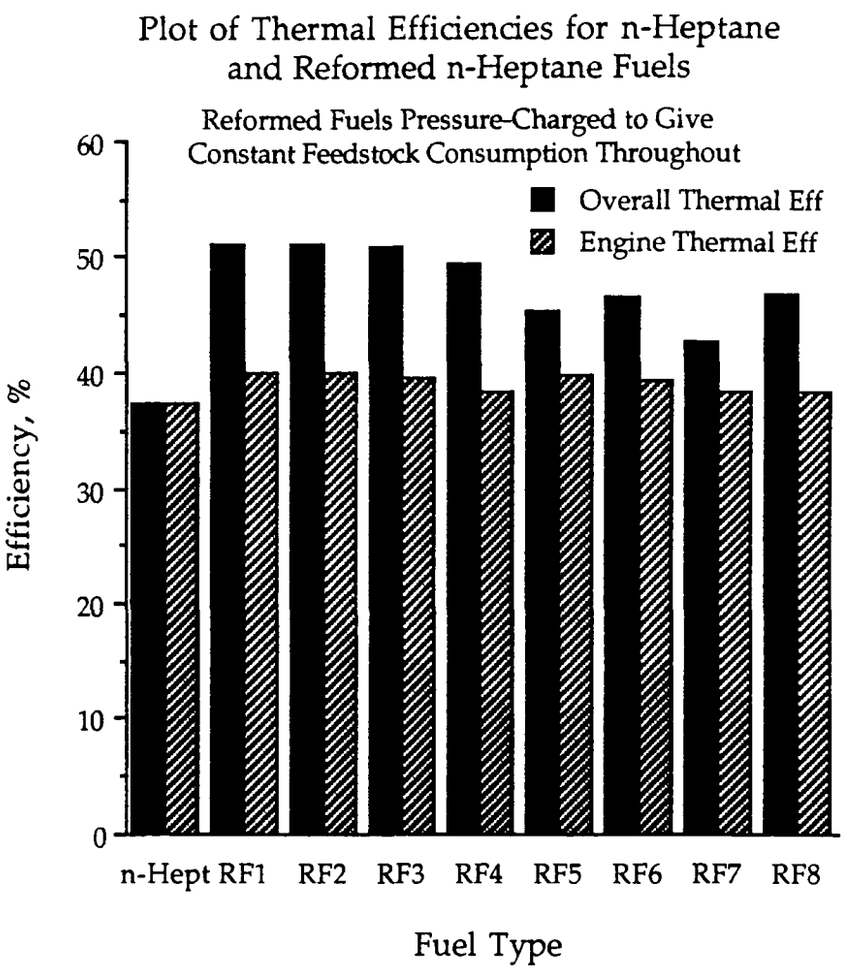


Fig 6.13

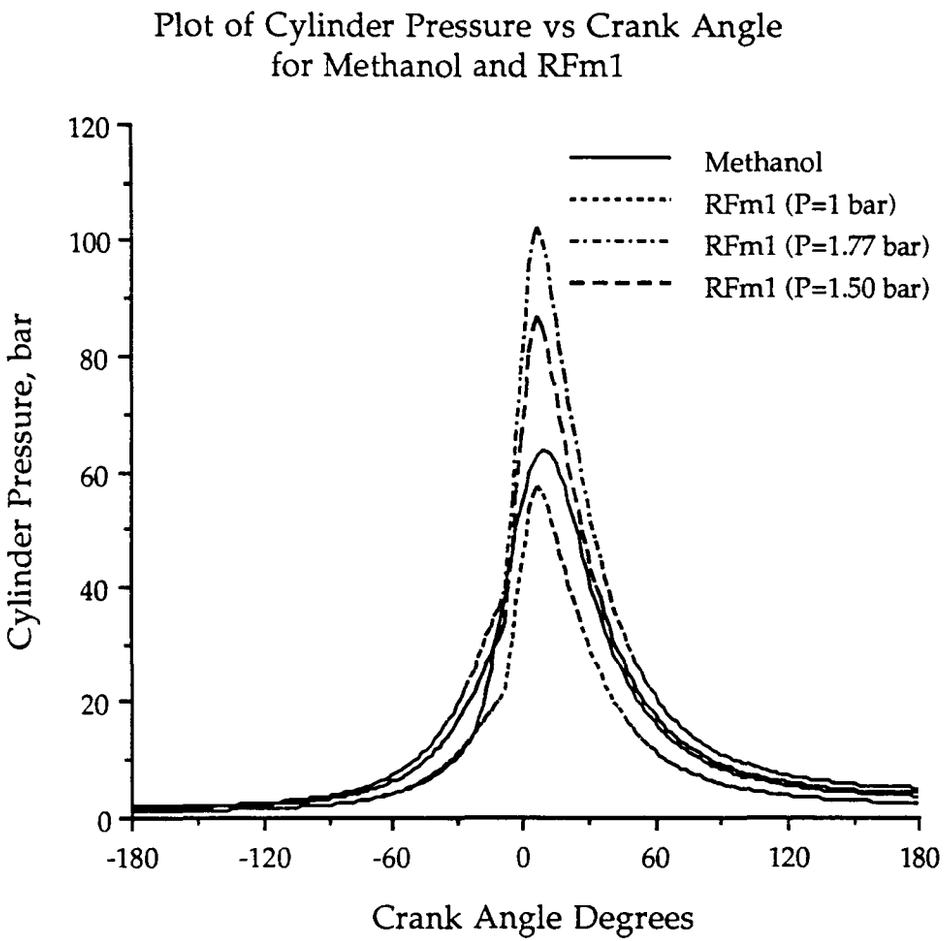


Fig 6.14a

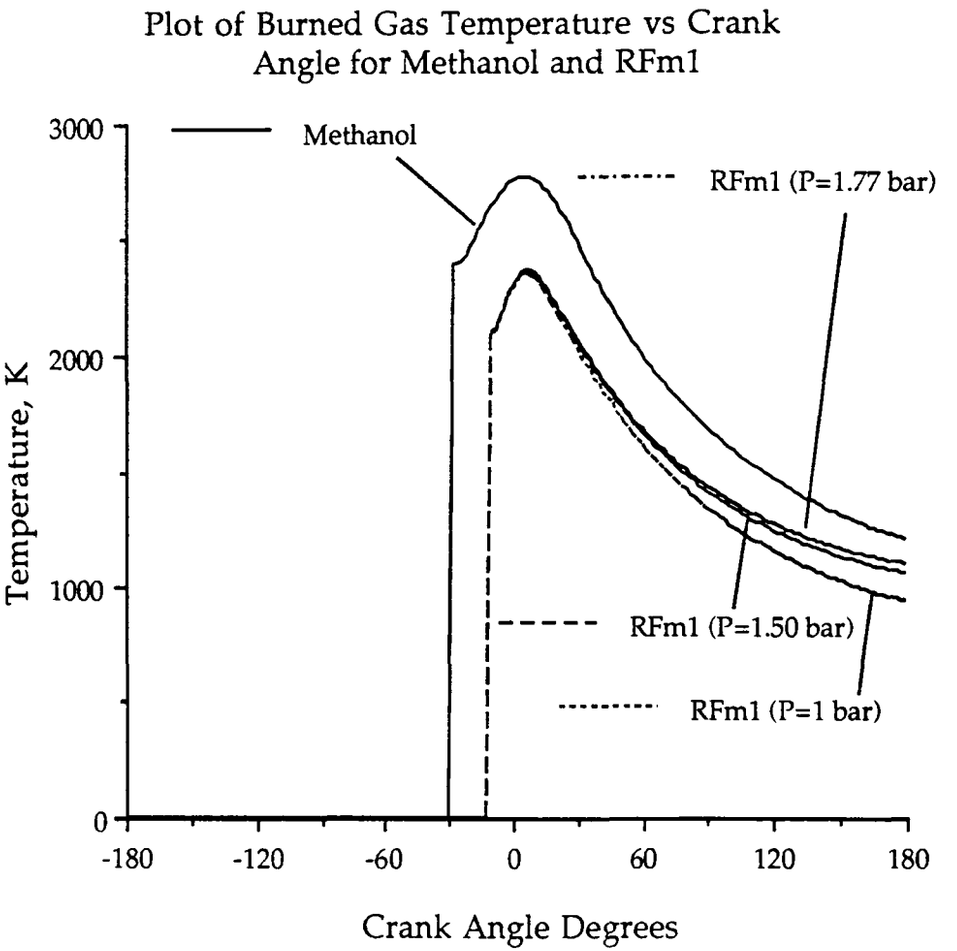


Fig 6.14b

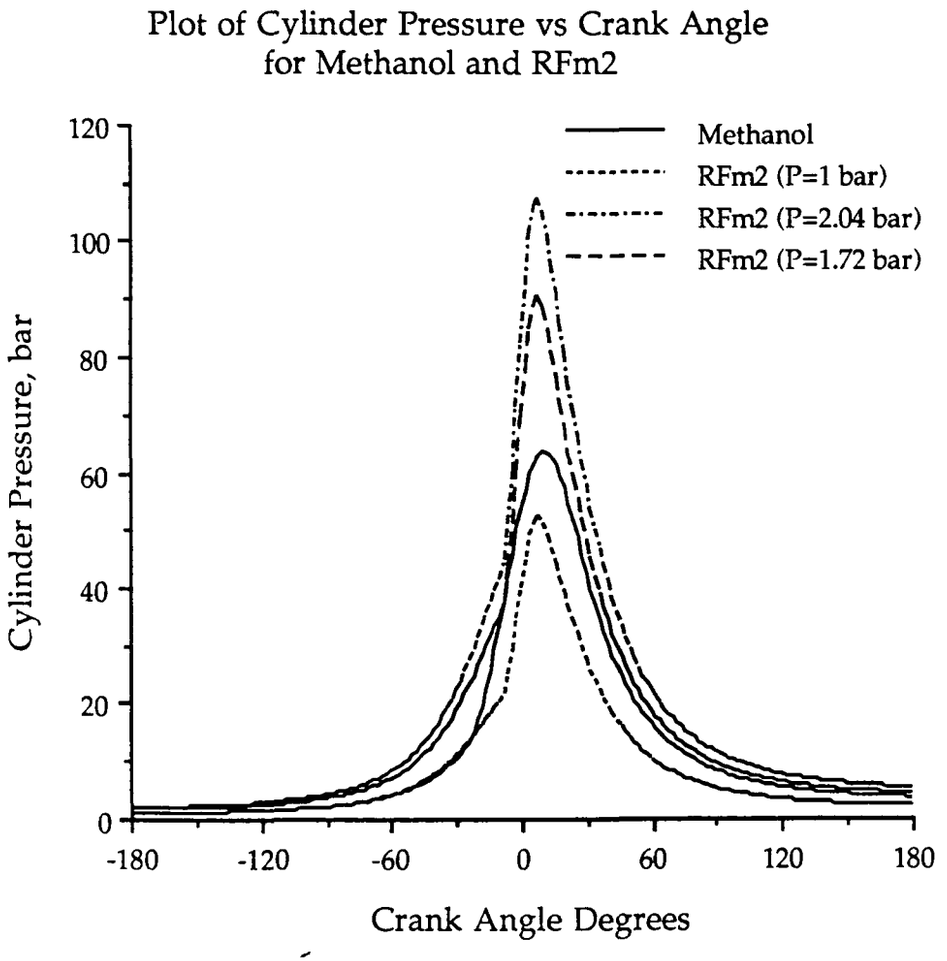


Fig 6.15a

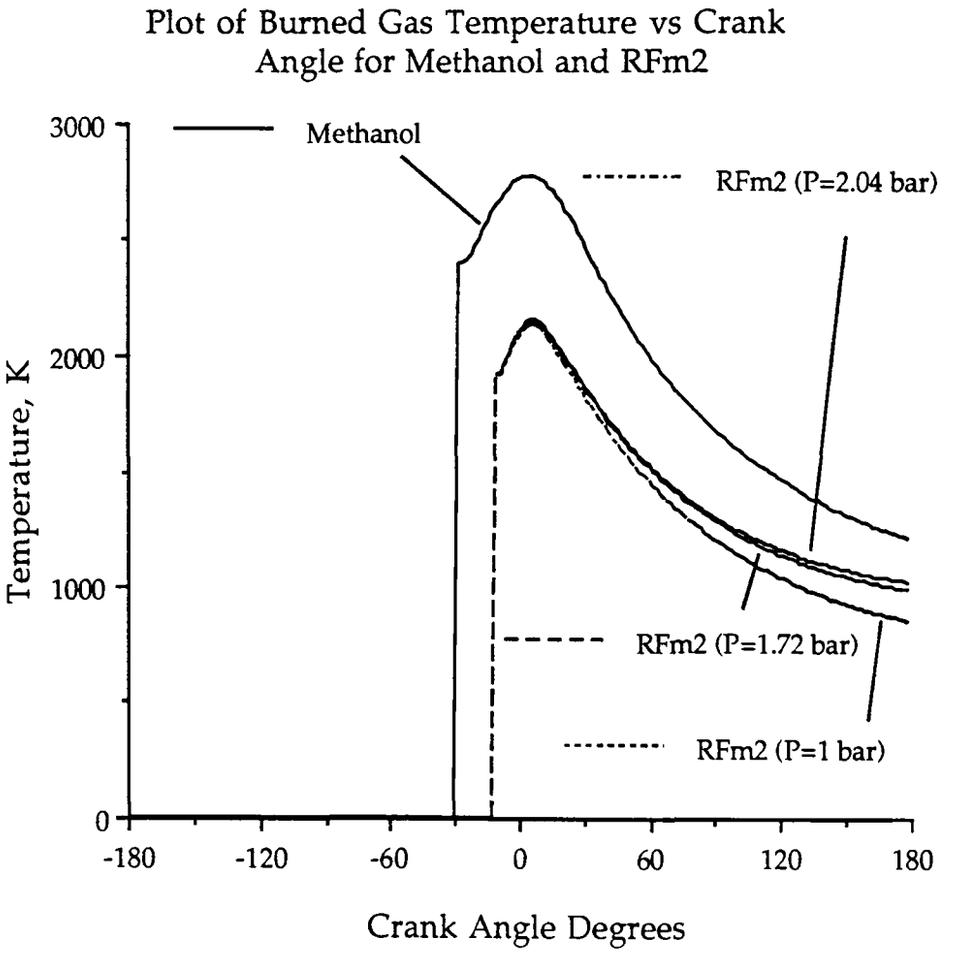


Fig 6.15b

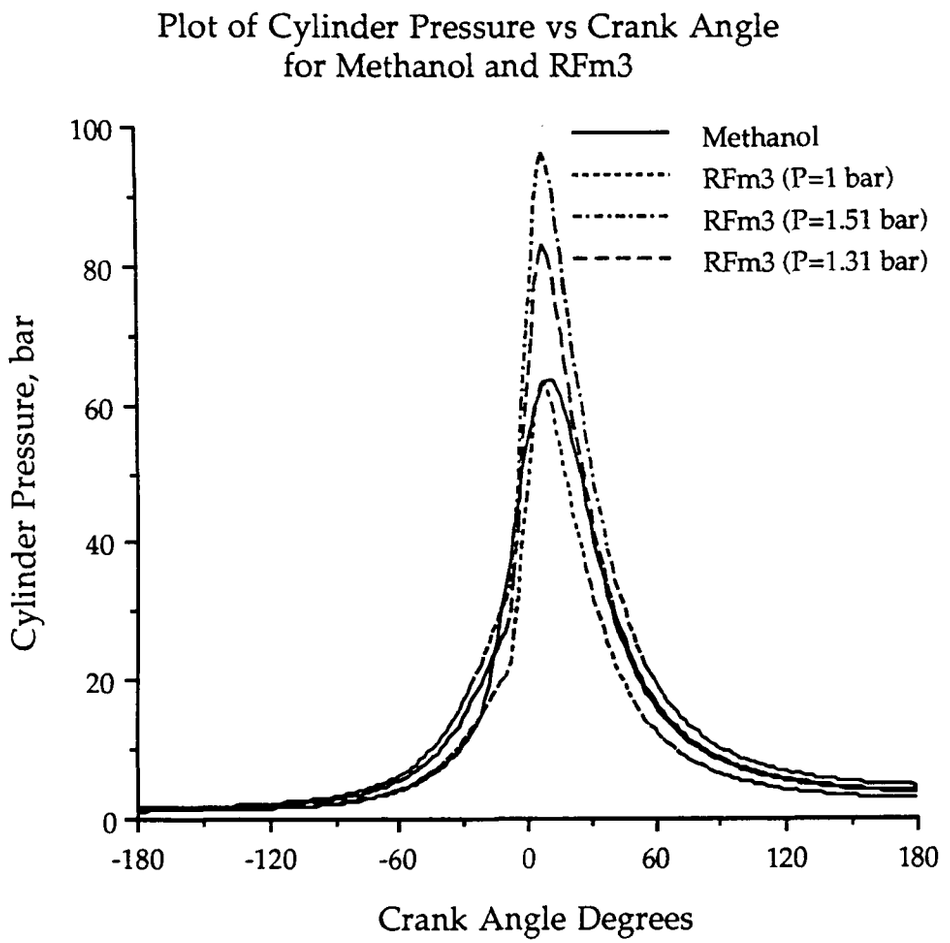


Fig 6.16a

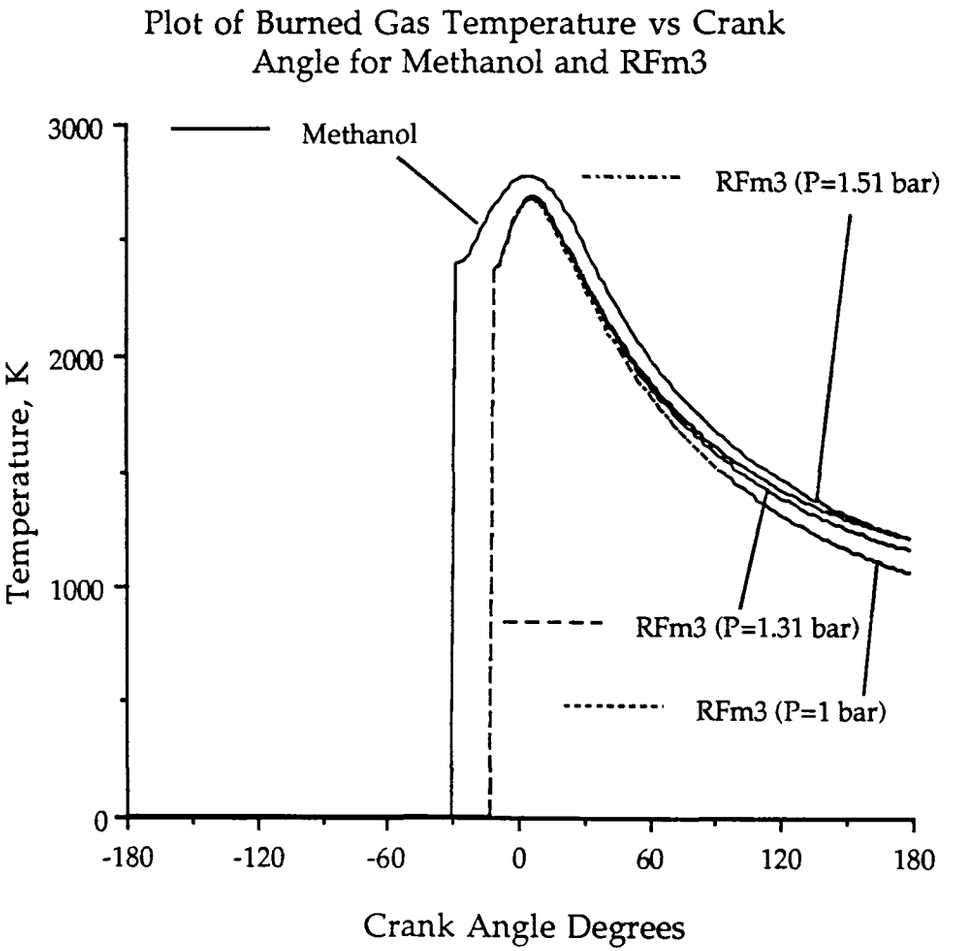


Fig 6.16b

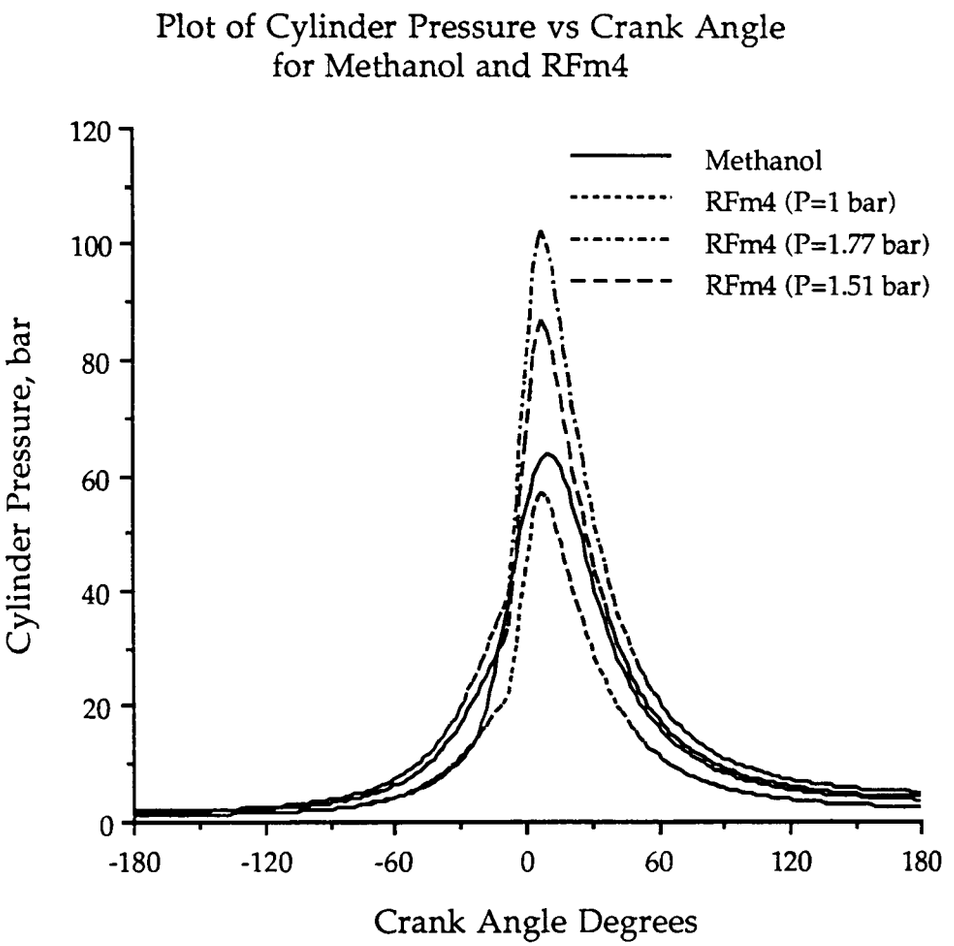


Fig 6.17a

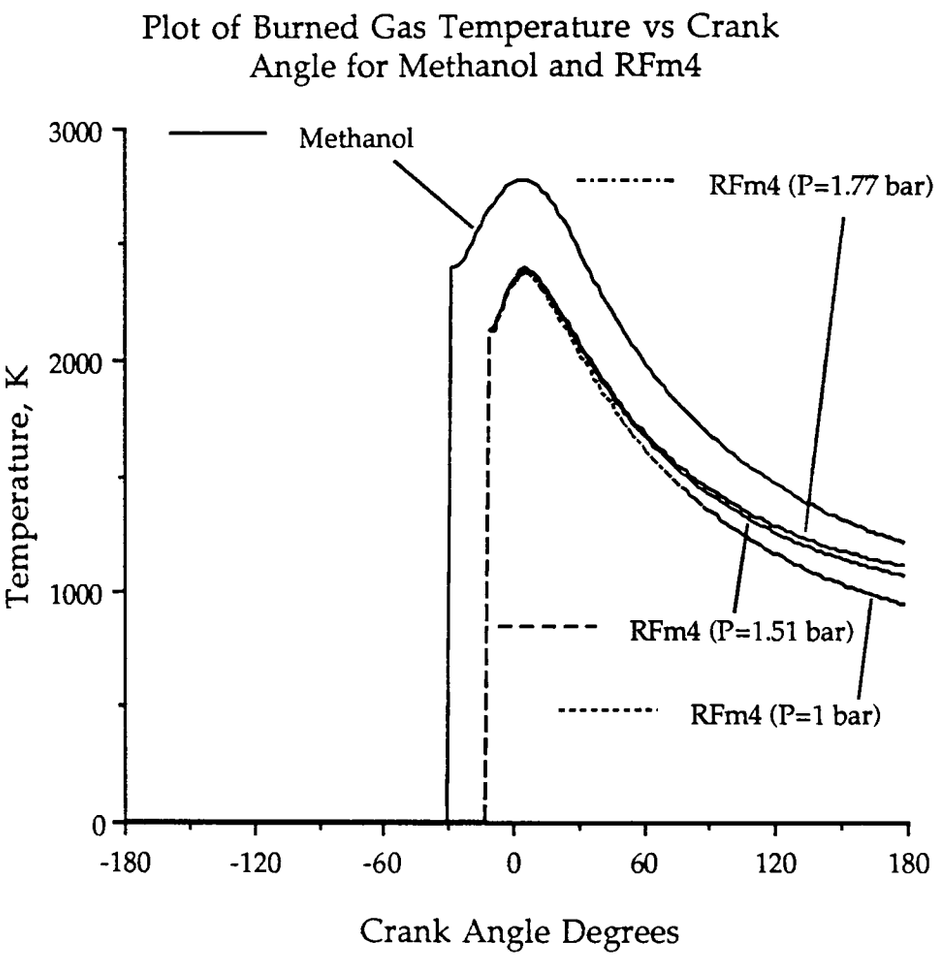


Fig 6.17b

Plot of Max Cycle Pressure and IMEP for Methanol and Reformed Methanol Fuels

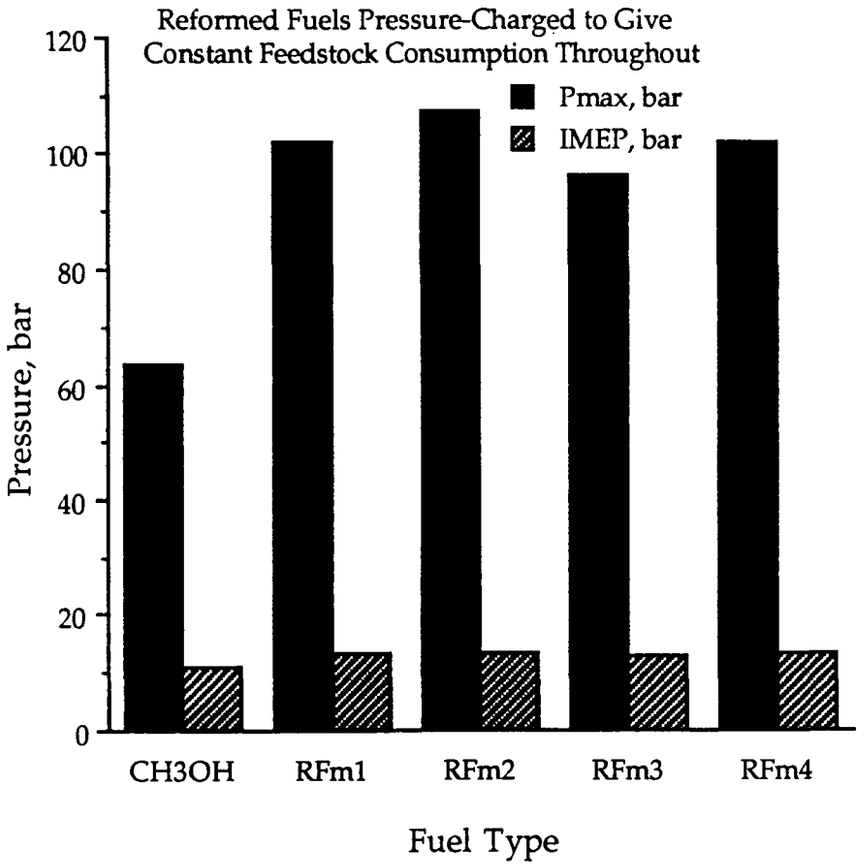


Fig 6.18

Plot of Cycle Burned Gas Temp and Reactor Temp Requirement for Methanol and Reformed Methanol Fuels

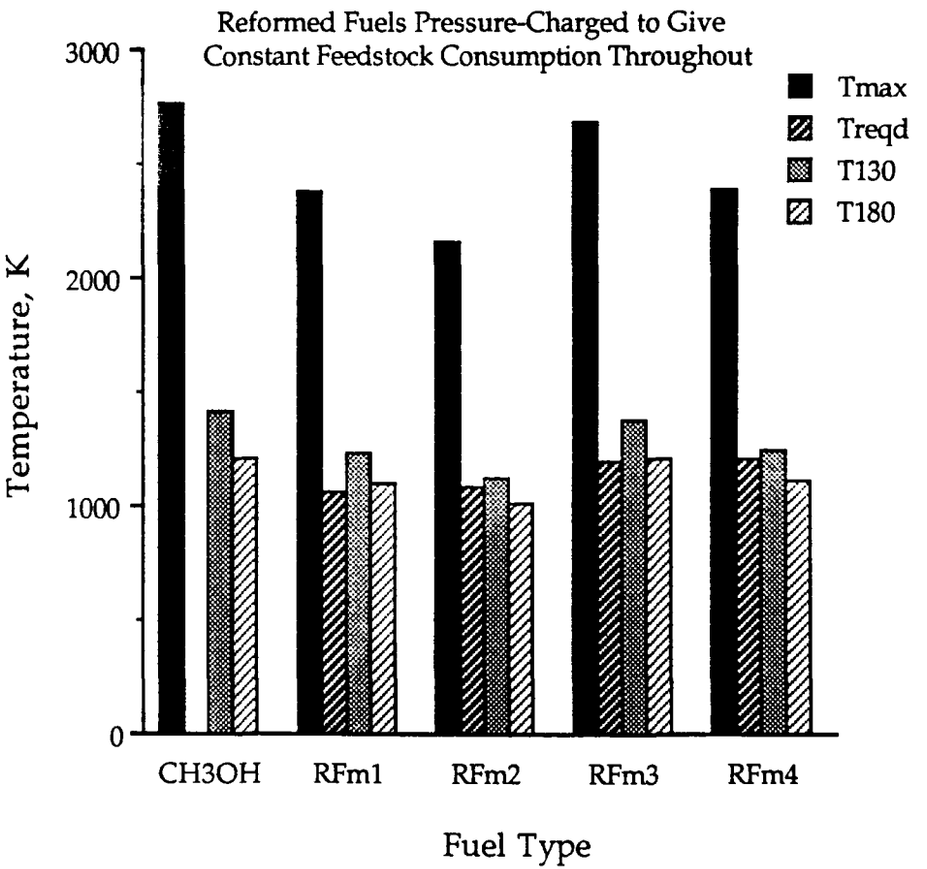


Fig 6.19

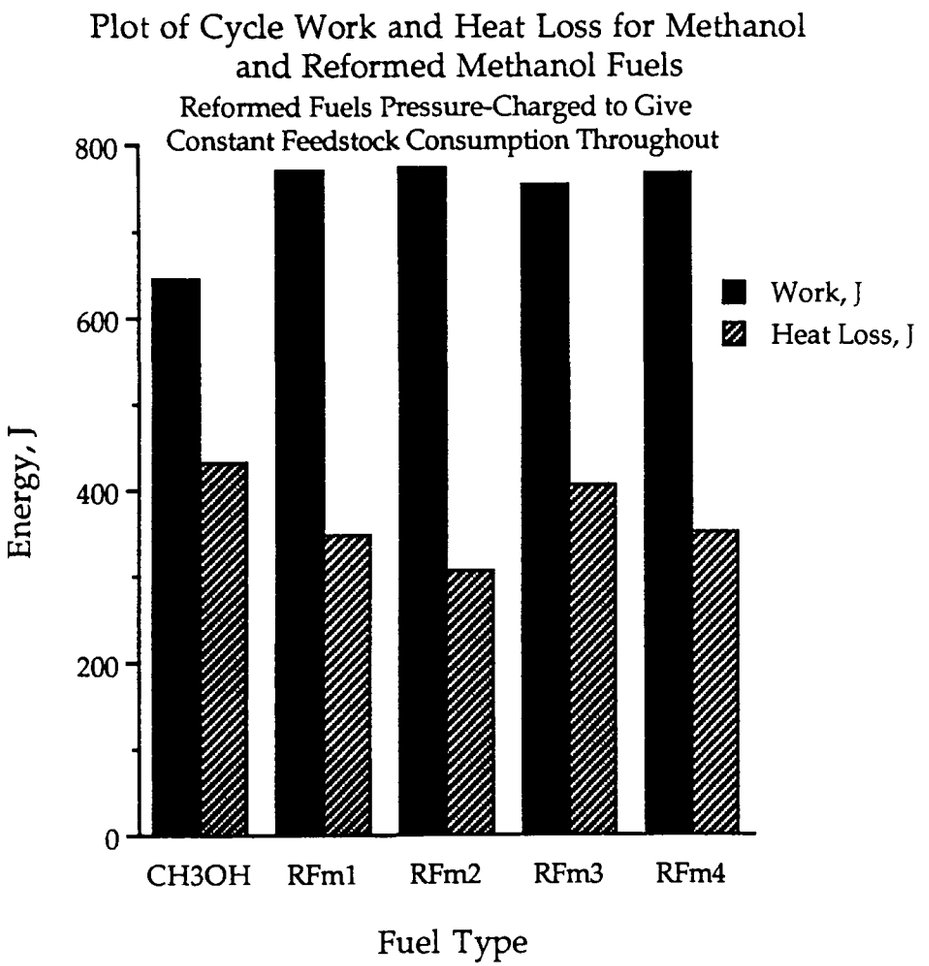


Fig 6.20

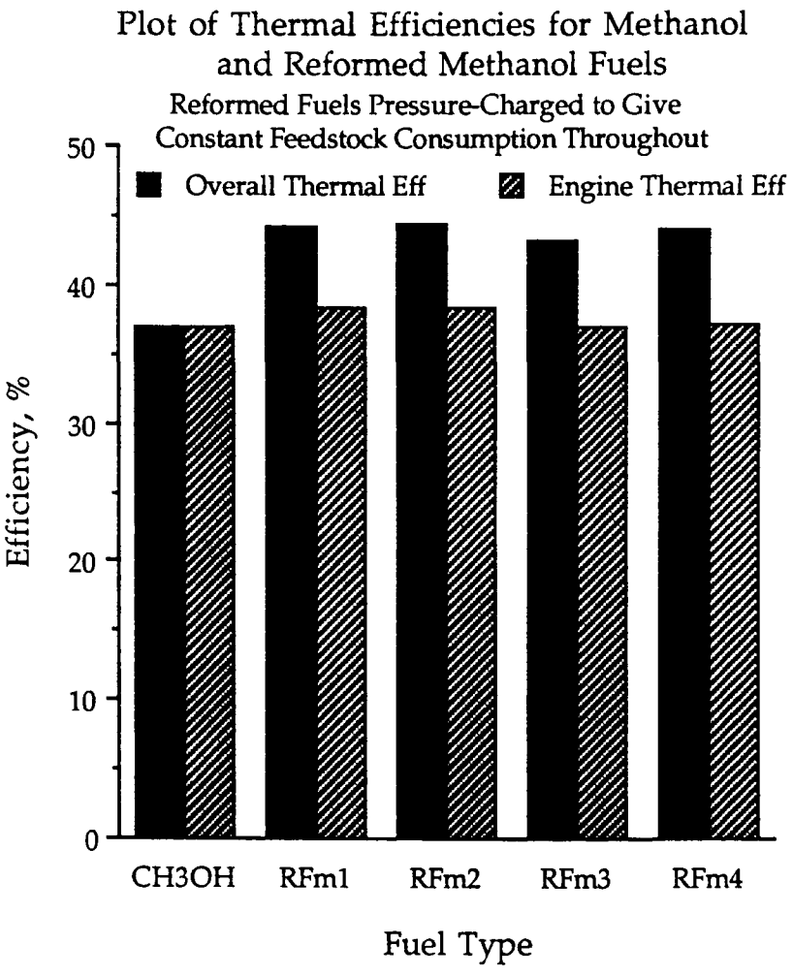


Fig 6.21

# 7 POLLUTANT EMISSION PREDICTIONS FOR ENGINE OPERATION ON REFORMED FUELS

The emission of toxic pollutants from the automotive engine has become a very important and widely debated issue over the past 25 years or so. Damage to life and the environment has become increasingly apparent (101), and legislation has quite rightly forced engine manufacturers to adopt sophisticated emission control strategies in order to meet the prescribed regulated limits (102, 103, 104).

Most of the current emissions legislation imposes limits on the permissible mass output of certain pollutants per mile of vehicle operation, as determined over a specific driving cycle which is performed under controlled conditions on a chassis dynamometer. The three main test procedures are those of the USA (105), Japan (106), and Europe (107), with many countries outside these areas adopting the American procedure, which is generally regarded as the more stringent standard. Rush and Larby presented an overview of the world-wide legislation situation in 1986; whilst the paper is very informative, it should be pointed out that some of the quoted limits have since been superseded (108).

To date, the legislation has been concerned mainly with the emission of carbon monoxide, unburned fuel (UBF - usually hydrocarbons), and oxides of nitrogen, which are mainly NO and $NO_2$ and are normally lumped together as $NO_x$. Future legislation is likely to include requirements limiting the permissible emission levels of aldehydes, and, in view of the recently much-publicized 'Greenhouse Effect', the levels of carbon dioxide. The general characteristics and formation mechanisms for the currently regulated pollutants are discussed by Bosch (109).

The predicted effect on the various emissions brought about by engine operation on exhaust-gas reformed fuels is discussed below, and it will become apparent that at this stage only a detailed theoretical investigation into the potential for $NO_x$ improvements can be undertaken.

## 7.1 The Effect of Exhaust-Gas Reforming on Currently Regulated Pollutants

### 7.1.1 Carbon Monoxide

Carbon monoxide formation in the engine arises primarily as a result of incomplete combustion in conditions of air deficiency, whilst a secondary mechanism is the thermal dissociation of carbon dioxide which occurs at the high temperatures which characterize the engine combustion process. Although equilibria predictions for such processes predict a certain amount of recombination as the mixture cools during the engine expansion stroke, experimental work has shown that in practice these reactions do not reach completion. This indicates that the reaction mechanism for the $CO/CO_2/O_2$ system is 'rate-controlled', which is particularly significant in the case of the high-speed internal combustion engine, and was discussed in section 5.1 (110).

As a major cause of CO formation is air-deficiency in the combustion mixture, it has to be concluded that the reformed fuel engine would be susceptible to such emissions if operated at air-to-fuel ratios lower than stoichiometric. Under more favourable conditions, CO formation resulting from localized rich zones caused by poor mixture homogeneity might be reduced in the reformed fuel engine, as the charge mixture should be more uniform, but it would be difficult to predict quantitative results without a very complex engine model.

It has been found in this project that peak cylinder temperature levels should be relatively low when operating with exhaust-reformed fuels, and it is therefore predicted that CO formation via the thermal dissociation route should be reduced as compared with conventional fuel operation.

### 7.1.2 Unburned Fuel (Hydrocarbons or Alcohols)

As in the case of carbon monoxide, air deficiency is a major cause of unburned fuel emissions, although other important sources are crevice volumes, mis-fires, flame quenching, and the adsorbtion/desorbtion mechanism at the cylinder-wall oil film. As the reformed fuel gas entering the engine cylinder should not contain more than traces of liquid hydrocarbon or alcohol fuels, it is suggested that the emission of such compounds from the engine should be extremely low. As in the case of CO, the level of sophistication which would be required of an engine model in order to predict unburned gaseous fuel emissions would be high, and it must hence be concluded that such levels would currently be best determined by practical rig-testing techniques.

### 7.1.3 Note on Aldehydes

Research into alternative fuels has led to concern over the emission of certain unregulated pollutants such as aldehydes, which appear to be particularly high from alcohol-fuelled engines. Chemicals such as formaldehyde, acetaldehyde and benzaldehyde are known contributors to photochemical smog, and are 'potentially carcinogenic', as well as being irritants of the skin, eyes, and mucous membranes (111); various empirical data pertaining to such emissions from gasoline, methanol and reformed-methanol engines have been published. König et al (47) report aldehyde

emissions from a methanol-fuelled engine some 2.5 to 3 times higher than from the same engine running at the same speed/load site on gasoline. It is also reported, however, that running on dissociated methanol gives reductions in aldehydes to levels lower than gasoline-fuelled values. These results are presented in the current work - see Fig 2.11.

Goodger mentions that the introduction of water into the methanol/air combustion system results in significant reductions in aldehyde levels, which is of interest in the current work in view of the unreacted water content of exhaust-gas reformed fuels (112).

Lipari and Colden report pure-methanol engine aldehyde levels some ten times greater than those for the equivalent gasoline-fuelled engine, when tested in accordance with the Federal Test Procedure, and it seems likely, therefore, that increasing use of alcohol fuels in the future will inevitably lead to the introduction of further legislation (35).

Many of these observations indicate that the proposed process of exhaust-gas reforming could result in important reductions in aldehyde levels, as compared with conventionally-fuelled engines, but no attempt has been made to quantify theoretical levels of improvement in this study.

### 7.1.4 Oxides of Nitrogen - $NO_x$

Nitric oxide (NO) and nitrogen dioxide ($NO_2$) formation is primarily attributable to the high temperatures which exist during the engine combustion process, and the two oxides are generally added together and expressed as an $NO_x$ concentration.

Of the two oxides, NO is quite the predominant species, and is formed by the oxidation of atmospheric nitrogen. The NO formation mechanism has been widely studied, and is particularly interesting as levels emitted from the engine are usually considerably higher than those predicted by equilibria computations, as a result of the effect of reaction kinetics (113, 114).

In view of this, predictive studies of such levels necessitate the adoption of an engine simulation package which incorporates the $NO_x$ kinetics model, but in the first instance, such a routine was not available. Hence, peak cycle temperature conditions were identified from the cycle analysis exercise and used in order to accurately compute peak equilibrium $NO_x$ levels by means of the EQCOMP.PAS Gibbs free energy equilibria routine. This enables an accurate comparison of baseline and reformed-fuel combustion peak equilibrium $NO_x$ levels. It was found that reformed fuels gave considerable $NO_x$ reductions, as predicted cycle temperatures were generally much lower with these fuels than with the standard fuels.

More recently, cycle analysis software has become available which does incorporate the $NO_x$ kinetics model, and it has thus been possible to predict the rate-controlled levels which might be emitted from the engine (115). Whilst the software gives grounds for comparison of rate-controlled levels, it should be pointed out that the code has not yet been quantitatively validated against a running engine. Further cycle simulation runs for the whole range of standard and reformed fuels have therefore been conducted from initial pressure conditions which give the same level of work output for the two fuelling modes. The results of peak equilibrium and rate-controlled $NO_x$ levels are given in Fig's 7.1 and 7.2. Peak equilibrium levels occur at peak cycle temperature conditions, whilst rate-controlled levels are quoted at the typical exhaust-valve opening crank angle of 130 degrees ATDC.

### 7.1.4.1 Discussion of $NO_x$ Predictions for n-Heptane Fuels

Fig 7.1 indicates that reformed fuel combustion should lead to significant reductions in $NO_x$ emissions. Plots of peak equilibrium and rate-controlled concentrations at 130°ATDC are given against an abscissa of peak cycle temperature, and the trends clearly follow the well established relationship which exists between $NO_x$ formation and combustion temperature. It should be pointed out that rate-controlled $NO_x$ concentrations have been read from a graphical output of cycle composition vs crank angle, explaining why values quoted in the text are round numbers.

A peak equilibrium level of 5955ppm is predicted for pure n-heptane, with a rate-controlled level of around 2950ppm at 130°ATDC. By comparison, the highest respective reformed n-heptane levels are 3061 and 305ppm for fuel RF4, which result from a peak combustion temperature reduced by approximately 250K as compared with the standard fuel. These $NO_x$ reductions are respectively equivalent to 48.5% and 89.7%, and all other reformed fuels give even greater predicted levels of improvement, as their peak cycle temperatures are lower still.

It is interesting to note that the apparent percentage reductions in rate-controlled levels are considerably larger than the predicted improvements in peak equilibrium level. This can be explained by consideration not only of peak temperature levels, but also the amount of time spent at these high temperatures during the cycle. Taking a temperature of 2000K as an arbitrary cut-off point, above which $NO_x$ might be considered to form in appreciable quantities, it can be seen that reformed fuel cycle temperatures exceed this level for much shorter durations than for the standard fuel. In the case of RF4 (see Fig 6.4b) the reformed fuel cycle temperature levels exceed 2000K for

around 56° crank angle, whilst the temperature is exceeded for 92° in the case of the pure n-heptane fuel under the same cycle work output conditions.

In the case of fuel RF5 (Fig 6.5b), which gives barely quantifiable rate-controlled $NO_x$ levels and a peak equilibrium level of just 812ppm, the crank angle elapsing during which the arbitrary 2000K threshold is exceeded is 32°.

It is therefore concluded that reformed fuels should give low $NO_x$ levels as compared with the standard n-heptane fuel, as a result of anticipated reductions in both peak cycle temperature and the duration spent at high temperatures. Predicted reductions in peak equilibrium levels are generally greater than around 48.5% for the fuels examined, with improvements in rate-controlled concentrations exceeding 89.7%.

#### 7.1.4.2 Discussion of $NO_x$ Predictions for Methanol Fuels

Fig 7.2 shows similar trends to those of Fig 7.1, ie sharp increases in $NO_x$ as temperature rises towards 2700K. In the case of the pure alcohol, the peak cycle equilibrium $NO_x$ level is 4475ppm, with a predicted rate-controlled concentration at 130°ATDC of around 2450ppm. Of the reformed fuels, $RF_m3$, which has a relatively high heating value per unit mass, gives highest peak equilibrium and rate-controlled values of 3120 and 1200ppm respectively, representing reductions of 30.3% and 51.0% below baseline.

Again, temperatures of 2000K and above exist for much shorter crank angle durations in the case of the reformed fuel cycles with, for example, $RF_m2$ cycle temperatures only being in this range for 24° compared with 90° for the standard fuel. This leads to barely quantifiable predictions of rate-controlled $NO_x$ levels for most of the reformed methanol fuels examined.

## 7.3 Conclusions of Pollutant Emission Predictions.

This brief predictive study of emission levels has sought to give a general insight into the potential for reductions in regulated pollutants when the engine is operated with exhaust-reformed fuels.

As mentioned, the levels of currently regulated pollutants such as CO and unburned fuel cannot easily be predicted, as they are largely functions of air to fuel ratio and engine geometry (crevice volumes, flame quenching etc.). For this reason, no theoretical prediction of the effect on such emissions has been attempted.

Theoretical predictions have, however, been made for peak equilibrium and rate-controlled $NO_x$ levels for reformed fuel combustion, using an engine model which incorporates the $NO_x$ kinetics mechanism. This has indicated that large improvements should be attainable, with predicted reductions in rate-controlled levels being considerably greater than those in peak equilibrium concentrations. Predicted reductions in peak and rate-controlled levels are in excess of around 48.5 and 89.7% respectively in the case of n-heptane fuels and 30.3% and 51.0% for the alcohol, when reformed fuel levels are compared to standard fuel baseline at the same level of cycle work output.

This work concludes the theoretical feasibility study. Subsequent chapters of the thesis deal mainly with the reformer/test-rig design and testing phases of the project, the main objective of which is to establish a practical understanding of the chemistry of the proposed exhaust-gas reforming process.

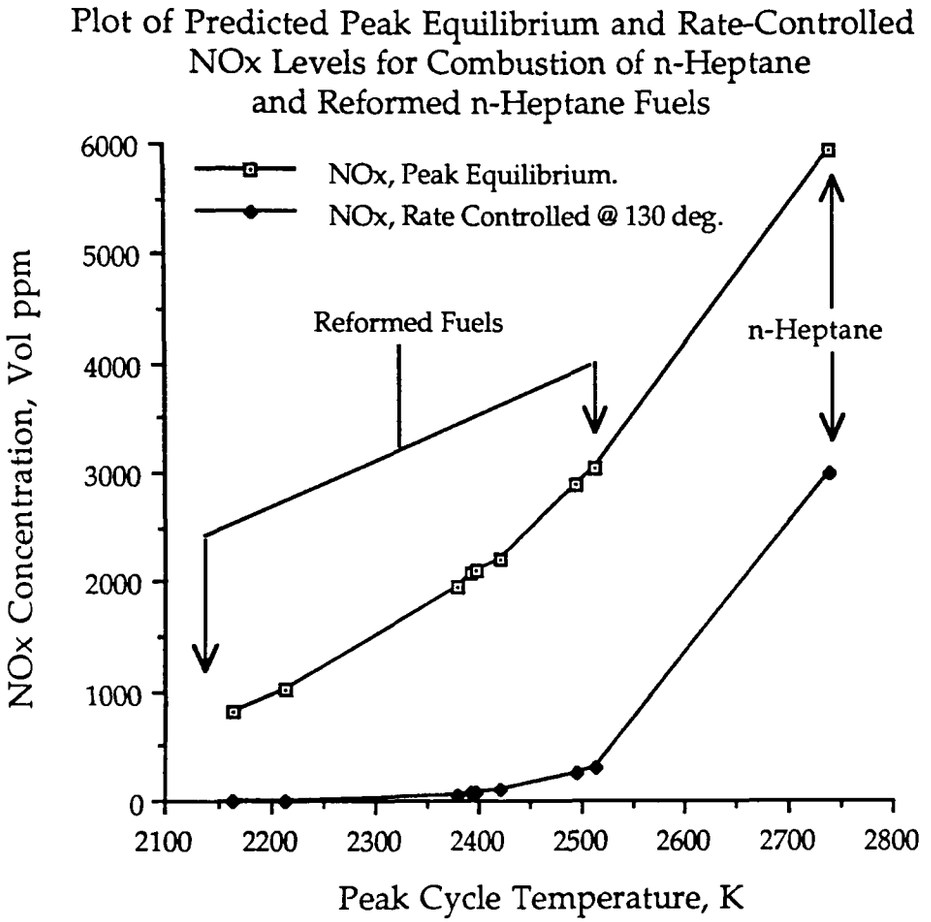
Plot of Predicted Peak Equilibrium and Rate-Controlled
NOx Levels for Combustion of n-Heptane
and Reformed n-Heptane Fuels
NOx, Peak Equilibrium.
NOx, Rate Controlled @ 130 deg.
Reformed Fuels
n-Heptane
NOx Concentration, Vol ppm
Peak Cycle Temperature, K
6000
5000
4000
3000
2000
1000
0
2100
2200
2300
2400
2500
2600
2700
2800

Fig 7.1

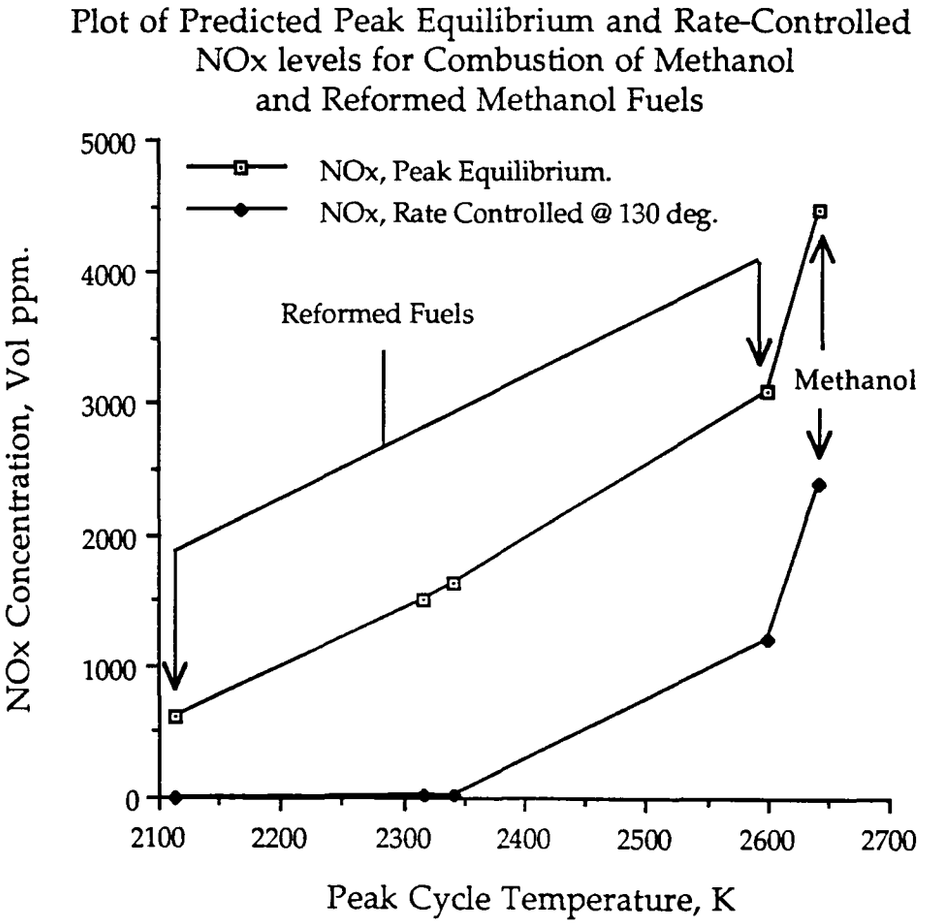
Plot of Predicted Peak Equilibrium and Rate-Controlled
NOx levels for Combustion of Methanol
and Reformed Methanol Fuels
NOx, Peak Equilibrium.
NOx, Rate Controlled @ 130 deg.
Reformed Fuels
Methanol
NOx Concentration, Vol ppm.
Peak Cycle Temperature, K
5000
4000
3000
2000
1000
0
2100
2200
2300
2400
2500
2600
2700

Fig 7.2

# 8 DESIGN OF PROTOTYPE REFORMING REACTOR AND TEST RIG

The theoretical work conducted so far has predicted potential improvements in thermal efficiency and emission performance for an engine operating on exhaust-gas reformed fuels in place of the conventional feedstocks. The objective of the work reported in the following two chapters was to design, construct and operate a laboratory test rig capable of producing such reformed fuels, and hence establish the practical feasibility of the proposed process.

The first task of this phase of the project was to finalise the design criteria for the prototype reforming reactor, and then to begin producing working drawings leading into manufacture. As this design work progressed, so too did the design and construction of the test rig itself. On completion, the reformer was assembled onto the rig and commissioning began, highlighting one or two shortcomings which were rectified prior to commencement of the test programme.

In the first instance the design of the reforming reactor will be described.

## 8.1 Design of the Reforming Reactor

The following list gives the main points thought to be important in the design of the reformer:

1) Catalyst formulation - naturally this is critical in order that the requisite reactions are actively promoted.

2) The reactor should be charged with a quantity of the chosen catalyst which is sufficient to deal with the throughput of reactants (see space velocity calculations below).

3) The catalyst should be arranged in such a way that presents an acceptably low restriction to the gas flow.

4) Good heat transfer conditions should exist between any surplus exhaust gases (ie those not required directly in the reforming process) and the catalyst matrix, in order that this important source of thermal energy is fully utilized.

5) The reactor should be able to withstand gas temperatures of up to around 1200°C without suffering mechanical or metallurgical degradation.

6) Facilities should naturally exist for the easy flow of reforming and surplus exhaust gases into and out of the device, and for the injection of the reformer feedstock and secondary steam.

7) Due consideration should be given to the instrumentation of the reactor. In particular, temperatures at inlet and exit from the catalyst, as well as part-way through it, would be of interest, and the siting of suitable thermocouple probes had thus to be considered from the outset.

Johnson Matthey Catalytic Systems Division were approached for advice in the selection of a suitable catalyst, and for guidance regarding catalyst volume. It was suggested that the use of a noble metal catalyst

deposited on a ceramic monolith support would best deal with the high temperature reforming environment, and Johnson Matthey offered to supply core-drilled round-section monoliths compatible with the proposed reformer dimensions. In the event, 35mm diameter samples of ceramic substrate having a cell density of 400 cells/sq inch were supplied. The washcoat deposited on the monolith consisted of a noble metal formulation of finely dispersed platinum and palladium particles.

For the purpose of space velocity calculations, the total catalyst volume of this type of support is simply based on the outer dimensions of the monolith, and it was decided, in conjunction with Johnson Matthey, that a total volume of around 2 litres should be adequate for the prototype reactor. Assuming that the rig would use a propane burner rated at 30kW output as the exhaust-gas generator (see discussion in later section), and that at most 50% of the gas produced would be directed to the reforming catalyst, the gas hourly space velocity (GHSV) can be calculated as follows:

$$\text{Gas Hourly Space Velocity} = \frac{\text{Catalyst Exhaust-Gas Flow Rate at STP}}{\text{Catalyst Bed Volume}} \left[\frac{\text{l}}{\text{l h}} = \text{h}^{-1}\right] \quad (8.1)$$

Stoichiometric burner operation at 30kW gives a calculated total mass flow rate of products of 39.0 kg/h, of which, for the purpose of this calculation, it is assumed 19.5 kg/h will pass through the catalyst. These gases have a molecular mass of 28.3, which gives a volumetric gas flow rate of 16567 l/h under standard conditions, giving a GHSV as follows:

$$\text{GHSV (30kW, 50\% Flow Split)} = 16\,567/2 = 8\,284\ \text{h}^{-1}$$

The nominal 2 litre volume is made up of 6 catalyst-charged tubes arranged in a shell and tube heat exchanger, as shown in Fig 8.1. It was felt that this arrangement gave the best compromise in terms of heat transfer between surplus exhaust gases and reforming catalyst, system back pressure, and ease of manufacture. As the diagram shows, only one end of the tube-stack is rigidly connected to the outer shell of the device, thus minimizing problems relating to differential expansion rates. Reforming flue gases are directed to the catalyst-bed via the central tube and the tube-stack end casing, with preheated feedstock and additional steam injected part way along the entry duct as required.

Inco Alloys International Inc. were approached regarding material selection for the reactor assembly, and it became apparent that a stainless steel containing nickel and chromium alloying elements would be best suited to the environmental demands of the unit (116). Inco subsequently provided the required tubing and sheet material in Inconel 600* and Incoloy 800* alloys free-of-charge, for which they are gratefully acknowledged.

Fully dimensioned engineering drawings of the reforming reactor were then completed, and the manufacture sub-contracted to Welding and Brazing Developments of Cannock, who specialize in the fabrication of high-temperature stainless steel alloys. The outer casing of the reactor was rolled from flat sheet and seam-welded, whilst the tubes which were to contain the catalyst were machined to give the minimum possible wall thickness, thereby maximizing the potential for good heat transfer. On completion of all machining operations, the reactor parts were fabricated into sub-assemblies, with all joints welded by means of the tungsten inert gas (TIG) technique

---

* Inconel and Incoloy are trademarks of the Inco family of companies

using Inconel* filler wire. The integrity of the completed fabrications was then verified using Ardrox® crack detection chemicals.

Final assembly of the reformer was carried out at the Automotive Engineering Centre, as this involved the careful installation of the catalyst monoliths and provisions for instrumentation. The monoliths were secured in the tube-stack using a composite comprising Macsicar 2 high temperature fire-clay and ceramic wool fibres. Reactor end-plates and flange joints were bolted down with stainless steel M10 cap screws and nuts, and were sealed with gaskets made from ceramic fibre paper and the fire-clay. At this stage the reactor was furnished with the following instrumentation:

Temperatures:

1) Reforming exhaust at inlet to the reactor.
2) Surplus exhaust at inlet to the reactor.
3) Reforming mixture 10mm into catalyst at entry.
4) Reforming mixture 1/2 way through catalyst.
5) Reforming mixture 10mm into catalyst at exit.
6) Surplus exhaust at reactor outlet.
7) Preheated and vaporized feedstock at inlet to reactor.
8) Secondary steam at inlet to reactor.

Pressures:

1) Reforming exhaust at inlet to reactor.
2) Surplus exhaust at inlet to reactor.
3) Reforming mixture at reactor outlet.
4) Surplus exhaust at reactor outlet.

All temperature probes are mineral-insulated Inconel-sheathed Type-K thermocouples, rated to 1200°C, whilst pressures are measured using Druck PDCR 910 strain-gauge pressure transducers which are mounted on a manifold remote from the reactor, and connected to the tapping points on the rig by lengths of 0.25" diameter stainless steel tubing.

The main problem encountered with the transducer hardware was related to the measurement of the three 'in-catalyst' temperatures, which in the first instance was accomplished by the insertion of 0.5mm diameter thermocouples into the catalyst matrix. Unfortunately, it was found on initial testing that these probes were not sufficiently robust to cope with the environment, and they were therefore replaced with 1mm diameter probes. These proved to be far more successful, although their insertion did completely block the particular cell of the matrix. It was felt, however, that in view of the high cell density, and the possibility of gas flow through the cell walls, the effect of this blockage on temperature readings would be negligible.

Photographs of the part-assembled reactor are shown in Figs 8.2a, b & c.

## 8.2 Design and Construction of the Test Rig.

It had been decided that the best way to test the reformer in the first instance would be by means of a static test rig, using a burner/combustion chamber assembly as a flue-gas generator. It was originally proposed that the burner be fuelled with natural gas from the mains, but it became apparent that a propane-fuelled burner would give a product gas composition more representative of that expected from a gasoline-fuelled engine. This is due to the hydrogen to carbon ratio of the fuels, which is 4.0, 2.67 and around 1.8 to 1.9 for the methane, propane and gasoline fuels respectively

A single shell and tube combustion chamber/heat exchanger assembly was specified to house the burner, and provides a means of generating flue-gases having a controlled temperature at inlet to the reactor. A schematic diagram of the test-rig hardware is shown in Fig 8.3.

The combustion chamber assembly was manufactured by W B Combustion of Cannock, and is again constructed largely in Inconel alloys. Flue gas temperature control is achieved by means of a thermocouple at the chamber outlet connected to a Eurotherm Type 815 temperature controller in a closed-loop configuration. The controller operates a motorized valve sited in the cooling-air inlet duct leading to the outer shell of the combustion chamber assembly. The operator simply inputs the required flue gas temperature at the rig control panel, and the system will then control to within about +/- 2°C of the set-point, once the combustion chamber is up to temperature.

As outlined above, the rig is fully instrumented with thermocouples and pressure transducers, and there are flow meters situated in all fluid inlet pipes (air, propane, feedstock, water), as well as orifice plates in the two gas outlet ducts which enable the flow split between reforming and surplus exhaust gases to be determined. The flow split between the two channels is controlled by a single butterfly valve sited in the surplus exhaust gas duct at the outlet of the reactor unit, which permits testing over a range of catalyst space velocities. Finally, there are a number of gas sampling points on the rig in order to facilitate the determination of flue and fuel gas compositions.

All pressure and temperature transducers are connected to multi-channel indicators which incorporate IEEE-488 interfaces (117), enabling the units to be connected directly to a data acquisition board fitted to the Apple

Macintosh IIci computer; this system is described below. In addition, Table 8.1 summarizes the instrumentation specification for the rig and reactor.

Once fully assembled, all of the exposed ducting, and the reactor itself, were enclosed in ceramic fibre blanketing for the purpose of minimizing heat losses from the system; the insulation also serves as an essential safety feature. Figs 8.4a, b and c show photographs of the assembled rig with the insulation removed.

### 8.3 Computer-Based Data Acquisition

As there were around 10 pressure and 10 temperature channels being monitored on the rig, it was thought that a computer-based data-logging capability would be useful. In order to facilitate this, the specification for the two multi-channel monitors procured for the purpose of pressure and temperature indication included the provision of IEEE interface hardware, which would enable data transfer between the instrument and computer over the General Purpose Interface Bus (GPIB).

The Macintosh IIci computer was fitted with a National Instruments NB-DMA-8-G GPIB data acquisition board, which acts as an interface between the computer and the information transfer bus, and enables control of data-logging activities for up to 13 discrete IEEE-compatible instruments on the parallel bus. In the current project, just the two above-mentioned 10-channel monitors were connected, and having organized the necessary hardware, the next step involved writing the instrument driver software. This was done in the LabVIEW (Laboratory Virtual Instrument Engineering Workbench) software environment, as described below (118).

### 8.3.1 Creation of LabVIEW Instrument Drivers

LabVIEW is a software environment in which application programs are created using a graphical programming language called G, and are referred to as *Virtual Instruments* or *VI's*. *VI's* usually have three main parts, namely the *Front Panel*, the *Block Diagram* and the *Icon/Connector Pane*. The Front Panel is the user interface, which enables the user to interact with the application, and provides a mechanism for manual data input and output. The Block Diagram is the *VI's* source code, or in effect the computer program, and the Icon/Connector Pane acts as a visual representation of the *VI*, and also enables the *VI* to be used as a *Sub-VI*, analogous to a sub-routine in conventional programming, in the block diagram of a larger *VI*.

LabVIEW is ideal for the problem in hand, ie writing instrument driver software, as the package is supplied with a library of *sub-VI*'s which perform various GPIB commands. For example, the *GPIB Write VI* will write a specified data string to a nominated GPIB device (instrument), whilst the *GPIB Read VI* can then be used to read a specified number of bytes of information from the addressed device. Using such *VI's* as *sub-VI's* in conjunction with other LabVIEW facilities leads to a larger application, enabling the user to remotely control real instruments via the representative front panel displayed on the computer. The *VI* front panel is constructed by the user in such a way that it gives a visual representation of the real instrument, with, for example, on/off, channel select and parameter-switching facilities. In addition, user-written *sub-VI's* can be incorporated which scale the acquired data for display in any chosen engineering unit, which was useful in the current work. The LabVIEW Front Panel and Block Diagram created for the purpose of controlling the CIL TA880 multi-channel temperature monitor are shown in Figs 8.5 and 8.6 respectively.

Referring to Fig 8.5, variable controls for selecting channel number for start and end of data logging scans and unit selection are shown, and each of these can easily be adjusted to the desired value by the user by means of the computer mouse. The GPIB primary address box must be set to the pre-determined address of the actual instrument, which in this case is 09 for the TA880. The GPIB Read count is set to 20 bytes, which enables the *VI* to read the required amount of data from the real instrument at each scan, and the write/read delay of 500ms is introduced in order to allow the TA880 to update its display between GPIB read operations. The matrix to the right-hand side of the *VI* front panel gives a display of the values of the 10 logged temperature channels, which can automatically be transferred into an external file on the hard drive of the computer if required.

The block diagram which runs behind the front panel, and is effectively the computer program, is shown in Fig 8.6. *Sub-VI* icons for GPIB Write and GPIB Read functions are clearly shown. No attempt will be made here to go into more detail, but it can be said that the intuitive nature of the LabVIEW programming environment made the writing of the instrument drivers relatively straight-forward, and has led to the development of a very user-friendly data acquisition application.

A similar Virtual Instrument was also created in order to control the Druck DPI 420 pressure indicator, which, in conjunction with the TA880 *VI*, enables full computer control of most pressure and temperature logging operations.

## 8.4 Gas Analysis.

For the purpose of setting the air to fuel ratio of the propane burner, a relatively simple Testoterm $O_2$ analyser, operating on the electromagnetic cell principle, has been employed. This gives a digital readout of the flue gas oxygen concentration to a resolution of 0.1%, with calibration carried out automatically on start-up using atmospheric air. Much of the testing was carried out under approximately stoichiometric burner operating conditions, in which case the burner air to fuel ratio (AFR) is adjusted to give a flue-gas oxygen level of around 0.2%. Testing with oxygen-enriched flue gases was conducted with the burner AFR set to give the desired levels of oxygen concentration as determined by the Testoterm analyser.

In the first instance, the Orsat apparatus was used as a means of obtaining a more complete analysis of the flue gas composition. This equipment gives a dry analysis of the sample, by means of chemical reagents which absorb $CO_2, O_2$ and CO as the sample is passed through the apparatus. In this case, resolution is to a level of 0.2%, and, notwithstanding the apparent simplicity of the technique, it appeared to give accurate and repeatable results when applied carefully to the analysis of flue gases. The apparatus was also used to analyse the proposed reformed fuels, and, in terms of the three gases mentioned above, it was found to be most useful. The main limitation of the apparatus, however, regards the determination of combustibles other than CO in the sample. Whilst provision apparently exists for the measurement of pure hydrogen, the presence of other combustible gases such as light hydrocarbons renders the oxidation technique employed inapplicable. More sophisticated techniques therefore had to be employed in order to fully analyse samples of gaseous reformed fuels.

In particular, use was made of the Gas Chromatograph-Mass Spectrometer (GC-MS) system, which was acquired recently for use in an allied research project (119). In this case, flue and reformed fuel gases were sampled from the test rig by means of a heated sample line, and introduced directly into the column of the gas chromatograph before passing through the mass spectrometer detector. These analyses gave some interesting results, but it became apparent that a certain amount of system development would be required before an accurate quantitative analysis could be achieved. It was therefore decided that the gas analysis work should be carried out on a sub-contract basis by a certified external laboratory. In order to facilitate this, industry-standard gas sampling equipment comprising a positive displacement pump, stainless steel sample cylinders, a pressure indicator and purge attachment were procured. This enabled pressurized samples of reformed fuel gas to be collected from the test rig and taken to British Gas Scientific Services laboratories, where a full gas analysis was undertaken. The gas analysis technique employed is based on gas chromatography separation followed by detection using flame ionization, thermal conductivity and non-dispersive infra-red analysers. Results thus obtained were found to be reliable and repeatable, leading to a high degree of confidence in the analysis.

### 8.5 Rig Commissioning.

Initial commissioning of the rig involved setting up the propane burner and gas controls to ensure safe and reliable operation of the combustion apparatus. Problems were encountered due to the back pressure presented by the reactor and flue ducts, which was relatively high compared with the restriction found in furnace applications more typical for this type of burner. Burner stability problems were overcome by ensuring good sealing around the back of the burner assembly, and by the use of a more suitable gas

pressure regulator than that which had been originally supplied. Minor problems relating to excessive condensation in the outlet ducting were cured by the application of additional water trap/drain arrangements.

### 8.6 Preliminary Test Programme

Having validated the general safety and integrity of the rig assembly up to flue gas temperature of around 950°C at combustion chamber outlet, the preliminary test programme commenced.

Initial testing was carried out with the burner propane flow-rate set at 20 l/min, and with the air flow rate set to give a flue gas composition containing some 0.2% oxygen, ie very nearly stoichiometric conditions; this setting would give a nominal output of just over 30kW. Burner operation was constrained to err on the lean side of stoichiometric, in order to minimize the possibility of carburizing conditions which might have a detrimental effect on the long-term durability of the rig.

Neglecting the small amount of excess air, the stoichiometric equation for the propane burner is as follows:

i) Burner combustion:

$$C_3H_8 + 5(O_2 + 3.76N_2) \rightarrow 25.8(0.116CO_2 + 0.155H_2O + 0.729N_2) \quad (8.2)$$

Stoichiometric AFR = 15.6 : 1

It was decided that initial trials would be conducted using RF-08 as the reformer feedstock. This fuel is a European reference grade unleaded gasoline

having an overall composition represented by $(CH_{1.79})_x$ (120). The idealized exhaust-gas reforming equation for the fuel, using flue gases generated by the propane burner (eqn 8.2) is given by:

ii) Reforming of European Reference Grade Unleaded Gasoline, RF-08

$$(CH_{1.79})_x + (3.69x)(0.116CO_2 + 0.155H_2O + 0.729N_2) \rightarrow (5.59x)(0.256CO + 0.263H_2 + 0.481N_2) \quad (8.3)$$

Stoichiometric Reforming Exhaust Gas to Feedstock Ratio = 7.57 : 1

At the 30kW stoichiometric burner operating condition, the total flue gas mass flow rate is around 0.650 kg/min. In the first instance, this flow is split equally between the reforming and surplus sections of the reactor, giving a catalyst flow rate of 0.325 kg/min. The stoichiometric gasoline flow rate through the catalyst is then simply calculated as follows:

$$\text{Stoich. Gasoline Flow Rate} = \frac{\text{Flue Gas Flow Rate}}{\text{Stoich. Reforming Exh. Gas to Feedstock Ratio}} \quad (8.4)$$

which in this case gives a figure of 0.043 kg/min and a volumetric liquid flow rate of 57.2 ml/min, based on a quoted specific gravity of 0.7503 (120).

In view of earlier theoretical predictions that stoichiometric reforming would tend to lead to the formation of carbon solids, it was decided that testing should be conducted at gasoline flow rates of between 20 and 40 ml/min, and at flue gas temperatures in the range of 850°C to 950°C at entry to the reformer. In addition to these trials, which were conducted using

stoichiometric burner flue gases, a short investigation of the effect of excess air in the combustion products was also undertaken.

On completion of this early investigative work, during which only the Orsat gas analysis technique was used, the reformer was stripped down and the catalyst removed for inspection, as little evidence of the proposed endothermic reforming reactions had been observed. It was suspected that the catalyst might have become damaged, or possibly poisoned by traces of sulphur contained within the feedstock (121).

Although the reactor hardware appeared to be in good condition, it was apparent that the catalyst monolith had suffered a thermal failure, resulting in several cell passages becoming completely blocked by what appeared to be re-solidified molten substrate material. Samples of this were sent to Johnson Matthey, who conducted an electron-probe X-ray micro-analysis, and confirmed that the failure was indeed the result of overheating to a temperature of around 1300 to 1400°C (122).

Evidence of this overheating had been noted during the early excess-air reforming trials, where flue gases containing some 3% oxygen were used as the reforming oxidant. The apparent overheating problem arose when shutting off the gasoline feedstock flow to the reactor, as under these conditions, a sharp and uncontrollable increase in temperature to over 1200°C was observed on one occasion. It was thought that this transient temperature excursion was due to the fact that as the feedstock flow rate reduced towards zero, a point would momentarily exist where there was a stoichiometric oxygen-to-gasoline ratio within the reactor. This would naturally lead to a highly exothermic reaction, and a resulting sharp rise in temperature.

This hypothesis appeared to be confirmed in later excess-air trials, where the excess air to the burner was trimmed off before shutting down the reformer feedstock flow, thus ensuring that gasoline to oxygen ratios were always extremely fuel-rich in terms of the oxidation stoichiometry. In doing this, no further overheating problems attributable to the feedstock oxidation were experienced.

The reformer was then rebuilt with a fresh charge of catalyst, and tested using n-heptane as the reformer feedstock. Again, the flow from the burner, which was fired under stoichiometric conditions at the nominal 30kW output, was split into two equal flows at entry to the reformer, and the preheated and vaporized n-heptane introduced into the reforming exhaust-gas stream. The stoichiometric equation for the reforming of n-heptane with burner flue gases is as follows:

$$C_7H_{16} + 25.83(0.116CO_2 + 0.155H_2O + 0.729N_2) \rightarrow 40.83(0.245CO + 0.294H_2 + 0.461N_2) \quad (8.5)$$

From which the stoichiometric exhaust gas to n-heptane reforming ratio is 7.31 : 1.

This leads to a stoichiometric n-heptane flow rate of 0.044kg/min, and hence a liquid flow rate of 64.0 ml/min. Again, in order to avoid C(s) formation problems, flow rates of 20 to 40 ml/min were used, with flue gas temperatures at inlet to the reformer of 850°C to 950°C. The results observed were of limited interest, as it was still not possible to detect any significant endothermic reaction. Having examined the effect of most other variables, it was concluded that the space velocity through the reformer must be too great to permit conversion of the feedstock.

The test rig was therefore modified to enable operation at much lower space velocities, and testing conducted at a reforming flue gas flow rate of around 0.12 kg/min, which under standard conditions equates to a GHSV of 3059 $h^{-1}$, a reduction by a factor of 2.7 compared with the earlier trials. Under these conditions, the stoichiometric n-heptane flow rate was 0.016 kg/min, or 23.8ml/min liquid flow rate, and hence testing was carried out at rates ranging between 10 and 20 ml/min; the results were now of considerable interest, with definite evidence of feedstock conversion. Having thus ascertained the general operating conditions under which feedstock conversion could be achieved, it was decided that a more rigorous investigative programme could be undertaken.

## 8.7 Summary of Rig Design, Construction and Commissioning

The reactor and test rig have been designed, constructed and commissioned, and preliminary tests conducted in order to validate the operation of the system. A great deal of experience was gained during this period, and it was felt that the system was now ready for application in a rigorous and closely-controlled study of the reforming process. This programme of work is reported in the following chapter.

| Parameter | Location | Transducer | Indicator | IEEE |
|---|---|---|---|---|
| Pressure | Burner Air Inlet | Druck | Druck | Y |
| " | Burner Propane Inlet | PDCR 910 | DPI 420 | Y |
| " | Feedstock Tank Outlet | " | " | Y |
| " | Feedstock at Reformer Inlet | " | " | Y |
| " | Ref. Flue Gas at Reactor Inlet | " | " | Y |
| " | Surplus Flue Gas Outlet Duct | " | " | Y |
| " | Reformed Fuel Outlet Duct | " | " | Y |
| " | Surp. Flue Gas at Reactor Inlet | " | " | Y |
| " | Surplus Flue Gas Outlet Duct | " | " | Y |
| " | Atmospheric Pressure | " | " | Y |
| Temperature | Burner Air Inlet | Type K | CIL | Y |
| " | Burner Propane Inlet | T/couple | TA 880 | Y |
| " | Feedstock Tank Outlet | " | " | Y |
| " | Feedstock at Reactor Inlet | " | " | Y |
| " | Ref. Flue Gas at Reactor Inlet | " | " | Y |
| " | Catalyst Matrix Inlet | " | " | Y |
| " | Catalyst Matrix Centre | " | " | Y |
| " | Catalyst Matrix Outlet | " | " | Y |
| " | Surplus Flue Gas Outlet Duct | " | " | Y |
| " | Reformed Fuel Outlet Duct | " | " | Y |
| Flow Rate | Feedstock at Tank Outlet | Platon Rotameter | | N |
| " | Gas at Burner Inlet | " | | N |
| " | Air at Burner Inlet | " | | N |
| " | Excess Steam Water Supply | " | | N |
| " | Reformed Fuel in Outlet Duct | Orifice, $H_2O$ Inc. Mano. | | N |
| Oxygen Conc. | Surplus Flue Outlet Duct | Testoterm Electrochem | | N |
| Gas Compos. | Reformed Fuel Outlet Duct | Orsat Apparatus (+Sub-Contracted) | | N |

Table 8.1

Details of Instrumentation on the Rig/Reactor Assembly

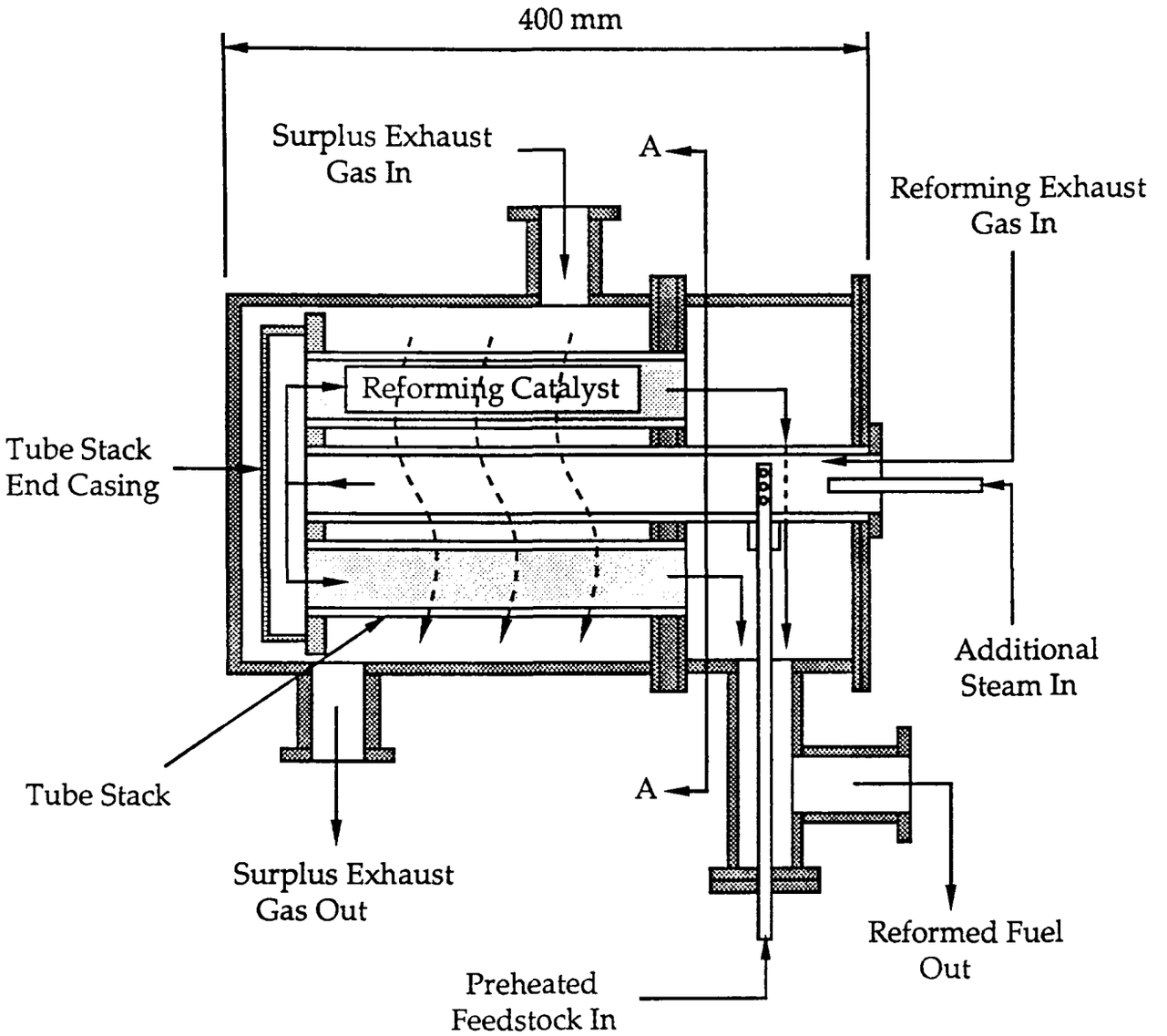


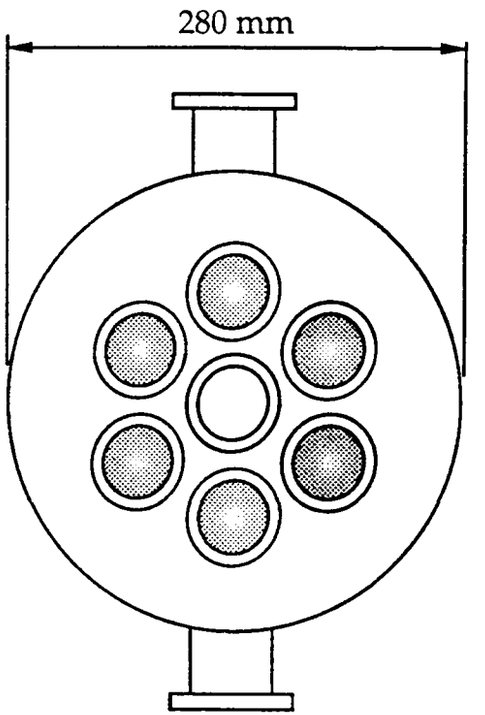


End View of Tube-Stack at A-A

Fig 8.1 Diagram of Prototype Reforming Reactor

Fig 8.2a

Photograph of Reforming Reactor Assembly

with End-Cover Removed

Fig 8.2b Photograph of Tubestack Showing Exhaust-Gas Inlet Duct, Feedstock Entry Port and Catalyst Monoliths

Fig 8.2c Photograph of Parlty-Assembled Reactor Showing Thermocouple Insertion into Catalyst Monoliths

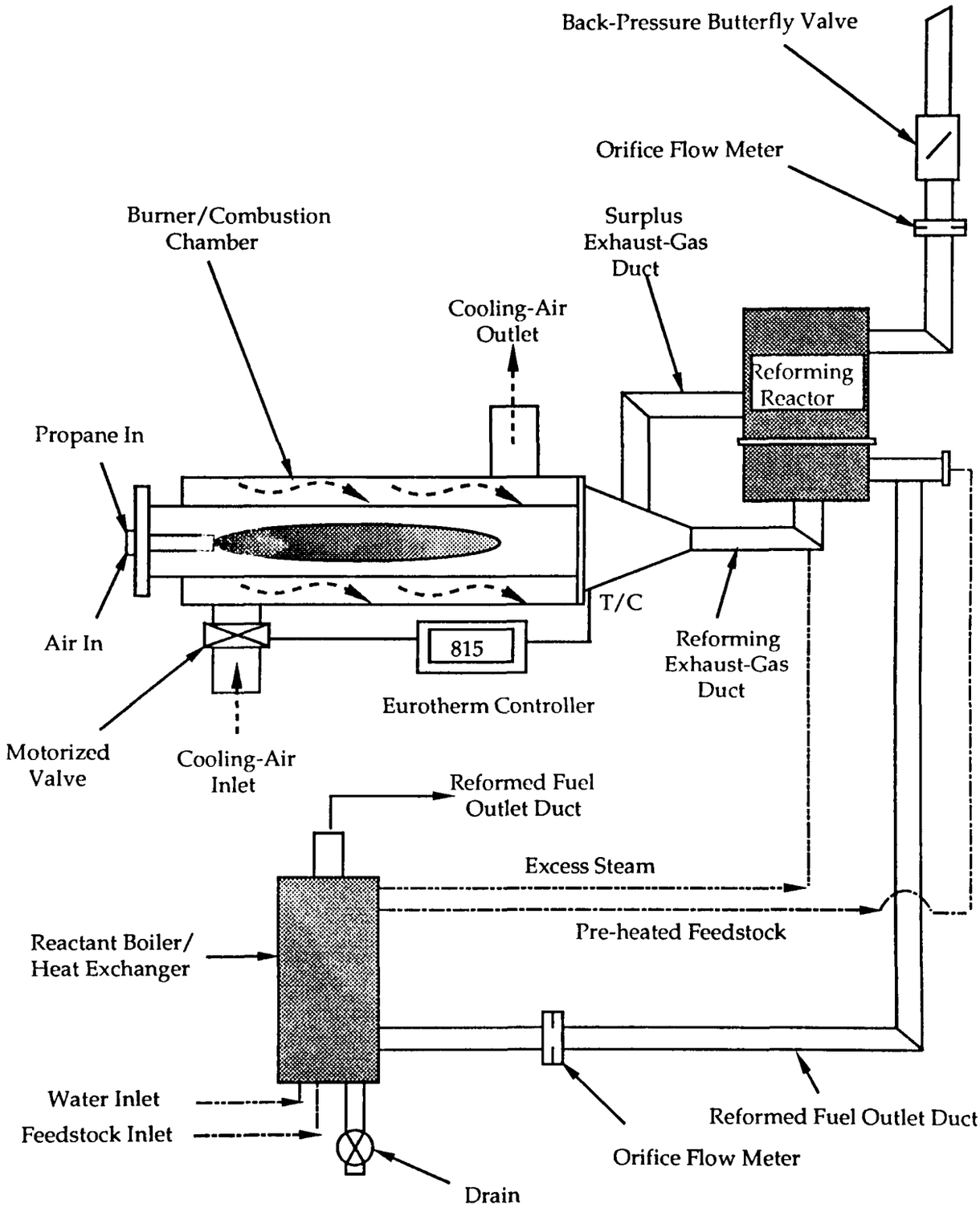


Fig 8.3 Diagram of Reformer Test Rig

Fig 8.4a

Photograph Showing General View of Test Rig

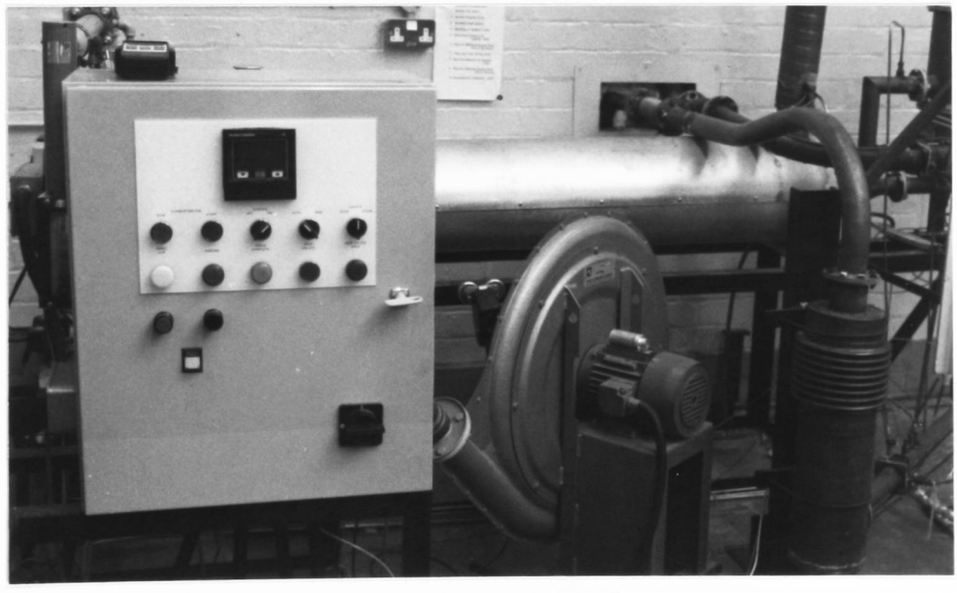

Fig 8.4b

Photograph Showing Rig Control Panel, Burner Air Blower and the Horizontally-Mounted Combustion Chamber Assembly

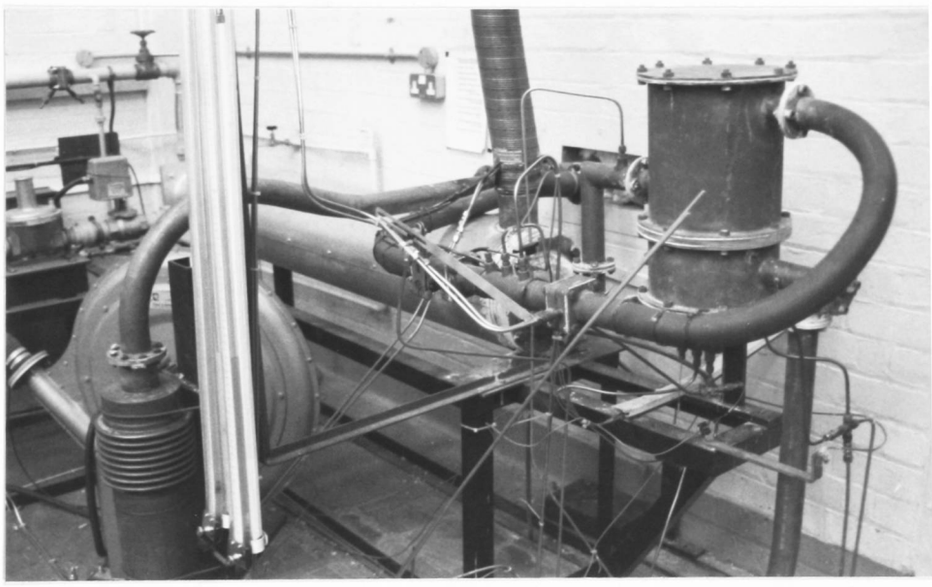

Fig 8.4c

Photograph Showing Installation of Reforming Reactor on the Test Rig

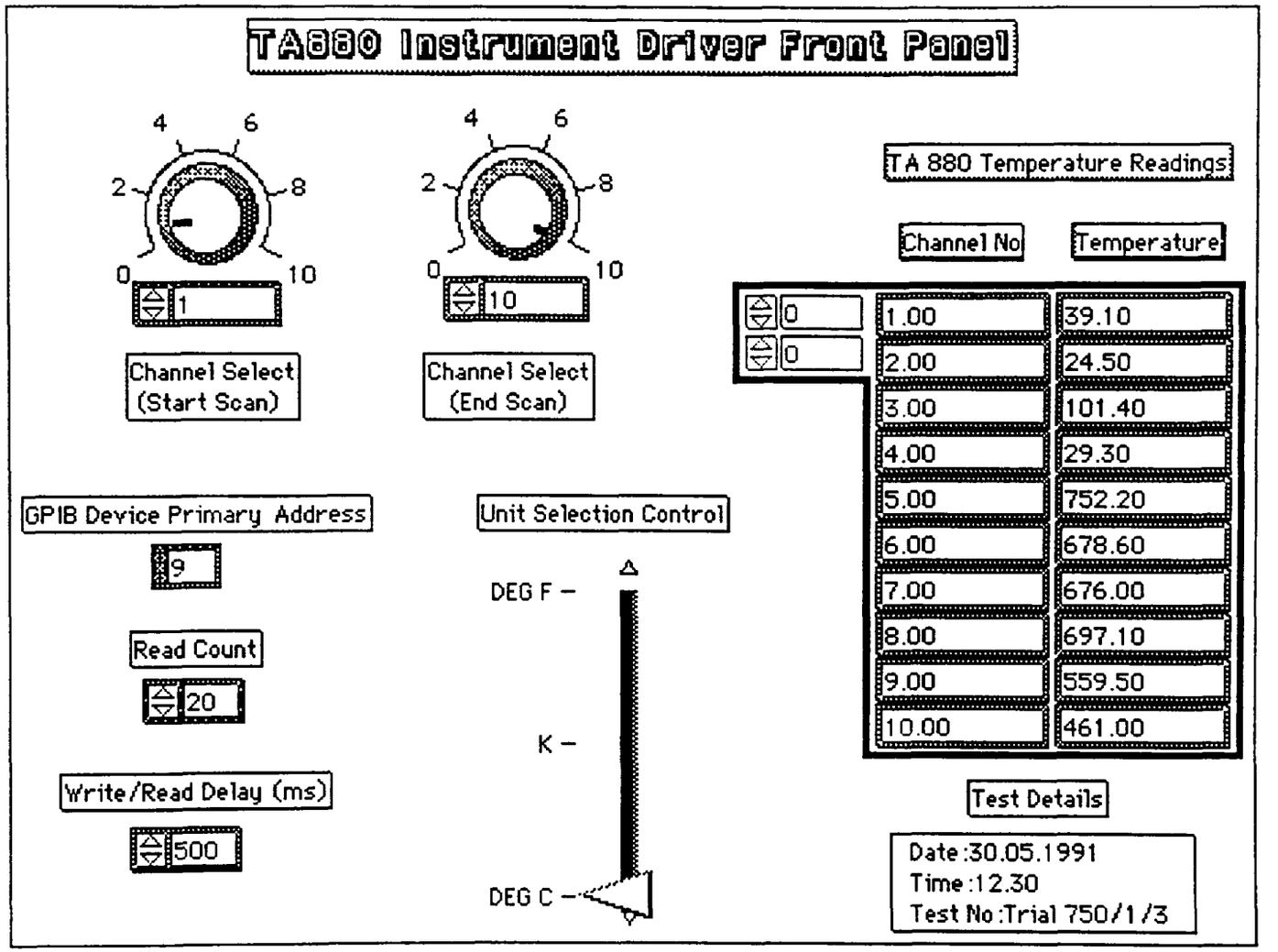


Fig 8.5 Front Panel of LabVIEW Virtual Instrument for
TA 880 Multi-Channel Temperature Monitor

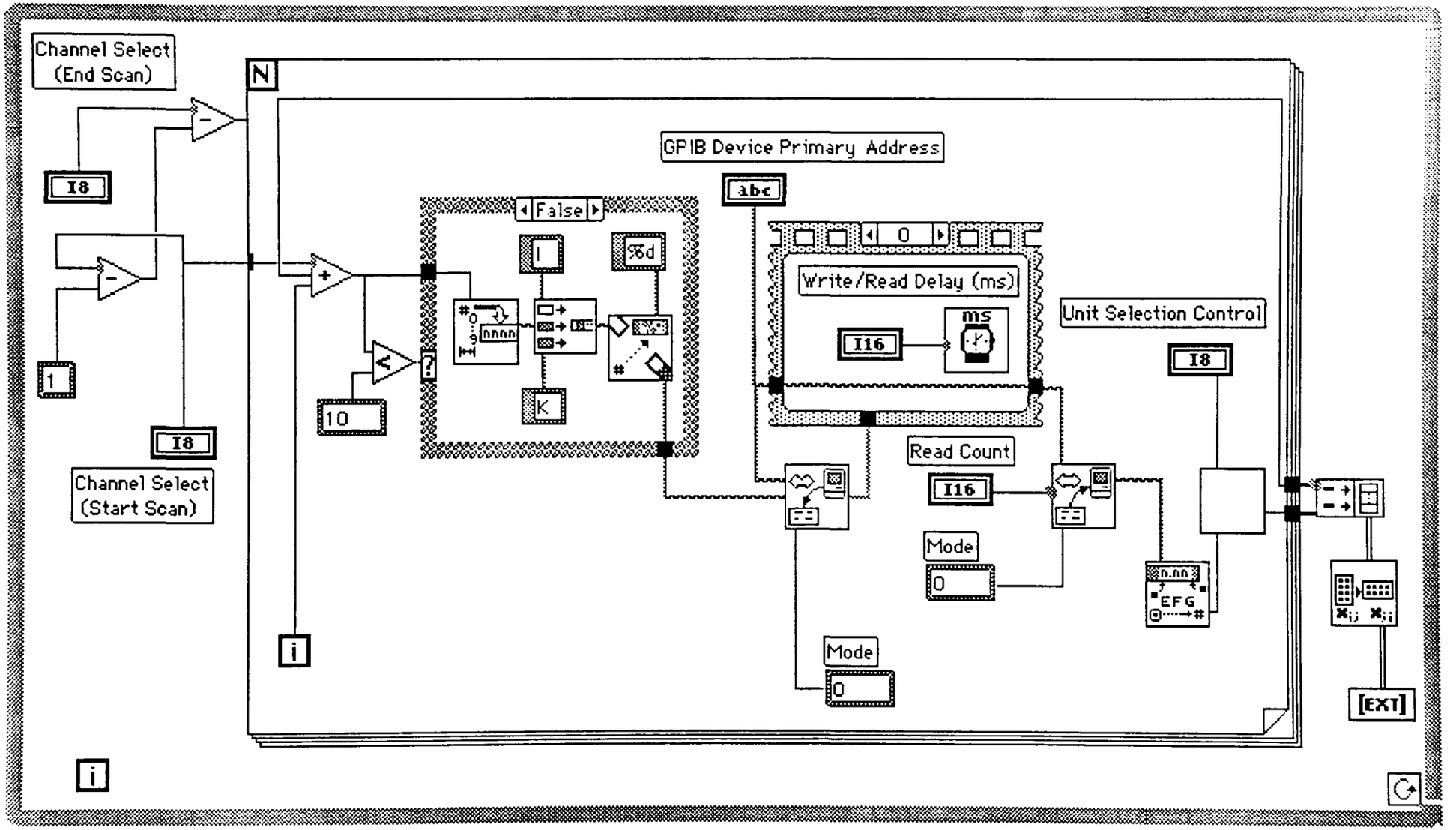


Fig 8.6 Block Diagram of LabVIEW Virtual Instrument
for TA 880 Multi-Channel Temperature Monitor

# 9 EXPERIMENTAL EVALUATION OF THE REFORMING PROCESS

The effect of several parameters is of interest in the detailed investigation of the reforming process, namely, feedstock type, reformer oxidant inlet temperature, catalyst space-velocity, flue-gas composition and reforming oxidant to fuel ratio. A very comprehensive test programme would be required in order to examine the effect of each of these fully, but as the cost of the sub-contracted gas analysis work was high, this was not feasible. Hence a more concise test programme, which would give clear indications of the effect of each variable, had to be devised, as outlined below.

## 9.1 Test Programme

### 9.1.1 Selection of Feedstocks

Preliminary work had been carried out using unleaded gasoline and n-heptane as the reformer feedstocks; it was the latter fuel which gave the more interesting results towards the end of the commissioning/validation exercise. It was therefore decided that an in-depth investigation of the reforming of this discrete hydrocarbon should be undertaken, in order to gain an insight into the capabilities of the process as applied to a relatively simple compound.

As unleaded gasoline is currently one of the most widely available motor fuels, the efficiency of the reforming process as applied to this feedstock is naturally of great interest, and hence the fuel was also chosen for a full investigation.

The study of the two feedstocks was conducted over an identical range of conditions in order that the effect of feedstock composition could be clearly observed. It should be pointed out at this stage that, in view of time and cost constraints, it has not been possible to carry out a practical investigation of the reforming of methanol, a feedstock which showed considerable potential in the earlier theoretical work. It is hoped that this shortcoming might be addressed at a later stage in the research.

### 9.1.2 Reformer Oxidant Inlet Temperature

The theoretical and early practical studies indicated that the temperature of the reaction equilibrium would have a very significant effect on the outcome of the reforming process. The flue gas (oxidant) generator, which consists basically of the propane burner and combustion chamber/heat exchanger assembly, was designed with a capability for producing flue gases at a set temperature at entry to the reformer ducting. This temperature level is set by the operator on the rig control panel, and, once the combustion apparatus has warmed up, gives flue gas temperatures of within $\pm 2^{\circ}C$ of the set-point.

As earlier studies predicted that lower reformer temperatures would lead to the formation of carbon solids and generally low levels of feedstock conversion, reformer gas inlet temperatures of $850^{\circ}C$ and $950^{\circ}C$ were chosen for this part of the investigation. In addition, as the effect of temperature was of particular interest, it was decided that a temperature sweep should be conducted for each fuel. In this case the reforming oxidant composition and oxidant to feedstock ratio are held constant over a range of reformer gas inlet temperature, in order that the effect of temperature can be studied in isolation.

### 9.1.3 Effect of Reactor Space Velocity

In most work involving the use of a catalyst, the space velocity of the reactants over the promoter is critical. Gas hourly space velocity (GHSV), as defined in eqn 8.1, gives a measure of reactant throughput relative to catalyst volume, and should hence be related to reaction kinetics. It can be appreciated that as the catalyst volume, once decided, is essentially fixed, the flow rate of reactants must be adjusted in order to give a space velocity in line with the reaction kinetics.

In view of the complexity of the task, and the limited amount of knowledge in the field, no theoretical work was carried out in the area of exhaust-gas reforming reaction kinetics. Early experimental trials using unleaded gasoline (ULG) at a gas hourly space velocity of around $8284h^{-1}$ failed to give any indication that the endothermic reforming reactions were proceeding, and it was concluded that this level of throughput was too great for the chosen noble metal catalyst formulation and volume, which was nominally 2 litres. Further work at a reduced space velocity of $3059h^{-1}$ using the n-heptane feedstock gave much more interesting results, with clear evidence of conversion to lighter hydrocarbons and possibly hydrogen.

It was therefore felt that a nominal space velocity of around $3000h^{-1}$ should be chosen for examination, as this appeared to signify a level at which the process was beginning to give good conversion. In order that the effect of further reductions in space velocity could be examined, trials were also conducted at a space velocity of $1000h^{-1}$, where it was hoped that near-equilibrium product compositions might be observed. This lower space velocity represents the minimum at which the rig can operate comfortably, as the lower limit of a number of the flow metering devices is approached.

### 9.1.4 Flue Gas Compositions

In line with the theoretical study, four flue gas compositions were selected for the rig-based investigation. These were the standard (unmodified) composition, and exhaust gases containing excess steam, excess oxygen, and excess steam+oxygen. The standard flue gases comprised stoichiometric combustion products from the propane burner, with a flue gas oxygen concentration of 0.2% vol set in order to ensure the avoidance of carburizing burner operating conditions.

Excess-steam exhaust gases are created by doubling the water content of the flue gases by means of secondary steam injection. This steam is generated in a heat exchanger situated in the hot reformed fuel outlet duct, and is injected into the reformer inlet duct near the feedstock entry port. It is possible to boil water and preheat the resulting steam to temperatures of around 400°C, and as the flow is relatively small, and is injected only into the actual reforming exhaust-gas stream, the cooling effect is minimal. The steam flow-rate is measured by means of a rotameter sited in the water supply piping, upstream of the boiler.

Excess oxygen is introduced into the flue gases by operating the propane burner at a lean air to fuel ratio. In line with the theoretical work, a level of 3.0% vol was chosen for the investigation, which means that the burner controls have to be set to give a flue gas oxygen reading of around 3.4% at the Testoterm analyser, which gives a dry analysis.

Finally, flue gases containing 100% excess steam and 3.0% oxygen are generated by injecting secondary steam into the oxygen-enriched flue gases.

### 9.1.5 Effect of Reforming Oxidant to Fuel Ratio

The stoichiometric reforming equations for each of the four burner flue gas compositions are written in order to determine stoichiometric oxidant to reformer-feedstock ratios. It was anticipated that reforming at this ratio would almost certainly lead to the formation of carbon solids, but at the same time it was predicted that good hydrogen yields might be observed under these conditions, and the ratio was therefore chosen for examination.

There was certainly no scope for particulate-free reforming at lower oxidant to fuel ratios, and hence the effect of the variable was further examined at a weaker ratio where the feedstock is reformed with a 100% oxidant excess. Thus two reactor excess oxidant factors, $\lambda_r$=1 and $\lambda_r$=2, were selected for the study, where $\lambda_r$ is as defined in eqn 5.10.

### 9.1.6 Summary of Test Sites

The study of the two feedstocks, n-heptane and ULG, is thus conducted over 16 discrete test sites at the two reactor gas inlet temperatures of 850°C and 950°C, giving 64 points in all. The matrix of test sites given below shows the 16 points examined for each feedstock and gas inlet temperature.

| | $\lambda_r$ | 1.0 | 2.0 | 1.0 | 2.0 | 1.0 | 2.0 | 1.0 | 2.0 |
|---|---|---|---|---|---|---|---|---|---|
| | Excess $H_2O$ | - | - | 100% | 100% | - | - | 100% | 100% |
| | Excess $O_2$ | - | - | - | - | +3% | +3% | +3% | +3% |
| GHSV | | | | | | | | | |
| $3000h^{-1}$ | | 3/1 | 3/2 | 3/3 | 3/4 | 3/5 | 3/6 | 3/7 | 3/8 |
| $1000h^{-1}$ | | 1/1 | 1/2 | 1/3 | 1/4 | 1/5 | 1/6 | 1/7 | 1/8 |

Table 9.1 Matrix of Test Sites Indicating Test Numbering System.

Table 9.1 shows the test numbering system employed. The inclusion of abbreviations describing reactor feedstock composition and gas inlet temperature leads to a full test number of the form given below:

RH/850/3/1 (Sample Test Number)

where RH represents reforming of n-heptane, 850 is the gas inlet temperature in degrees C, the descriptor '3' indicates a gas hourly space velocity of $3000h^{-1}$, and the final digit describes the reactor excess oxidant factor and oxidant composition, as indicated in Table 9.1

In addition to these tests at discrete points, temperature sweeps were conducted using each of the feedstocks. In each case the 100% excess-steam flue gas composition was used at a reforming excess oxidant factor, $\lambda_r$, of 1.5, and a GHSV of $1000h^{-1}$. Temperature was varied from 600 to 950°C in 50°C increments, giving 8 points for each fuel and thus a further 16 sites in total.

### 9.1.7 Test Procedure

In the case of all test sites the procedure adopted is essentially the same. The rig is allowed to fully warm up to the required temperature with burner controls and excess steam flows adjusted to give the desired flue gas composition, as determined by the requisite flow meters and the flue gas oxygen analyser. The butterfly valve in the surplus exhaust outlet duct is then set to give the required space velocity through the catalyst, which is measured by means of an orifice plate situated in the reformed fuel outlet duct. Note that the orifice plate was located in this duct as it was considerably cooler than the inlet ducts, leading to a reduced tendency for the orifice to distort under the severe environmental conditions. Flue gas composition,

pressure, and temperature are used in order to calculate the gas density and hence mass flow rate for the observed orifice pressure drop via the standard orifice equation. When conditions stabilize, all pressure, temperature and flow data are recorded either manually or through the Macintosh IIci computer, and the gasoline/n-heptane feedstock flow is switched on.

A 12 volt automotive fuel pump is used in order to inject the feedstock into the reactor, via 0.25" diameter stainless steel tubing and a port in the reforming exhaust-gas inlet duct; the flow rate is controlled and monitored by flow metering valves and a calibrated rotameter. The rig is allowed to settle for approximately 15 minutes, after which time the feedstock boiler and preheater are able to fully vaporize the fuel, heating to temperature levels of around 300 to 400°C. Catalyst temperatures are closely monitored during this period, and when they have stabilized, a sample of the fuel gas is taken from the reformed fuel outlet duct by means of the hand pump and sample cylinders mentioned in section 8.4. On completion of 16 test points, the batch of samples were taken to British Gas Scientific Services for analysis.

## 9.2 Results

### 9.2.1 Gas Analysis and Thermal Efficiency Results for Discrete Test Points

As mentioned earlier, it was not possible to conduct extensive sweeps across wide ranges of reactor excess oxidant factor, space velocity, etc., on account of the high cost of the gas analysis work. It is not feasible, therefore, to attempt to present plots of gas composition and thermal efficiency against such variables, although there is sufficient data to enable the clear identification of certain salient trends. Hence the gas analysis results are presented as bar charts of individual or conveniently-grouped gas

concentration levels against test number; thermal efficiency is also plotted against this abscissa. Each plot is drawn for a specific feedstock and gas inlet temperature, and shows results for the two space velocities studied. Where applicable, corresponding equilibrium levels from the earlier predictive study are shown, enabling direct comparison of observed and theoretical results.

Plots for the n-heptane feedstock are grouped together in Fig's 9.1 to 9.7, whilst graphs for ULG are given in Fig's 9.8 to 9.14. Results of individual gas concentrations at gas inlet temperatures of 850 and 950°C are shown alongside each other for the purpose of comparison. Referring to Table 9.1, it is also possible to observe the effects of reactor excess oxidant factor, $\lambda_r$, and flue gas composition in these plots.

Results are thus presented as follows:

| | Fig No |
|---|---|
| Hydrogen Yield for Reforming of n-Heptane at 850 and 950°C | 9.1a, b |
| Carbon Monoxide Yield for Reforming of n-Heptane at 850 and 950°C | 9.2a, b |
| Methane Yield for Reforming of n-Heptane at 850 and 950°C | 9.3a, b |
| Ethane/Ethene Yield for Reforming of n-Heptane at 850 and 950°C | 9.4a, b |
| C3/C6 HC's Yield for Reforming of n-Heptane at 850 and 950°C | 9.5a, b |
| Carbon Dioxide Yield for Reforming of n-Heptane at 850 and 950°C | 9.6a, b |
| Thermal Efficiency for Reforming of n-Heptane at 850 and 950°C | 9.7a, b |
| | |
| Hydrogen Yield for Reforming of ULG at 850 and 950°C | 9.8a, b |
| Carbon Monoxide Yield for Reforming of ULG at 850 and 950°C | 9.9a, b |
| Methane Yield for Reforming of ULG at 850 and 950°C | 9.10a,b |
| Ethane/Ethene Yield for Reforming of ULG at 850 and 950°C | 9.11a,b |

### 9.2.2 Gas Analysis and Thermal Efficiency Results for Temperature Sweeps

A comprehensive sweep across a range of reformer gas inlet temperature was conducted, as this is a particularly important variable, and the results of the study are shown in Fig's 9.15 to 9.21. In each of these Fig's, reactor excess oxidant factor was set to 1.5, with the flue gas composition containing 100% excess steam used as the reforming oxidant. Again, plots of individual and conveniently-grouped gas concentrations and reactor thermal efficiency are presented, in this case against reformer gas inlet temperature. In order that the effect of the two different feedstock compositions can be clearly observed, corresponding plots for n-heptane and ULG are given alongside each other on the page, as follows:

## 9.3 Discussion of Test Results

### 9.3.1 Reforming of n-Heptane at Discrete Points

Fig's 9.1, 9.2, and 9.3 show yields of hydrogen, carbon monoxide and methane respectively for the reforming of n-heptane at gas-hourly space velocities (GHSV's) of 1000 and 3000$h^{-1}$ and at gas inlet temperatures of 850 and 950°C. The test number shown on the plots contains an asterisk in place of the space velocity descriptor, as two space velocity points and the equilibrium level, where applicable, are given for each test number. Note that odd-numbered test points, which represent stoichiometric reforming ($\lambda_r$=1), are grouped together, as are even-numbered tests, which represent reforming at $\lambda_r$=2. The four blocks of data given for the two excess oxidant factors correspond to reforming with unmodified, excess steam, excess oxygen and excess steam+oxygen exhaust gases respectively, as test number increases from 1 to 7 ($\lambda_r$=1) and 2 to 8 ($\lambda_r$=2) (Ref Table 9.1).

Fig 9.1b highlights some interesting trends in hydrogen concentration for the reforming of n-heptane at 950°C. Firstly, it is apparent that space velocity has a very significant effect on observed composition. Results at the lower level of 1000$h^{-1}$ are broadly in line with equilibrium predictions, whilst at the higher level of 3000$h^{-1}$ hydrogen yields are generally much lower than the theoretical levels. In the light of earlier work this was to be expected, and indicates that the space velocity of 1000$h^{-1}$ is low enough to permit the reforming reactions to approach equilibrium at this temperature, whilst the higher space velocity is not. It is felt that the correlation between theoretical and observed results is remarkably good in view of the complex nature of the test work, which involves the control of several critical and inter-dependent variables.

It is suggested that reductions in GHSV below $1000h^{-1}$ would not result in significant improvements in hydrogen yield for the n-heptane feedstock at 950°C, as the levels already appear to be close to equilibrium. Increases in the catalyst velocity certainly tend to reduce yields, although the point between $1000h^{-1}$ and $3000h^{-1}$ at which the effect becomes significant has not been accurately established.

Trials at $1000h^{-1}$ and 850°C generally show hydrogen yields slightly below computed equilibrium levels, which can presumably be attributed to slower reaction kinetics over the catalyst at this lower temperature.

Referring again to Fig 9.1b, the effect of reactor excess oxidant factor, $\lambda_r$, is also clearly illustrated. Odd-numbered test points represent reforming at $\lambda_r$=1.0, whilst even-numbered test points are at $\lambda_r$=2.0, and it is evident, by comparing test points 1 with 2, 3 with 4, etc, that moving from stoichiometric to a 100% excess oxidant reforming ratio leads to a reduction in hydrogen yield at a GHSV of $1000h^{-1}$, regardless of reforming oxidant composition. This is to be expected, as under 'lean' reforming conditions the product gas will inevitably contain diluting quantities of unreacted oxidant.

By comparing the four odd-numbered test points, the effect of flue gas composition can be observed. Test point 1, at a GHSV of $1000h^{-1}$ and a gas inlet temperature of 950°C, gives a hydrogen yield of 24.4% with standard exhaust gases, whilst the excess steam exhaust gases used in test point 3 give a hydrogen concentration of 30.5%. The effect of excess oxygen in the exhaust gases (point 5) is to reduce hydrogen yield to 25.1%, whilst the oxidant containing both excess oxygen and steam gives a hydrogen yield of 32.2% for test point 7, the highest hydrogen level observed throughout the whole test programme.

Fig's 9.2a and b show trends in carbon monoxide levels similar to those described above for hydrogen. The lower GHSV gives yields broadly in line with predicted levels, whilst concentrations at the higher GHSV of $3000h^{-1}$ clearly fall short of equilibrium predictions. Yields are most favourable at 950°C (Fig 9.2b), where again the expected trend of reducing yield with increasing values of $\lambda_r$ can be identified by comparing corresponding even and odd-numbered test points. A peak level of 20.9% is shown for test point 5, which represents the highest carbon monoxide yield observed in the study. This notably occurs with an oxygen-enriched oxidant, and it can be seen that the effect on carbon monoxide yield of the introduction of excess steam into the flue gases is minimal, which was certainly not true in the case of hydrogen, which increased markedly with increasing water.

Fig's 9.3a and b are also interesting, as in this case it can be seen that observed methane levels tend to exceed equilibrium predictions. The fact that hydrogen and carbon monoxide yields generally fall just short of predicted levels at $\lambda_r=1$ is consistent with these apparently high methane levels, which exist because reforming reactions have not reached equilibrium. Methane levels of between 0 and 4% are observed at 950°C compared with predicted levels of between around 0 and 1%, and again a clear relationship between yield and excess oxidant factor can be identified.

The ethane/ethene concentrations shown in Fig 9.4 must also be attributed to reaction kinetics, as they are essentially non-equilibrium products; predicted equilibrium levels have been omitted from the plots as they were extremely low. The combined C2 hydrocarbon results do not show any clear trend with temperature or exhaust gas composition, although it can be seen that the higher levels occur at odd-numbered test points which signify stoichiometric reforming ($\lambda_r=1$). Levels shown in Fig 9.4b tend to show a

clear trend with GHSV, with generally lower levels observed at the lower space velocity which supports the argument that these are non-equilibrium reaction products.

These observations are corroborated by the results shown in Fig 9.5, where C3 to C6 hydrocarbons are grouped together. There is a more defined trend with temperature for these results, with levels at 950°C being generally lower than at 850°C, indicating more complete conversion of the feedstock at the higher temperature.

Carbon dioxide yields are shown in Fig 9.6. These levels essentially represent quantities of carbon dioxide which pass through the reformer as unconverted reactants. Clear trends with GHSV are apparent, with higher velocities giving yields somewhat displaced from equilibrium predictions, whilst results at $1000h^{-1}$ approach the theoretical levels more closely.

Interpretation of the thermal efficiency results given in Figs 9.7a and b has proved difficult, particularly at the higher temperature. Efficiencies at 850°C appear to follow predicted levels quite well for the lower GHSV, with values falling broadly between 95 and 115% and reducing with the injection of excess oxygen (test points 5,7,6 & 8) as expected. Results at $3000h^{-1}$ generally fall short of predicted levels, which is to be expected as the reforming reactions do not appear to reach equilibrium under these conditions.

With the exception of the peak value of 128% observed at test point 2, GHSV=$1000h^{-1}$, the results at 950°C do not correlate very well with computed predictions. This is particularly interesting in the case of the lower GHSV, as the observed gas compositions appeared to be quite close to equilibrium under these conditions.

Observed thermal efficiency values are generally much lower than predicted, whilst the dependence of efficiency on $\lambda_r$, which can be observed by comparing points 1 with 2, 3 with 4 etc, is much more pronounced than expected. It is suggested that these anomalies might be elucidated by the following hypotheses:

1) At the high temperature, 'kinetic' carbon will almost certainly be deposited on the catalyst, and this would tend to be much worse at $\lambda_r$=1 than at $\lambda_r$=2. Such a deposition naturally has a detrimental effect on the thermal efficiency of the reaction if the potential heating value of the particulate is omitted from the efficiency calculation, as is the case here, where levels of deposition have not been quantified.

There was definite evidence of C(s) deposition on the catalyst, as the temperature of the monolith would often rise sharply on the introduction of excess air into the flue gases following reformer trials. This temperature increase was apparent even after allowing a considerable time to elapse following shut-down of the reformer feedstock, and it could not, therefore, be attributed to the oxidation of other combustible residuals. It is suggested that kinetic C(s) formation results as the feedstock impinges on the highly active catalyst surface.

2) Potential C(s) problems are exacerbated by the fact that the actual ratio of reforming exhaust gas to feedstock at the higher temperature will tend to be somewhat lower than the nominal setting. This is largely the result of high hydrogen yields, which give a reformed fuel having a relatively low density, leading to an increase in pressure drop across the measuring orifice plate for a given mass flow rate, as compared with more dense exhaust gases. In consequence, more of the

flue gases entering the reformer assembly become diverted through the surplus exhaust duct, leading to fuel enrichment in the reformer catalyst relative to the nominal setting of the exhaust-gas to fuel ratio. Hydrocarbons levels in general were higher than equilibrium predictions, and it is suggested that this could in part be attributable to the fuel-rich excursion.

3) The measurement of the hot reformed fuel gas flow-rate has a direct bearing on the thermal efficiency calculation, and this is performed using a stainless steel orifice plate. There is some doubt as to the accuracy of this technique at the elevated temperatures of the reformed fuel outlet duct, which is typically 300 to 600°C, as there would presumably be some thermal effect on the shape and/or size of the orifice, but no information regarding potential inaccuracies has been found. Reformed fuel density is based on the gas composition, pressure and temperature observed in the duct, and the mass flow rate then calculated using the standard orifice equation.

It is difficult to eliminate the shift in reforming stoichiometry mentioned in point (2) above, as the orifice flow rate has to be set up prior to switching on the raw fuel to the reformer, when a known exhaust gas composition is passing through the plate. This enables the requisite calculations to be performed, and the back-pressure butterfly valve to be adjusted in order to give the required gas flow through the catalyst.

### 9.3.2 Reforming of RF-08 ULG at Discrete Points

Results for the reforming of RF-08 ULG over the range of eight discrete test points are presented in Fig's 9.8 to 9.14. Observation of these results

indicates that reforming of the motor fuel feedstock presents a more demanding challenge than that of n-heptane.

Fig 9.8 shows hydrogen yields at 850 and 950°C and clearly demonstrates a dependence on space velocity and gas inlet temperature. Most favourable conditions are at 950°C and a GHSV of $1000h^{-1}$, where a maximum hydrogen concentration of 19.8% is observed for exhaust gases containing excess steam and oxygen at $\lambda_r=1$ (test point 7, GHSV=$1000h^{-1}$). These are precisely the same test conditions which gave optimum yields in the n-heptane reforming exercise.

Carbon monoxide levels given in Fig 9.9 demonstrate similar trends with temperature and GHSV, with a peak level of 12.0% indicated at test point RH/950/1/6. Methane yields illustrated in Fig 9.10 show a strong dependence on $\lambda_r$, with levels at stoichiometric ($\lambda_r=1$) typically an order of magnitude higher than at $\lambda_r=2$. Although no equilibria computations were conducted for this fuel, it is suggested that these methane yields arise from non-equilibrium conditions, and would be accompanied by the deposition of carbon solids.

Hydrocarbons levels shown in Fig 9.11 and 9.12 also show a relationship with $\lambda_r$, and in addition a general trend with GHSV, particularly at 950°C. The plots indicate that equilibrium conditions are not being reached either at a space velocity of $3000h^{-1}$, or, to a lesser degree, at $1000h^{-1}$.

Reactor thermal efficiency results presented for ULG in Fig 9.14 show a dependence on temperature, and, in the case of results at 950°C, a clear trend with GHSV, with the slower velocity giving highest efficiencies. The results in general are much lower than those observed for n-heptane, and this is

attributed to the following observations. Firstly, it seems likely that certain fractions of the feedstock might pass through the reformer without reaction, which in the case of heavier hydrocarbons would lead to non-detection, as the gas analysis technique has an upper limit of C6. Secondly, there was again evidence of C(s) deposition which at times appeared to be quite heavy in view of the amount of time it took to 'regenerate' the reactor by means of careful oxidation following reforming trials. Finally, as mentioned above, the accuracy of the orifice flow measurement technique as applied to the hot reformed fuel is uncertain.

It has to be concluded, therefore, that the reforming of the complex motor fuel cannot be so easily achieved as the conversion of the single n-heptane hydrocarbon feedstock.

### 9.3.3 Temperature Sweep Results for n-Heptane and ULG

The temperature sweep plots presented in Fig's 9.15 to 9.21 show gas concentrations and thermal efficiencies for the reforming of ULG and n-heptane over a range of reformer gas inlet temperature extending from 600 to 950°C. The value of $\lambda_r$ is set to 1.5 throughout, GHSV is $1000h^{-1}$, and the reforming oxidant is the exhaust composition enriched with 100% excess steam. Corresponding plots for each feedstock are shown alongside each other on the page, and can be compared directly.

Plots of hydrogen and carbon monoxide yield shown in Fig's 9.15 and 9.16 respectively confirm that the reforming of n-heptane was rather more successful than ULG. Peak hydrogen and carbon monoxide yields of 23.3 and 11.6% respectively are observed for the single hydrocarbon feedstock, compared with levels of 16.2 and 5.3% for the motor fuel. It is also apparent

from the shape of the curves that the process as applied to n-heptane begins to give good hydrogen and carbon monoxide yields at lower temperatures than in the case of ULG reforming.

Another point worthy of note is that in all four plots, yields are still rising at 950°C, which tends to suggest that under these reforming oxidant and space velocity conditions, higher yields could be achieved if temperatures were increased further.

Methane levels shown for the two raw fuels (Fig 9.17) show similar trends for each, although levels for ULG are again slightly lower than those for n-heptane. In this case there is no evidence to suggest that increases in gas temperature beyond 950°C would lead to further increases in methane yield.

Hydrocarbons plots shown in Fig's 9.18 and 9.19 are interesting, as they tend to indicate a levelling off or reduction in yield as temperatures increase towards 950°C. In the case of the lighter C2 hydrocarbons, levels for n-heptane reforming are generally higher than for the motor fuel, whilst the C3-C6 species concentrations are broadly lower than for the motor fuel.

The tendency for reduced hydrocarbons levels with increasing temperature is to be expected, as higher temperatures should lead to better conversion of the hydrocarbon fuels. In the case of ULG, higher concentrations of C3-C6 species are the result of lower levels of conversion of the motor fuel, and, quite possibly the presence of unreacted fuel fractions in this range. It is also suggested that small quantities of C7+ hydrocarbons could be present in the fuel gas mixture as unreacted hydrocarbons, but as mentioned earlier, the gas analysis technique used did not give levels for species higher than C6.

Carbon dioxide concentrations shown in Fig 9.20 are also as expected, with levels falling with increasing gas inlet temperature. Reductions in carbon dioxide are much lower in the case of ULG than n-heptane, and this is again attributed to the generally lower levels of reactivity observed for the gasoline-based reforming mixture.

Finally, plots of thermal efficiency given in Fig 9.21 show that levels are in the main higher for n-heptane than for ULG. A peak efficiency of 120.2% is observed at 900°C for n-heptane, whilst the maximum ULG reaction thermal efficiency value of around 70% is observed at 950°C, and shows signs of increasing further with increasing gas inlet temperature.

It is suggested that this low level of efficiency for gasoline relative to n-heptane is due to carbon deposition within the reactor and poor conversion of higher hydrocarbons which are not subsequently detected in the gas analysis. This leads to a low calculated reformed fuel heating value, and hence a low reactor thermal efficiency.

## 9.4 Conclusions of Test Programme.

The chemistry of the exhaust-gas reforming process has been examined on an experimental test rig, and has yielded some very interesting results.

In the case of an n-heptane fuel, respective hydrogen and carbon monoxide yields of 32.2 and 20.9% can be achieved at a gas inlet temperature of 950°C and a gas hourly space velocity of $1000h^{-1}$; these levels are within 2.5% of the theoretical predictions. Under these conditions, the levels of light hydrocarbons such as methane, ethane and ethene tend to be somewhat higher than equilibrium levels, and it is suggested that this is due to the effect

of reaction kinetics and catalyst formulation. Another important factor is the shift from the nominal set value of $\lambda_r$ towards fuel-rich values when reforming at higher temperatures. The shift is due to the relatively low density of the hydrogen-rich fuels produced under these conditions, which ultimately causes a reduction in the flow rate of reforming flue gases through the catalyst. It is an unfortunate feature of the test set-up which cannot be easily eliminated, and would exacerbate C(s) formation problems and the tendency to yield hydrocarbons levels higher than expected.

These factors also appear to have had a detrimental effect on reaction thermal efficiency, and whilst a peak level of 128.0% was observed at test-point RH/950/1/2 (n-heptane, T=950°C, GHSV=1000$h^{-1}$, - see Table 9.1), levels generally fell between around 95 and 115% for n-heptane.

ULG reforming results showed lower levels of conversion to hydrogen and carbon monoxide, with maximum observed levels of 19.8 and 12.0% respectively; thermal efficiency values are correspondingly low as compared with n-heptane levels. It became apparent that achieving high levels of conversion with the motor fuel presents a far greater challenge than with the single hydrocarbon. C(s) problems also appeared to be more pronounced with the gasoline, evidence of which was the sharp rise in temperature which inevitably occurred as soon as excess air entered the reactor following the ULG trials.

It is suggested that the relatively low levels of thermal efficiency observed for the gasoline, which were typically between 70 and 90%, are primarily the result of poor overall fuel conversion, C(s) deposition, and the presence in the reformed fuel of higher unreacted hydrocarbons (above C6) which lie outside the measuring range of the gas analysis equipment.

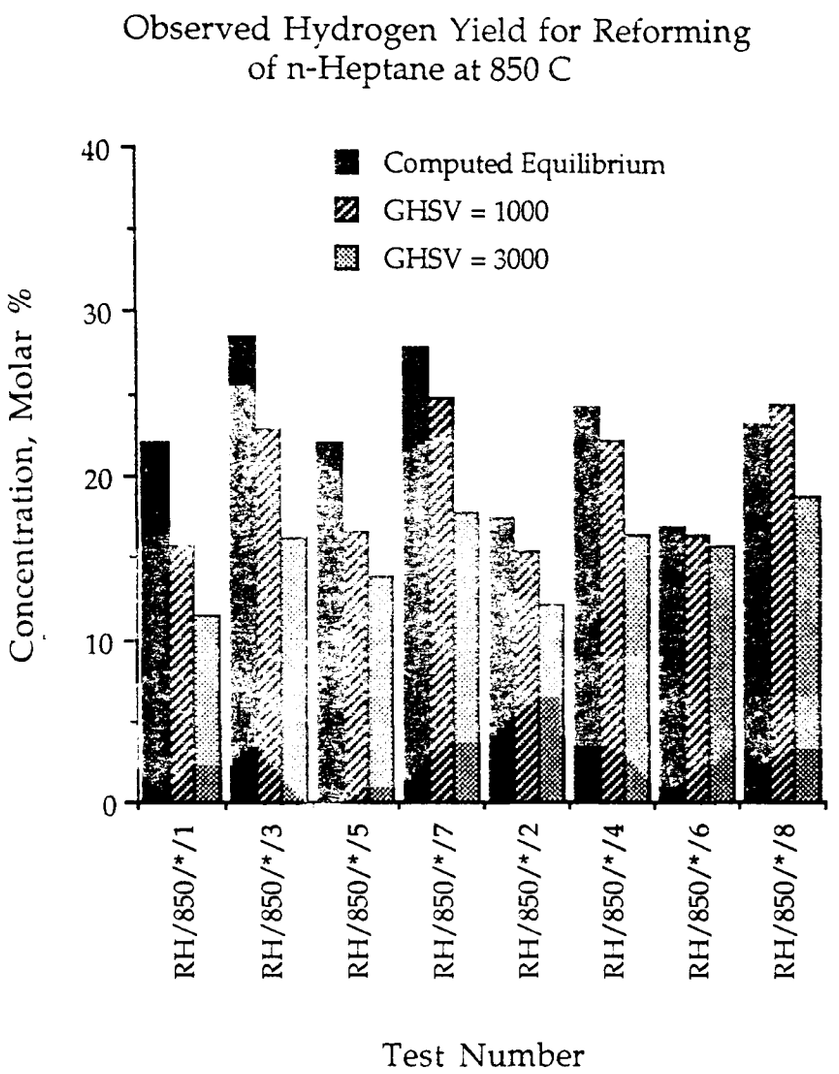


Fig 9.1a

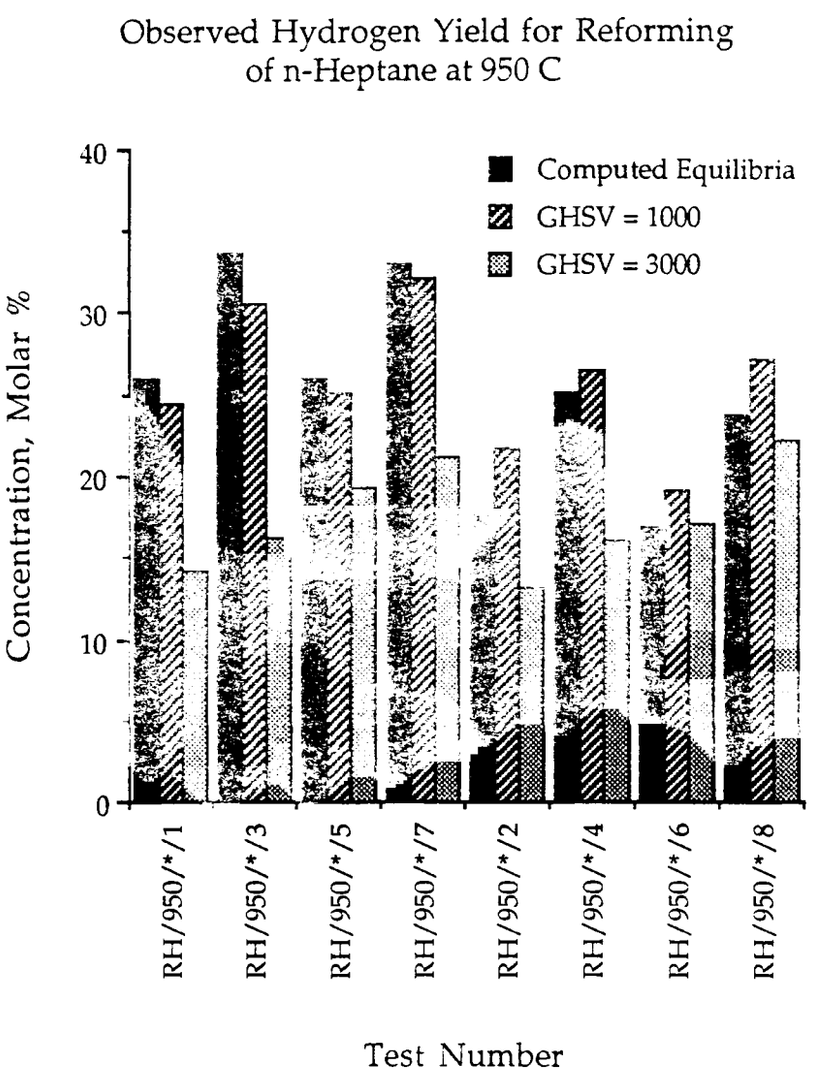


Fig 9.1b

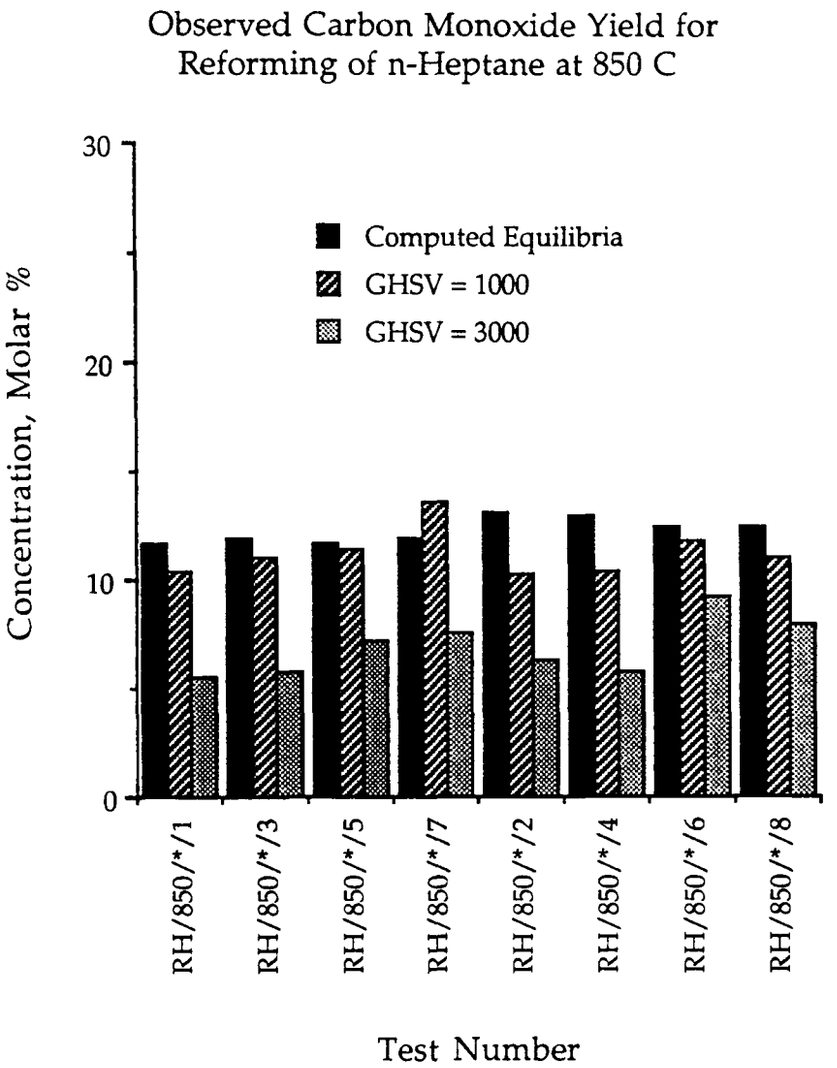


Fig 9.2a

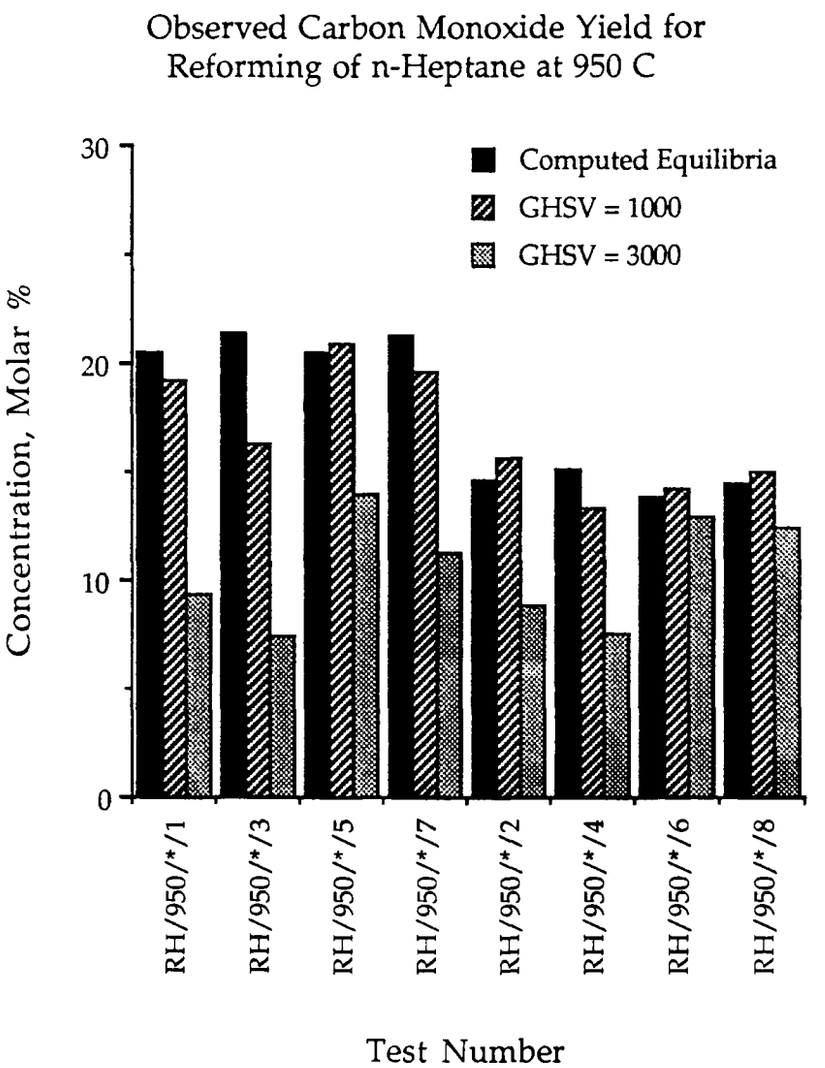


Fig 9.2b

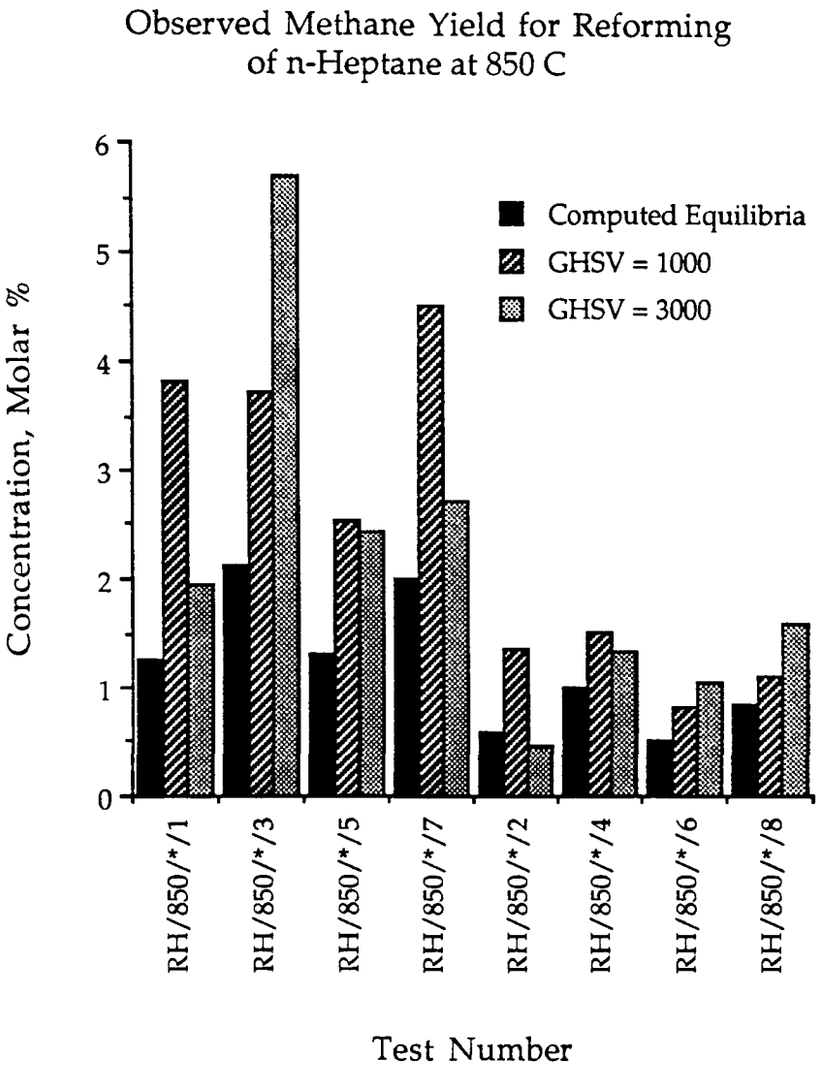


Fig 9.3a

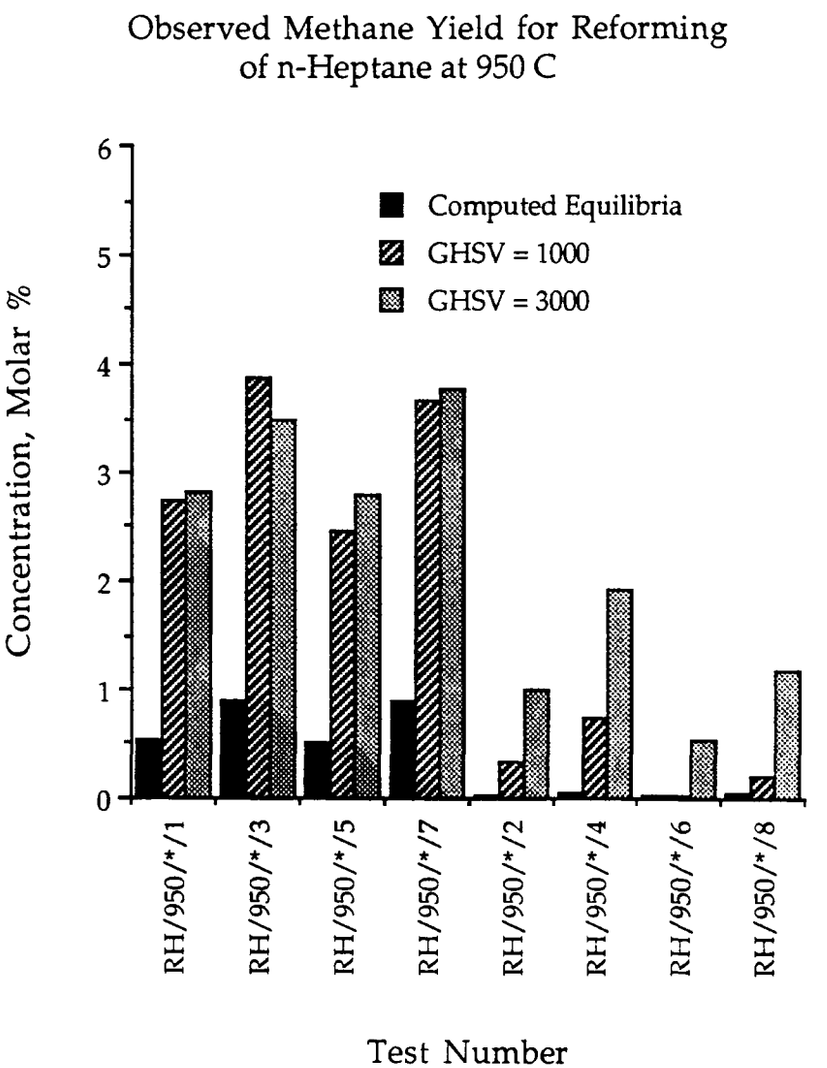


Fig 9.3b

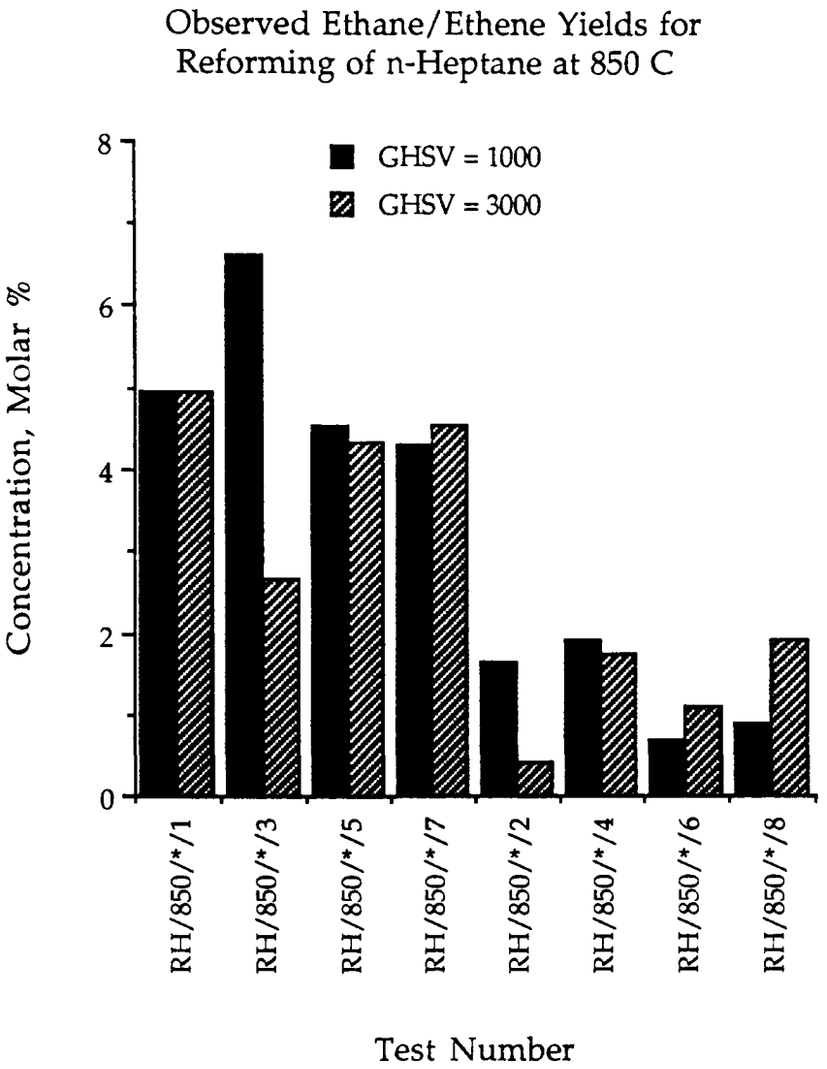


Fig 9.4a

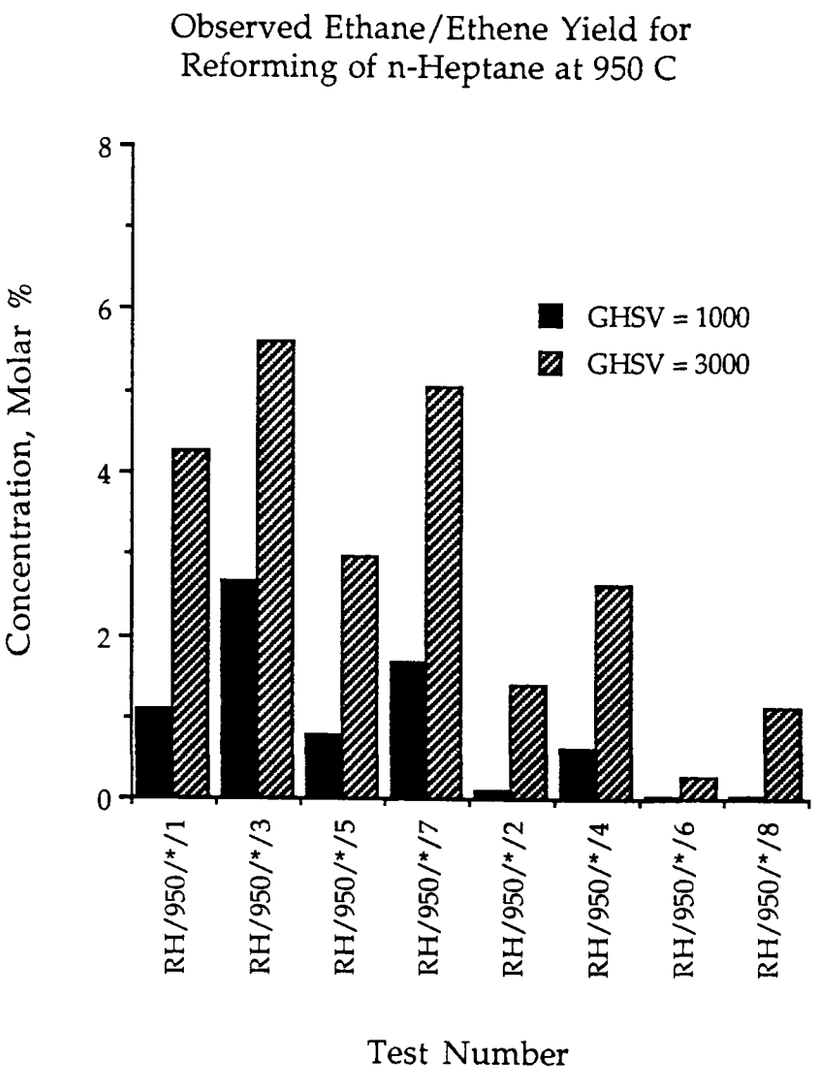


Fig 9.4b

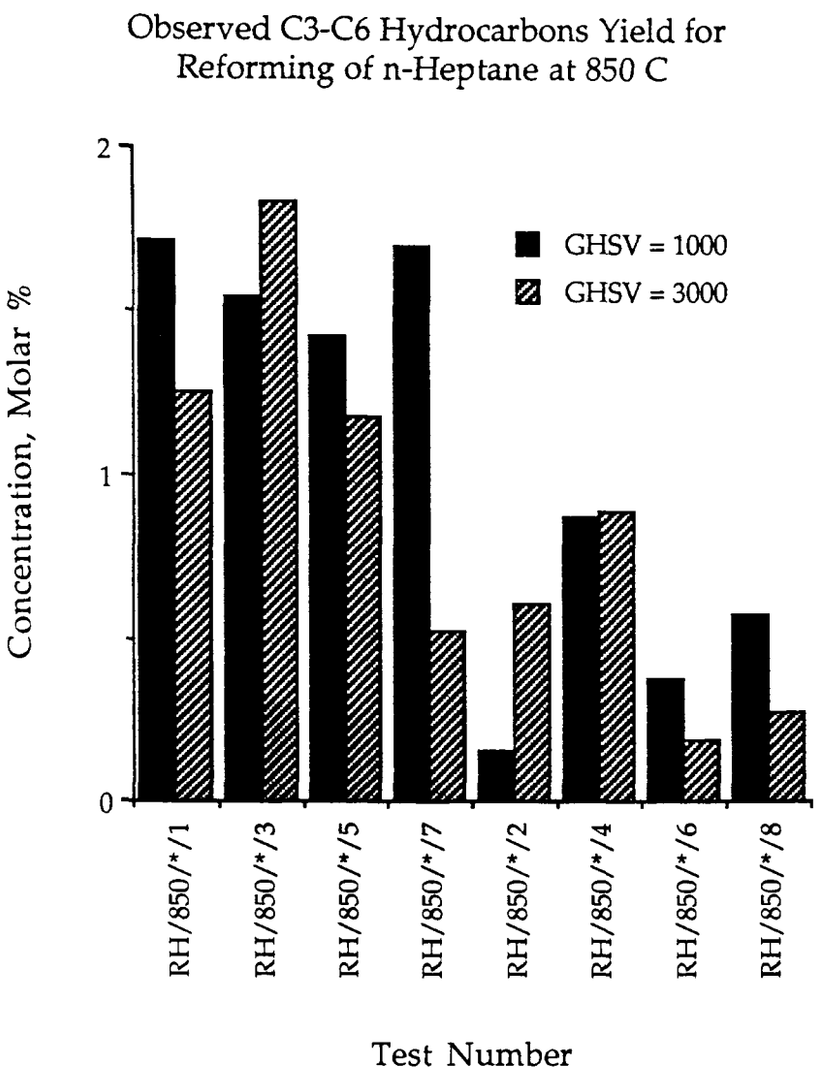


Fig 9.5a

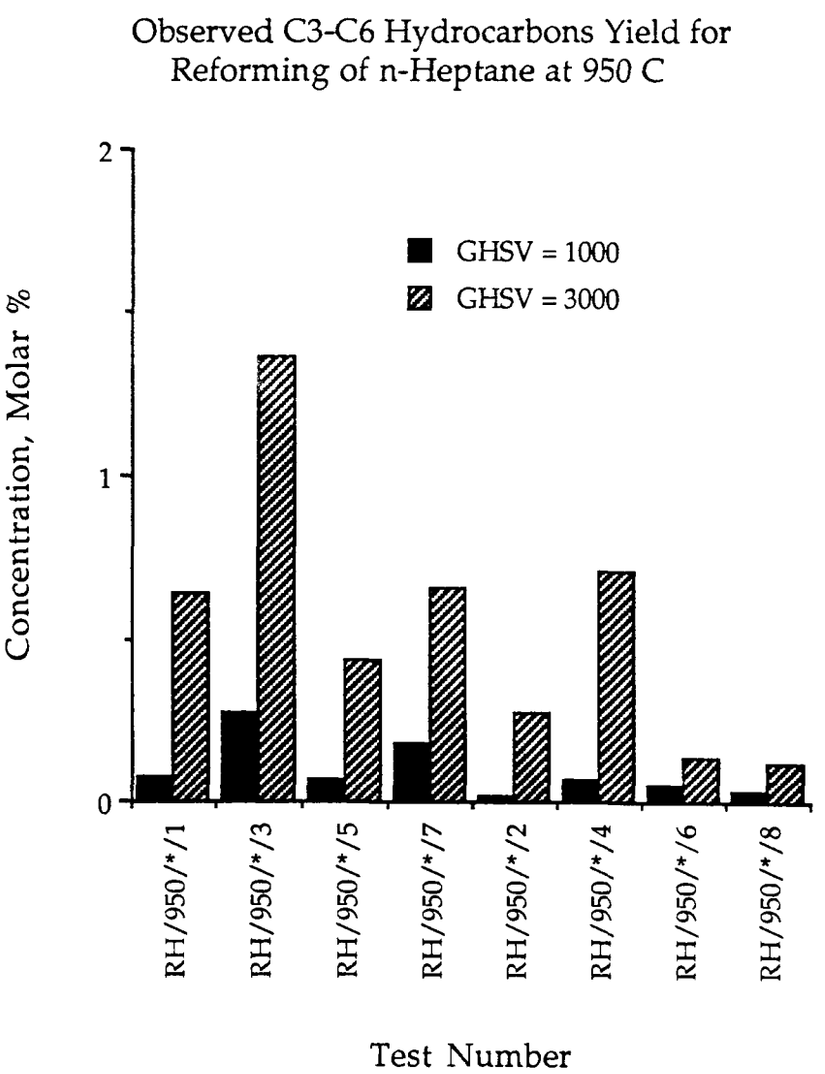


Fig 9.5b

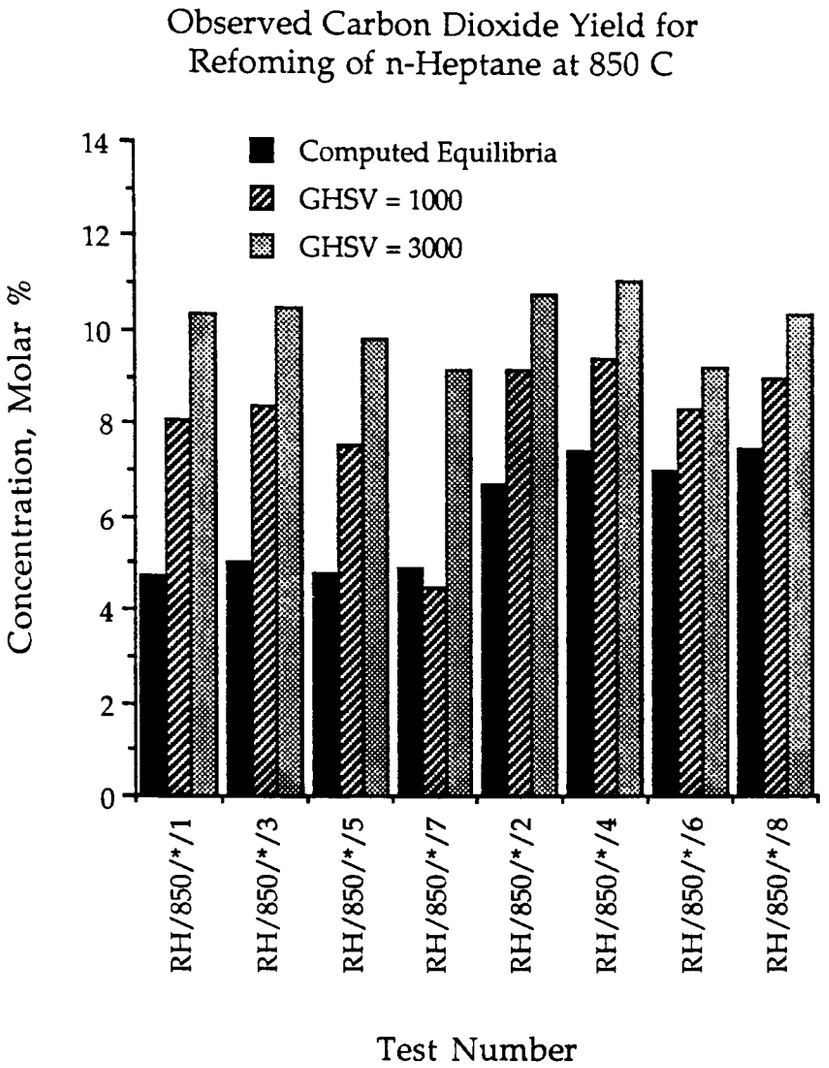


Fig 9.6a

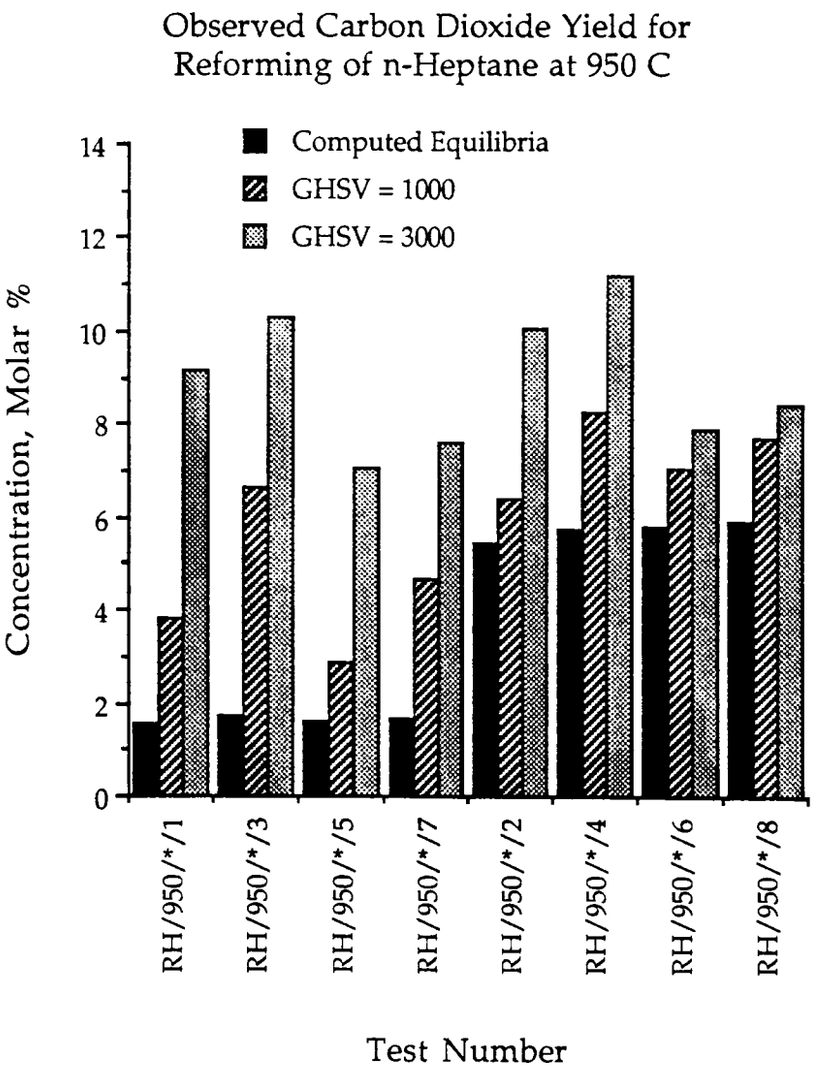


Fig 9.6b

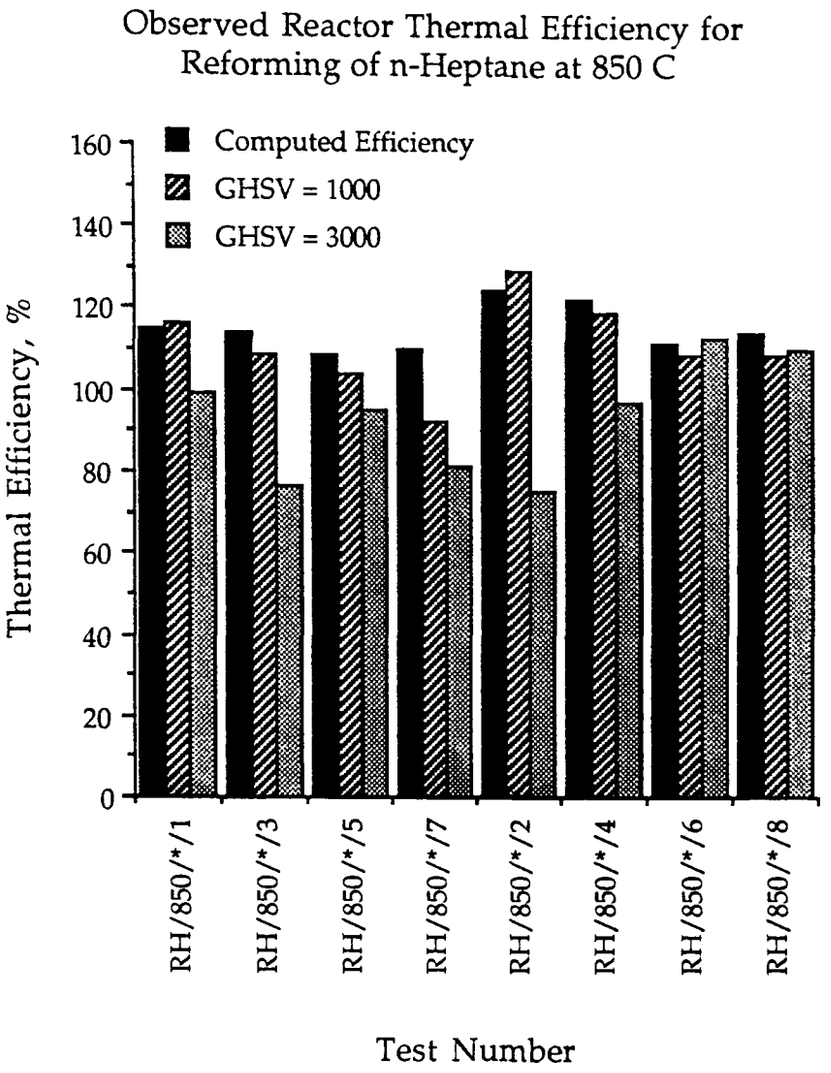


Fig 9.7a

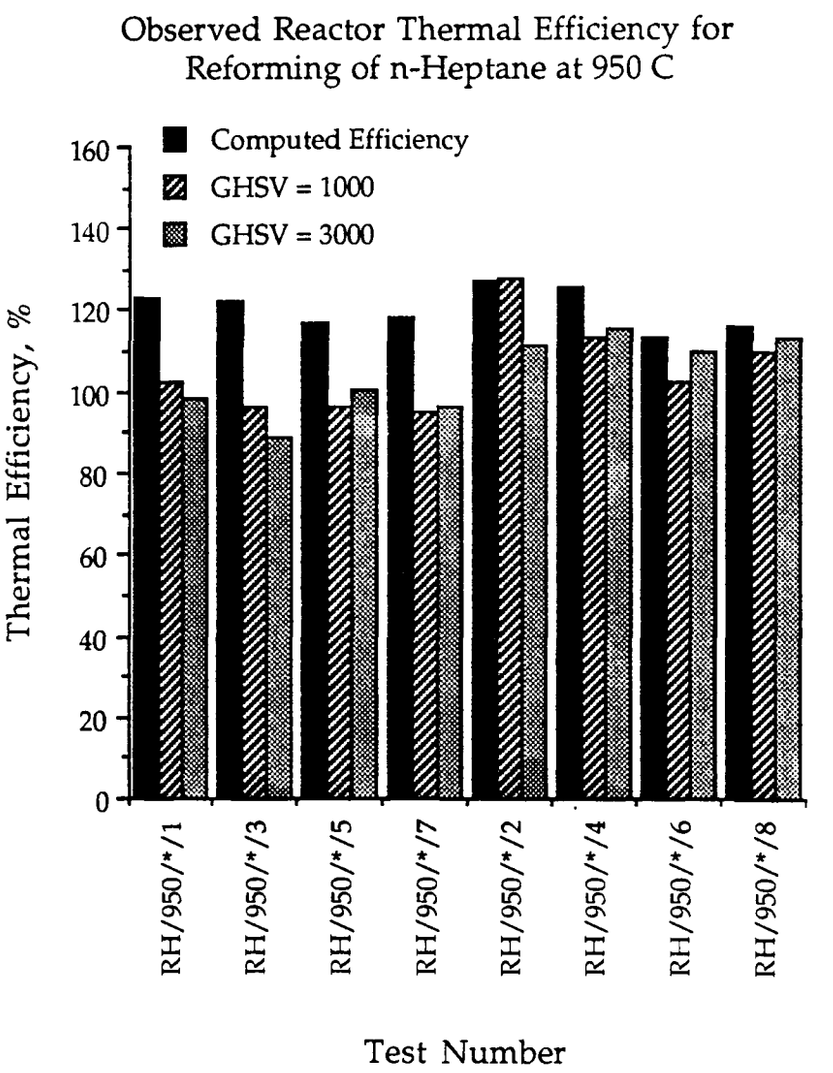


Fig 9.7b

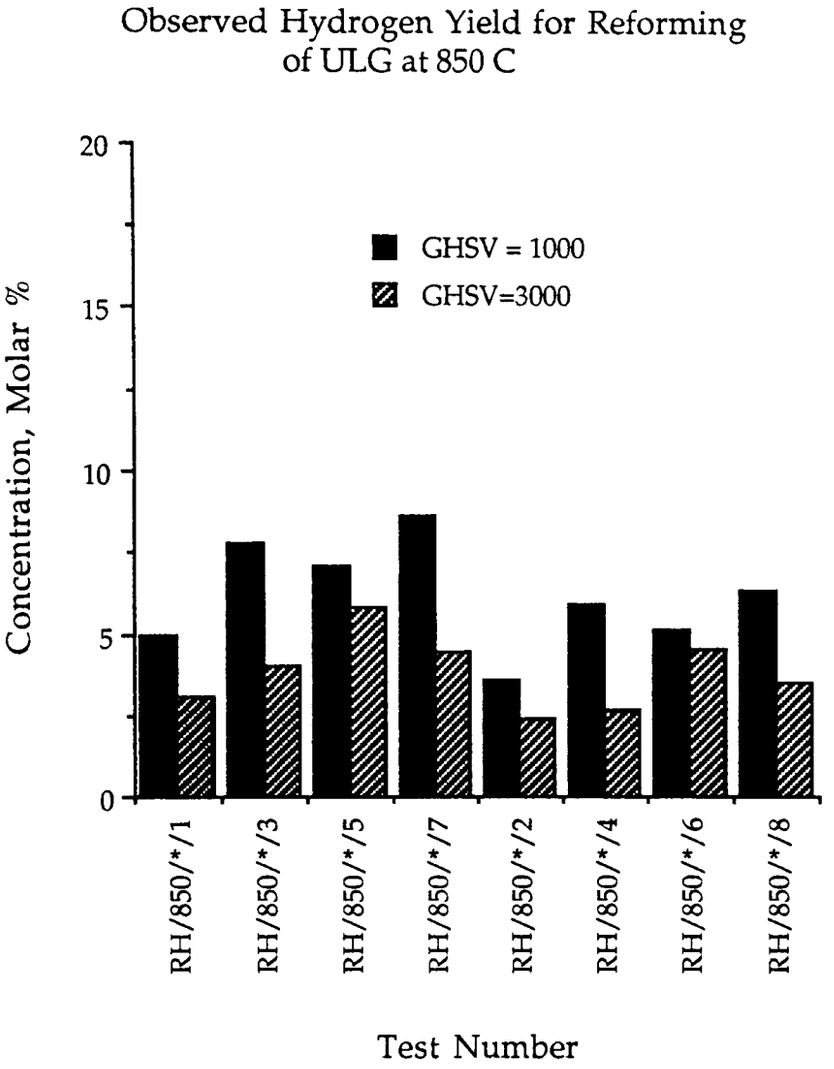


Fig 9.8a

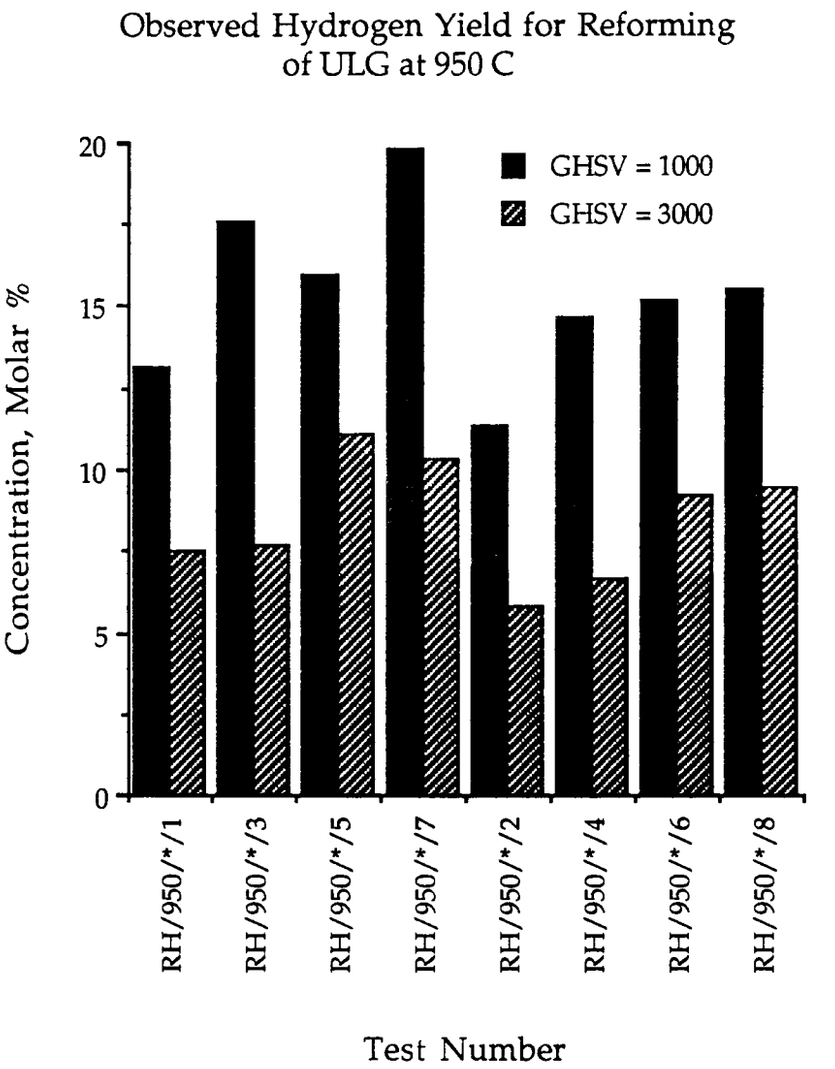


Fig 9.8b

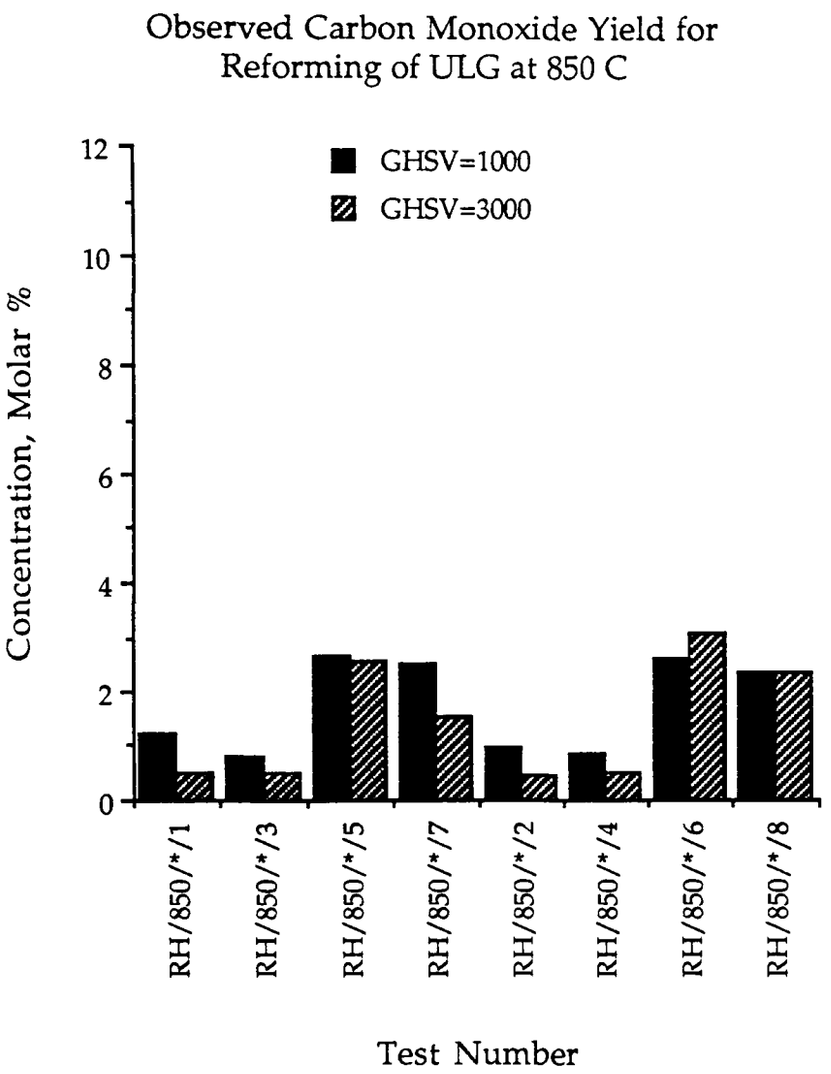


Fig 9.9a

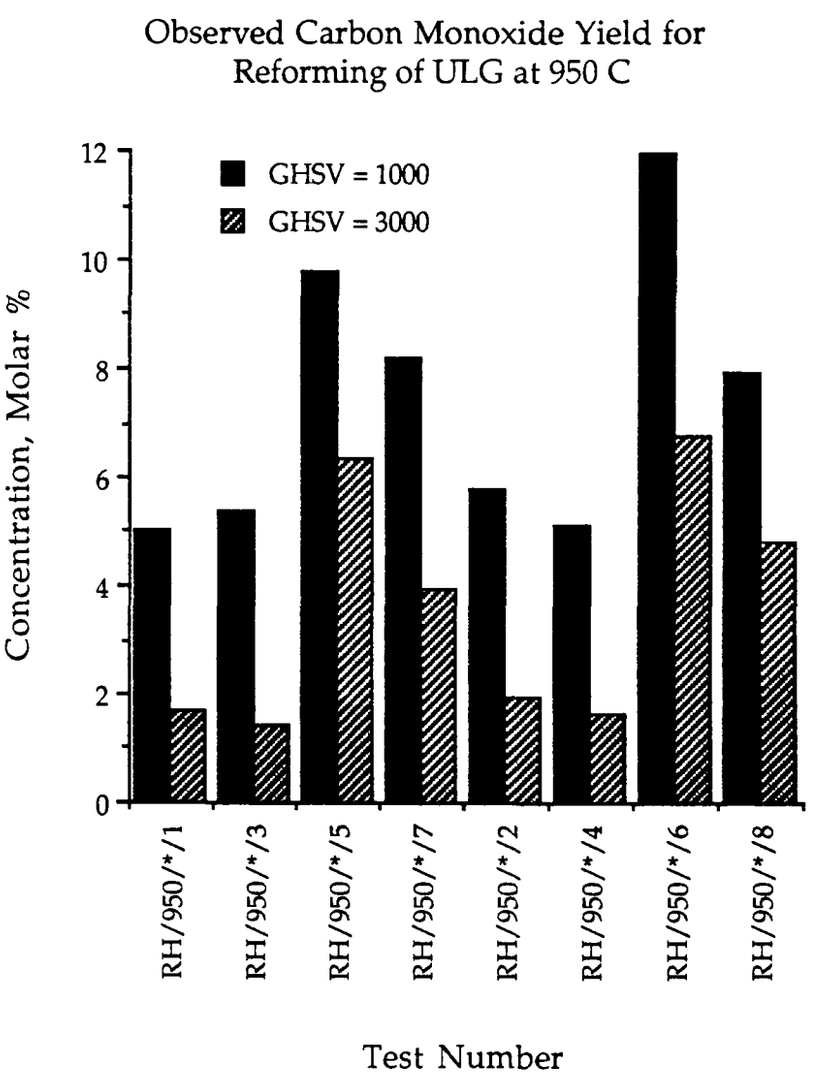


Fig 9.9b

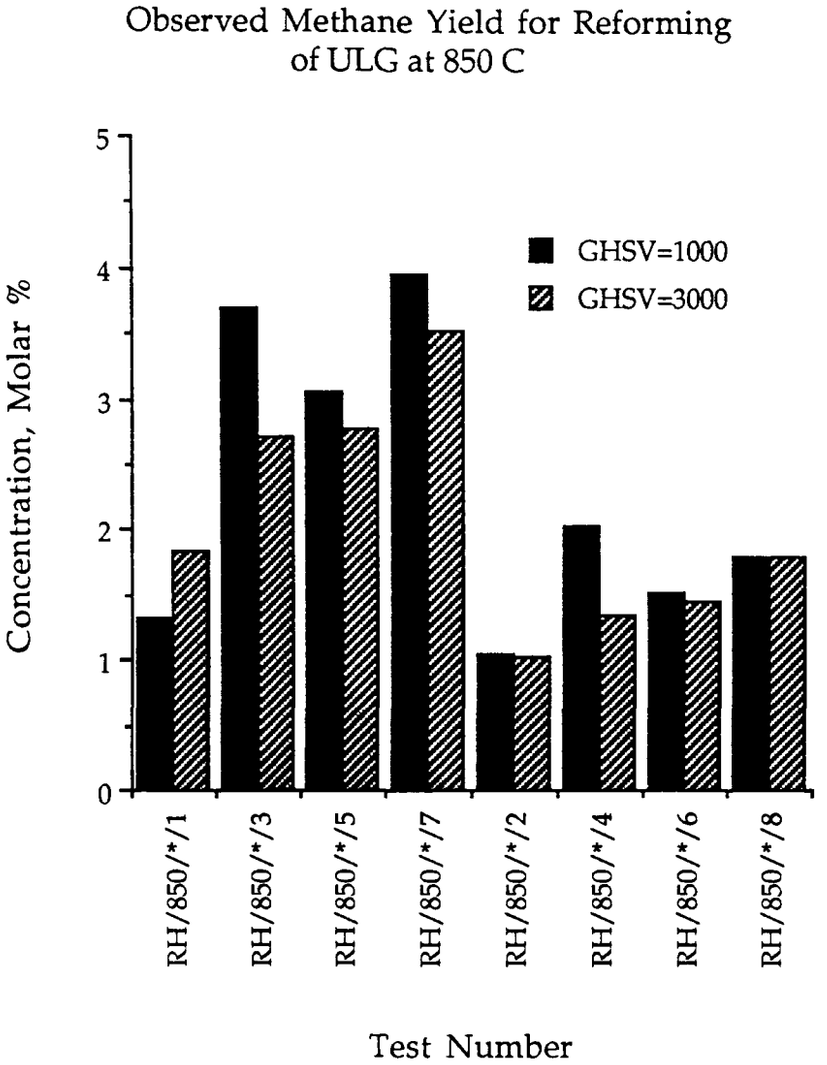


Fig 9.10a

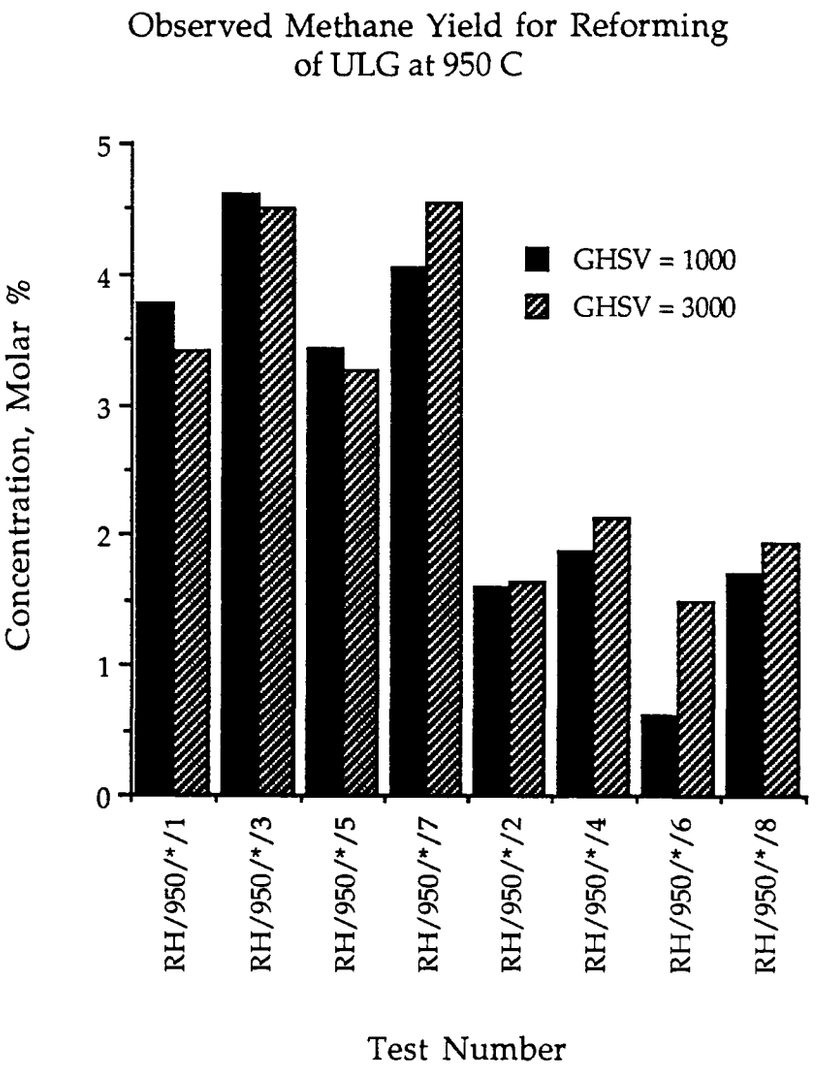


Fig 9.10b

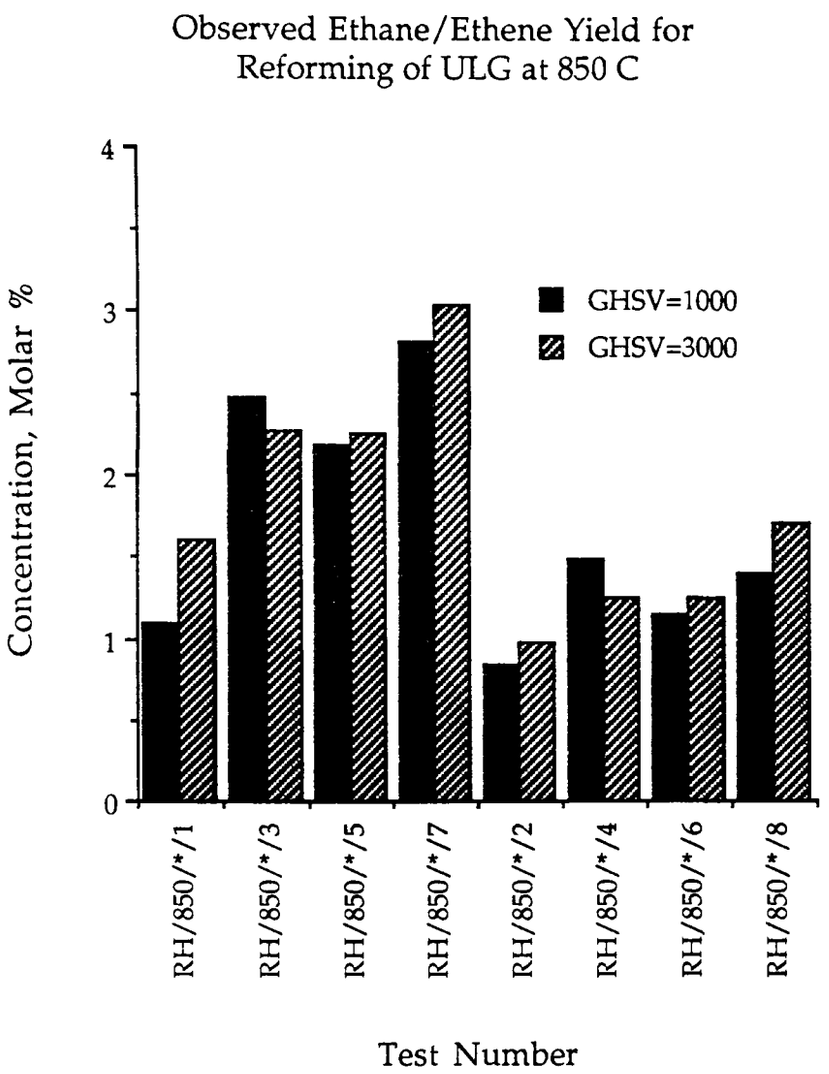


Fig 9.11a

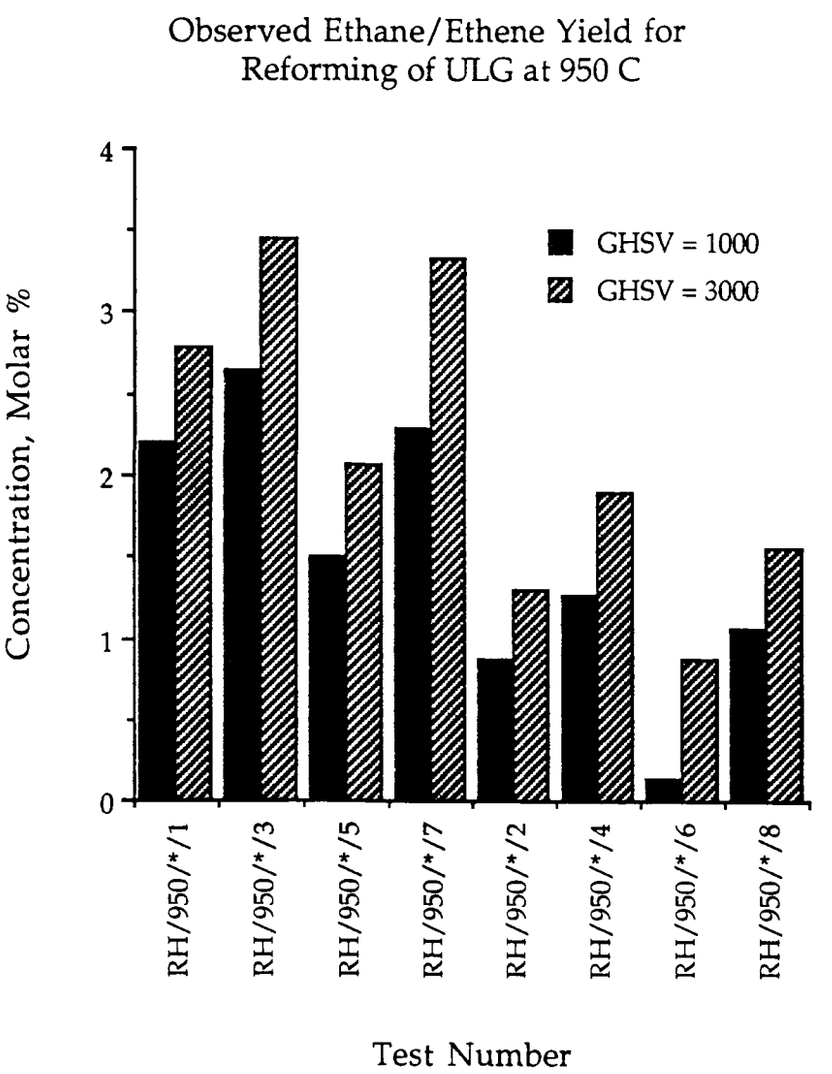


Fig 9.11b

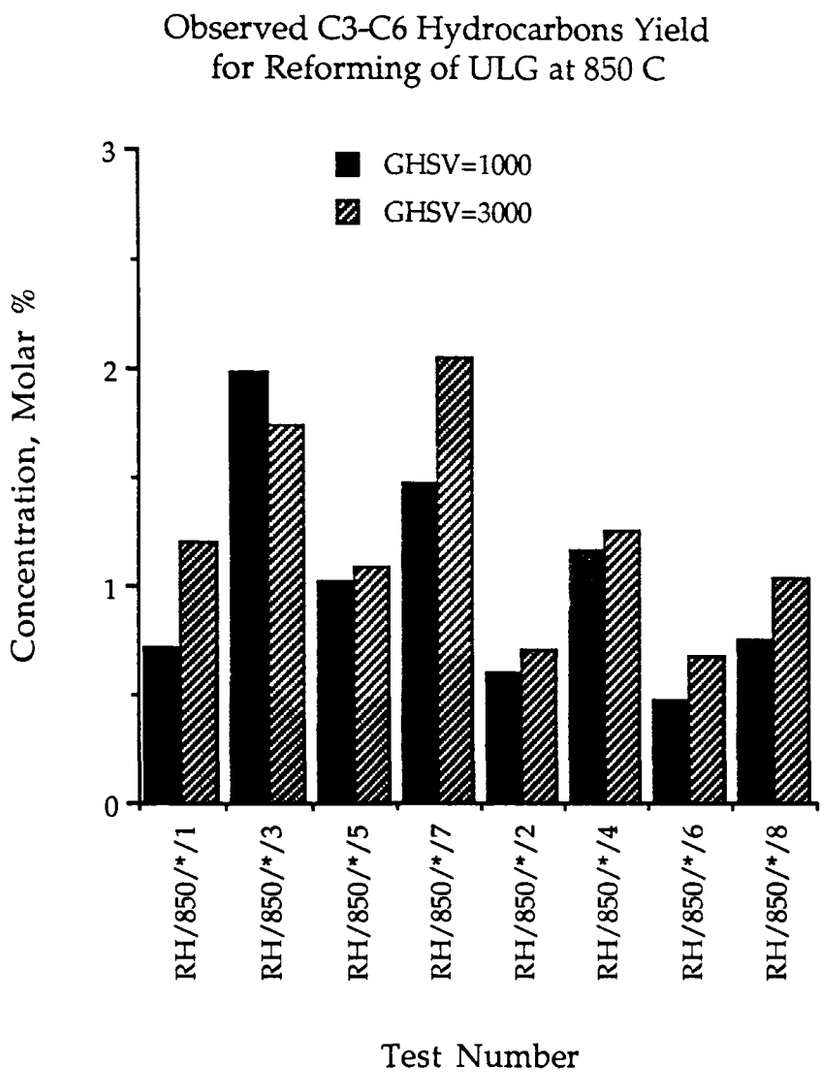


Fig 9.12a

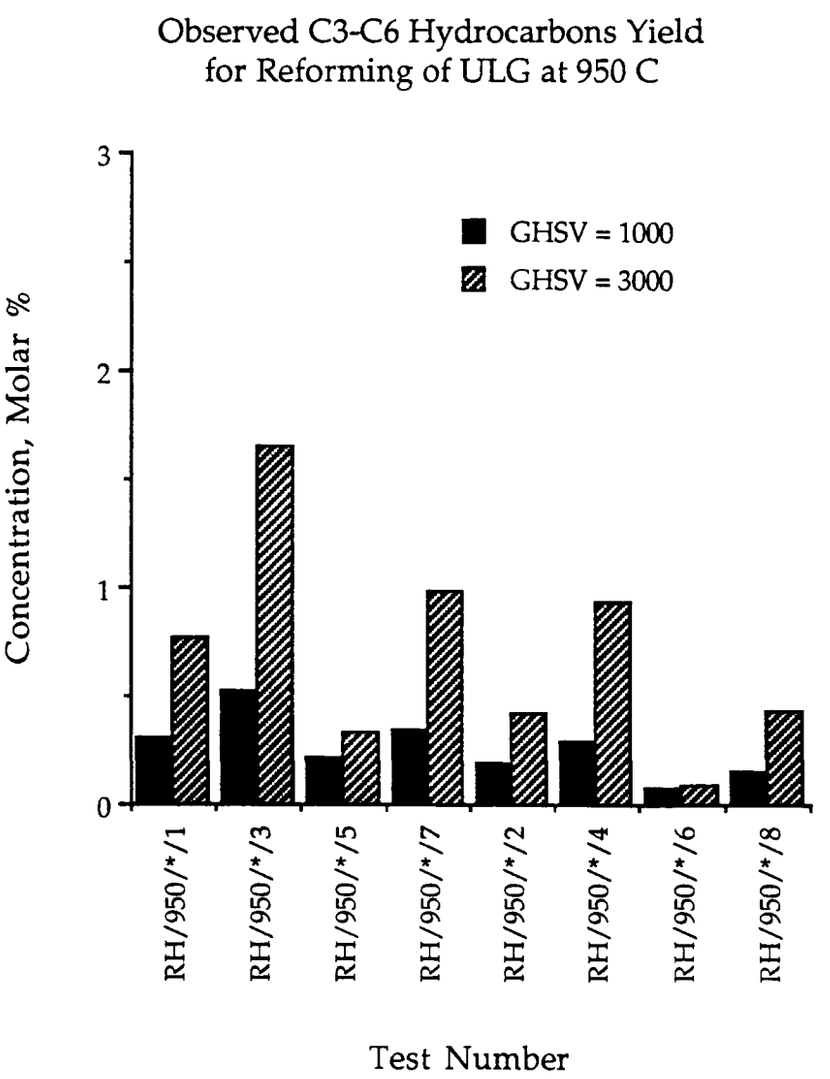


Fig 9.12b

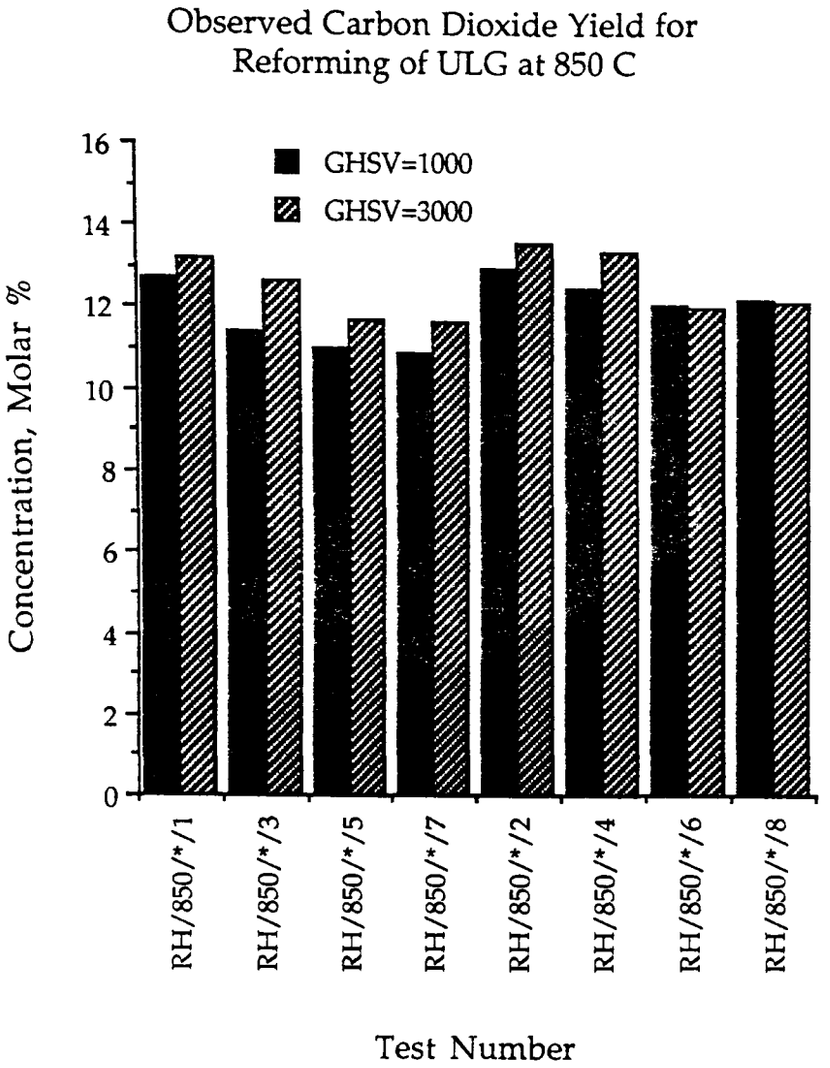


Fig 9.13a

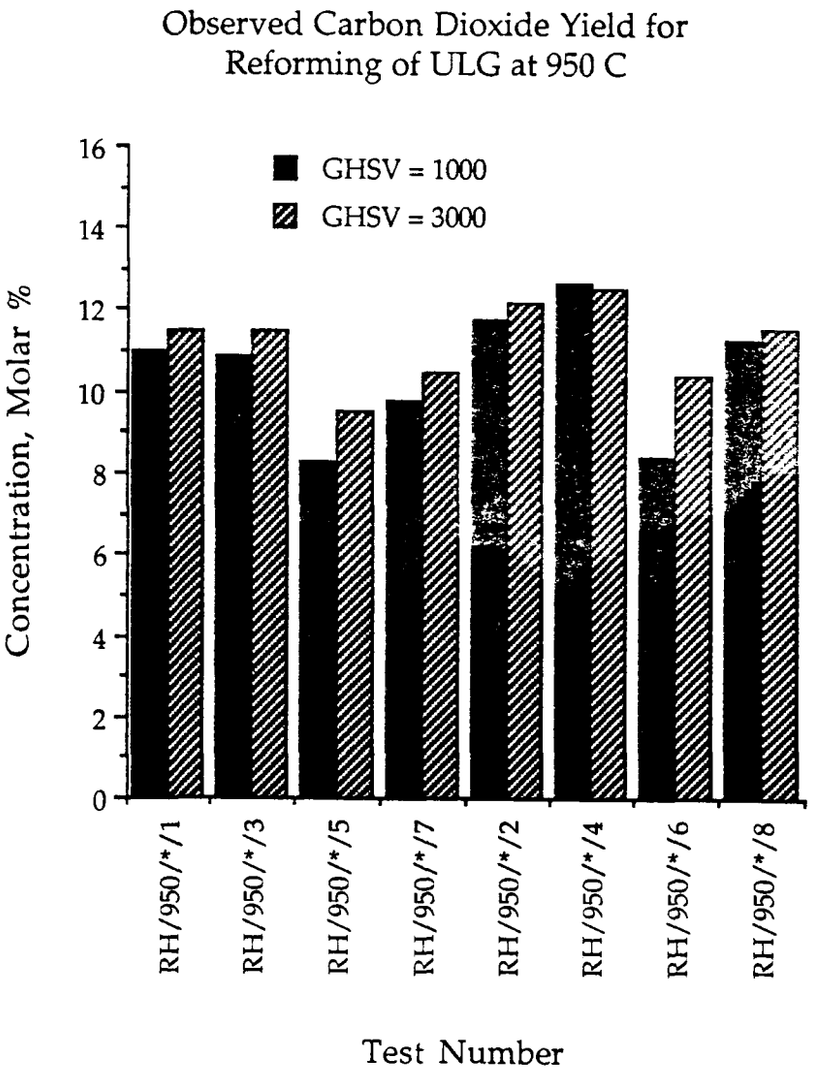


Fig 9.13b

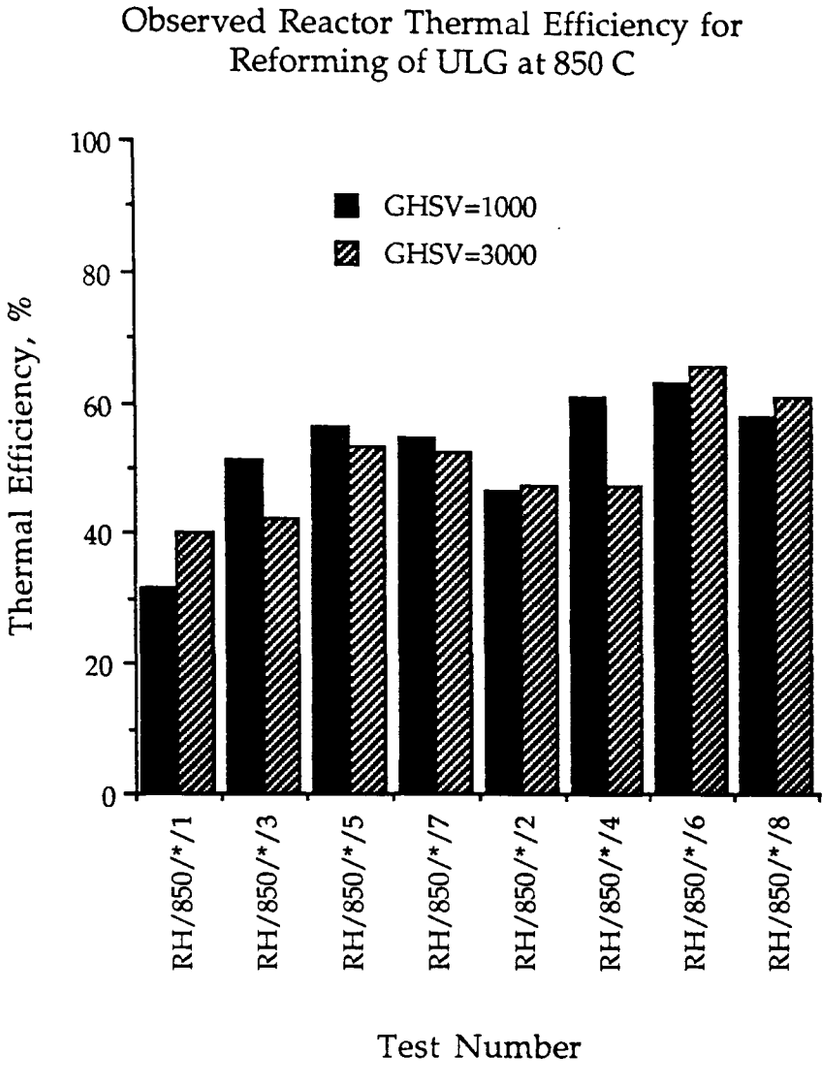


Fig 9.14a

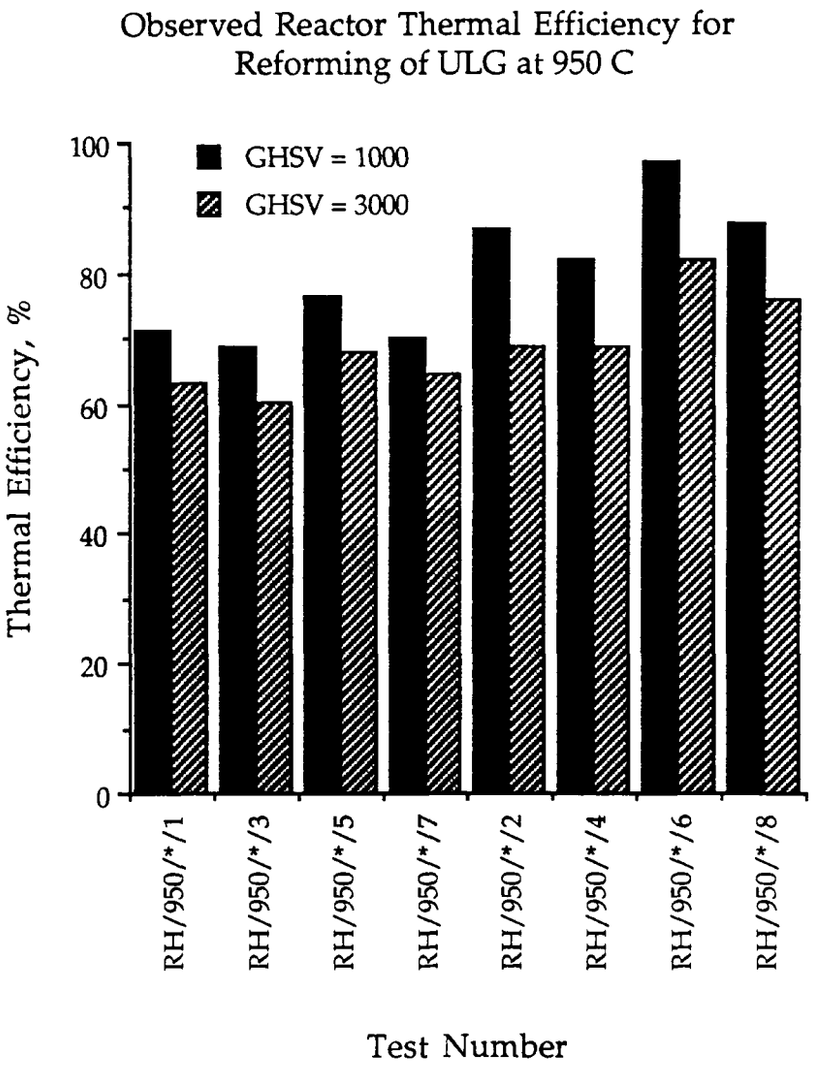


Fig 9.14b

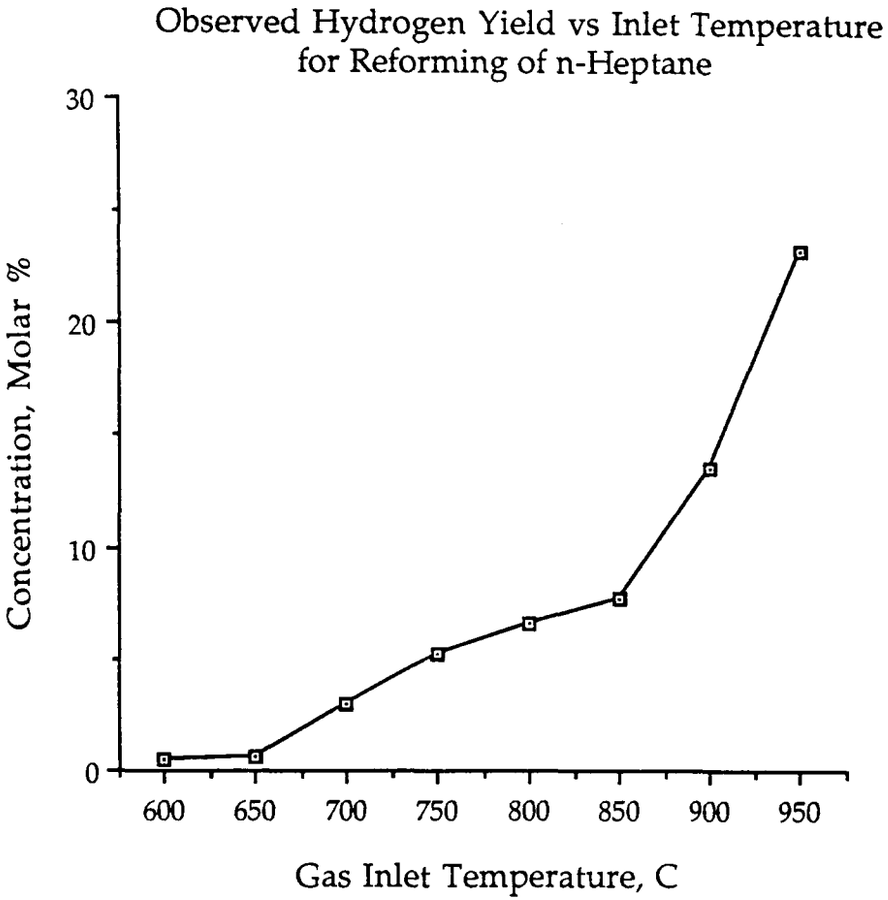


Fig 9.15a

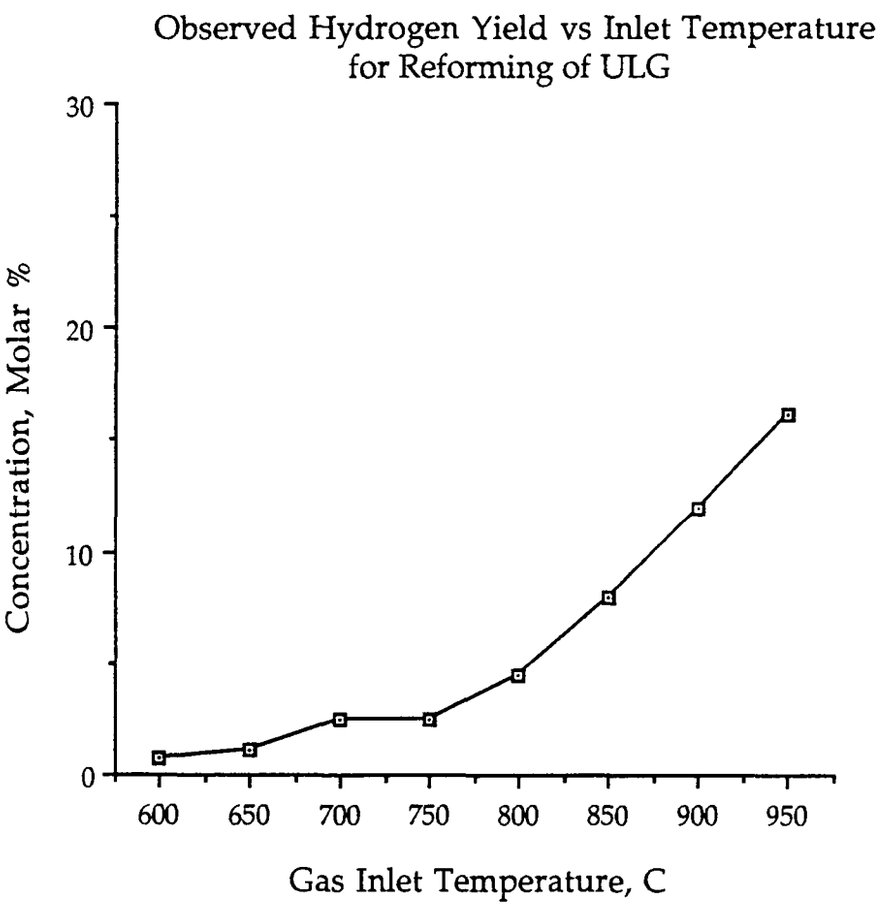


Fig 9.15b

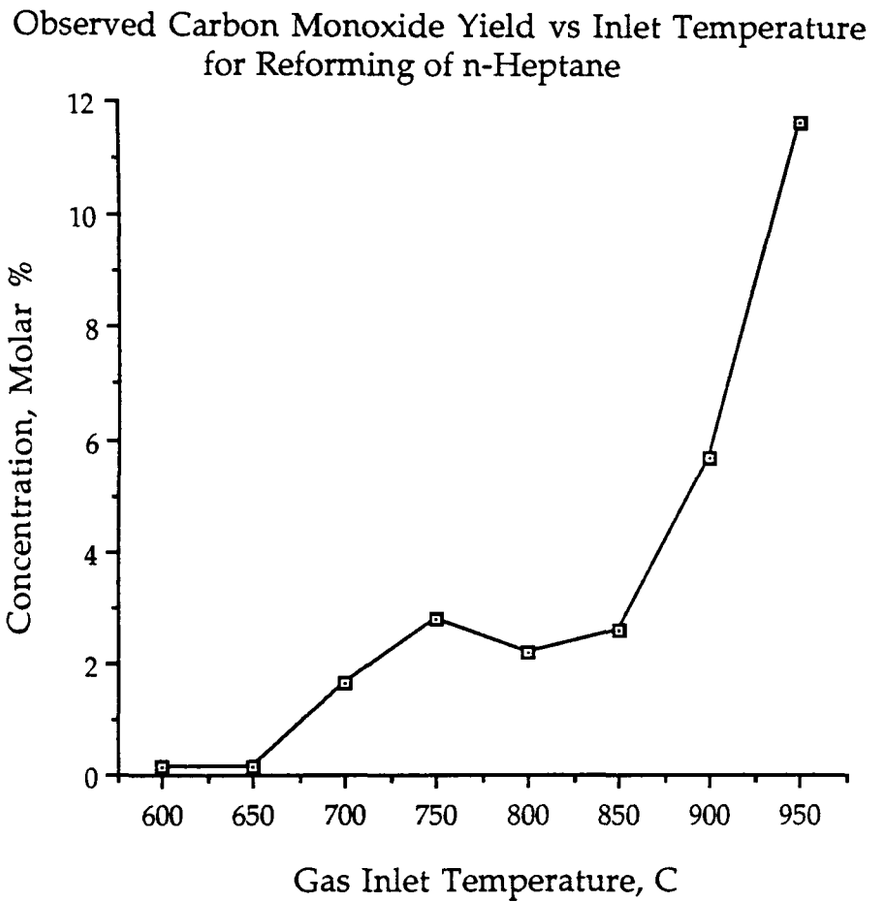


Fig 9.16a

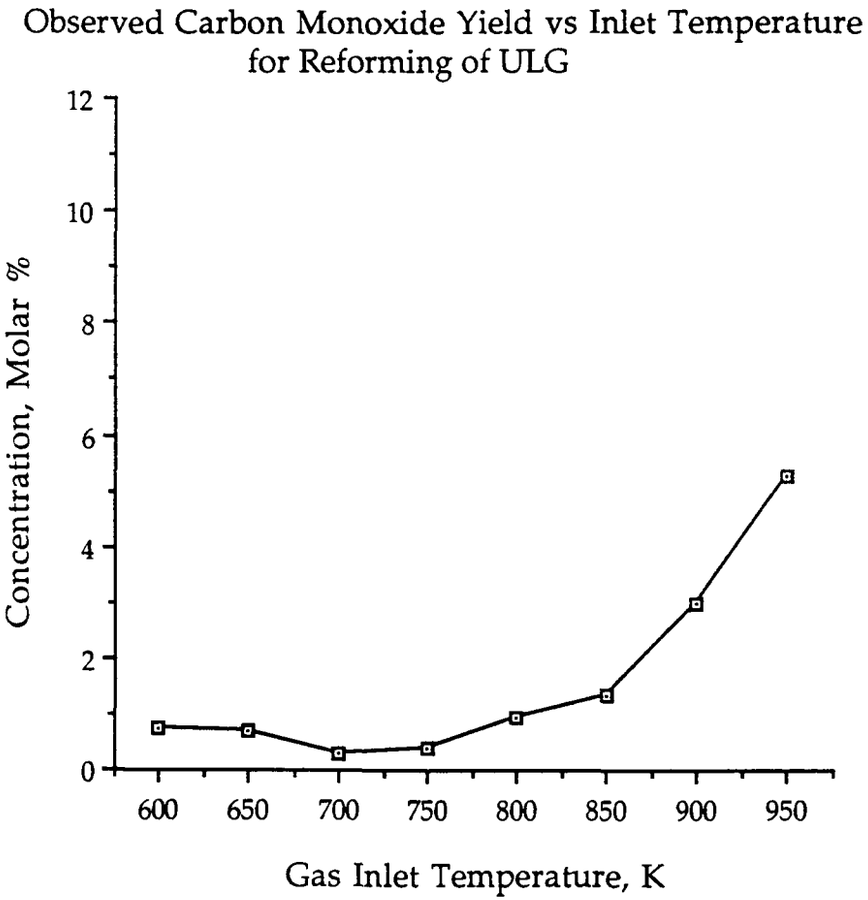


Fig 9.16b

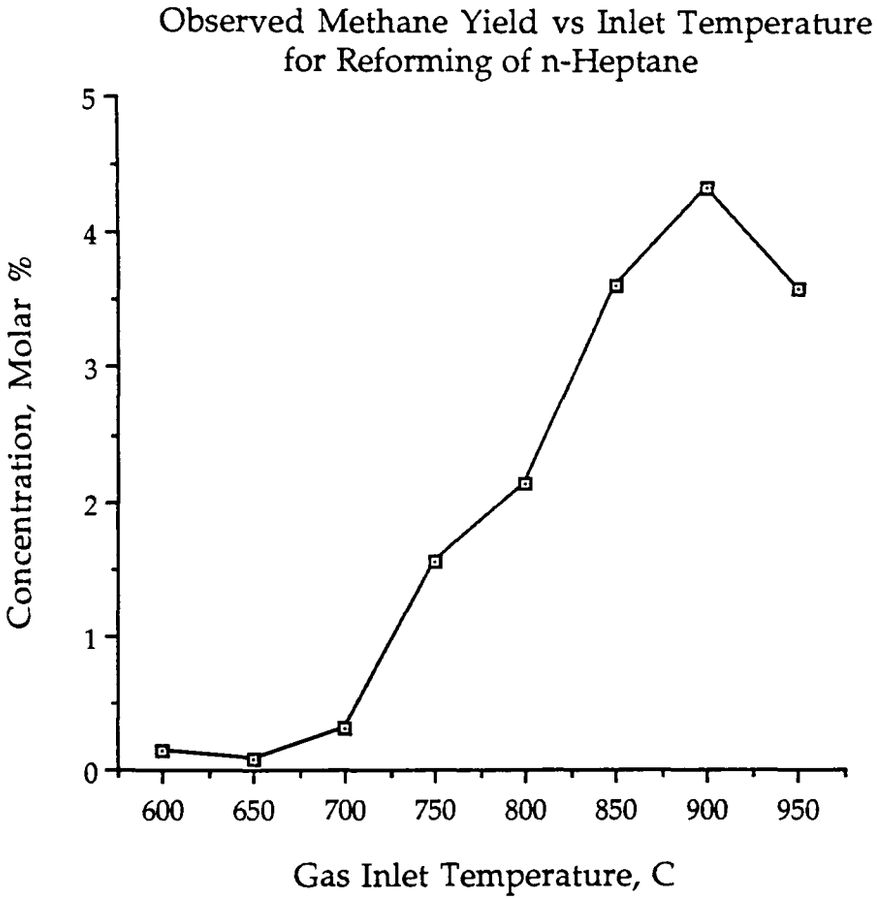


Fig 9.17a

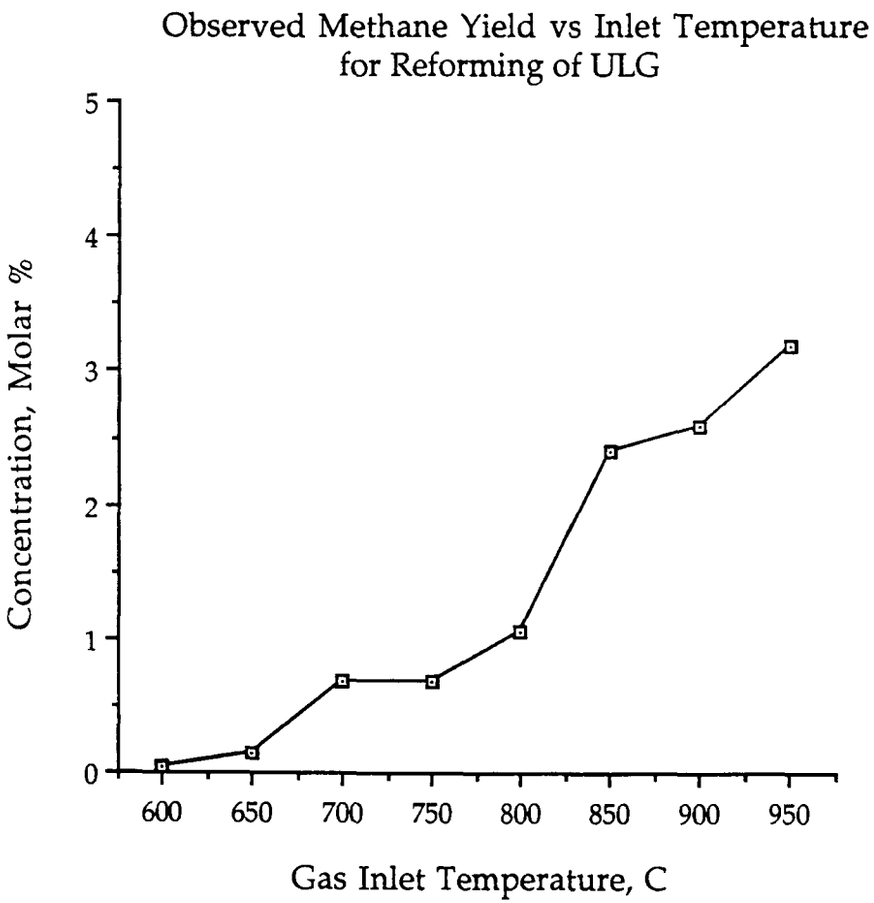


Fig 9.17b

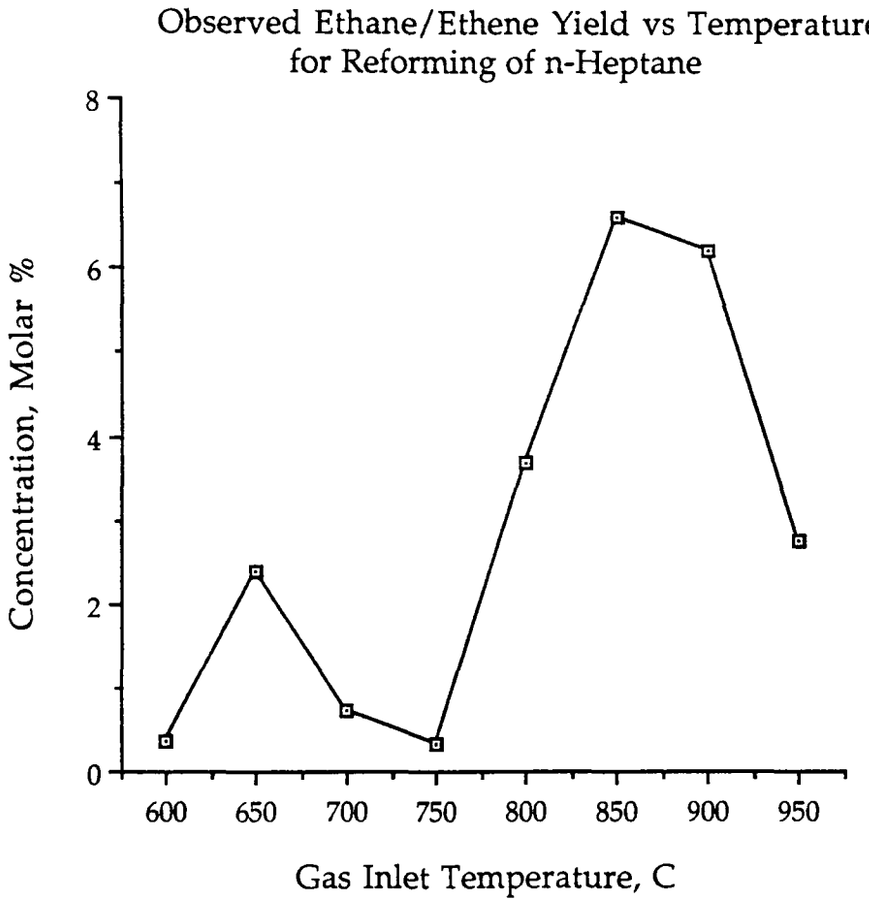


Fig 9.18a

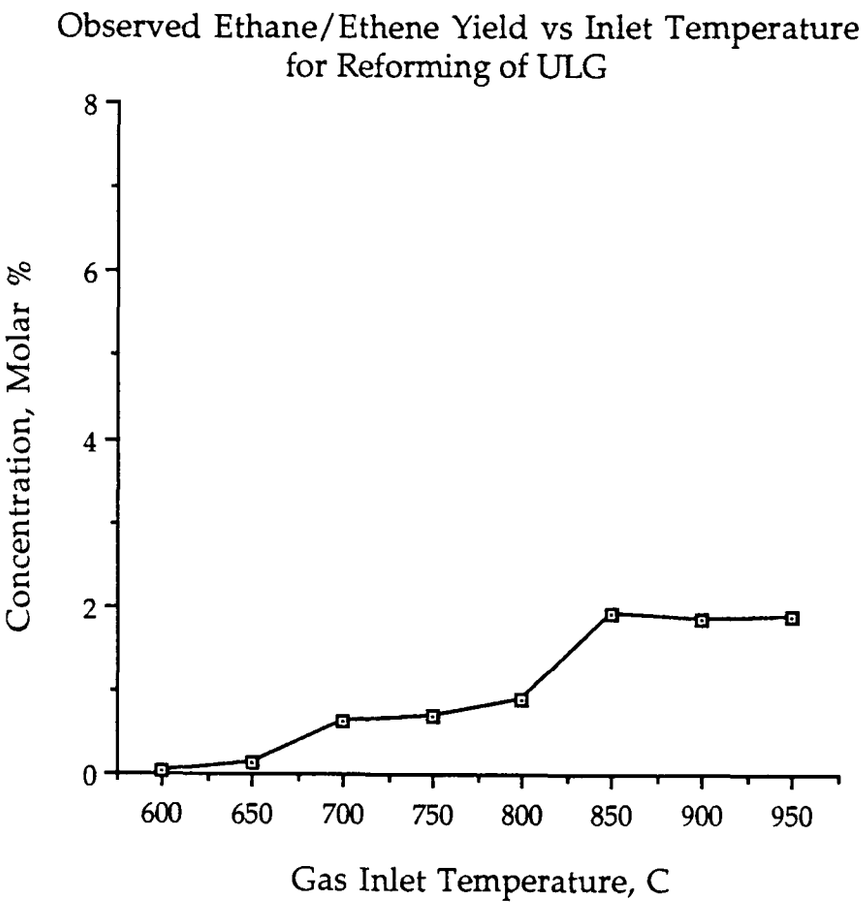


Fig 9.18b

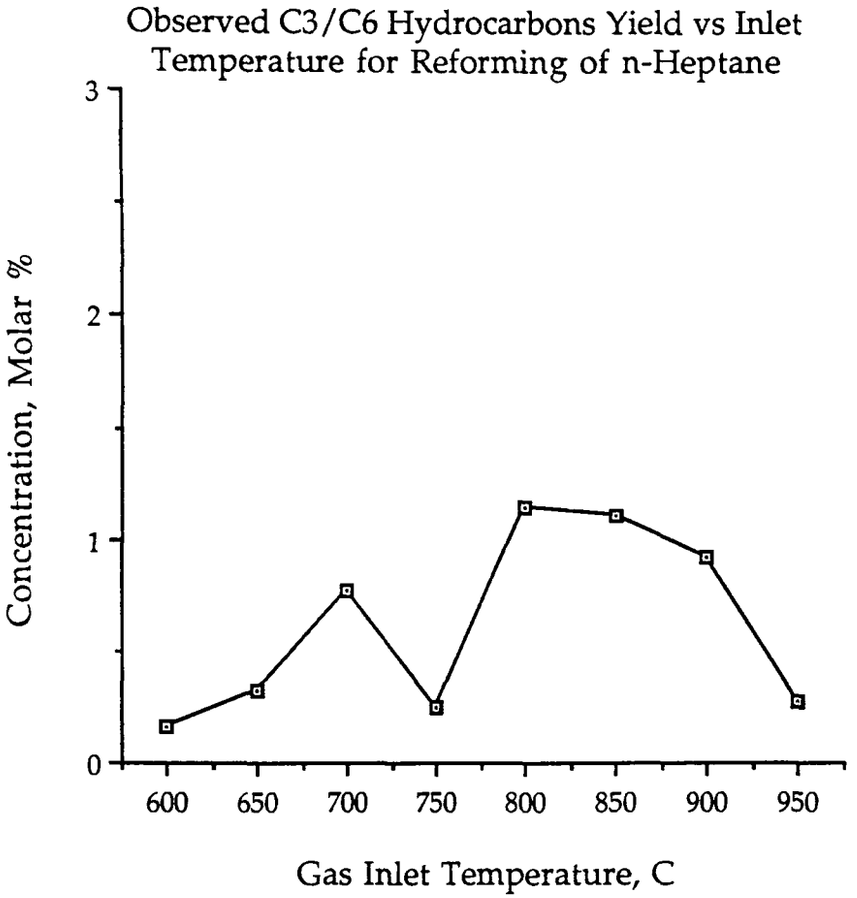


Fig 9.19a

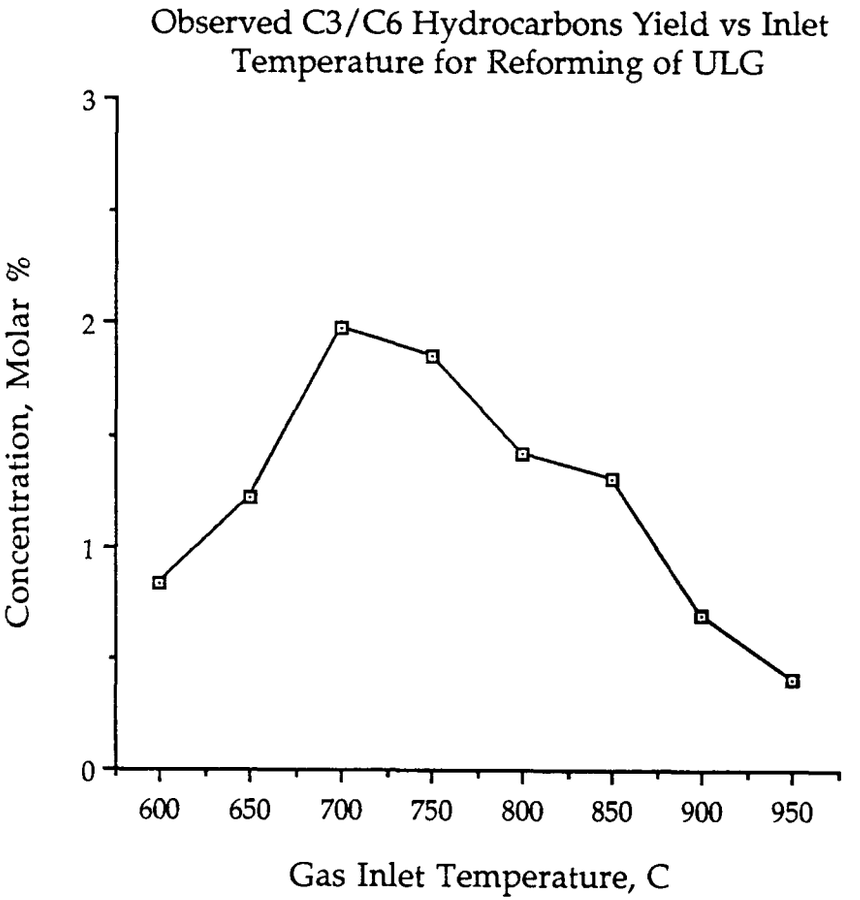


Fig 9.19b

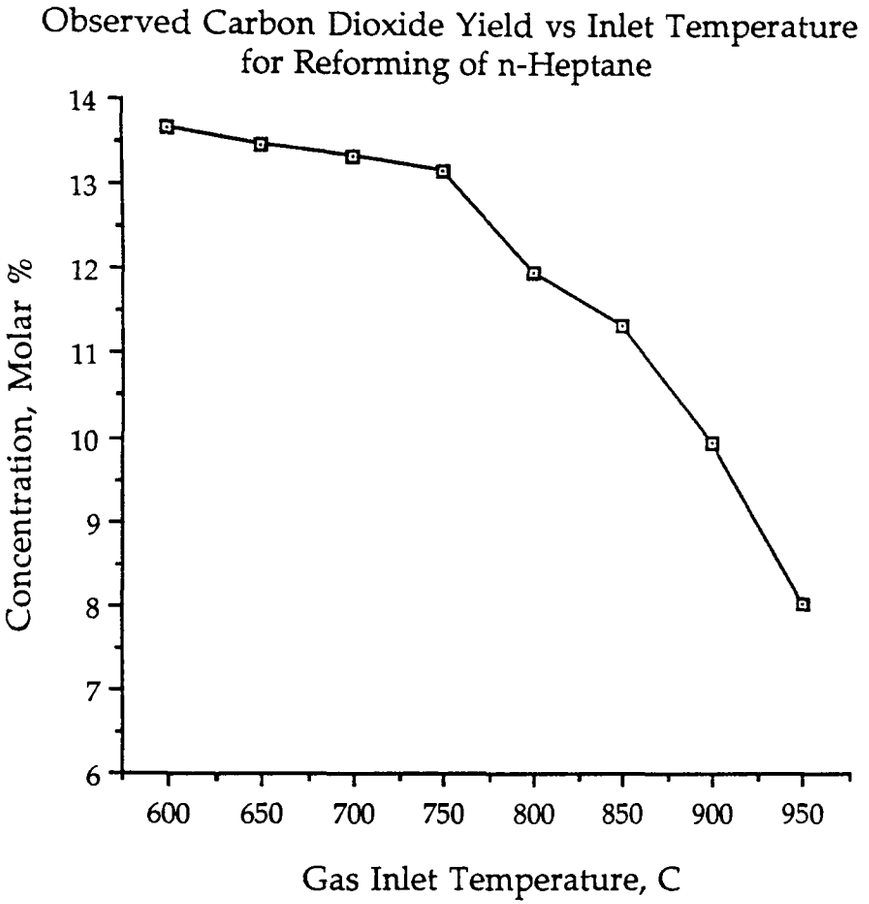


Fig 9.20a

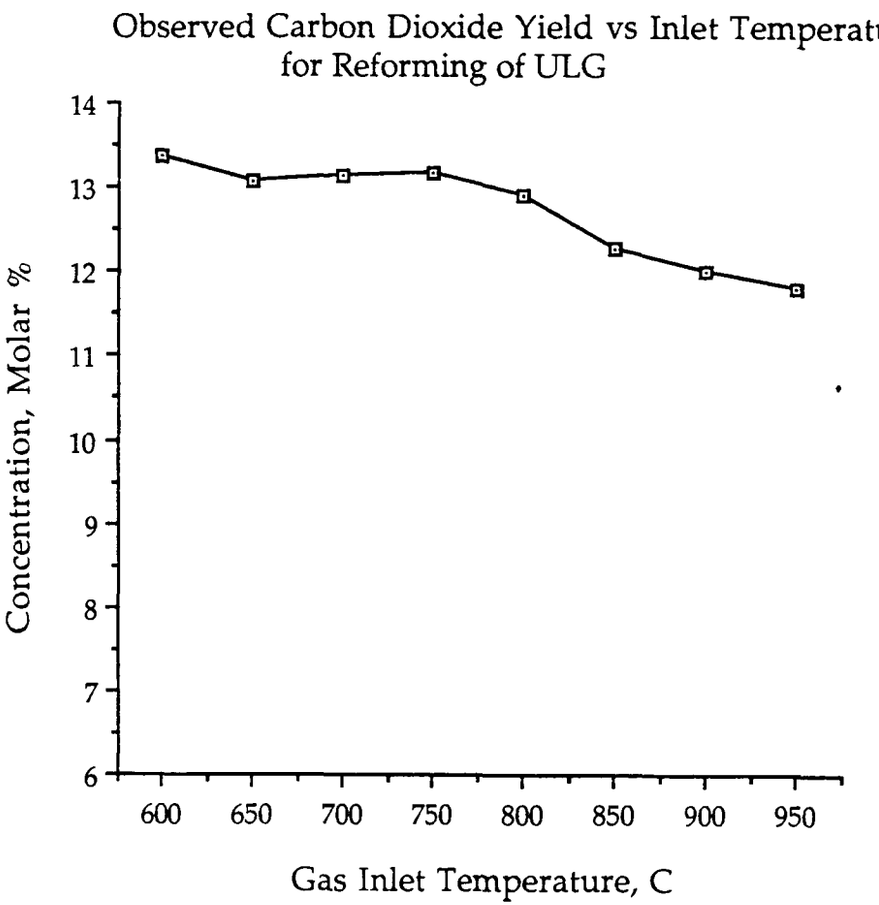


Fig 9.20b

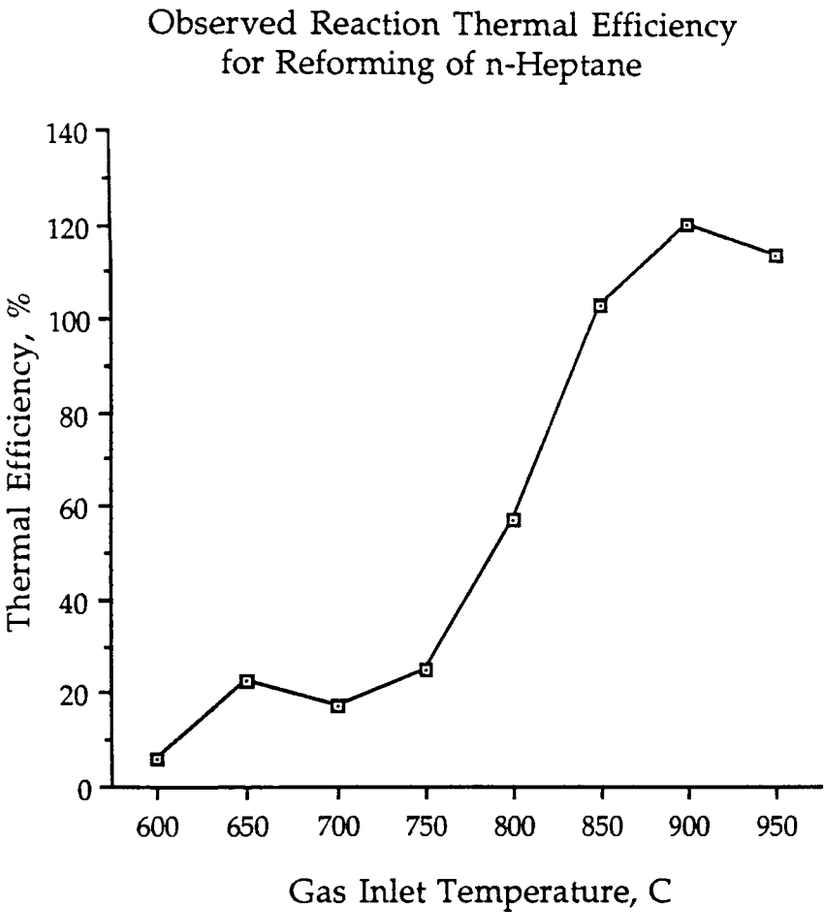


Fig 9.21a

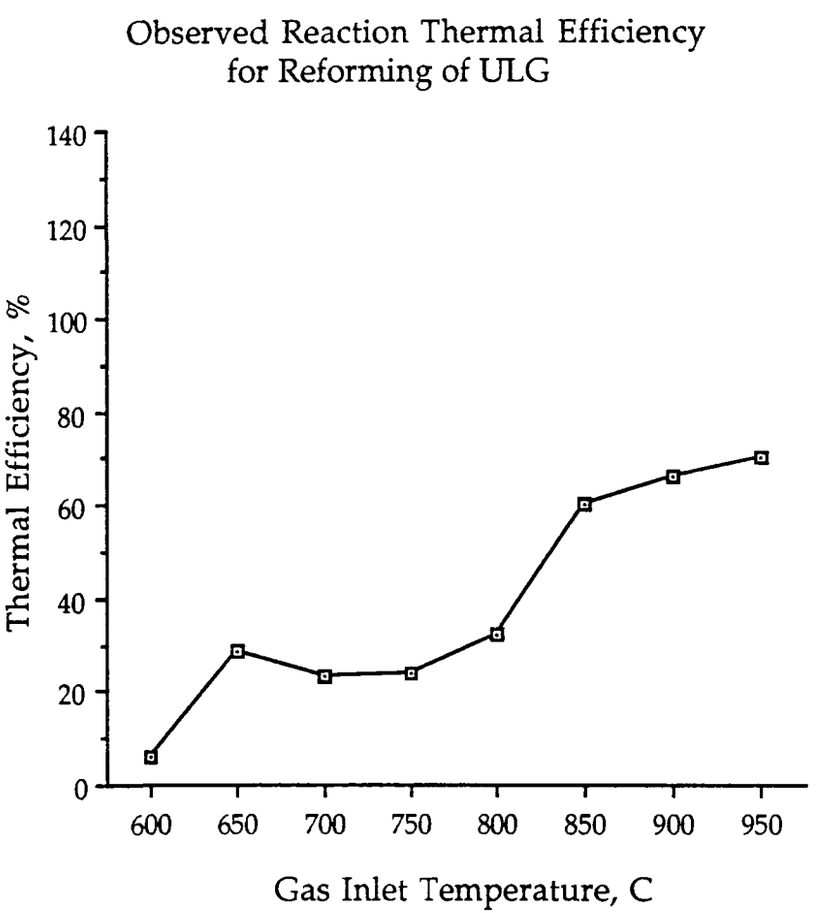


Fig 9.21b

# 10 CONSIDERATIONS RELATING TO THE PRACTICAL FEASIBILITY OF A VEHICLE INSTALLATION

It had originally been hoped that the exhaust-gas reforming process might be applied to the engine feedstock and enable engine operation solely on a reformed fuel/air charge, leading to improvements in overall efficiency and reductions in pollutant emissions. As the project developed, however, it became apparent that the objective of operating an inherently transient automotive engine on a pure reformed gasoline/air charge would be difficult, if not impossible, to achieve. Reasons for this are discussed below.

## 10.1 Observations Based on the Theoretical Work

The theoretical predictive study of reforming equilibria and energy requirements gave encouraging results in terms of the fuel compositions which could be produced by the reforming process. Hydrogen and carbon monoxide levels approaching those given in the idealized reforming equations were predicted, with good reformer thermal efficiencies indicating improvements in fuel calorific value across the reformer, as a result of heat recovery from the hot exhaust gases.

The theoretical study also, however, highlighted a number of limitations, not least of which are the high temperature levels predicted as being required to drive the endothermic reforming reactions.

One of the first points which became apparent was that a simple consideration of the engine energy balance, and reforming reaction energy requirements, was totally inadequate as a means of assessing the feasibility of the process. Using such a simple analysis, it can apparently be shown that

sufficient thermal energy exists in hot exhaust gases to drive the requisite reforming reactions to completion. On closer examination, however, it can be seen that reforming reactions can only be actively promoted at temperatures exceeding an absolute minimum of around 650°C, and hence only a relatively small amount of the energy content of hot exhaust gases can actually be reclaimed by the process itself. As the gases cool below this level they can be used to preheat the reformer reactants by means of indirect heat exchange, but they cannot otherwise contribute directly to the endothermic energy requirement.

Hence high temperature requirements of around 800 to 950°C are predicted for engine exhaust gases entering the reformer, and whilst cycle analysis work predicts that such temperatures might be attainable under certain conditions, it is apparent that it would be difficult to achieve these levels over the wide range of engine operating conditions experienced in the current passenger car. The problem of low exhaust-gas temperatures at part load might be overcome by the adoption of smaller engines running at higher loads or, perhaps, cylinder disenablement for low-load operation.

A further problem highlighted in the theoretical work relates to the levels of pressure-charge which would be required in order to maintain either a constant level of feedstock consumption or work output as compared with the engine operating cycle on the standard fuels. It might be possible to run the reactor at an elevated pressure to facilitate reformed-fuel boost, although this would inevitably lead to an increase in engine back-pressure, and hence a reduction in IMEP. It is suggested that the main problem with pressurized reformed fuels, however, would result from the extremely low ignition energy of hydrogen in the fuel gas, which may lead to pre-ignition and

uncontrolled combustion when operating the engine at high loads. This phenomenon has been highlighted by many previous workers.

### 10.2 Observations Based on the Experimental Work

Once the test-rig had been commissioned, a wide-ranging investigation of the effect of several parameters was conducted, in order that the reformer operating conditions of most interest could be established. This led into the more specific investigation of a discrete range of test points, the prime objective of which was to establish optimum operating conditions for the reforming process.

It was possible to produce reformed n-heptane fuels having hydrogen and carbon monoxide concentrations of around 32 and 20% respectively, and optimum reaction thermal efficiencies typically around 110 to 115%. There was evidence that equilibrium conditions were being closely approached in practice, and it was felt that the earlier theoretical work was well-supported by these experimental results. It was encouraging to note the degree to which the reforming reactions could be promoted in practice.

However, the experimental work highlighted a number of problems, some of which had become apparent in the earlier predictive work, whilst others had not.

Firstly, it was confirmed that exhaust-gas temperature requirements of around 850 to 950°C would be required at inlet to the reformer if good levels of feedstock conversion were to be achieved. In the case of both n-heptane and ULG feedstocks, rig operation at temperatures lower than this led to sharp reductions in hydrogen and carbon monoxide yields, and tended to give

increases in certain hydrocarbon concentrations. Greater quantities of unreacted feedstock would also presumably exist in the product gases, although as mentioned, it was not possible to quantify hydrocarbons levels for species above C6. This reduction in conversion results in a commensurate decrease in observed reactor thermal efficiency.

Carbon solids formation which had been predicted in the earlier work was confirmed in the practical studies, although it is suspected that a certain amount of the soot deposition was the result of kinetically-controlled decomposition of the feedstock on the highly reactive catalyst surface, which is an effect quite separate from the predicted equilibrium formation. This problem appeared to be most prominent with the ULG feedstock, but it is suggested that it could largely be avoided by careful control of the ratio of reforming oxidant to fuel, oxidant composition, and temperature.

The overriding practical limitation highlighted by the experimental work, however, relates to the maximum reactor gas hourly space velocity (GHSV) which can be tolerated. Initial testing showed that little or no feedstock reforming occurred at higher levels of GHSV, whilst progressive reductions in the relative catalyst throughput led to steady improvements in conversion. Ultimately the rig was operated at a space velocity of $1000h^{-1}$, which, in view of flow metering limitations, represented the practical minimum level of operation of the system. Under these conditions, good feedstock conversion was observed, but the arithmetic product of reformed fuel flow rate and higher heating value amounts to a fuel power level of around just 8kW, which is obviously inadequate in terms of fuelling a typical automotive power unit. The situation could be improved by increasing the catalyst volume, thus permitting increased reactant throughput for a given

space velocity, but this would lead to a physically larger reactor and increased warm-up times, as discussed below.

A problem which became apparent during the rig testing was the length of time which elapsed between powering up the rig and the reactor reaching its required operating temperature. This was typically around 1 hour, which would be totally unacceptable for most vehicle installations, although it is suggested that the time could be reduced by careful attention to detail in the design of the reformer system.

### 10.3 Conclusions of Feasibility Discussion

Theoretical and rig-based studies indicate that exhaust-gas reforming reactions can produce hydrogen-containing fuels having improved calorific values as compared with the feedstock, although exhaust-gas temperature requirements are rather high. In addition, the quantities of fuel producible with the current reactor would not be sufficient to power an automotive engine.

A redesigned reformer, containing a greater volume of catalyst, possibly having an improved formulation, might solve this problem, although reactor size would tend to increase, with potential space and warm-up time penalties.

It is suggested that the process might be most feasible as a means of generating a hydrogen-containing fuel gas for use as a supplementary fuel, in order to extend the lean flammability limit of a gasoline/air charge. Theoretical predictions of reformed fuel laminar flame speeds suggest that hydrogen-rich reformed fuel gases could increase the flame speed of a

conventional charge, indicating some potential for the enrichment strategy. If only a portion of the feedstock needed to be reformed prior to aspiration into the engine as a supplementary fuel, reformer sizing might be more compatible with vehicle packaging and warm-up requirements for a chosen level of reactor space velocity. In such an installation, certain mechanical aspects of the engine construction might need to be specifically designed with the reformer in mind. The following features are some of those which might be particularly important:

1) Insulation of pistons/bores, leading to reduced thermal losses to coolant and a corresponding increase in exhaust-gas temperatures. This might be achieved by the application of ceramic materials.

2) Heat insulated exhaust ports and ducting to reformer, in order to minimize heat losses from the hot combustion products.

3) A potential for variable exhaust valve timing, or possibly a novel porting arrangement, would be desirable, in order to ensure that sufficiently high reformer gas inlet temperatures can be maintained over a wide range of engine operating conditions.

Naturally, the reformer control system would be complex, with control requirements for reformer oxidant to feedstock ratio, gas inlet temperature and oxidant composition (excess oxygen and/or steam). Additional complexities relate to the engine fuel management hardware, which would be required to give the correct ratios of gasoline, reformed fuel and air over the full range of system operation.

As mentioned earlier, the exhaust-gas reforming of methanol has only been studied theoretically, and the results were encouraging in terms of predicted fuel compositions, thermal efficiencies, exhaust-gas temperature requirements, and a reduced tendency for C(s) formation. Further practical studies of the process might therefore indicate a higher feasibility for the onboard reforming process as applied to the alcohol, as compared with the hydrocarbon fuels.

# 11 PROJECT CONCLUSIONS AND RECOMMENDATIONS

## 11.1 Executive Summary of Project Conclusions

Hydrocarbon fuels have been successfully exhaust-gas reformed in the laboratory, by means of a test rig comprising a propane-fuelled exhaust-gas generator and a prototype catalytic reforming reactor.

Mixtures of n-heptane and combustion products have been converted into reformed fuels having hydrogen and carbon monoxide concentrations within 2.5% of theoretical equilibrium levels. Successful conversion of a ULG fuel was generally more difficult to achieve, with much lower yields of the above-mentioned combustibles observed under similar test conditions. The experimental studies confirm the tendency for C(s) formation as a result of reforming reactions for the two hydrocarbon fuels, and conditions must therefore be carefully controlled if heavy deposition is to be avoided.

Significant improvements in fuel heating value were observed for trials with n-heptane, as a result of endothermic heat recovery from the hot exhaust gases, whilst reductions in heating value are indicated for ULG, as a result of the poor conversion of this fuel.

Theoretical work predicts significant improvements in flame speed, cycle efficiency, and $NO_x$ levels for the combustion of reformed fuels as compared with standard fuels. In addition, the theoretical studies of the exhaust-gas reforming of methanol were most encouraging, with lower temperature requirements and a much-reduced tendency towards carbon deposition as compared with the hydrocarbons.

## 11.2 Project Conclusions

1) Practical testing of the prototype reformer indicates that good conversion of an n-heptane feedstock can be achieved, albeit at relatively high temperatures and low catalyst gas hourly space velocities (GHSV's). Theoretically predicted trends of equilibria with temperature, oxidant to fuel ratio, and oxidant composition have been confirmed in practice, and a reformed fuel having hydrogen and carbon monoxide levels of 32.2% and 19.6% respectively was observed, at a reactor gas inlet temperature setting of 950°C (1223K) and a GHSV of $1000h^{-1}$.

2) The conversion of RF-08 ULG to hydrogen and carbon monoxide, via the exhaust-gas reforming mechanism, appears to be considerably more difficult to achieve than the conversion of n-heptane. Peak hydrogen and carbon monoxide levels for this feedstock are again observed at high reactor gas inlet temperatures of around 950°C, with values of 19.8% and 12.0% respectively.

3) The highest observed reactor thermal efficiency, which represents the ratio of reformed fuel heating value to that of the reformer feedstock, is 128.0%; this value was observed for the n-heptane feedstock. However, levels for this fuel generally fell between 95 and 115%, whilst the thermal efficiencies for the ULG fuel were lower, at best falling between around 70 and 90%. It is suggested that the poor results for the gasoline are attributable to heavy C(s) deposition, and the possible presence of unreacted feedstock components in the product gases, which lie outside the range of the gas analysis equipment.

4) The low levels of gas hourly space velocity required with the current reactor, in order to give favourable conversion conditions, resulted in rather low rates of generation of the reformed fuels. In the case of the n-heptane

feedstock, the best level of 'fuel power', the arithmetic product of reformed fuel heating value and flow rate, was around 8kW. Such a level would not be sufficient to power a typical automotive engine.

5) Evidence of C(s) formation was observed during certain experimental trials, and was generally most pronounced with the ULG fuel. Deposition of the condensed species is attributed both to equilibrium and kinetic formation, and was exacerbated by uncontrolled shifts in oxidant to fuel ratio to values somewhat lower than the nominal settings, which occurred during high-temperature trials. The reactor could be regenerated following C(s) deposition by means of controlled oxidation, brought about by carefully purging the reactor with burner flue gases containing small quantities of excess air.

6) Theoretical reformed fuel laminar flame speed calculations, based on computations of equilibrium reformed fuel compositions, predict increases in burning velocity by a factor of between 2.6 and 3.3 as compared with pure n-heptane, which has a burning velocity of 39.7cm/s. Calculation of these flame speeds enabled the effect of improved flame propagation to be accounted for in the cycle analysis investigation, but it is felt that the calculations should be confirmed experimentally, as the theoretical methodology adopted in the current project has not been validated for reformed fuels.

7) Cycle analysis simulations, based on computed reformed fuel equilibria, predict increases in overall engine efficiency broadly in line with predicted improvements in calorific value, as compared with standard fuels. However, at a constant level of feedstock consumption, which would require that the reformed fuel/air mixture is pressure-charged into the cylinder, it was found that improvements in engine cycle efficiency over and above the effect due to increases in fuel calorific value are predicted. It is concluded that this is

primarily attributable to reductions in burn duration and heat transfer losses which characterize reformed fuel combustion.

8) At a constant level of work output, which would require an intermediate level of pressure boost for the reformed fuel charge, reductions in predicted rate-controlled $NO_x$ levels of around 89.7 and 51.0% are predicted at 130° ATDC (Exhaust Valve Opening) for n-heptane and methanol fuels respectively. These reductions result from decreased cycle temperatures and shorter durations spent at high cycle temperatures which characterize the combustion of the reformed fuels.

9) Theoretical predictive studies of the exhaust-gas reforming of methanol indicate that the process is far less prone to C(s) formation than that applied to the hydrocarbon, whilst temperature requirements tend to be considerably lower. Fuel $RF_m1$ has hydrogen and carbon monoxide yields of 27.2 and 9.7% respectively, a reactor thermal efficiency of 115.8%, and an exhaust gas temperature requirement at inlet to the reactor of around 1060K. Notably, this reformed fuel is predicted at $\lambda_r$=1, ie stoichiometric reforming, and is well outside the C(s) formation zone. C(s)-free reforming under such stoichiometric conditions did not appear to be feasible for the hydrocarbon fuels studied.

In the light of these project conclusions, recommendations for further work related to this study should aim to address a number of issues, as outlined below.

## 11.3 Project Recommendations/Further Work

1) The Mk I prototype reformer has performed well, and has shown no tendency for mechanical failure under the most severe environmental conditions. The maximum rate at which reformed fuels can be generated, however, has been found to be too low to satisfy the requirements of a typical automotive engine. It is suggested, therefore, that a Mk II reactor should be designed and constructed with careful attention to the following details:

i) Provision must be made for a greater volume of catalyst which, in conjunction with the observed optimum catalyst space velocity, will lead to the generation of reformed fuels at higher mass flow rates.

ii) It should be possible to further improve the heat transfer between surplus exhaust gases and the catalyst monoliths, thereby improving overall heat recovery, and increasing catalyst reaction temperatures.

iii) Thinner section materials should be used throughout the construction of the reactor, in order to reduce warm-up time, which is currently unacceptable at around 1 hour.

2) It is suggested that the effectiveness of a range of catalyst formulations should be examined, in order that the feasibility of substantially increasing reformed fuel production rates beyond current levels can be established. A more active, and possibly more heavily-loaded catalyst washcoat may be beneficial in terms of raising the maximum tolerable space velocity, and might also lead to reductions in reaction temperature requirements.

3) The interesting theoretical predictions for the exhaust-gas reforming of methanol have not been confirmed experimentally, and it is suggested that in view of the potential benefits predicted for this feedstock, the work should be conducted. The reforming of a methane feedstock should also be studied, as there is an increasing awareness of the potential of compressed natural gas as an automotive fuel, and of mains natural gas as an engine fuel for combined heat and power (CHP) systems.

4) The feasibility of the exhaust-gas reforming process should now be examined more closely as a means of producing a hydrogen-rich gas for use as a charge supplement, leading to ultra-lean combustion of otherwise standard fuel/air mixtures. It is suggested that a Mk II reactor should be designed, constructed, and optimized, and used as a means of producing a hydrogen-rich supplementary fuel gas for use in engine-based lean combustion studies.

5) The laminar flame speed of reformed fuels needs to be studied experimentally. A flame propagation rig is currently being developed in the Automotive Engineering Centre as part of an under-graduate final year project, and it is hoped that this will facilitate the quantification of reformed fuel burning velocities (123).

6) The potential of exhaust-gas reforming in applications other than automotive power unit systems should be explored. As mentioned above, CHP might be one such area, whilst another possible application is in gas-fired furnace heaters, where the potential for improvements in efficiency and reductions in $NO_x$ emissions might be attractive. In contrast with the highly transient automotive engine, the steady-state operating mode of these stationary applications might render them inherently more compatible with the exhaust-gas reforming concept.

## REFERENCES


1) Kukkonen, C A. *Hydrogen as an Alternative Automotive Fuel.* SAE Paper 810349, 1981.

2) Thring, R H. *Alternative Fuels for Spark-Ignition Engines.* SAE Paper 831685, 1983.

3) Milkins, E E, Watson, H C, Zhou, Z H, and Edsell, J. *Comparison of Ultimate Fuels - Hydrogen and Methane.* SAE Paper 871167, 1987.

4) Finegold, J G, Lynch, F E, Baker, N R, Takahashi, R, and Bush, A F. *The UCLA Hydrogen Car: Design, Construction, and Performance.* SAE Paper 730507, 1973.

5) Lucas, G G, and Richards W L. *The Hydrogen/Petrol Engine - The Means to Give Good Part-Load Thermal Efficiency.* SAE Paper 820315, 1982.

6) Strickland, G. *Hydrogen Storage Technology for Metal Hydrides* in *Hydrogen for Energy Distribution.* Institute of Gas Technology, Chicago, 1979.

7) Rosso, M J, Adlhart, O J, and Marmolejo, J A. *A Fuel Cell Energy Storage System for Space Station Extravehicular Activity.* SAE Paper 881105, 1988.

8) Strebig, K C, and Waytulonis, R W. *The Bureau of Mines' Hydrogen Powered Mine Vehicle.* SAE Paper 871678, 1987.

9) Olavson, L G, Baker, N R, Lynch, F E, and Mejia, L C. *Hydrogen Fuel for Underground Mining Machinery.* SAE Paper 840233, 1984.

10) Twigg, M V. *I C I Catalyst Handbook.* Second Edition, Chapter 5, Wolfe Publishing Ltd, London, 1989.

11) British Petroleum. *Gasmaking.* B P Technical Services, London, 1965.

12) Pearce, R, and Patterson, W R. *Catalysis and Chemical Processes.* Chapter 6, Blackie & Son Ltd, London, 1981.

13) Houseman, J, and Cerini, D J. *On-Board Hydrogen Generator for a Partial Hydrogen Injection Internal Combustion Engine.* SAE Paper 740600, 1974.

14) Lee, R C, and Wimmer, D B. *Exhaust Emission Abatement by Fuel Variations to Produce Lean Combustion.* SAE Paper 680769, 1968.

15) Newkirk, M S and Abel, J L. *The Boston Reformed Fuel Car.* SAE Paper 720670, 1972.

16) Murray, R G and Schoeppel, R J. *Emission and Performance Characteristics of an Air-Breathing Hydrogen-Fueled Internal Combustion Engine.* Intersociety Energy Conversion Engineering Conference, Paper 719009, SAE Inc, New York, 1971.

17) Martin, M D. *Gaseous Automotive Fuels from Steam Reformed Liquid Hydrocarbons.* SAE Paper 780457, 1978.

18) Parks, F B. *A Single-Cylinder Engine Study of Hydrogen-Rich Fuels.* SAE Paper 760099, 1976.

19) Sher, E and Hacohen, Y. *Measurements and Predictions of the Fuel Consumption and Emission of a Spark Ignited Engine Fuelled with Hydrogen-Enriched Gasoline.* Proc Instn Mech Engrs, Vol 203, No A3, 155-162, 1989.

20) Strehlow, R A. *Fundamentals of Combustion,* Chapter 7, International Textbook Company, Pennsylvania, 1968.

21) Houseman, J and Hoehn, F W. *A Two-Charge Engine Concept.* Paper presented at the International Stratified Charge Conference, Troy, Michigan, October 30 - November 1 1974, SAE 741169, 1974.

22) Houseman, J and Cerini, D J. *Onboard Hydrogen Generation for Automobiles.* 11th Intersociety Energy Conversion Engineering Conference, Paper 769001, SAE Inc, New York, 1976.

23) Fox, H M of Phillips Petroleum Company. *Method and Apparatus for Reducing Engine Exhaust Pollutants.* USA Patent 3 717 129, 1973.

24) Anon. *Germans Attack Auto-Pollution with a Cracking Carburetor.* Machine Design, Vol 45, Part 18, p34, 1973.

25) Anon. *Emissions Slashed by Fuel Reformer.* Machine Design, Vol 45, Part 19, p42, 1973.

26) Wright, R A. *Industry Report.* Automotive News, 30 April 1973.

27) Gray, L C, and Alson, J A. *The Case for Methanol.* Scientific American, pp86-92, November 1989.

28) DeLuchi, M A, Johnson, R A, and Sperling, D. *Methanol vs. Natural Gas Vehicles: A Comparison of Resource Supply, Performance, Emissions, Fuel Storage, Safety, Costs, and Transitions.* SAE Paper 881656, 1988.

29) Mason, J L. *Vehicular Fuel Economy and The Greenhouse Effect.* The 1990 I Mech E/SAE Exchange Lecture, I Mech E Headquarters, London, 15 May 1990.

30) Menrad, H, Bernhardt, W, and Decker, G. *Methanol Vehicles of Volkswagen - A Contribution to Better Air Quality.* SAE Paper 881196, 1988.

31) Kester, F L, Konopka, A J, and Camara, E H. *Onboard Steam Reforming of Methanol to Fuel the Automotive Hydrogen Engine.* Intersociety Energy Conversion Engineering Conference, Paper 759175, SAE Inc, New York, 1975.

32) McCall, D M, Lalk, T R, Davison, R R, and Harris, W B. *Performance and Emissions Characteristics of a Spark Ignition Engine Fueled with Dissociated and Steam-Reformed Methanol.* SAE Paper 852106, 1985.

33) Smith, L R, and Urban, C M. *Unregulated Exhaust Emissions from Methanol-Fueled Cars.* SAE Paper 820967, 1982.

34) Scull, N, Kim, C, and Foster, D E. *Comparison of Unburned Fuel and Aldehyde Emissions from a Methanol-Fueled Stratified Charge and Homogenous Charge Engine.* SAE Paper 861543, 1986.

35) Lipari, F, and Colden, F L. *Aldehyde and Unburned Fuel Emissions from Developmental Methanol-Fueled 2.5L Vehicles.* SAE Paper 872051, 1987.

36) Sawicki, E, Hauser, T R, Stanley, T W, and Elbert, W. *The 3-Methyl-2-benzothiazolone Hydrazone Test.* Analytical Chemistry, Vol 33, Part 1, pp93-96, 1961.

37) Lipari, F and Swarin, S J. *Determination of Formaldehyde and other Aldehydes in Automobile Exhaust with an Improved 2,4-Dinitrophenyl-Hydrazine Method.* Journal of Chromatography, Vol 247, pp297-306, Elsevier Scientific Publishing Company, Amsterdam, 1982.

38) Finegold, J G. *Hydrogen: Primary or Supplementary Fuel for Automotive Engines.* SAE Paper 760609, 1976.

39) Menard, W A, Moynihan, P I, and Rupe, J H. *New Potentials for Conventional Aircraft When Powered by Hydrogen-Enriched Gasoline.* SAE Paper 760469, 1976.

40) Stebar, R F, and Parks, F B. *Emission Control with Lean Operation Using Hydrogen-Supplemented Fuel.* SAE Paper 740187, 1974.

41) Jenkins, J W of Johnson Matthey plc. *Catalytic Generation of Hydrogen from Hydrocarbons.* European Patent Publication No 0 262 947, 1988.

42) Jenkins, J W of Johnson Matthey plc. *Catalytic Hydrogen Generator for use with Methanol.* European Patent Publication No 0 217 532, 1987.

43) Clemmens, W B, and Martin, J C. *Methanol Decomposition Through Rich Oxidation in a Self-Ignited Catalytic Reactor.* SAE Paper 900582, 1990.

44) Yoo, S J, and Lee, C I. *Feasibility Evaluation of Reformed Methanol Usage to Spark Ignition Engine.* SAE Paper 871166, 1987.

45) Brinkman, N D, and Stebar, R F. *A Comparison of Methanol and Dissociated Methanol Illustrating Effects of Fuel Properties on Engine Efficiency - Experiments and Thermodynamic Analyses.* SAE Paper 850217, 1985.

46) Yamaguchi, I, Takishita, T, Sakai, T, Ayusawa, T, and Kim, Y K. *Development Research on Dissociated Methanol Fueled Spark Ignition Engine.* Paper No 852201, Proc of 4th Joint Symposium on Internal Combustion Engines, Jan 1984.

47) König, A, Ellinger, K-W, and Korbel, K. *Engine Operation on Partially Dissociated Methanol.* SAE Paper 850573, 1985.

48) Sato, T, Tanaka, M, and Agawa, K. *A Study on the Reformed-Methanol Engine.* SAE Paper 861237, 1986.

49) Sakai, T, Yamaguchi, I, Asano, M, Ayusawa, T and Kim, Y K. *Transient Performance Development on Dissociated Methanol Fueled Passenger Car.* SAE Paper 871169, 1987.

50) Lindström, O B. *Fuel Treatment for Combustion Engines.* USA Patent 3 918 412, 1975.

51) Sjöström, K. *Steam Reforming of n-Heptane at Low Concentrations for Hydrogen Injection into Internal Combustion Engines.* Ind Eng Chem Process Des Dev, Part 19, pp148-153, 1980.

52) Parsons, B N V. *An Internal Combustion Engine and a Method of Operating the Engine.* European Patent Application 85302249.9, 1985.

53) Parsons, B N V. *Exhaust Gas Reforming.* Unpublished Internal Report, Jaguar Cars, Coventry, 1984.

54) Sepos, T G. *Feasibility Study of Steam Reforming for Automotive Fuel Use.* Final Year Project Thesis, Dept of Mechanical Engineering, University of Birmingham, 1987.

55) Quader, A A. *Why Intake Charge Dilution Decreases Nitric Oxide Emission from Spark Ignition Engines.* SAE Paper 710009, 1971.

56) Williams, C, and Southall, M. *Atmospheric Pollution from Petrol Engines: A Further Exercise in the Control of Oxides of Nitrogen by Exhaust Recirculation.* MIRA Report 1971/5, Nuneaton, England, 1971.

57) Jones, M R, Dunn, J W, and Wyszynski, M L. *Thermodynamic Feasibility Studies of the Exhaust-Gas Reforming of Hydrocarbon Fuels.* I Mech E International Conference: Automotive Power Systems - Environment and Conservation, Paper No C394/014, Chester, England, September 10-12 1990.

58) Sjöström, K, Eriksson, S, and Landqvist, G. *Onboard Hydrogen Generation for Hydrogen Injection into Internal Combustion Engines.* SAE Paper 810348, 1981.

59) Machmouchi, H C. *Computer Programme for Calculation of Complex Chemical Equilibrium Compositions.* MSc Thesis, Dept of Mechanical Engineering, University of Birmingham, 1987.

60) West, H. *Calculation of Equilibrium Compositions and Applications to Automotive Fuel Reforming.* Final Year Project Thesis, Department of Mechanical Engineering, University of Birmingham, 1988.

61) Bailey, B K, and Russel, J A. *Emergency Transportation Fuels: Properties and Performance.* SAE Paper 810444, 1981.

62) Dorn, P, and Mourao, A M. *The Properties and Performance of Modern Automotive Fuels.* SAE Paper 841210, 1984.

63) Reynolds, W C, and Perkins, H C. *Engineering Thermodynamics.* pp425-445, McGraw-Hill, New York, 1970.

64) Haywood, R W. *Equilibrium Thermodynamics.* pp247-266, John Wiley & Sons, Chichester, 1980.

65) Anon. *JANAF Thermochemical Tables.* Dow Chemical Company, Michigan, 1986.

66) Stull, D R, Westrum, E F, and Sinke, G C. *The Chemical Thermodynamics of Organic Compounds.* John Wiley & Sons, New York, 1969.

67) Eastop, T D, and McConkey, A. *Applied Thermodynamics for Engineering Technologists.* pp544-554, Longman, London, 1979.

68) Benson, R S. *Advanced Engineering Thermodynamics.* Chapter 4, Pergamon Press, London, 1967.

69) Smith, E B. *Basic Chemical Thermodynamics.* Fourth Edition, Oxford Science Publications, Oxford, 1990.

70) Benson, R S, and Whitehouse, N D. *Internal Combustion Engines, Volume 2.* Pergamon Press, Oxford, 1979.

71) Denbigh, K. *The Principles of Chemical Equilibrium.* Third Edition, Chapters 2, 3, 4, Cambridge University Press, London, 1971.

72) Van Zeggeren, F and Storey, S H. *The Computation of Chemical Equilibria.* Cambridge University Press, London, 1970.

73) Olikara, C, and Borman, G L. *A Computer Program for Calculating Properties of Equilibrium Combustion Products with Some Applications to I C Engines.* SAE Paper 750468, 1975.

74) Zeleznik, F J, and Gordon, S. *Calculation of Complex Chemical Equilibria.* Ind Eng Chem, Vol 60, No 6, June 1968.

75) Svehla, R A, and McBride, B J. *Fortran IV Computer Program for Calculation of Thermodynamic and Transport Properties of Complex Chemical Systems.* NASA Report TN D-7056, Lewis Research Center, Cleveland, Ohio, 1973.

76) Gordon, S and McBride, B J. *Computer Program for Calculation of Complex Chemical Equilibrium Compositions, Rocket Performance, and Chapman-Jouguet Detonations.* NASA Special Publication SP-273, Lewis Research Center, Cleveland, Ohio, 1971.

77) Stroud, K A. *Engineering Mathematics.* Second Edition, Chapter 10, Macmillan Press, London, 1982.

78) Zemansky, M W. *Heat and Thermodynamics.* Chapter 16, McGraw-Hill, New York, 1957.

79) Gordon, S. *Complex Chemical Equilibrium Calculations.* Paper in *Kinetics and Thermodynamics in High-Temperature Gases.* NASA Special Publication SP-239, Lewis Research Centre, Cleveland, Ohio, 1970.

80) Zeleznik, F J, and Gordon, S. *Simultaneous Least-Squares Approximation of a Function and its First Integrals with Application to Thermodynamic Data.* NASA Report TN D-767, Lewis Research Center, Cleveland, Ohio, 1961.

81) Benson, R S and Baruah, P C. *Performance and Emission Predictions for a Multi-Cylinder Spark Ignition Engine.* Proc Inst Mech Engrs, Vol 191, Part 32/77, pp339-354, London, 1977.

82) Baruah, P C, Benson, R S, and Gupta, H N. *Performance and Emission Predictions for a Multi-Cylinder Spark Ignition Engine with Catalytic Converter.* SAE Paper 780672, 1978.

83) Bosch GmbH. *Automotive Handbook.* p216, Robert Bosch, Stuttgart, 1986.

84) Chan, S H. *Computer Simulation of Engine Cycles and Combustion Thermodynamics.* MSc Thesis, Dept of Mechanical Engineering, University of Birmingham, 1987.

85) Ferguson, C R. *Internal Combustion Engines - Applied Thermosciences.* Chapter 3, 4, John Wiley and Sons, New York, 1986.

86) Robertson, M D. *Computer Simulation of Arbitrary Heat Release.* Final Year I C Engines Course Report, Dept of Mechanical Engineering, University of Birmingham, 1988.

87) Heywood, J B. *Internal Combustion Engine Fundamentals.* Chapter 9, McGraw-Hill Book Company, New York, 1988.

88) Kanury, A M. *Introduction to Combustion Phenomena.* pp130-131, Gordon & Breach Scientific Publications, New York, 1975.

89) Barnett, H C, and Hibbard, R R. *Basic Considerations in the Combustion of Hydrocarbon Fuels with Air.* NACA Report No 1300, Lewis Flight Propulsion Laboratory, Cleveland, Ohio, 1957.

90) Heimel, S, and Weast, R C. *Effect of Initial Mixture Temperature on the Burning Velocity of Benzene-Air, n-Heptane-Air, and Iso-Octane-Air Mixtures.* Sixth Symposium (International) on Combustion, pp296-302, Yale University, New Haven, Connecticut, August 19-24 1956. Published by Chapman & Hall, London.

91) Metghalchi, M, and Keck, J C. *Burning Velocities of Mixtures of Air with Methanol, Isooctane, and Indolene at High Pressure and Temperature.* Combustion and Flame 48: 191-210, Elsevier Science Publishing, New York, 1982.

92) Milton, B E, and Keck, J C. *Laminar Burning Velocities in Stoichiometric Hydrogen and Hydrogen-Hydrocarbon Gas Mixtures.* Combustion and Flame 58: 13-22, Elsevier Science Publishing, New York, 1984

93) Yu, G, Law, C K, and Wu, C K. *Laminar Flame Speeds of Hydrocarbon + Air Mixtures with Hydrogen Addition.* Combustion and Flame 63: 339-347, Elsevier Science Publishing, New York, 1986.

94) Morgan, G H, and Kane, W R. *Some Effects of Inert Diluents on Flame Speeds and Temperatures.* Fourth Symposium (International) on Combustion, pp313-320, Massachusetts Institute of Technology, Cambridge, Massachusetts, September 1-5 1952. Published by Williams and Wilkins, Baltimore.

95) Mellish, C E, and Linnett, J W. *The Influence of Inert Gases on some Flame Phenomena.* Fourth Symposium (International) on Combustion, pp407-420, Massachusetts Institute of Technology, Cambridge, Massachusetts, September 1-5 1952. Published by Williams and Wilkins, Baltimore.

96) Bradley, J N. *Flame and Combustion Phenomena.* Chapter 5, Methuen & Co, London, 1969.

97) Gaydon, A G, and Wolfhard, H G. *Flames, Their Structure, Radiation and Temperature.* Third Edition, Chapter 5, Chapman and Hall, London, 1970.

98) Price, T W, and Potter, J H. *Factors Affecting Flame Velocity in Stoichiometric Carbon Monoxide Oxygen Mixtures.* Fourth Symposium (International) on Combustion, pp363-369, Massachusetts Institute of Technology, Cambridge, Massachusetts, September 1-5 1952. Published by Williams and Wilkins, Baltimore.

99) Scheller, K. *On the Burning Velocity of Moist Carbon Monoxide-Oxygen-Nitrogen Mixtures.* Sixth Symposium (International) on Combustion, pp280-288, Yale University, New Halen, Connecticut, August 19-24 1956. Published by Chapman & Hall, London.

100) Lewis, B, and von Elbe, G. *Combustion, Flames and Explosions of Gases.* Chapter 7, Academic Press, New York, 1951.

101) Grasso, P. *Health Effects of Automotive Exhaust Gases.* 8-12, Petroleum Review, Institute of Petroleum, January 1990.

102) Walzer, P, Altendorf, J P, Geiger, I, and Waschatz, U. *A New Exhaust Emissions Concept.* SAE Paper 881156, 1988.

103) Koberstein, E, Engler, B H, and Völker, H. *Catalytic Automotive Exhaust Purification-The European Situation 1985.* SAE Paper 852094, 1985.

104) Gomez, A J, and Reinke, P E. *Lean Burn: A Review of Incentives, Methods and Tradeoffs.* SAE Paper 880291, 1988.

105) United States Environmental Protection Agency. *40 Code of Federal Regulations: Protection of the Environment. Parts 81 to 89.* National Technical Information Service, Springfield, 1986.

106) Japan Environment Agency Air Quality Bureau. *Automotive Pollution Control Division Exhaust Emissions Certification Test Procedure 10-Mode and 11-Mode Driving Cycle.* Japan Environment Agency, 1986.

107) Economic Commission for Europe. *Agreement Concerning the Adoption of Uniform Conditions of Approval and Reciprocal Recognition of Approval for Motor Vehicle Equipment and Parts, Regulation 15.* Brussels Office of Official Publications, 1981.

108) Rush, M W, and Larby, R J. *An Overview of Worldwide Vehicle Exhaust Emission Legislation.* Presented at 'Moteurs et Carburants des Vehicules de l'An 2000', Brussels, 21 October 1986.

109) Bosch GmbH. *Emission Control for Spark Ignition Engines.* Robert Bosch, Stuttgart, 1985.

110) Benson, R S, and Whitehouse, N D. *Internal Combustion Engines, Volume 1.* Pergamon Press, Oxford, 1979.

111) Kraft, J and Kuhler, M. *Aldehydes from Motor Vehicles: Toxicity and Air Quality.* SAE Paper 851661, 1985.

112) Goodger, E M. *Alternative Fuels - Chemical Energy Resources.* Chapter 7, Macmillan Press, London, 1980.

113) Heywood, J B. *Pollutant Formation and Control in Spark Ignition Engines.* Prog. Energy Combust. Sci., Vol 1, pp135-164, 1976.

114) Lavoie, G A, Heywood, J B, and Keck, J C. *Experimental and Theoretical Investigation of Nitric Oxide Formation in Internal Combustion Engines.* Combust. Sci. Technology, Vol 1, pp313-326, 1970.

115) Wyszynski, M L. *Virtual Internal Combustion Engine (VICE)®.* Engine cycle simulation software written at the University of Birmingham, June 1990.

116) Higgins, R A. *Engineering Metallurgy Part 1-Applied Physical Metallurgy.* Fourth Edition, Chapter 18, Holder and Stoughton, London 1980.

117) Anon. *IEEE Standard Digital Interface for Programmable Instrumentation.* IEEE Standard 488, 1981.

118) Anon. *Data Acquisition and Instrument Control using Apple Macintosh Computers - A Hands-On Seminar.* Held at the Excelsior Hotel, Birmingham, by National Instruments of Newbury, September 1989.

119) West, H. *The Reduction of Pollutant Emissions from Internal Combustion Engines.* Internal Progress Report, Dept of Mechanical Engineering, University of Birmingham, April 1991.

120) Anon. *Analysis Certificate No. 03871 for CEC Legislative Fuel RF-08-A-85.* Johann Haltermann GmbH, Hamburg, 1984.

121) Hughes, R. *Deactivation of Catalysts.* Chapter 5, Academic Press, London, 1984.

122) Anon. *Examination of RF-08 Monolith by the Electron Probe X-Ray Micro Analyser.* Analysis carried out by Johnson Matthey Technology Centre, Sonning Common, January 1991.

123) Moore, C A. *Design and Construction of a Low-Cost Test Rig for the Investigation of Flame Propagation.* Final Year Project Thesis, School of Manufacturing & Mechanical Engineering, University of Birmingham, 1992.

# APPENDIX I

Not available in the digital version of this thesis

# APPENDIX II

| Oxidant | Gas Concentration, Molar Fraction | | | | | Oxidant Details | | Stoich. |
|---|---|---|---|---|---|---|---|---|
| | CO | $CO_2$ | $H_2O$ | $N_2$ | $O_2$ | Ex $H_2O$ | Ex $O_2$ | OX:F |
| OX1 | 0.003 | 0.122 | 0.139 | 0.734 | 0.002 | - | - | 7.55 |
| OX2 | 0.003 | 0.107 | 0.244 | 0.644 | 0.002 | 100% | - | 5.38 |
| OX3 | 0.003 | 0.108 | 0.123 | 0.740 | 0.026 | - | 3% | 7.09 |
| OX4 | 0.002 | 0.096 | 0.220 | 0.659 | 0.023 | 100% | 3% | 5.32 |
| | | | | | | | | |
| $OX_m1$ | - | 0.115 | 0.230 | 0.655 | - | - | - | 3.74 |

Table A5.1 Details of Reforming Oxidant Compositions and Stoichiometric Reforming Oxidant to Feedstock Ratios.

| Fuel | Gas Concentration, Molar Fraction | | | | | | OX | $T_{req}$ | $T_{eq}$ | $\lambda_r$ | Stoi. | $\eta_{rth}$ |
|---|---|---|---|---|---|---|---|---|---|---|---|---|
| | CO | $CH_4$ | $CO_2$ | $H_2$ | $H_2O$ | $N_2$ | | K | K | | AFR | % |
| RF1 | .130 | .006 | .067 | .174 | .044 | .579 | 1 | 1300 | 923 | 2.0 | 0.937 | 124.5 |
| RF2 | .184 | .001 | .035 | .215 | .031 | .534 | 1 | 1435 | 1023 | 1.5 | 1.224 | 127.2 |
| RF3 | .189 | - | .029 | .212 | .035 | .535 | 1 | 1535 | 1123 | 1.5 | 1.221 | 127.8 |
| RF4 | .191 | .002 | .038 | .295 | .044 | .430 | 2 | 1395 | 1023 | 1.5 | 1.656 | 126.0 |
| RF5 | .124 | .005 | .070 | .169 | .047 | .585 | 3 | 1105 | 923 | 2.0 | 0.891 | 111.5 |
| RF6 | .180 | .001 | .037 | .211 | .033 | .538 | 3 | 1290 | 1023 | 1.5 | 1.190 | 117.1 |
| RF7 | .140 | .016 | .063 | .259 | .057 | .465 | 4 | 1125 | 923 | 1.5 | 1.482 | 113.3 |
| RF8 | .188 | .002 | .039 | .284 | .045 | .442 | 4 | 1305 | 1023 | 1.5 | 1.586 | 119.1 |

Table A5.2 Details of Reformed n-Heptane Fuels Selected for Cycle Analysis Simulation.

| Fuel | Gas Concentrations, Molar Fraction | | | | | | OX | $T_{req}$ | $T_{eq}$ | $\lambda_r$ | Stoi. | $\eta_{rth}$ |
|---|---|---|---|---|---|---|---|---|---|---|---|---|
| | CO | $CH_4$ | $CO_2$ | $H_2$ | $H_2O$ | $N_2$ | | K | K | | AFR | % |
| $RF_m1$ | .097 | .013 | .100 | .272 | .122 | .396 | $_m1$ | 1060 | 900 | 1.0 | 1.369 | 115.8 |
| $RF_m2$ | .074 | .005 | .106 | .223 | .138 | .453 | $_m1$ | 1080 | 900 | 1.5 | 0.973 | 117.1 |
| $RF_m3$ | .179 | .005 | .060 | .388 | .090 | .278 | $_m1$ | 1200 | 1000 | 0.5 | 2.254 | 119.0 |
| $RF_m4$ | .124 | - | .079 | .282 | .125 | .390 | $_m1$ | 1205 | 1000 | 1.0 | 1.347 | 119.4 |

Table A5.3 Details of Reformed Methanol Fuels Selected for Cycle Analysis Simulation.

Note that in Tables A5.2 and A5.3, $T_{eq}$ represents simulated reformer equilibrium temperature, and $T_{req}$ is the predicted reformer gas inlet temperature requirement. $\lambda_r$ is reformer excess oxidant factor, Stoi. AFR is the stoichiometric AFR for the combustion of reformed fuel, and $\eta_{rth}$ is the computed reformer thermal efficiency of the reaction which produces the reformed fuel.

```
1       CASE NUMBER (KASE)
TP      ASSIGNED CONDITIONS (TP = CONSTANT TEMP & PRESS)

        TEMPERATURES
1               NUMBER OF SPECIFIED TEMPERATURES
800             TEMPERATURES (KELVIN)

        PRESSURES
1               NUMBER OF SPECIFIED PRESSURES
1.0             PRESSURES (ATMOSPHERES)

        OX/FUEL RATIOS
FI  1           EQUIV RATIO (FI), % FUEL (%F) OR OX/FUEL RATIO (OF)
1.0             VALUES

8               NO OF GASEOUS SPECIES (NS)
Y  0.001        CONVERGENCE CRITERIA ( 'N' - DEFAULT OF 0.000005 )

COMPONENT ELEMENTS, MOL. WEIGHTS & OXIDATION STATES:
 4 ELEMENTS        MW        V+     V-
 H                 1.00797   1      0
 N                 14.0067   0      0
 O                 15.9994   0      -2
 C                 12.01115  4      0

REACTANT DETAILS

                   H    N    O    C    %WT    H0(CAL/MOLE)
1 FUEL:
CH3OH              4    0    1    1    1.000      0

3 OXIDANTS:
CO2                0    0    2    1    0.184      0
H2O                2    0    1    0    0.150      0
N2                 0    2    0    0    0.666      0

3.74            STOICH OX/FUEL RATIO

SPECIES         INITIAL ESTIMATES FOR MOLE FRACTIONS
C(S)                0.0001
CH4                 0.0001
CO                  0.02
CO2                 0.005
H2                  0.02
H2O                 0.005
N2                  0.05
O2                  0.0001
```

Fig A5.1 Input File for Reforming Simulation Using EQCOMP.PAS

```
**********************************************************************
*******      CALCULATION OF EQUILIBRIUM COMPOSITIONS        *********
* FOR APPLICATION TO STEAM REFORMING OF AUTOMOTIVE FUELS *
*********    WRITTEN BY HEATHER WEST & MARTIN JONES         ********
*BIRMINGHAM UNIVERSITY - DEPT. OF MECHANICAL ENGINEERING *
********************              1988                ********************
**********************************************************************
```

Input is from: C:reactm.DAT

RESULTS FILE

sort is: TP
assigned temperature 1 is: 800
assigned pressure 1 is: 1
assigned equivalence ratio 1 is: 1.00
number of species is: 8
convergence criteria is: 0.001000

| | Element | M | V+ | V- |
|---|---|---|---|---|
| 1 | H | 1.00797 | 1 | 0 |
| 2 | N | 14.00670 | 0 | 0 |
| 3 | O | 15.99940 | 0 | -2 |
| 4 | C | 12.01115 | 4 | 0 |

Initial estimate of Molecular Weight is: 10.03009 g/gmole
species being considered:-
C(S) CH4 CO CO2 H2 H2O
N2 O2

RATIO 1, PRESSURE 1 = 1.00 ATM., TEMP 1 = 800 K

Reactant Compositions:

| | H | N | O | C | % wt | H0(cal/mole) |
|---|---|---|---|---|---|---|
| Fuels: | | | | | | |
| CH3OH | 4.000 | 0.000 | 1.000 | 1.000 | 1.000 | -57040.00000 |
| Oxidants: | | | | | | |
| CO2 | 0.000 | 0.000 | 2.000 | 1.000 | 0.184 | -94040.53035 |
| H2O | 2.000 | 0.000 | 1.000 | 0.000 | 0.150 | -57790.25575 |
| N2 | 0.000 | 2.000 | 0.000 | 0.000 | 0.666 | -0.11528 |

ratio 1 HSUBO is: -536.20763 (kg-mol)(K)/kg
B0 1 is: 0.03948 (kg-atoms)/kg
B0 2 is: 0.03752 (kg-atoms)/kg
B0 3 is: 0.01975 (kg-atoms)/kg
B0 4 is: 0.00988 (kg-atoms)/kg

Solutions to ratio 1, pressure 1, temp. 1 :

| PI | 1 | 2 | 3 | 4 | 5 | dlnn |
|---|---|---|---|---|---|---|
| 1 | -10.782 | -12.961 | -32.542 | -1.232 | -0.219 | 0.300 |
| 2 | -9.610 | -12.489 | -41.917 | -1.232 | 0.004 | -0.697 |
| 3 | -9.328 | -12.450 | -43.109 | -1.232 | 0.016 | -0.602 |
| 4 | -9.336 | -12.566 | -43.510 | -1.232 | -0.016 | 0.062 |
| 5 | -9.315 | -12.573 | -43.708 | -1.232 | -0.000 | -0.000 |
| 6 | -9.311 | -12.573 | -43.752 | -1.232 | -0.000 | 0.000 |
| 7 | -9.311 | -12.573 | -43.754 | -1.232 | -0.000 | 0.000 |

******** EQUILIBRIUM COMPOSITION ********

| NAME | n (mole fract) | S | $H_0$ | $C_P$ | G1 |
|---|---|---|---|---|---|
| C(S) | 0.01204630311 | 2.38475 | 1.15241 | 0.02876 | -1.23234 |
| CH4 | 0.05031950344 | 27.95184 | -7.54709 | 0.40981 | -38.48829 |
| CO | 0.03535211416 | 27.32007 | -14.33570 | 0.54540 | -44.99817 |
| CO2 | 0.12712077782 | 0.95900 | -55.73026 | 1.33174 | -88.75188 |
| H2 | 0.18864446764 | 19.17685 | 2.21070 | 2.00421 | -18.63403 |
| H2O | 0.15975509336 | 26.90327 | -33.65036 | 2.74769 | -62.38774 |
| N2 | 0.42676174044 | 26.56898 | 2.26149 | 4.36064 | -25.15901 |
| O2 | 0.00000000002 | 28.36259 | 2.38093 | 4.36064 | -50.48811 |

THERMODYNAMIC PROPERTIES:

PRESSURE: 1.000 atm, TEMPERATURE: 800 K
FI: 1.00 OX:FUEL RATIO: 3.740
% FUEL: 21.097 STOICH. OX:FU RATIO: 3.740
MOL. WT.: 22.75013 DENSITY : 0.34656 KG/M3
ENTHALPY : -3494.09472 KJ/KG ENTROPY : 9.92088 KJ/KG K
HFR = -4461.01640 KJ/KG HFP = -4234.20715 KJ/KG
HEAT OF REACTION @ 298 K = -1.075 MJ/KG FEED FUEL

Exh. to reactants mass ratio =1.58
Enth.of exh. out =-3055.819 KJ/KG
Enth. of products =-3494.095 KJ/KG
Tot enth out =-3225.821 KJ/KG
Enth of fuel=-5303.916 KJ/KG
Trial and error tot. enth. in=-3222.064 KJ/KG
Reqd. oxidant enth. in =-3036.516 KJ/KG

Reqd. Oxidant Temp. = 830 K

LHV of Reformed Fuel= 20.985 MJ/KG

Reactor Thermal Efficiency = 105.40 %

Fig A5.2 Output File for Reforming Simulation Using EQCOMP.PAS

# APPENDIX III

| Fuel | $P_1$, bar | $P_{max}$, bar | IMEP, bar | $\eta_{overall}$,% | $\eta_{cycle}$,% |
|---|---|---|---|---|---|
| $C_7H_{16}$ | 1.00 | 64.12 | 11.52 | 37.32 | 37.32 |
| | | | | | |
| RF1 | 1.00 | 53.42 | 6.49 | 46.85 | 36.68 |
| RF1 | 2.23 | 120.51 | 15.76 | 51.08 | 39.99 |
| RF1 | 1.67 | 89.82 | 11.51 | 49.83 | 39.01 |
| RF2 | 1.00 | 57.36 | 7.29 | 47.47 | 36.73 |
| RF2 | 2.01 | 116.54 | 15.80 | 51.19 | 39.92 |
| RF2 | 1.50 | 86.79 | 11.51 | 50.01 | 38.69 |
| RF3 | 1.00 | 57.41 | 7.29 | 47.47 | 36.76 |
| RF3 | 2.01 | 116.00 | 15.72 | 50.96 | 39.46 |
| RF3 | 1.50 | 86.85 | 11.51 | 50.08 | 38.78 |
| RF4 | 1.00 | 61.72 | 7.91 | 46.18 | 35.83 |
| RF4 | 1.80 | 112.40 | 15.24 | 49.38 | 38.32 |
| RF4 | 1.40 | 86.70 | 11.51 | 47.98 | 37.23 |
| RF5 | 1.00 | 52.56 | 6.32 | 41.91 | 36.63 |
| RF5 | 2.05 | 108.91 | 14.02 | 45.42 | 39.70 |
| RF5 | 1.71 | 90.62 | 11.51 | 44.74 | 39.11 |
| RF6 | 1.00 | 57.01 | 7.22 | 43.50 | 36.56 |
| RF6 | 1.86 | 107.09 | 14.39 | 46.61 | 39.18 |
| RF6 | 1.52 | 87.10 | 11.51 | 45.67 | 38.34 |
| RF7 | 1.00 | 59.90 | 7.56 | 40.37 | 36.38 |
| RF7 | 1.65 | 99.31 | 13.17 | 42.64 | 38.43 |
| RF7 | 1.46 | 87.70 | 11.51 | 42.17 | 38.00 |
| RF7* | 1.65 | 91.99 | 13.16 | 42.64 | 38.43 |
| RF7** | 1.65 | 84.11 | 13.04 | 42.24 | 38.07 |
| RF7*** | 1.65 | 75.97 | 12.81 | 41.41 | 37.32 |
| RF8 | 1.00 | 61.28 | 7.82 | 44.05 | 36.04 |
| RF8 | 1.74 | 107.21 | 14.43 | 46.80 | 38.29 |
| RF8 | 1.41 | 86.97 | 11.51 | 46.05 | 37.68 |

Table A6.1 Summary of n-Heptane Reformed Fuel Cycle Analysis Pressure and Efficiency Results

| Fuel | $P_1$, bar | $T_{max}$, K | $T_{130}$, K | $T_{180}$, K | $T_{req}$, K | HHV1 | HHV2 |
|---|---|---|---|---|---|---|---|
| | | | | | | MJ/kg | MJ/kg |
| $C_7H_{16}$ | 1.00 | 2863 | 1426 | 1214 | - | - | 48.20 |
| | | | | | | | |
| RF1 | 1.00 | 2227 | 1027 | 869 | 1300 | 3.82 | 61.57 |
| RF1 | 2.23 | 2253 | 1177 | 1066 | 1300 | 3.82 | 61.57 |
| RF1 | 1.67 | 2246 | 1133 | 1007 | 1300 | 3.82 | 61.57 |
| RF2 | 1.00 | 2435 | 1124 | 947 | 1435 | 5.06 | 62.30 |
| RF2 | 2.01 | 2461 | 1278 | 1148 | 1435 | 5.06 | 62.30 |
| RF2 | 1.50 | 2452 | 1224 | 1075 | 1435 | 5.06 | 62.30 |
| RF3 | 1.00 | 2439 | 1125 | 947 | 1535 | 5.05 | 62.24 |
| RF3 | 2.01 | 2465 | 1279 | 1149 | 1535 | 5.05 | 62.24 |
| RF3 | 1.50 | 2456 | 1225 | 1076 | 1535 | 5.05 | 62.24 |
| RF4 | 1.00 | 2589 | 1201 | 1009 | 1395 | 6.85 | 62.12 |
| RF4 | 1.80 | 2610 | 1347 | 1199 | 1395 | 6.85 | 62.12 |
| RF4 | 1.40 | 2602 | 1292 | 1125 | 1395 | 6.85 | 62.12 |
| RF5 | 1.00 | 2187 | 1008 | 854 | 1105 | 3.63 | 55.14 |
| RF5 | 2.05 | 2211 | 1143 | 1030 | 1105 | 3.63 | 55.14 |
| RF5 | 1.71 | 2207 | 1115 | 993 | 1105 | 3.63 | 55.14 |
| RF6 | 1.00 | 2417 | 1116 | 939 | 1290 | 4.93 | 57.35 |
| RF6 | 1.86 | 2441 | 1256 | 1121 | 1290 | 4.93 | 57.35 |
| RF6 | 1.52 | 2435 | 1217 | 1069 | 1290 | 4.93 | 57.35 |
| RF7 | 1.00 | 2470 | 1146 | 965 | 1125 | 5.96 | 53.49 |
| RF7 | 1.65 | 2487 | 1264 | 1119 | 1125 | 5.96 | 53.49 |
| RF7 | 1.46 | 2484 | 1239 | 1086 | 1125 | 5.96 | 53.49 |
| RF7* | 1.65 | 2458 | 1270 | 1125 | 1125 | 5.96 | 53.49 |
| RF7** | 1.65 | 2427 | 1282 | 1135 | 1125 | 5.96 | 53.49 |
| RF7*** | 1.65 | 2396 | 1298 | 1150 | 1125 | 5.96 | 53.49 |
| RF8 | 1.00 | 2566 | 1189 | 1000 | 1305 | 6.56 | 58.91 |
| RF8 | 1.74 | 2586 | 1326 | 1177 | 1305 | 6.56 | 58.91 |
| RF8 | 1.41 | 2580 | 1281 | 1118 | 1305 | 6.56 | 58.91 |

Table A6.2 Summary of n-Heptane Reformed Fuel

Cycle Analysis Temperature Results, Giving Fuel Heating Values

Note that HHV1 is heating value in MJ per unit mass of reformed fuel, and HHV2 is per unit mass of reformer feedstock

$\eta_{overall}$ is based on work output and feedstock fuel power input to the reformer, and $\eta_{cycle}$ is based on work output and engine fuel power input.

* Timing retarded 4 degrees from standard

**Timing retarded 8 degrees from standard

***Timing retarded 12 degrees from standard

| Fuel | $P_1$, bar | $P_{max}$, bar | IMEP, bar | $\eta_{overall}$, % | $\eta_{cycle}$,% |
|---|---|---|---|---|---|
| $CH_3OH$ | 1.00 | 63.46 | 11.26 | 36.92 | 36.92 |
| | | | | | |
| $RF_m1$ | 1.00 | 57.30 | 7.15 | 41.44 | 35.97 |
| $RF_m1$ | 1.77 | 102.10 | 13.46 | 44.08 | 38.27 |
| $RF_m1$ | 1.50 | 86.50 | 11.25 | 43.56 | 37.81 |
| $RF_m2$ | 1.00 | 52.31 | 6.16 | 41.10 | 35.54 |
| $RF_m2$ | 2.04 | 107.60 | 13.53 | 44.30 | 38.31 |
| $RF_m2$ | 1.72 | 90.65 | 11.25 | 43.79 | 37.87 |
| $RF_m3$ | 1.00 | 63.27 | 8.32 | 41.14 | 35.13 |
| $RF_m3$ | 1.51 | 96.41 | 13.21 | 43.27 | 36.95 |
| $RF_m3$ | 1.31 | 83.19 | 11.26 | 42.56 | 36.35 |
| $RF_m4$ | 1.00 | 57.12 | 7.10 | 41.13 | 35.24 |
| $RF_m4$ | 1.77 | 102.15 | 13.41 | 43.96 | 37.16 |
| $RF_m4$ | 1.51 | 86.83 | 11.25 | 43.28 | 37.08 |

Table A6.3 Summary of Methanol Reformed Fuel Cycle Analysis Pressure and Efficiency Results

| Fuel | $P_1$, bar | $T_{max}$, K | $T_{130}$, K | $T_{180}$, K | $T_{req}$, K | HHV1 | HHV2 |
|---|---|---|---|---|---|---|---|
| | | | | | | MJ/kg | MJ/kg |
| $CH_3OH$ | 1.00 | 2770 | 1409 | 1205 | - | - | 22.73 |
| | | | | | | | |
| $RF_m1$ | 1.00 | 2356 | 1106 | 937 | 1060 | 5.52 | 26.18 |
| $RF_m1$ | 1.77 | 2374 | 1231 | 1099 | 1060 | 5.52 | 26.18 |
| $RF_m1$ | 1.50 | 2370 | 1201 | 1058 | 1060 | 5.52 | 26.18 |
| $RF_m2$ | 1.00 | 2134 | 996 | 848 | 1080 | 3.98 | 26.28 |
| $RF_m2$ | 2.04 | 2153 | 1126 | 1016 | 1080 | 3.98 | 26.28 |
| $RF_m2$ | 1.72 | 2150 | 1101 | 983 | 1080 | 3.98 | 26.28 |
| $RF_m3$ | 1.00 | 2672 | 1259 | 1057 | 1200 | 9.27 | 26.62 |
| $RF_m3$ | 1.51 | 2689 | 1374 | 1206 | 1200 | 9.27 | 26.62 |
| $RF_m3$ | 1.31 | 2684 | 1338 | 1158 | 1200 | 9.27 | 26.62 |
| $RF_m4$ | 1.00 | 2373 | 1112 | 940 | 1205 | 5.60 | 26.53 |
| $RF_m4$ | 1.77 | 2392 | 1240 | 1106 | 1205 | 5.60 | 26.53 |
| $RF_m4$ | 1.51 | 2388 | 1210 | 1065 | 1205 | 5.60 | 26.53 |

Table A6.4 Summary of Methanol Reformed Fuel

Cycle Analysis Temperature Results, Giving Fuel Heating Values

# APPENDIX IV

| | Gas Concentration, Molar % | | | | | | $\eta_{rth}$ |
|---|---|---|---|---|---|---|---|
| Test Point | $H_2$ | CO | $CH_4$ | $C_2$ | $C_{3-6}$ | $CO_2$ | % |
| 1/1 | 15.81 | 10.37 | 3.81 | 4.97 | 1.72 | 8.05 | 115.90 |
| 1/2 | 15.33 | 10.30 | 1.36 | 1.64 | 0.15 | 9.13 | 129.50 |
| 1/3 | 22.87 | 11.01 | 3.73 | 6.63 | 1.55 | 8.39 | 108.80 |
| 1/4 | 22.23 | 10.42 | 1.52 | 1.90 | 0.87 | 9.38 | 119.10 |
| 1/5 | 16.66 | 11.42 | 2.53 | 4.53 | 1.43 | 7.55 | 103.70 |
| 1/6 | 16.43 | 11.81 | 0.82 | 0.70 | 0.38 | 8.34 | 108.50 |
| 1/7 | 24.80 | 13.54 | 4.50 | 4.30 | 1.70 | 4.50 | 92.30 |
| 1/8 | 24.44 | 11.06 | 1.10 | 0.90 | 0.57 | 8.98 | 108.40 |

Table A9.1

Gas Analysis Results for n-Heptane.

Gas Inlet Temperature=850°C

GHSV=1000$h^{-1}$

| | Gas Concentration, Molar % | | | | | | $\eta_{rth}$ |
|---|---|---|---|---|---|---|---|
| Test Point | $H_2$ | CO | $CH_4$ | $C_2$ | $C_{3-6}$ | $CO_2$ | % |
| 1/1 | 11.48 | 5.49 | 1.95 | 4.95 | 1.26 | 10.35 | 99.00 |
| 1/2 | 12.14 | 6.31 | 0.47 | 0.40 | 0.61 | 10.77 | 75.30 |
| 1/3 | 16.18 | 5.77 | 5.68 | 2.68 | 1.84 | 10.47 | 76.60 |
| 1/4 | 16.40 | 5.80 | 1.33 | 1.74 | 0.89 | 11.09 | 97.00 |
| 1/5 | 13.86 | 7.22 | 2.44 | 4.34 | 1.18 | 9.84 | 95.00 |
| 1/6 | 15.68 | 9.20 | 1.06 | 1.09 | 0.19 | 9.23 | 113.10 |
| 1/7 | 17.82 | 7.52 | 2.73 | 4.54 | 0.52 | 9.15 | 81.16 |
| 1/8 | 18.79 | 7.97 | 1.58 | 1.90 | 0.27 | 10.34 | 110.40 |

Table A9.2

Gas Analysis Results for n-Heptane.

Gas Inlet Temperature=850°C

GHSV=3000$h^{-1}$

| | Gas Concentration, Molar % | | | | | | $\eta_{rth}$ |
|---|---|---|---|---|---|---|---|
| Test Point | $H_2$ | CO | $CH_4$ | $C_2$ | $C_{3-6}$ | $CO_2$ | % |
| 1/1 | 24.40 | 19.29 | 2.74 | 1.11 | 0.08 | 3.80 | 102.90 |
| 1/2 | 21.77 | 15.64 | 0.33 | 0.10 | 0.02 | 6.39 | 128.00 |
| 1/3 | 30.52 | 16.29 | 3.88 | 2.67 | 0.27 | 6.62 | 96.60 |
| 1/4 | 26.44 | 13.37 | 0.75 | 0.62 | 0.07 | 8.27 | 113.30 |
| 1/5 | 25.10 | 20.94 | 2.45 | 0.77 | 0.07 | 2.87 | 96.50 |
| 1/6 | 19.21 | 14.23 | 0.03 | 0.03 | 0.05 | 7.06 | 102.80 |
| 1/7 | 32.21 | 19.56 | 3.67 | 1.67 | 0.18 | 4.69 | 95.00 |
| 1/8 | 27.26 | 14.99 | 0.21 | 0.05 | 0.03 | 7.69 | 109.90 |

Table A9.3

Gas Analysis Results for n-Heptane.

Gas Inlet Temperature=950°C

GHSV=1000$h^{-1}$

| | Gas Concentration, Molar % | | | | | | $\eta_{rth}$ |
|---|---|---|---|---|---|---|---|
| Test Point | $H_2$ | CO | $CH_4$ | $C_2$ | $C_{3-6}$ | $CO_2$ | % |
| 1/1 | 14.17 | 9.40 | 2.81 | 4.27 | 0.64 | 9.15 | 98.50 |
| 1/2 | 13.14 | 8.89 | 1.00 | 1.41 | 0.27 | 10.08 | 111.40 |
| 1/3 | 16.17 | 7.38 | 3.50 | 5.59 | 1.37 | 10.32 | 88.80 |
| 1/4 | 16.12 | 7.54 | 1.93 | 2.64 | 0.71 | 11.19 | 115.40 |
| 1/5 | 19.32 | 14.03 | 2.79 | 2.96 | 0.44 | 7.03 | 100.30 |
| 1/6 | 17.15 | 12.91 | 0.54 | 0.28 | 0.14 | 7.90 | 110.20 |
| 1/7 | 21.25 | 11.32 | 3.78 | 5.05 | 0.66 | 7.61 | 96.60 |
| 1/8 | 22.14 | 12.38 | 1.19 | 1.12 | 0.12 | 8.45 | 113.70 |

Table A9.4

Gas Analysis Results for n-Heptane.

Gas Inlet Temperature=950°C

GHSV=3000$h^{-1}$

| | Gas Concentration, Molar % | | | | | | $\eta_{rth}$ |
|---|---|---|---|---|---|---|---|
| Test Point | $H_2$ | CO | $CH_4$ | $C_2$ | $C_{3-6}$ | $CO_2$ | % |
| 1/1 | 4.92 | 1.22 | 1.32 | 1.10 | 0.72 | 12.69 | 31.60 |
| 1/2 | 3.62 | 0.95 | 1.05 | 0.83 | 0.60 | 12.91 | 46.60 |
| 1/3 | 7.81 | 0.80 | 3.70 | 2.48 | 1.99 | 11.43 | 51.40 |
| 1/4 | 5.87 | 0.89 | 2.04 | 1.49 | 1.17 | 12.45 | 61.00 |
| 1/5 | 7.09 | 2.65 | 3.06 | 2.19 | 1.02 | 10.99 | 56.60 |
| 1/6 | 5.15 | 2.64 | 1.52 | 1.14 | 0.48 | 12.06 | 63.40 |
| 1/7 | 8.66 | 2.50 | 3.95 | 2.82 | 1.48 | 10.89 | 54.80 |
| 1/8 | 6.35 | 2.35 | 1.79 | 1.41 | 0.76 | 12.15 | 58.00 |

Table A9.5

Gas Analysis Results for ULG.

Gas Inlet Temperature=850°C

GHSV=1000$h^{-1}$

| | Gas Concentration, Molar % | | | | | | $\eta_{rth}$ |
|---|---|---|---|---|---|---|---|
| Test Point | $H_2$ | CO | $CH_4$ | $C_2$ | $C_{3-6}$ | $CO_2$ | % |
| 1/1 | 0.72 | 0.52 | 1.83 | 1.61 | 1.20 | 13.21 | 40.10 |
| 1/2 | 0.60 | 0.44 | 1.03 | 0.97 | 0.71 | 13.53 | 47.50 |
| 1/3 | 1.99 | 0.52 | 2.72 | 2.28 | 1.74 | 12.63 | 42.40 |
| 1/4 | 1.17 | 0.49 | 1.35 | 1.25 | 1.26 | 13.34 | 47.40 |
| 1/5 | 1.02 | 2.54 | 2.77 | 2.26 | 1.09 | 11.72 | 53.40 |
| 1/6 | 0.48 | 3.06 | 1.45 | 1.25 | 0.68 | 11.96 | 65.80 |
| 1/7 | 1.48 | 1.56 | 3.52 | 3.04 | 2.05 | 11.64 | 52.40 |
| 1/8 | 0.76 | 2.35 | 1.79 | 1.71 | 1.04 | 12.13 | 60.90 |

Table A9.6

Gas Analysis Results for ULG.

Gas Inlet Temperature=850°C

GHSV=3000$h^{-1}$

| | Gas Concentration, Molar % | | | | | | $\eta_{rth}$ |
|---|---|---|---|---|---|---|---|
| Test Point | $H_2$ | CO | $CH_4$ | $C_2$ | $C_{3-6}$ | $CO_2$ | % |
| 1/1 | 13.12 | 5.05 | 3.79 | 2.20 | 0.31 | 11.00 | 71.30 |
| 1/2 | 11.41 | 5.82 | 1.60 | 0.88 | 0.19 | 11.77 | 86.80 |
| 1/3 | 17.59 | 5.39 | 4.62 | 2.65 | 0.52 | 10.89 | 68.60 |
| 1/4 | 14.73 | 5.15 | 1.87 | 1.27 | 0.29 | 12.64 | 81.90 |
| 1/5 | 16.02 | 9.80 | 3.43 | 1.50 | 0.22 | 8.28 | 76.40 |
| 1/6 | 15.18 | 11.97 | 0.63 | 0.14 | 0.07 | 8.39 | 97.20 |
| 1/7 | 19.82 | 8.20 | 4.05 | 2.29 | 0.34 | 9.77 | 70.10 |
| 1/8 | 15.58 | 7.97 | 1.72 | 1.06 | 0.15 | 11.25 | 87.40 |

Table A9.7

Gas Analysis Results for ULG.

Gas Inlet Temperature=950°C

GHSV=1000$h^{-1}$

| | Gas Concentration, Molar % | | | | | | $\eta_{rth}$ |
|---|---|---|---|---|---|---|---|
| Test Point | $H_2$ | CO | $CH_4$ | $C_2$ | $C_{3-6}$ | $CO_2$ | % |
| 1/1 | 7.52 | 1.69 | 3.41 | 2.79 | 0.77 | 0.77 | 63.20 |
| 1/2 | 5.79 | 1.93 | 1.64 | 1.30 | 0.42 | 0.42 | 68.60 |
| 1/3 | 7.71 | 1.42 | 4.50 | 3.46 | 1.66 | 1.66 | 60.10 |
| 1/4 | 6.63 | 1.62 | 2.13 | 1.89 | 0.93 | 0.93 | 68.90 |
| 1/5 | 11.09 | 6.35 | 3.27 | 2.06 | 0.33 | 0.33 | 67.90 |
| 1/6 | 9.23 | 6.76 | 1.49 | 0.88 | 0.09 | 0.09 | 82.20 |
| 1/7 | 10.32 | 3.97 | 4.56 | 3.33 | 0.99 | 0.99 | 64.60 |
| 1/8 | 9.50 | 4.80 | 1.95 | 1.56 | 0.43 | 0.43 | 75.90 |

Table A9.8

Gas Analysis Results for ULG.

Gas Inlet Temperature=950°C

GHSV=3000$h^{-1}$

| Gas Inlet Temp, °C | Gas Concentration, Molar % | | | | | | $\eta_{rth}$ |
|---|---|---|---|---|---|---|---|
| | $H_2$ | CO | $CH_4$ | $C_2$ | $C_{3-6}$ | $CO_2$ | % |
| 600 | 0.45 | 0.13 | 0.14 | 0.37 | 0.16 | 13.67 | 5.91 |
| 650 | 0.67 | 0.16 | 0.08 | 2.38 | 0.32 | 13.46 | 22.40 |
| 700 | 3.01 | 1.64 | 0.32 | 0.73 | 0.77 | 13.33 | 17.40 |
| 750 | 5.17 | 2.78 | 1.56 | 0.32 | 0.25 | 13.16 | 25.10 |
| 800 | 6.63 | 2.21 | 2.14 | 3.69 | 1.15 | 11.99 | 57.20 |
| 850 | 7.72 | 2.58 | 3.61 | 6.61 | 1.11 | 11.33 | 102.90 |
| 900 | 13.52 | 5.66 | 4.34 | 6.21 | 0.92 | 9.95 | 120.20 |
| 950 | 23.25 | 11.63 | 3.59 | 2.75 | 0.27 | 8.03 | 113.90 |

Table A9.9

Gas Analysis Results for n-Heptane Temperature Sweep.
GHSV=1000$h^{-1}$, Excess-Steam Flue Gases, $\lambda_r$=1.5.

| Gas Inlet Temp, °C | Gas Concentration, Molar % | | | | | | $\eta_{rth}$ |
|---|---|---|---|---|---|---|---|
| | $H_2$ | CO | $CH_4$ | $C_2$ | $C_{3-6}$ | $CO_2$ | % |
| 600 | 0.78 | 0.77 | 0.05 | 0.04 | 0.84 | 13.36 | 6.00 |
| 650 | 1.14 | 0.71 | 0.15 | 0.14 | 1.22 | 13.07 | 28.40 |
| 700 | 2.44 | 0.32 | 0.68 | 0.63 | 1.98 | 13.15 | 23.30 |
| 750 | 2.50 | 0.38 | 0.69 | 0.69 | 1.86 | 13.17 | 23.80 |
| 800 | 4.43 | 0.96 | 1.05 | 0.88 | 1.42 | 12.89 | 32.00 |
| 850 | 8.00 | 1.34 | 2.41 | 1.92 | 1.31 | 12.27 | 59.90 |
| 900 | 12.00 | 3.00 | 2.60 | 1.85 | 0.70 | 12.00 | 66.00 |
| 950 | 16.20 | 5.30 | 3.20 | 1.90 | 0.41 | 11.80 | 70.00 |

Table A9.10

Gas Analysis Results for ULG Temperature Sweep.
GHSV=1000$h^{-1}$, Excess-Steam Flue Gases, $\lambda_r$=1.5.